Understanding and Quantifying Motor Vehicle Emissions with Vehicle Specific Power and TILDAS Remote Sensing

by

José Luis Jiménez-Palacios

Double Mechanical Engineer Degree (1993)
Universidad de Zaragoza (Spain)
Université de Technologie de Compiègne (France)

Submitted to the Department of Mechanical Engineering
In Partial Fulfillment of the Requirements for the Degree of
Doctor of Philosophy in Mechanical Engineering

at the

Massachusetts Institute of Technology

February 1999

Signature of Author…………………………………………………………………
Department of Mechanical Engineering
December 5, 1998

Certified by…………………………………………………………………
Gregory J. McRae
Bayer Professor of Chemical Engineering
Thesis Supervisor

Accepted by…………………………………………………………………...
Ain A. Sonin
Mechanical Engineering Department Graduate Chair

Understanding and Quantifying Motor Vehicle Emissions with Vehicle Specific Power and TILDAS Remote Sensing

by

José Luis Jiménez-Palacios

ABSTRACT

Motor vehicles are one of the largest sources of air pollutants worldwide. Despite their importance, motor vehicle emissions are inadequately understood and quantified. This is due in part to large variations in individual vehicle emissions with changing operating conditions, and to significant differences between vehicles.

To better relate emissions with operating conditions, a new parameter termed "specific power" (SP) is presented. SP is the instantaneous tractive power per unit vehicle mass. This parameter has three main advantages: it can be calculated from roadside measurements, it captures most of the dependence of light-duty vehicle emissions on driving conditions, and it is directly specified in emissions certification cycles. The dependence of CO, HC, and NO_x emissions on SP is better than on several other commonly used parameters, such as speed, acceleration, power, or fuel rate. Using SP as the basic metric allows meaningful comparisons to be made between data from different remote sensing sites, dynamometer driving cycles, and emission models. Modern U.S. vehicles are likely to operate under commanded enrichment when SP exceeds the maximum value on the Federal Test Procedure (~22 kW/Metric Ton). This may allow transient high emissions to be screened out during future remote sensing campaigns.

Remote sensing can address the problem of inter-vehicle differences by quickly and cheaply measuring the emissions of large numbers of vehicles. Here, a tunable infrared laser differential absorption spectrometer (TILDAS) remote sensor was used to gather the first on-road measurements of N_2O and NO_2, and the first high precision measurements of NO. NO was detected with a sensitivity of 5 ppm, which allowed even Ultra Low Emission Vehicles to be measured. On-road accuracy was demonstrated by comparing the TILDAS results with the on-board measurements of a heavy-duty diesel truck (HDDT). The remote sensor could operate with an optical path length of 88 meters, more than five times that of competing instruments. The NO and N_2O emission distributions of passenger cars (PCs) and light-duty trucks (LDTs) were found to be highly skewed, while the NO emission distribution for HDDTs was not. N_2O emissions from PCs and LDTs are estimated to contribute between 0.5% and 0.9% to U.S. greenhouse gas emissions.

Acknowledgments

My Ph.D. has been a multifaceted and enriching journey. I have profoundly changed, yet in some ways I am still very much the same person who started this program. Five years of my life and lots of different people and experiences after, I am happy to see this journey finished. This is my chance to recognize those who contributed to make it possible.

First of all, I would like to thank my Ph.D. advisor, Greg McRae, for his support during my graduate studies. He always had encouraging and positive things to say about my work, and was an endless source of suggestions. He also made me realize the importance of our field by circling the globe 25 times while I was his grad student.

Next I would like to express my gratitude to Dave Nelson, Mark Zahniser, Barry McManus, and Chuck Kolb of Aerodyne Research, and to Michael Koplow of Emdot Corporation. They introduced me to the TILDAS technique and were patient with my mistakes along the way. Working with them was one of the most rewarding experiences of these few years, and most importantly, was always fun.

I also want to thank my other thesis committee members, Bob Slott, John Heywood, and Ahmed Ghoniem. Each one of them brought a very different perspective and working style which made for very enriching interactions. I also had many stimulating discussions about my thesis work with Betty Pun, Ed Brown, Monika Mayer, Jochen Harnish, Frank Verdegem, Peter McClintock, Carlos Martinez, and Dave Kayes.

The many people of the McRae research group have provided a stimulating and fun work environment. I thank them for their companionship and all the fun moments spent together, and, last but not least, for their help with preparing my talks and especially my thesis defense. I will miss you! I also congratulate Liz Webb for managing the secretarial work with so much enthusiasm and efficiency.

I also spent one year of my Ph.D. working at the MIT Combustion Research Facility until its closure. I want to thank Janos Beer, Laszlo Barta, and the CRF research group for making that year very rich in learning and enjoyment.

César Dopazo of the University of Zaragoza helped me to come to MIT and generously supported me here for six months with his own group's research funding, a gesture I have not forgotten and for which I want to express again my gratitude.

I also wish to acknowledge the South Coast Air Quality Management District for sponsoring a field measurement campaign; in-kind support from NASA and Hughes "Smog Dog;" help during remote sensing campaigns from Steve Schmidt of Arthur D. Little, Nelson Sorbo of Hughes Environmental Services, and Ed Brown, Foy King, and Bruce Harris of EPA; and financial support from "La Caixa" Fellowship Program and from the EPA Office of Research and Development (grant number R824794-01-0).

I have been very lucky to have many friends in my years at MIT. To them I want to express my deepest gratitude for their humor, companionship, eagerness to follow when I suggested yet another trip to explore the wild USA or another dance class, and also their support when research was thin and my morale was low. You know who you are and I need not say more.

Finally I would like to thank my family. Their love (and illegal shipments of Spanish ham) has always been with me. I want to dedicate this thesis to them.

Table of Contents

List of Figures

Chapter 5. The TILDAS Remote Sensor 141

List of Tables

Nomenclature

A/C	Air Conditioning
A/F	Air-to-Fuel Ratio
ARB02	A dynamometer test cycle designed by the California Air Resources Board
CAA	Clean Air Act
CAP	Compliance Assurance Program
CARB	California Air Resources Board
CH_2O	Formaldehyde
CO	Carbon monoxide
CO_2	Carbon Dioxide
DMV	Department of Motor Vehicles
EGR	Exhaust Gas Recirculation
EMFAC	California's emissions factor model
EPA	U.S. Environmental Protection Agency
FIR	Far Infrared
FTIR	Fourier Transform Infrared Spectrometer
FTP	Federal Test Procedure
FWHM	Full Width at Half Maximum
GC	Gas Chromatography
gpg	Grams of pollutant emitted per gallon of fuel consumed
gpm	Grams of pollutant emitted per mile traveled
GVW	Gross Vehicle Weight
GVWR	Gross Vehicle Weight Rating
HC	Hydrocarbons
HDT	Heavy-Duty Truck
HDDT	Heavy-Duty Diesel Truck
HFET	Highway Fuel Economy Test
HL07	Dynamometer driving cycle representing aggressive driving
HWFET	See HFET
HWHM	Half Width at Half Maximum
I/M	Inspection and Maintenance Program
IM240	240-second driving cycle used in inspection and maintenance programs
IPCC	Intergovernmental Panel on Climate Change
K	Kelvin
kW	Kilowatt
LDT	Light-Duty Truck
LDV	Light-Duty Vehicles
LEV	Low-Emission Vehicle
MIR	Mid Infrared

MMTCE	Millions of Metric Tons of Carbon Equivalent
MOBILE	EPA's mobile source emissions model
NARSTO	North American Research Strategy for Tropospheric Ozone
NDIR	Non-Dispersive Infrared
NDUV	Non-Dispersive Ultraviolet
NH_3	Ammonia
NIR	Near Infrared
NMHC	Non-Methane Hydrocarbons
NMOG	Non-Methane Organic Gases
N_2O	Nitrous oxide
NO	Nitric oxide
NO_2	Nitrogen dioxide
NO_x	Oxides of nitrogen (the sum of NO and NO_2. N_2O is not included).
OBD	On-Board Diagnostics
OXY	Oxidation Catalyst
PC	Passenger Car
ppm	Parts-per-million
ppmv	Parts-per-million by volume
RS	Remote Sensing
RSD	Remote Sensing Device
SCAQMD	South Coast Air Quality Management District
SCAQS	South Coast Air Quality Study
SFTP	Supplemental Federal Test Procedure
SI	International system of units
SP	Specific Power
SULEV	Super Ultra Low Emission Vehicle
TCE	Tons of Carbon Equivalent
TDL	Tunable Diode Laser
TDLAS	Tunable Diode Laser Absorption Spectroscopy
THC	Total Hydrocarbons
Tier 0	A set of Federal emission standards for passenger cars and light-duty trucks
Tier 1	A set of Federal emission standards for passenger cars and light-duty trucks
Tier 2	A set of Federal emission standards for passenger cars and light-duty trucks
TILDAS	Tunable Infrared Laser Differential Absorption Spectroscopy
TLEV	Transitional Low-Emitting Vehicle
TWC	Three-Way Catalyst
ULEV	Ultra Low Emission Vehicle
US06	Regulatory driving cycle representing aggressive driving
UV	Ultraviolet
VIN	Vehicle Identification Number
VMT	Vehicle-Miles Traveled

VOC	Volatile Organic Compounds
VSP	Vehicle Specific Power
WOT	Wide Open Throttle

Chapter 1. Introduction

1.1. Air Pollution

Air pollution spans a wide range of spatial and temporal scales. Urban air quality problems affect most large cities around the world (WHO/UNEP, 1992). Tropospheric ozone in particular persists in the U.S. despite more than 30 years of regulation and billions of dollars spent on emissions controls, although it is slowly improving as a result of these efforts (U.S. EPA, 1998f). Air quality in many developing countries is deteriorating (WHO/UNEP, 1992) because these countries generally lack the resources to invest in emission controls.

Global air pollution problems have captured public attention, first because of stratospheric ozone depletion, and more recently due to the debate about global warming. In response to the latter concern, steps to stabilize and reduce the emissions of greenhouse gases were agreed in the 1997 Kyoto protocol. If the predictions of significant warming are confirmed, widespread changes in human activities will be needed to fend off disastrous consequences.

1.2. The Contribution of Motor Vehicles to Air Pollution

Automobile-related air pollution did not attract much attention until about 1950. Emissions from coal combustion and other uncontrolled industrial sources had been the main sources of air pollution until then. The importance of automobiles was first recognized in the Los Angeles area, where a new pollutant which irritated the eyes and respiratory system was observed, mostly during the summer. Growing numbers of gasoline-powered cars without any emission control system and the particular meteorological conditions of the Los Angeles basin combined to produce a serious smog problem that persists to this day. Automobile manufacturers first denied that cars were the cause of the problem, but eventually the scientific evidence was too clear to be denied (de Nevers, 1995).

The strategy chosen to deal with the problem was to impose limits on how much pollution new cars could emit, the so-called "emission standards." The first such regulations were enacted in California in 1965 (Calvert *et al.*, 1993). U.S. legislation

followed in 1968. The early 1970s were marked by conflict between the U.S. EPA and the automobile manufacturers because the emissions regulations were not achievable using existing technology (de Nevers, 1995). The manufacturers did succeed in developing the technology needed to meet these increasingly stricter regulations, summarized in Figure 1-1.
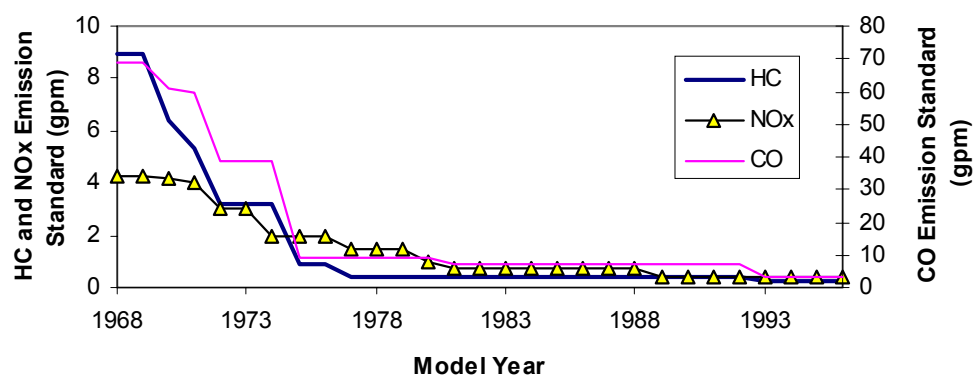
Figure 1-1: California new passenger car emission standards
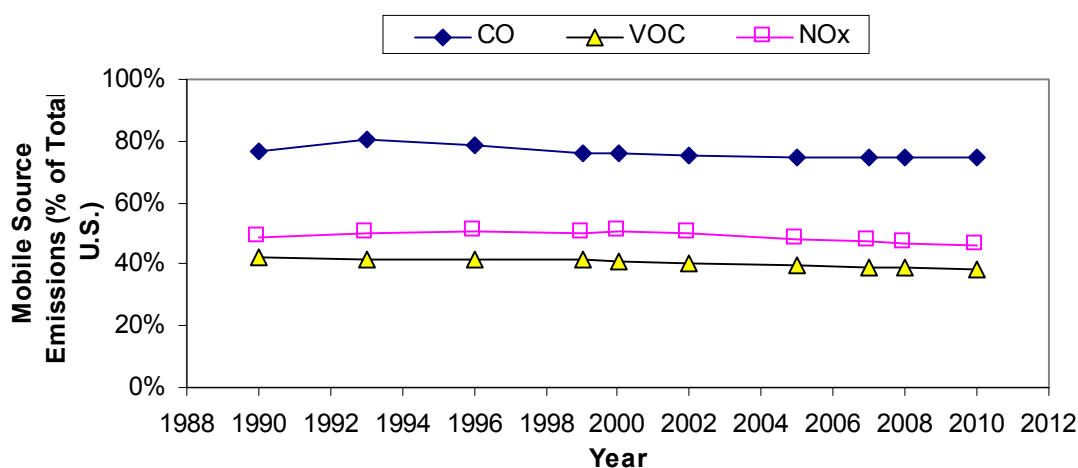
Figure 1-2: Contribution of mobile sources to total U.S. emissions[1] (U.S. EPA, 1997d)

Despite this success producing less polluting new cars, the air quality improvements that were anticipated when those regulations were designed have not been fully achieved. In 1993-95 still 44% of the U.S. population lived in areas which violated the ozone air quality standard, shown in Figure 1-3. Motor vehicles are still one of the

---

[1] The total U.S. emissions are projected to decline from 1990 to 2010 by 19% for CO, 27% for VOC, and 11% for NOx *(U.S. EPA, 1997d)*.

largest sources of air pollutant emissions in the US, contributing 79% of the total CO, 42% of the VOC, 50% of the NO_x, and 29% of the greenhouse gases in 1996 (U.S. EPA, 1996b; U.S. EPA, 1998c). This dominance is projected to continue in the future, as illustrated by Figure 1-2.

Many U.S. States are finding it difficult to meet the current ozone and PM air quality standards by the deadlines established in the Clean Air Act (U.S. EPA, 1997a). For these reasons still stricter emission standards are being planned and implemented (U.S. EPA, 1996a; U.S. EPA, 1997a; CARB, 1998c; U.S. EPA, 1998h), including a "Super Ultra Low Emissions Vehicle" standard of 0.02 gpm NO (or a factor of 200 smaller than pre-control levels) in California (CARB, 1998c).

Figure 1-3: Nonattainment areas for as of September 1997(from U.S. EPA, 1997c)

Despite their prominent position in the air pollution landscape, motor vehicle emissions are inadequately understood and quantified. A recent NARSTO review of mobile source emissions states: "at present, large and significant uncertainties exists in the estimates of the motor vehicle inventory. These uncertainties exist for all vehicle types and classes throughout North America" (Sawyer *et al.*, 1998b).

The primary focus of this thesis is on approaches that can provide a better understanding and quantification of motor vehicle emissions. Such information is vitally needed to design cost-effective control strategies.

1.2.1. Capturing the Effect of Driving Conditions on Motor Vehicle Emissions

Many factors influence the emissions of a vehicle, including age, miles driven, emission control technology, deterioration of the emission controls, tampering, ambient temperature, and altitude. At present the emissions from the vehicle fleet are estimated by models that attempt to account for many of those factors. Since these models are used by air pollution control agencies in the design of new control strategies (U.S. EPA, 1993b; CARB, 1998a), it is critical that the models reflect the true emissions as closely as possible.

Unfortunately, significant problems exist. The SCAQS-1 Tunnel Study of 1987 in the Los Angeles area "caused much consternation and head-scratching in the U.S. among those involved in the development and use of mobile source emission factors" (Halberstadt, 1990) by finding CO and HC emission rates that were higher than those predicted by the models by factors of approximately 3 and 4, respectively (Pierson *et al.*, 1990). Subsequent studies have found that despite many improvements, emission models still cannot consistently predict real-world emissions better than within about factor of 2, although the size of the discrepancies has been reduced (Fujita *et al.*, 1992; Kirchstetter *et al.*, 1996; Robinson *et al.*, 1996; Singer and Harley, 1996; Dreher and Harley, 1998; Gertler *et al.*, 1998; Ipps and Popejoy, 1998).

Driving conditions strongly affect emissions but their effects are not well quantified. As a result it is difficult to compare results based on different methods such as instrumented vehicles, tunnel studies, remote sensing, dynamometer driving cycles, and emissions modeling (or the results of different studies with the same method). A common approach is to relate emissions to average speed (Carlson and Austin, 1997; CARB, 1998a). However, Webster and Shih (1996) showed that emissions could vary by an order of magnitude for the same vehicle and average speed, due to small differences in speed on a one-second time scale. Roadway grade is known to affect emissions (Cicero-Fernandez and Long, 1995; Cicero-Fernandez and Long, 1996), but current inventory models do not account for it (Beardsley, 1998; Long, 1998).

A large fraction of the emissions from light-duty vehicles and trucks comes from a small fraction of the fleet with a malfunctioning control system (Stedman *et al.*, 1994). Inspection and Maintenance (I/M) programs are aimed at reducing these emissions. Remote sensing can be used as a way to identify high emitters to be directed to inspection and maintenance (I/M) facilities for testing, or to identify low emitters for exemption

from I/M testing ("clean screening"). These actions can lead to more acceptable I/M programs and more cost-effective improvements in air quality (Calvert *et al.*, 1993; Beaton *et al.*, 1995). These applications, however, have been hampered by the variability of vehicle emissions, such as the transient high emissions of properly operating vehicles. These high emissions lead to false high emitter identification and have been one of the main reasons why remote sensing has not been widely accepted for the detection of high emitters (Lorang, 1998). A reliable method to screen out these occurrences is needed.

Chapter 3 of this thesis presents a new definition of specific power that captures the dependence of emissions on driving conditions and is a good predictor of transient high emissions. A very important property of this parameter is that it is measurable from the roadside, and thus, it can be used by studies not having direct access to the vehicle such as tunnel studies and remote sensing.

1.2.2. Quantifying Vehicle Emissions with High Precision Remote Sensing

Considerable effort has been expended to develop approaches to better quantify motor vehicle emissions under actual operating conditions (Cadle *et al.*, 1997; Cadle *et al.*, 1998). Tunnel studies (Pierson *et al.*, 1990; Kirchstetter *et al.*, 1996; Robinson *et al.*, 1996; Gertler *et al.*, 1998) such as the SCAQS-1 mentioned above can be used to obtain average fleet emission factors, while ambient air measurements in the vicinity of large roadways (Fujita *et al.*, 1992; Ipps *et al.*, 1998) can assess the pollutant emission ratios (CO/NO_x and HC/NO_x). However, neither of these methods can provide information about vehicle-to-vehicle variations in emissions. Although it is possible to fit individual vehicles with on-board instrumentation capable of pollutant monitoring, such instrumentation is necessarily limited to a small number of test vehicles and cannot measure the emissions of non-cooperative vehicles.

Remote sensing instruments using open path spectroscopy can measure the emissions of thousands of vehicles per day. These measurements are made simultaneously and immediately behind the moving vehicle and, thus, have the potential to provide the best possible information on actual in-use vehicle emission profiles. Remote sensing of CO and HC has been operational for a number of years. Measurements of NO have lagged due to sensitivity problems. Current remote sensors cannot reliably measure the emissions from very clean vehicles, nor can they quantify other important species such as N_2O or NH_3.

The range of current instruments is also very limited. Bishop and Stedman (Bishop and Stedman, 1996c) report in a recent description of their NDIR-UV instrument that "the system is designed to operate on a single lane road […] Multiple lane operation has been reported but is not recommended." A longer pathlength would allow greater flexibility in the placement of the sensors. It would also diminish concerns of motorist and operator safety which greatly limit site selection (Walsh and Gertler, 1997), of vandalism of unmanned remote sensors, and of the suspected driving changes by drivers aware of the presence of the remote sensor (Walsh *et al.*, 1997).

Despite the more than 10 years since remote sensing was invented, some important aspects of remote sensing measurements have not been quantified or documented. Chapter 4 presents an analysis of a number of important issues which are necessary for a proper interpretation of these measurements.

In Chapter 5 of this thesis, a high-precision, long-pathlength remote sensor is presented. This instrument is based on Tunable Infrared Laser Differential Absorption Spectroscopy (TILDAS), and has been developed to overcome some of the limitations of existing remote sensors. It represents a major breakthrough with a sensitivity of 5 ppm of the exhaust for NO, which allows the measurement of the emissions of even Ultra Low Emission Vehicles. The measurement of minor species such as N_2O, NO_2, and NH_3 is also possible. A long path length capability has been demonstrated, which makes the TILDAS technique particularly well suited for on and off-road vehicle emissions measurements.

The TILDAS remote sensing instrument was used to answer some of the outstanding questions about motor vehicle emissions. Chapters 6 and 8 contain the analysis of the NO and N_2O emissions of more than 1400 light duty vehicles and light duty trucks. Chapter 7 presents the results of NO and NO_2 remote sensing of heavy-duty diesel trucks. A number of insights about the emission magnitudes, distributions, correlations, and formation mechanisms have been obtained from an in-depth analysis of these results.

1.2.3. Thesis Structure

This thesis is organized in the following manner:

- Chapter 2 summarizes the relevant background.

- Chapter 3 introduces a new parameter, Specific Power, and shows its usefulness for remote sensing and emissions modeling.

- Chapter 4 analyzes some of the practical issues associated with remote sensing measurements.

- Chapter 5 presents the TILDAS technique and its application to remote sensing.

- Chapter 6 contains the analysis of a measurement campaign of NO emissions from passenger cars and light-duty trucks.

- Chapter 7 presents the analysis of the NO and NO_2 emissions remotely sensed from heavy-duty diesel trucks.

- Chapter 8 is devoted to the analysis of the remote sensing measurements of nitrous oxide (N_2O) from cars and light-duty trucks.

- Chapter 9 contains the directions for future research.

- Chapter 10 presents the conclusions of this thesis.

1.2.4. Publications

Five conference papers have been presented on this work at the time of this writing, and another one will be submitted to the 9th CRC workshop on vehicle emissions. Part of chapter 5 has been published in *Applied Physics B* **62**(4), 1998. Part of chapter 6 has been accepted for publication in the *Journal of Air and Waste Management Association*. Condensed versions of chapters 3 and 8 will be submitted to *Environmental Science and Technology*. A version of chapter 7 will be submitted to the *Journal of Air and Waste Management Association*.

Chapter 2. Background

2.1. Spectroscopic Basis of Remote Sensing

2.1.1. Physical Basis for Remote Sensing: Beer's Law

The intensity of a light beam is proportional to the number of photons transmitted per unit time. Photons may be absorbed by gas molecules, raising that molecule to some excited state. For a given frequency, each molecule can be thought of having an apparent cross-sectional area ("absorption cross section", $\sigma(\nu)$) for photon absorption by the molecule.

The mathematical expression for the change in intensity, *dI*, of a parallel light beam of a single frequency (ν), as is traverses an infinitesimally small distance, *dx*, is given by Beer's Law *(Willard et al., 1988)*:

$$dI = \sigma(\nu)\, N\, I\, dx \tag{2-1}$$

where N is the number density of the absorbing molecule, in molecules/cm^3.
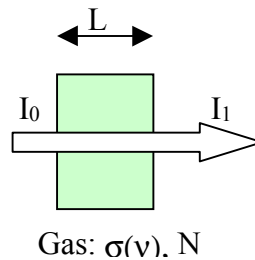
Figure 2-1: *Schematic of the transmission of a parallel beam through a gas*

If a monochromatic beam traverses a finite thickness L of a gas with spatially uniform composition (as depicted in Figure 2-1), equation (2-1) can be integrated:

$$\int_{I_0}^{I_1} \frac{dI}{I} = \int_0^L -\sigma(\nu)\, d \tag{2-2}$$

$$\frac{I_1}{I_0} = \exp(-\sigma(\nu)\, NL) \tag{2-3}$$

Beer's law indicates that the decrease in intensity is proportional to the incident intensity, and has an inverse exponential dependence in the concentration of the absorbing species and the pathlength of the measurement. The quantity $\sigma(\nu)NL$ is known as *optical depth.*

For the purposes of remote sensing, only the absorption due to the vehicle plume should be considered, while the absorption of the background atmosphere should be subtracted. If a light beam passes sequentially through 2 different volumes containing 2 gases that absorb at the same frequency, as depicted in Figure 2-2(a), it can be shown that:

$$\frac{I_1}{I_0} = \exp\left[-\sigma_1(\tilde{\nu})N_1L_1 - \sigma_2(\nu)N_2L_2\right] \qquad (2\text{-}4)$$

Or in other words the optical depths of the two volumes can be added when calculating the combined absorption. The same is true when both gases are contained within the same volume, as depicted in Figure 2-2(b). In this later case the optical depth will be $(\sigma_1(\nu)N_1 + \sigma_2(\nu)N_2)L$.
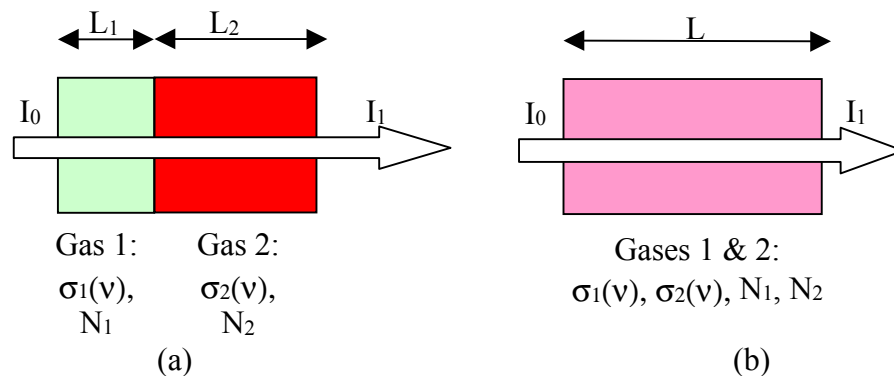
Figure 2-2: Schematic of 2 situations with more than one absorbing gas

2.1.2. Molecular Absorption of Infrared Radiation

The portion of the electromagnetic spectrum extending from the end of the red region on the visible light to the microwave region is called the infrared region. This region is customarily divided in three subregions (Willard *et al.*, 1988): the near infrared region (NIR), which extends from 4,000 to 12,500 cm^{-1} (2.5 to 0.8 $\mu m)^2$, the mid-

---

[2] To convert from cm^{-1} to μm use the formula: Wavelength $(\mu m) = 1 / (10^{-4} * \text{Frequency } (cm^{-1}))$

infrared region (MIR), which extends from 200 to 4,000 cm^{-1} (50 to 2.5 μm), and the far infrared region (FIR), which extends from 10 to 200 cm^{-1} (1,000 to 50 to μm).

The interactions between electromagnetic radiation and gas molecules in this region are mostly due to vibration of the atoms in a molecule with respect to one another and rotation of the molecule about an axis passing through the center of gravity (Herzberg, 1950). Due to quantum mechanical reasons, the allowed energies for these vibrational and rotational movements are limited to a series of discrete energy levels (Herzberg, 1950).

The vibrating molecule can absorb electromagnetic radiation if the molecule produces an oscillating electrical dipole moment that can interact with the electric field of the radiation (Willard *et al.*, 1988). Molecules which produce no dipole moment when they vibrate such as O_2 and N_2 do not interact with radiation by this mechanism. Molecules such as CO, NO, and CO_2 whose dipole moments varies while they vibrate, can absorb photons of energies that correspond to their quantized vibrational energy levels.

For each vibrational transition, simultaneous rotational transitions may occur. Each vibrational transition is observed as a "branch" or a "band" in the electromagnetic spectrum, composed of discrete lines that correspond to different rotational transitions. For example Figure 2-3 shows the absorption lines of part of the fundamental band of nitric oxide at around 1900 cm^{-1}.
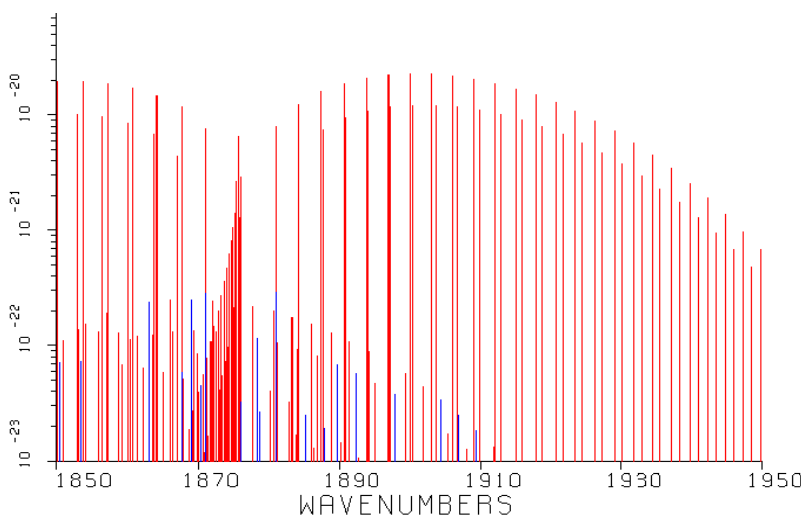
Figure 2-3: NO absorption bands around 1900 cm^{-1} showing individual absorption lines

2.1.3. Absorption Lineshapes

Beer's law, which relates the fractional absorption of a light beam when it traverses an absorbing gas, was presented in section 2.1.1. For an individual absorption line (such as the NO lines in Figure 2-3) the absorption cross-section can be expressed as (Willard *et al.*, 1988; Nagali and Hanson, 1997):

$$\sigma(\nu) = S \cdot \phi_\nu$$

where S is the line strength (in cm^{-1}/molecule cm^{-2}) and ϕ_ν ($1/cm^{-1}$) is the line shape function.
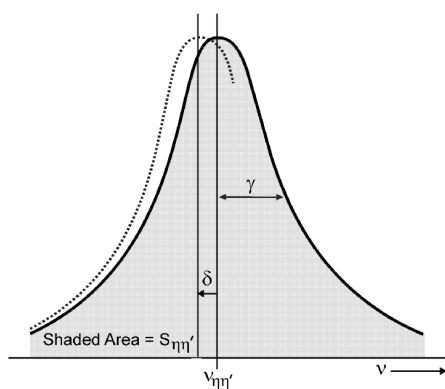
Figure 2-4: Schematic of line shape and the fundamental spectroscopic parameters of a line transition (the dotted line refers to a perturbed transition) (Rothman et al., 1998)

At atmospheric pressure[3], the shape of an individual molecular absorption line is dominated by the broadening provoked by intermolecular collisions (Herzberg, 1950). The resulting line shape function can be described by a Lorentzian function (Nagali *et al.*, 1997):

$$\phi(\nu) = \frac{1}{\pi} \cdot \frac{\gamma}{(\nu - \nu_0 + \delta)^2 + (\gamma)^2}$$

---

[3] At very low pressures (< 10 Torr) the line shape is determined by Doppler broadening, arising from random thermal motion of the gas molecules. For intermediate pressures (10-100 Torr) the line shape is a convolution of the Doppler and collision broadening effect, known as a Voigt line shape (Schiff *et al.*, 1994b).

where ν is the frequency (in cm^{-1}), γ is the collision half width[4] and δ is the collision shift. This functional shape can be used to model high resolution spectra such as those in Figure 5-4.

The width of the line is directly proportional to the absolute pressure:

$$\gamma = b\,P \tag{13.6}$$

where b is the pressure broadening coefficient (cm^{-1} atm^{-1}). b is determined by the broadening effect of air at low mixing ratios. At high mixing ratios the self-broadening effect becomes important.
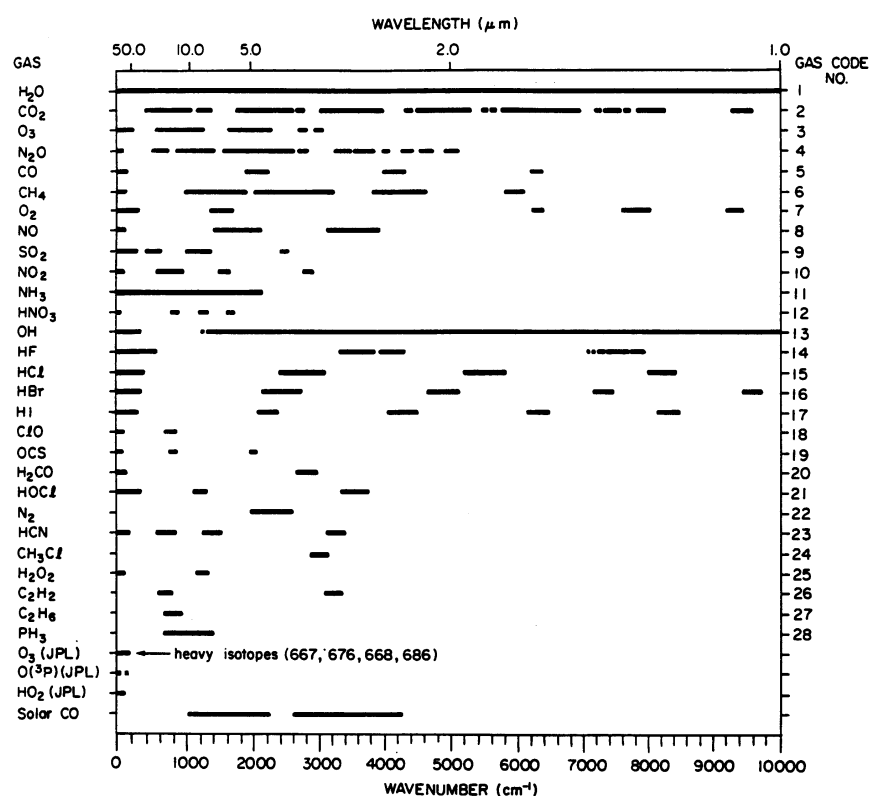
Figure 2-5: Spectral map showing the location of the absorption bands of the molecular species included in the 1996 HITRAN database (Rothman et al., 1998)

2.1.4. Spectral Databases

The positions and parameters of the molecular absorption bands and lines in the infrared have been subject to intensive research, both because of their potential

---

[4] HWHM or half width at half maximum.

applications and because they can be used to investigate the molecular structure (Herzberg, 1950). Several databases exist that compile existing information for individual lines, such as the HITRAN (Rothman *et al.*, 1987; Rothman *et al.*, 1992a; Rothman *et al.*, 1998) and GEISA (Jacquinet-Husson *et al.*, 1998). A spectral map with the location of the absorption bands of the molecules included in the 1996 version of HITRAN is shown in Figure 2-5 (Rothman *et al.*, 1998).

2.1.5. Effect of Gas Temperature and Pressure on Molecular Absorption Lines

The spectral parameters of an absorption line introduced in section 2.1.3 are functions of temperature and pressure. For the line strength[5] and the line width (Rothman *et al.*, 1998):

$$S(T) = S(T_0) \frac{Q(T_0)}{Q(T)} \frac{\exp(-c_2 \cdot E_\eta / T)}{\exp(-c_2 \cdot E_\eta / T_0)}$$

$$\gamma(T) = (\frac{T_0}{T})^n \cdot \gamma(T_0)$$

where T_0 and T are the reference and actual temperatures respectively, $Q(T)$ is the partition function, E_η is the ground state energy of the transition, c_2 is the second radiation constant,[6] and n is the coefficient of temperature dependence of the air-broadened half-width.

The line strength of an individual line can increase or decrease as temperature increases, while the line width generally decreases as temperature increases.[7]

All of the above parameters for the lines used in this study have been obtained from the HITRAN database. Some errors in HITRAN were discovered for the NO fundamental band at around 1900 cm^{-1}. The estimation of better parameters for those transitions is described in the next section.

---

[5] An additional term that accounts for the effect of stimulated emission on S(T) (Rothman *et al.*, 1998) has been omitted here since it is irrelevant at the temperatures of this study.

[6] $C_2 = h*c/k = 1.4388$ cm K

[7] According to the classical theory , n should have the value 0.5. However many experimental results show quite different values of n (Smith *et al.*, 1992; Spencer *et al.*, 1997).

2.2. On-Road Remote Sensing

2.2.1. Remote Sensing Setup

Cross-road remote sensing of vehicle emissions was pioneered by Don Stedman and Gary Bishop of the University of Denver in 1987 (Bishop *et al.*, 1989). The basic idea is to use the fact that the different exhaust gases absorb light at different frequencies to try to quantify them. The setup is illustrated in Figure 2-6. A light source(s) which contains at least 2 different frequency regions is shined across the road to a detector. When a vehicle goes by, its exhaust gases traverse the optical path of the laser light causing some absorption which is detected and recorded. The analysis of the relative absorption permits the quantification of a ratio of 2 gases, such as NO/CO_2, which is the primary result of the technique. From this ratio emission factors can be calculated as detailed in Appendix A.
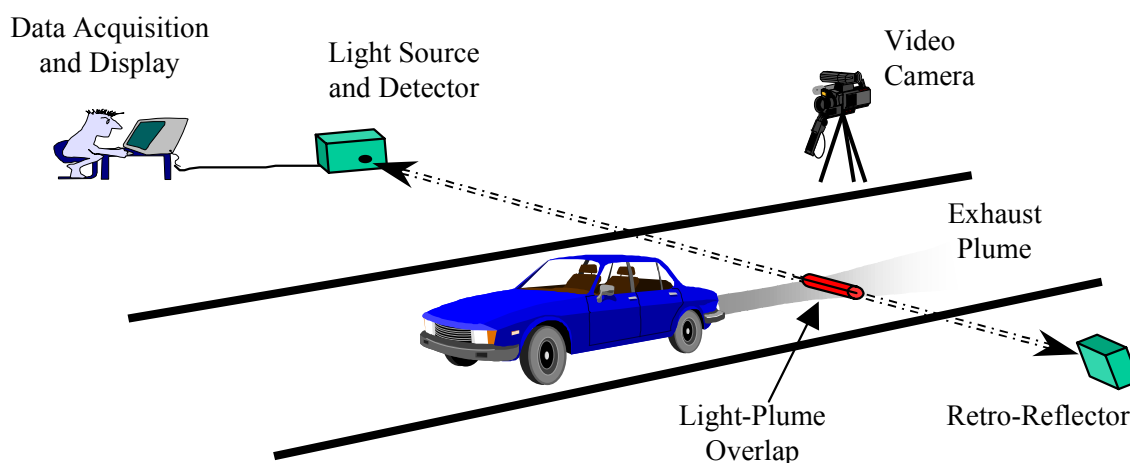
Figure 2-6: Setup for on-road remote sensing of automobile emissions

2.2.2. Principle of the Remote Sensing Measurement

The use of CO_2 as a reference gas allows one to make quantitative measurements of exhaust species without knowledge of the exhaust plume location or extent of dilution. Exhaust water vapor could also be used in principle for this purpose, but its much larger atmospheric background as compared to CO_2 make it impractical.

Since all gases in the exhaust plume are transported together by turbulent diffusion, the ratio of the measured column densities of NO and CO_2 provides an

emission index for NO. The emission index is simply the number of NO molecules per CO_2 molecule in the exhaust plume. This is the fundamental quantity measured by this instrument.

We can use the measured emission index to determine the concentration of NO present in the exhaust of an on-road vehicle. Since the complete combustion of gasoline produces a known CO_2 concentration, one can determine the NO concentration in the exhaust plume of the vehicle (in parts-per-million or ppm) in the following manner:

$$[NO] = \frac{NO\,(ppm\text{-}meter)}{CO_2\,(ppm\text{-}meter)} * [CO_2]_s$$

where $[CO_2]_S$ is the concentration of carbon dioxide produced in the stoichiometric combustion of gasoline. The emission index can be easily converted to units of grams of NO per unit of fuel, which can be used in fuel-based emission inventories (Singer *et al.*, 1996).

If a vehicle produces a significant concentration of CO or hydrocarbons, the above expression will overestimate the NO concentration, since the amount of CO_2 produced would be smaller than with complete combustion. If the CO and HC concentrations are also measured, the emission index could be corrected for this (Bishop *et al.*, 1996c):

$$[NO] = \frac{NO\,(ppm\text{-}m)}{CO_2\,(ppm\text{-}m) + CO(ppm\text{-}m) + 3*HC(ppm\text{-}m)} * [CO_2]_s$$

where it is assumed that the exhaust hydrocarbons have 3 carbon atoms on average (Bishop *et al.*, 1996c).

2.2.3. Spectroscopic Techniques Used for On-Road Remote Sensing

1) Non-Dispersive Infrared

Non dispersive infrared (NDIR) instruments to measure CO emissions were pioneered at the University of Denver in 1987 (Bishop *et al.*, 1989), and also demonstrated by General Motors (Stephens and Cadle, 1991). These two groups have also developed NDIR instruments which measure a portion of the VOC emissions (Cadle

and Stephens, 1994; Guenther *et al.*, 1995). SBRC developed an NDIR instrument to measure NO emissions (Jack *et al.*, 1995).

The University of Denver instrument is commercialized by Remote Sensing Technologies (RSTi). The GM instrument was commercialized and further developed by the "Smog Dog" group of the Hughes Santa Barbara Research Center (SBRC) (Jack *et al.*, 1995). Smog Dog was acquired by RSTi in 1997, making RSTi the only commercial supplier of remote sensing instrumentation.

The basic design of the NDIR remote sensing approach is shown in Figure 2-7 (Cadle *et al.*, 1994). The light from a broadband infrared source is sent across the exhaust of a passing vehicle and is then separated according to frequency by a series of beam splitters. The reflected beam of each beam splitter traverses an bandpass optical filter and the reaches an optical detector.
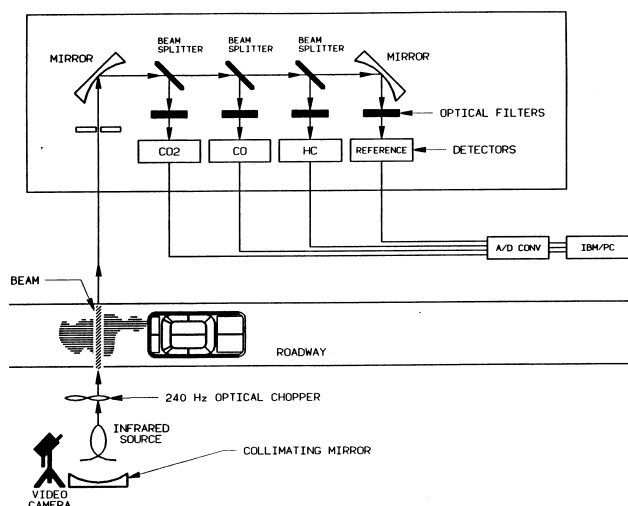
Figure 2-7: Schematic of the GM NDIR remote sensing instrument (Cadle *et al.*, 1994)

The shape of the optical filter used for the hydrocarbon channel is shown in the top part of Figure 2-8 (Guenther *et al.*, 1991). The middle and bottom graphs show the absorption in the same frequency region due to propane. Since only light that can traverse the optical filter reaches the detector, absorption due to propane will cause a decrease on the transmitted light. The instrument is then calibrated with mixtures containing different amounts of propane and the calibration curve is used in the remote sensing measurements.

The main problem with this approach are interferences from other absorbing gases. The filters used are very broad compared with individual absorption features (e.g. more than 100 cm^{-1} in the one shown in Figure 2-8, compared with 0.25 cm^{-1} for a typical absorption line at atmospheric pressure). Thus the likelihood of other species absorbing in the same region as the filter is very large. For example the graph in the bottom of Figure 2-8 shows absorption due to water vapor in the exhaust in the same region used for hydrocarbon measurement. A possible solution is to try to measure the interfering species at a different frequency and correct the measurement, e.g. the Hughes NO instrument measures NO absorption in the infrared and corrects the measurement for water vapor interferences (Jack *et al.*, 1995).
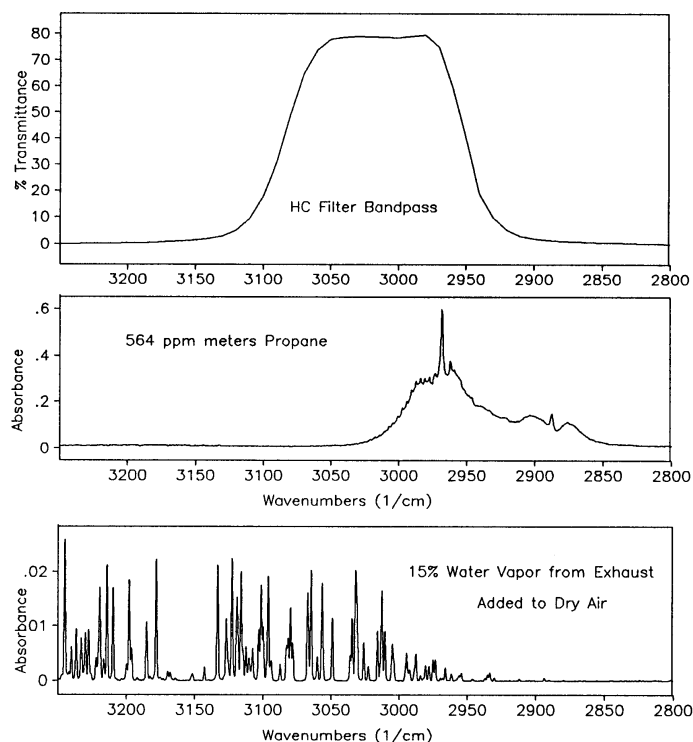
Figure 2-8: NDIR bandpass filter and absorption bands of propane and water (Guenther *et al.*, 1991)

2) Ultraviolet Absorption

UV absorption instruments have been developed to overcome the problem with water vapor interference in the NDIR measurement of NO. The University of Denver group developed an instrument based on this principle (Zhang *et al.*, 1996a) for which it claimed a precision (1σ) of about 300 ppm NO in the exhaust of the vehicle. Sjödin *et al.*

(1996) attempted the development of a similar instrument based on UV DOAS which claimed a similar precision.

Since most vehicles are thought to emit less than 300 ppm NO, a more sensitive instrument was needed. The University of Denver group has developed a new ultraviolet-based remote sensor with a standard deviation of about 20 ppm NO in the exhaust under parking lot conditions (Popp *et al.*, 1997). On-road data obtained with this instrument have recently been presented (Popp *et al.*, 1998a).

3) Near Infrared Tunable Diode Lasers

Schiff *et al.* (1994a) reported on the development of a near-infrared tunable diode laser system for remote sensing.[8] These researchers sensed the CO/CO_2 ratios of a vehicle running on a dynamometer, and also measured H_2O and CH_4 emissions. The detection limits reported are on the range of 5-50 ppm-m (depending on the species).

Since a TILDAS column density detection limit of 0.1 ppm (10 Hz) for NO translates into a sensitivity of about 3 ppm of the exhaust when measuring real cars, I estimate that NIR TDLs could achieve sensitivities on the order of 150-1500 ppm of the vehicle exhaust, which is comparable to what has been achieved using NDIR and UV techniques.[9,10] An attempt to extend this approach to NO emissions was impeded by the lack of an adequate diode laser (Slott, 1997).

4) Gas-Filter Correlation

A gas-filter correlation (GFCR) instrument is in the early stages of development (Sachse, 1998). The GFCR technique has been developed for satellite-based remote sensing of atmospheric gases. This instrument will have the capability of measuring CO and NO (using GFCR) and HCs (using the standard NDIR technique). The potential sensitivity of the system is estimated at 10 ppm of the exhaust for CO and NO.

---

[8] This instrument is described in more detail in a later publication (Schiff *et al.*, 1996).

[9] This estimate assumes that the signal-to-noise ratio would be the same for the NIR TDL measurements as for the TILDAS measurements. Some differences may exist owing to differences in laser diode power output, detector response and noise, interferences, etc.

[10] Near infrared diode lasers at longer wavelengths have become available since the time of this study, allowing the use of stronger absorption transitions for some molecules (Allen, 1998). Thus the presently achievable sensitivities using this technique may be lower than these numbers.

2.2.4. Applications of Remote Sensing

The ability to measure instantaneous on-road vehicle emissions by remote sensing has many potential applications. Dozens of studies have been carried out to evaluate and implement some of them. The most important applications proposed or accomplished to date are:

- High emitter detection for immediate pullover or direction to inspection and maintenance programs (Bishop *et al.*, 1993; Bishop *et al.*, 1996c; Sjödin *et al.*, 1996; Sorbo *et al.*, 1997)

- Low emitter detection for exemption from inspection and maintenance programs (Sjödin *et al.*, 1996; Baker *et al.*, 1997; Kishan *et al.*, 1998; St. Denis, 1998; Wenzel and Sawyer, 1998a)

- Pre-screening of vehicles in inspection and maintenance facilities (Petherick, 1996; Petherick, 1997).

- Public information systems that display the emission status of cars as they drive by (Bishop *et al.*, 1996a).

- Measurements at toll booths to charge higher tolls for gross polluters (Bishop *et al.*, 1996c).

- Measurements of employees for employer-paid repairs (Bishop *et al.*, 1996c).

- Fleet Characterization (Zhang *et al.*, 1993; Stedman *et al.*, 1994; Zhang *et al.*, 1994; Zhang *et al.*, 1995; Zhang *et al.*, 1996a; Bishop *et al.*, 1997; Stedman *et al.*, 1997a; Popp *et al.*, 1998a)

- Compilation of emissions inventories (Singer *et al.*, 1996; Dreher *et al.*, 1998).

- Evaluation of inspection and maintenance programs or the impact or other emission reduction programs such as reformulated fuels (Sjödin *et al.*, 1997a; Stedman *et al.*, 1997b; Stedman *et al.*, 1998)

- Evaluation of the rates of deterioration and technological improvement of the emission control systems (Slott, 1996).

- Detection of specific vehicle models with poor emission performance (Sjödin *et al.*, 1996; Wenzel and Ross, 1996; Wenzel and Ross, 1997; Wenzel *et al.*, 1998b).

- Comparing the emissions of vehicles with different technologies and/or fuels (Sjödin *et al.*, 1996; Riveros *et al.*, 1998; Stedman *et al.*, 1997a; Mercer and McArragher, 1997).

2.3. Tunable Diode Lasers

2.3.1. Characteristics of Tunable Diode Lasers

TDLs are semiconductor chips of lead salts (PbS, PbSe, PbTe) and their mixed alloys with themselves and other materials (Schiff *et al.*, 1994b). These semiconductors form p-n junctions with small energy band gaps. When a forward biased current for 0.1 to 1 A is applied across the junction, a population inversion is produced. Electrons are pushed up to the conduction band from the valance band.   The electron-hole recombination causes the emission of light associated with the band gap energy, typically 3 - 30 μm. This process is illustrated in Figure 2-9.
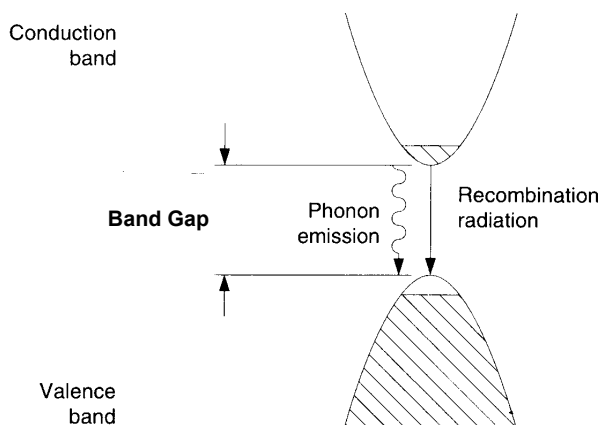
Figure 2-9: Electron-Hole Combination Process Resulting in Laser Emission (Silfvast, 1996)

Diode lasers usually operate below 120 K,[11] and they are generally housed in liquid nitrogen or liquid helium dewars. Closed-loop cryostat are also available that achieve temperatures down to 12 K.   The laser frequency is tuned by varying the temperature and the electrical current through the diode. In practice, the temperature is held constant with a feedback control system and the diode current is varied for fine frequency tuning.

The frequency of the emitted light increases as the temperature of the diode increases and/or the bias current passed through the diode increases. This does not happen in a continuous way, rather the diode emits light in a series of frequency

---

[11] Although a TDL used in this study operated as high as 155 K.

"modes," or frequency intervals where the diodes are continuously tunable. These modes are separated by "mode breaks", frequency intervals in which the diode does not emit any light. One of the biggest drawbacks of tunable diode lasers is the instability of modes. The frequency of the light emitted at a given temperature/current combination drifts with time. If the laser is warmed up to room temperature mode structures may change significantly, and some previously used absorption lines may no longer be within the lasing region. The presence of mode breaks and mode instability makes selecting and operating the tunable diode lasers a time consuming task.

2.3.2. Applications of TDLs to Atmospheric Measurements

Typical line widths of individual absorption lines at atmospheric pressure are on the order of 0.05 cm^{-1}. An adequate measurement of an individual line requires an spectral resolution of about 0.005 cm^{-1} (10 points per line). Non-dispersive Infrared (NDIR) and Fourier Transform Infrared (FTIR) spectrometers use broad band light sources and are generally incapable of such resolution.

TDLs have line widths of the order of 0.001 cm^{-1} or smaller (Schiff *et al.*, 1994b) and are tunable in frequency. They can be used to scan over an individual absorption line, the main requirement being that the molecule should have an infrared line spectrum which is resolvable. This includes most molecules with up to 5 atoms and some larger molecules (Werle, 1998).

The application of tunable diode lasers to atmospheric measurements is known as TDL spectroscopy, Tunable Diode Laser Absorption Spectroscopy (TDLAS), and Tunable Infrared Laser Differential Absorption Spectroscopy (TILDAS). The first and third names are used indistinctly in this thesis.

Atmospheric trace gas measurements with tunable diode laser spectroscopy generally use reduced pressure sampling to take advantage of the much narrower absorption lines under these conditions. This technique is less frequently used in open path remote sensing applications (Kolb *et al.*, 1995) although the first applications of TDLs to atmospheric measurements were open path measurements of ambient CO in cities (Hinkley and Kelley, 1971; Ku *et al.*, 1975).

The TILDAS technique has been used to measure SO_2, NO_2, HNO_3, N_2O, and HBr in directly sampled automotive exhaust (Harris *et al.*, 1987; Carduner *et al.*, 1992;

Jobson *et al.*, 1994; Zahniser, 1998) and N_2O in sampled aircraft engine exhaust (Wiesen *et al.*, 1996). A TILDAS system has been used in this thesis to perform open path atmospheric pressure measurements of NO, NO_2, N_2O, CO, CO_2, exhaust opacity, and gas temperature in exhaust gases from on road vehicles. This system is described in Chapter 5.

Chapter 3. A New Definition of Specific Power and its Application to Emission Studies

In this chapter a new parameter termed "specific power" (SP) is presented. SP is the ratio of instantaneous vehicle power to vehicle mass. This parameter is very useful in the analysis of remote sensing data, chassis dynamometer data, and in emissions modeling for three main reasons: it can be calculated from roadside measurements, it captures most of the dependence of light-duty vehicle emissions on driving conditions, and it is directly specified in emissions certification cycles.

In this chapter it is shown that the dependence of CO, HC, and NO_x emissions on SP is better than on several other commonly used parameters, such as speed, acceleration, absolute power, or fuel rate. Modern U.S. vehicles are likely to operate under commanded enrichment when SP exceeds the maximum value on the Federal Test Procedure (~22 kW/Metric Ton). This may allow transient high emissions to be screened out during future remote sensing campaigns. It is also shown that using SP as the basic metric allows meaningful comparisons to be made between data from different remote sensing sites, dynamometer driving cycles, and emission models.

This chapter is organized as follows: section 3.1 presents the definition of specific power and introduces its advantages. Section 3.2 shows the usefulness of the parameter by analyzing second-by-second emissions data acquired from several vehicles tested on four different driving cycles. Sections 3.3 and 3.4 discuss the applications of this parameter to remote sensing and emissions modeling. Finally, section 3.5 summarizes the conclusions of this chapter.

3.1. A New Definition of Specific Power

3.1.1. Definition

Vehicle *Specific Power*[12] (SP) is defined here as the instantaneous power per unit mass of the vehicle.[13] The instantaneous power generated by the engine is used to overcome the rolling resistance and aerodynamic drag,[14] and to increase the kinetic and potential energies of the vehicle. It equals the product of speed and an equivalent acceleration, which includes the effects of roadway grade and rolling resistance, plus a term for aerodynamic drag which is proportional to the cube of the instantaneous speed:

$$\mathrm{Vehicle\,Specific\,Power} = \frac{\frac{d}{dt}(KE+PE) + F_{\mathrm{rolling}} \cdot v + F_{\mathrm{Aerodynamic}} \cdot v}{m} =$$

$$= \frac{\frac{d}{dt}(\frac{1}{2}m \cdot (1+\varepsilon_i) \cdot v^2 + mgh) + C_R mg \cdot v + \frac{1}{2}\rho_a C_D A(v+v_w)^2 \cdot v}{m} =$$

$$= v \cdot (a \cdot (1+\varepsilon_i) + g \cdot grade + g \cdot C_R) + \frac{1}{2}\rho_a \frac{C_D \cdot A}{m}(v+v_w)^2 \cdot v$$

where:

- m : vehicle mass
- v : vehicle speed
- a : vehicle acceleration
- ε_i : "Mass factor", which is the equivalent traslational mass of the rotating components (wheels, gears, shafts, etc.) of the powertrain. The suffix i indicates that ε_i is gear-dependent.[15]

---

[12] Not to be confused with "engine specific power," defined as the maximum power output of a reciprocating engine per unit piston area, which is a measure of how well an engine designer has used the available piston area (Heywood, 1988).

[13] This definition can be expanded to include the power dissipated by engine friction and power demand of accessories such as air conditioning. These have not been included in the present definition because their estimation from roadside measurements is much more difficult and uncertain. Also, engine friction is generally small compared to the range of values of Specific Power.

[14] The sum of aerodynamic and rolling resistance is called "road-load power" (Heywood, 1988).

[15] The term m*v*a*ε_i is called the "acceleration resistance" (Bauer, 1996). Typical values of ε_i for a manual transmission are 0.25 in 1st gear, 0.15 in 2nd gear, 0.10 in 3rd gear, 0.075 in 4th gear (Emmelman and

- h : altitude of the vehicle
- grade : vertical rise/slope length[16]
- g : acceleration of gravity (9.8 m/s^2)
- C_R : coefficient of rolling resistance (dimensionless)[17, 18]
- C_D : drag coefficient (dimensionless)
- A: frontal area of the vehicle
- ρ_a : ambient air density (1.207 kg/m^3 at 20 °C = 68 °F)[19]
- v_w : headwind into the vehicle

The units of Specific Power are those of power per unit mass. The metric (SI) fundamental unit is W/kg, which is the same as kW/Metric Ton.[20] The later unit is more physically meaningful for road vehicles and has been used throughout this chapter. Equivalently the units of speed * acceleration can be used (e.g. m/s * m/s^2 = m^2/s^3, which is the same as W/kg or kW/Metric Ton). To convert from either of the SI units to mph^2/s, the SI number must be multiplied by 5.006.

Using typical values for all parameters we arrive to the following expression (in metric units):

$$SP \ (kW/\,Metric\,Ton \ = \ W/kg \ = \ m^2/s^3\,) =$$

$$= v \cdot (1.1 \cdot a + 9.81 \cdot grade + 9.81 \cdot 0.0135) + \frac{1}{2} \cdot 1.207 \cdot 0.0005 \cdot (v + v_w)^2 \cdot v$$

$$= v \cdot (1.1 \cdot a + 9.81 \cdot grade\,(\%) + 0.132) + 3.02 \cdot 10^{-4} \cdot (v + v_w)^2 \cdot v$$

$$(with \ v \ and \ v_w \ in \ m/s \ and \ a \ in \ m/s^2)$$

Hucho, 1998). If the transmission is automatic, hysteresis effects may be important (Emmelman *et al.*, 1998).

[16] Rigorously sin(atan(grade)) should be used instead of grade, but the error of this approximation is small (less than 1% relative error for grades below 14%).

[17] The value of C_r depends on the road surface and tire type and pressure, with a small dependence on vehicle speed. Typical values range from 0.0085 to 0.016 (Bauer, 1996). A value of 0.0135 has been used here for all vehicles.

[18] Rigorously cos(atan(grade)) should be used instead of grade, but the error of this approximation is small (less than 1% relative error for grades below 11%).

[19] The ideal gas law (Pv/T=P/(ρT) = constant) can be used to correct to other temperature and pressure conditions. The formula is $\rho = \rho_0*(P/P_0)*(T_0/T) = 1.207*(P/101.33)*(293.16/T)$, with ρ in kg/m3, P in kiloPascals (kPa), and T in Kelvin (K). This correction may be important, e.g. if the measurements are performed at -10°C (-14°F) and 1 atmosphere the air density will be 10% higher than at 20°C.

[20] One kW/Metric Ton equals 6.08 ·10^{-4} hp/lb.

And in units of mph^2/s:

$$SP \ (\text{mph}^2/\text{s}) =$$

$$v \cdot (1.1 \cdot a + 21.9 \cdot \text{grade}(\%) + 0.296) + 1.35 \cdot 10^{-4} \cdot (v + v_w)^2 \cdot v$$

$$(\text{with } v \text{ and } v_w \text{ in mph and } a \text{ in mph/s})$$

Note that these expressions are based on average values of the rolling resistance coefficient, the aerodynamic drag term coefficient (C_D*A/m), and the value of air density at 20°C (68°F). Better estimates of the actual values of these parameters should be used whenever possible.

This new definition of Specific Power is a generalization of the "Positive Kinetic Energy" proposed by Watson *et al*. (1983) and the "Specific Power" used by EPA and others, defined as 2*speed*acceleration (U.S. EPA, 1993a; Webster *et al.*, 1996; An and Scora, 1997; Carlson *et al.*, 1997). A recent study proposed a parameter termed "Relative Engine Load"[21] to characterize the power demand on a vehicle based on speed, acceleration, and grade measurements (McClintock, 1998). This parameter is based on an empirical approximation to the road-load power in IM240 tests and is numerically close to the new definition of Specific Power proposed when average values are used for the rolling resistance and aerodynamic coefficients.

The Specific Power of interest for remote sensing is that of the instant in which the emissions which are leaving the tailpipe were generated in the engine. The distance traveled by the vehicle while the exhaust gases travel from the engine to the end of the tailpipe has been estimated (section 4.2.3) based on second-by-second driving-cycle data to be between 0.1 and 25 meters for positive Specific Powers.[22]

The first three terms of the new Specific Power definition can be readily calculated from measurements of vehicle speed and acceleration. The fourth term, the load due to aerodynamic drag, depends on the factor (C_D*A/m) which is different for each specific vehicle model and payload.[23] An estimate of the range of values of this

---

[21] " Relative Engine Load" $(\text{mph}^2/\text{s}) = v \cdot (a + 21.82 \cdot \text{grade}(\%) + 0.065) + 0.014 \cdot v^2$ (v in mph and a in mph/s)

[22] During the remote sensing measurements shown in Figure 3-31, Figure 3-32, Chapter 6, and Chapter 8, speed and acceleration were measured between 11 and 1 meters before the location of the remote sensor based on an approximate calculation of this effect.

[23] The value of that ratio for individual models could be obtained in principle from EPA certification data, because each manufacturer must supply information on the "road load power" requirements of the vehicle

parameter has been calculated from the data for six vehicle classes reported by Emmelman and Hucho (Emmelman *et al.*, 1998). These estimates are shown in Figure 3-1. The 5 European passenger car classes are ordered from smaller to larger vehicle size, class A being the smallest.[24]

The figure shows that the average value of the parameter C_DA/m varies by only about a factor of two between the different vehicle class/payload combinations. If more detailed information is not available, an average value for all vehicles can be used with ±30% error for these classes and a given payload.
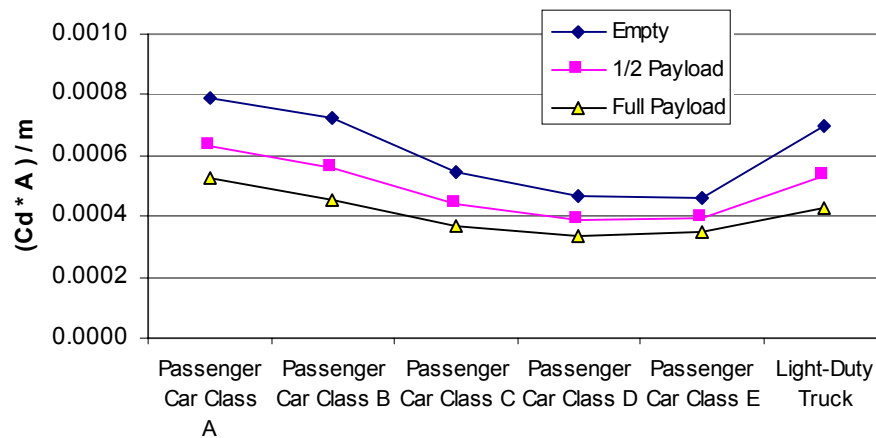
Figure 3-1: Values of the parameter (C_D*A/m) for several passenger car classes and for light duty trucks

3.1.2. Illustration of the Values of Specific Power for a Driving Cycle

Each one of the terms of the Specific Power equation have been calculated for each second[25] of the US06 emissions certification cycle to compare their relative

---

prior to certification testing. This information is needed to determine the settings of the chassis dynamometer.

[24] Typical vehicles of each passenger car class:
- Class A: Ford Fiesta; VW Polo; Opel Corsa.
- Class B: Ford Escort; VW Golf (Rabbit); Open Kadett.
- Class C: Audi 80; VW Passat; Open Vectra (Cavalier).
- Class D: BMW 520i; Mercedes 200E; Opel Omega.
- Class E: BMW 730i; Mercedes 300E; Opel Senator 3.0.

[25] The driving cycle is specified as a trace of speed vs. time with 1-second time resolution, so a finer calculation is not possible.

importance. The speed vs. time trace of this cycle, and the contribution of each term in the Specific Power equation are shown in Figure 3-2 and Figure 3-3 respectively.[26, 27] The three terms are of comparable magnitude. The speed*acceleration term reaches the highest values for strong accelerations and decelerations and the aerodynamic drag term is dominant at high speeds.
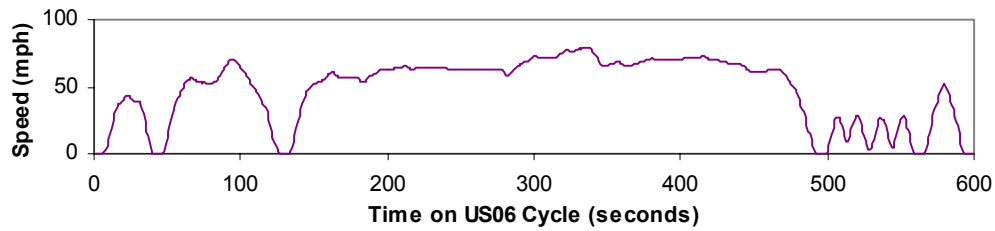
Figure 3-2: Speed vs. time trace for the US06 dynamometer test cycle
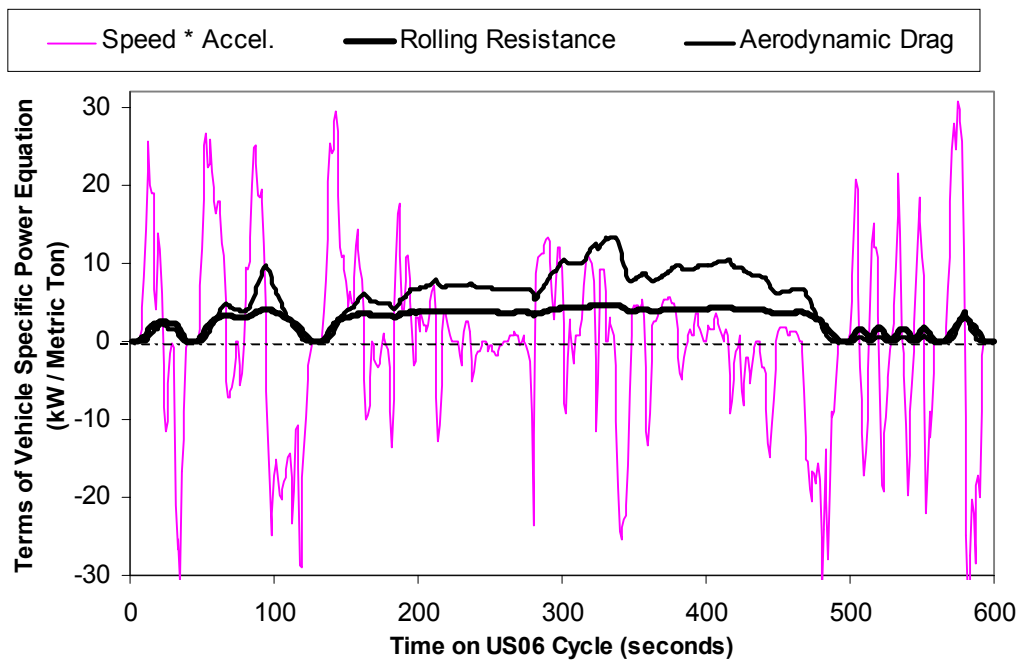
Figure 3-3: Values of the three components of the Specific Power vs. time during the US06 cycle

---

[26] Values of 0.0005 for the term (C_D*A/m) and 0.0135 for C_r were used in this calculation as a compromise value within the range of values for different vehicles.

[27] The effect of grade is not represented in the cycle, so the second term of the Specific Power equation is always equal to 0 here.

3.1.3. Distribution of Specific Power in Driving Cycles and Remote Sensing Studies

Vehicle emissions have a strong dependence on Specific Power, as will be shown in section 3.2. Therefore the distribution of Specific Powers allows the comparison of emissions data acquired in different ways, such as different driving cycles and/or remote sensing sites. A procedure to carry out this comparison is described in sections 3.3.6 and 3.4.2.

A comparison of the Specific Power distributions in three driving cycles, FTP, IM240, and US06[28, 29] and two remote sensing campaigns is shown in Figure 3-4. The FTP and IM240 driving cycles comprise more limited Specific Powers, with a maximum around 22 kW/Metric Ton for both cycles. On the other hand the US06 cycle, which is designed to represent emissions in aggressive driving, reaches much higher values (up to 53 kW/Metric Ton).
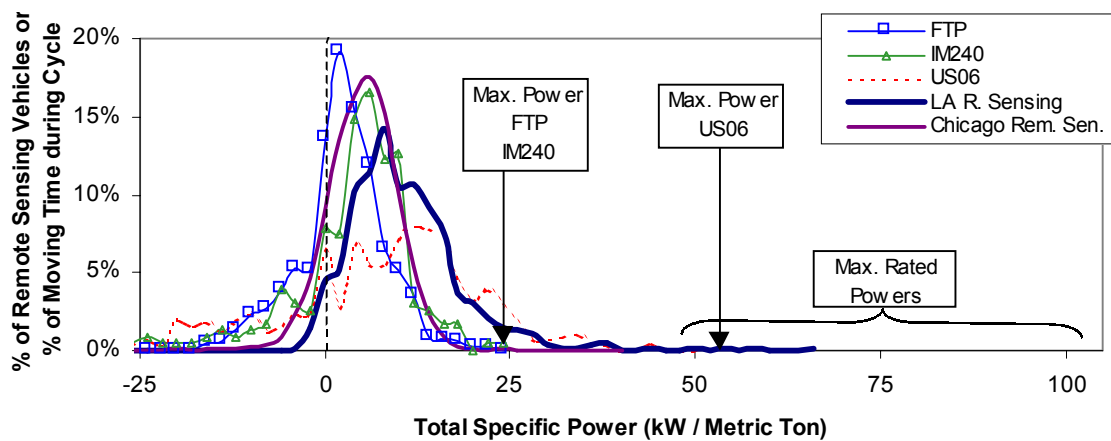
Figure 3-4: Distributions of Specific Powers in 3 driving cycles and 2 remote sensing studies, and maximum rated Specific Powers of current production vehicles

---

[28] The FTP cycle is the driving cycle for emissions certification of new vehicles in the U.S. The US06 cycle will be used for certification starting with model year 2000 (U.S. EPA, 1996a). The IM240 cycle is a 6-minute cycle designed by EPA and used by the U.S. states with enhanced inspection and maintenance programs.

[29] The seconds in which the vehicle is not moving have been excluded from the distributions.
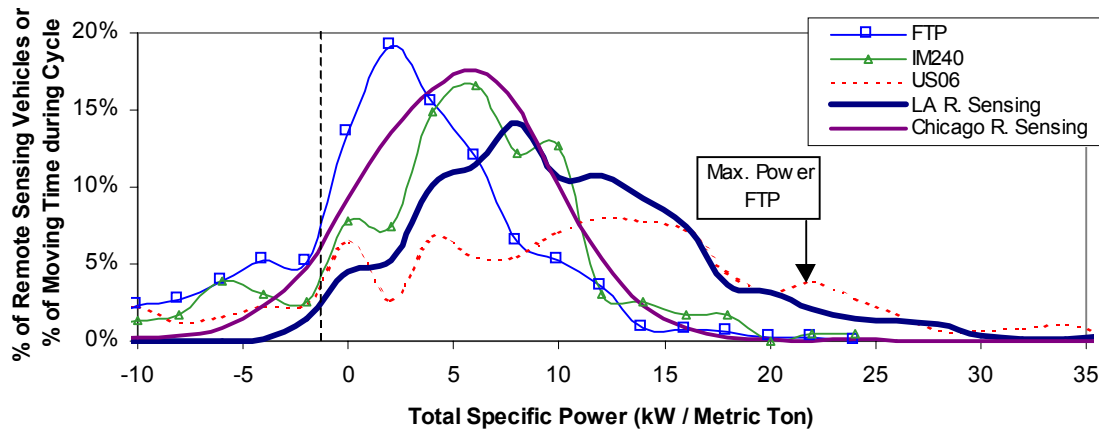
Figure 3-5: Detail of the distributions of Specific Powers in 3 driving cycles and 2 remote sensing studies

The two remote sensing studies shown in the figure have very different Specific Power distributions, due to the different characteristics of the remote sensing sites. The study carried out in Los Angeles (Chapter 6) contains very high Specific Powers, comparable to those on the US06 cycle. The measurements carried out in Chicago (Popp *et al.*, 1998a) had generally much lower Specific Powers, with a very similar distribution to that of the IM240 cycle. The impact of this difference on emissions is discussed in section 3.3.6.

Another interesting difference in Specific Power is present between bags 1 and 3 of the FTP (cold and hot start) and bag 2 (warm running), as shown in Figure 3-6. Bags 1 and 3 include significantly higher powers than bag 2.
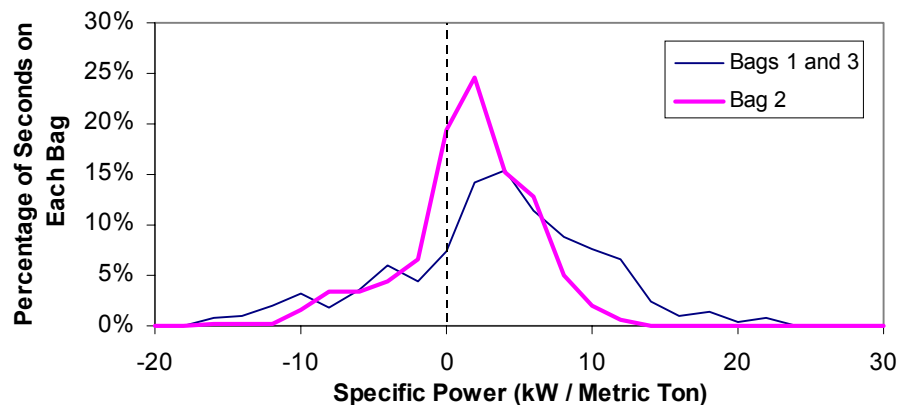
Figure 3-6: Distribution of Specific Powers in each bag of the FTP

3.1.4. Advantages of Specific Power for Emissions Studies

The main advantages of using Specific Power as an independent variable for studying the hot stabilized[30] emissions of passenger cars and light-duty trucks are three: specific power is directly measurable, it captures most of the dependence of emissions on engine operating parameters, and certification driving cycles are specified in terms of specific power.

1) <u>Specific Power is directly measurable</u>

A very important advantage of Specific Power with respect to other characterizations of the engine load is that no data or assumptions about any parameters which cannot be measured from the roadside are needed for the calculation of SP to an acceptable degree of accuracy. This is in contrast with many emissions studies and models which use non roadside-measurable parameters, such as engine speed, absolute power, fraction of available power, maximum vehicle power, throttle position, fuel rate, mass air flow, and manifold vacuum (see section 3.4.3).

2) <u>Specific Power captures an important part of the dependence of emissions on engine operating parameters</u>

Emissions from a given warmed-up gasoline-powered car or light-duty truck depend on several operating parameters, but mainly on air-to-fuel ratio, engine power, and engine speed (Heywood, 1988; Barth and Norbeck, 1997). Although Specific Power does not capture the effects of all of these parameters, it does capture a significant part:

- Specific Power is proportional to engine power, the constant of proportionality being the inverse of the mass of the vehicle.

- In modern properly operating[31] closed-loop controlled vehicles, the air-to-fuel ratio (A/F) is related to the value of the Specific Power. A/F is maintained around stoichiometric conditions by a closed-loop control system during normal operation, to maximize the three-way catalyst efficiency for all pollutants (Kummer, 1980). The air-to-fuel ratio may be rich at high values of Specific Power due to "commanded

---

[30] If the vehicle has been recently started and its catalyst and oxygen sensor are not fully warmed up the emissions depend very strongly on catalyst temperature (Kummer, 1980; Koltsakis and Stamatelos, 1997). These conditions are explicitly excluded here.

[31] Modern vehicles with problems in the air-to-fuel control system may revert to a fuel-rich "limp operating mode," leading to excess CO and HC emissions.

enrichment" events (see section 3.3) and lean for negative values due to "fuel cut-off" events (Haskew *et al.*, 1994; An *et al.*, 1997).

▪ The new definition of Specific Power given in section 3.1 includes the effects of roadway grades, rolling resistance, and aerodynamic resistance that earlier definitions of specific power omitted (U.S. EPA, 1993a; Webster *et al.*, 1996; Carlson *et al.*, 1997). EPA recently estimated that about 45% of the vehicle-miles traveled in the U.S. take place in grades larger than 1%[32, 33] (U.S. EPA, 1993a), and driving on uphill grades can increase emissions by a factor of two (Cicero-Fernandez *et al.*, 1995; Cicero-Fernandez *et al.*, 1996). Despite these facts, neither the current EPA emissions model, (MOBILE5), nor the version currently under development (MOBILE6), nor California's emission model (EMFAC) include the effect of roadway grade (Beardsley, 1998; Long, 1998).

Effects with an influence on emissions that are not captured by the new definition of Specific Power are:

▪ Engine speed. Although some attempts to model the engine speed of a passing vehicle have been pursued (Barth *et al.*, 1998), there is no accurate way to estimate this parameter due to the many different gear systems used. Fortunately the dependence of emissions on engine speed at a given power is limited (Heywood, 1988; De Soete, 1989).

▪ Engine friction losses. These losses could be modeled (Barth *et al.*, 1997)[34] but they are generally small compared to the range of specific powers of interest.

▪ Transmission losses. The efficiency of automatic transmissions can vary significantly. Most of this variability is associated with torque converter slip. The definition of SP given here ignores this loss and makes no distinction between automatic and manual transmissions. The overall effect of the transmission slip on the SP is expected to be

---

[32] Half on positive grade and half on negative grade. A grade of ±1% at 50 mph contributes ±2.2 kW/Metric Ton to the Specific Power, or 1/10 of the maximum FTP SP value.

[33] Data from Germany indicate a similar prevalence of roadway grades (Emmelman *et al.*, 1998).

[34] The model proposed by Barth et al. (Barth *et al.*, 1997) is $P_{friction} = \phi * K * N * V$, where ϕ is the fuel to air ratio, k is the engine friction factor, N is the engine speed, and V is the engine displacement. Thus the model of the friction losses depends on three non-measurable parameters (ϕ could be determined from the emission meausrements.

small except when a vehicle is accelerating from low speed and slip is high (Koplow, 1998).

- Power consumption of accessories such as air conditioning. Air conditioning in particular can impose an important extra load on the engine, which translates into an increase of emissions.[35] The fraction of the fleet equipped with air conditioning reaches more than 90% for model year 1996 (Koupal, 1998). For these reasons, models of the load imposed by air conditioning as a function of environmental conditions (temperature, humidity, solar load) are being developed (Koupal, 1998) and could be added to the calculation of Specific Power.[36]

- Payload weight. The maximum payload of a passenger car or light-duty truck varies from about 30% to 60% of the vehicle's weight (Emmelman *et al.*, 1998). This means that two vehicles of the same model with the same Specific Power could have such differences in absolute power depending on how many passengers and load a given vehicle is carrying.[37] An analysis of this effect is presented in section 3.2.6.

It is possible in principle to determine the mass of a vehicle during remote sensing with a "weight-in-motion" measurement system (U.S. DOT, 1997b). Then engine power could be calculated by multiplying Specific Power by the measured mass. However, it is not clear that knowing the absolute power instead of Specific Power will provide better information for remote sensing and emissions models (see sections 3.2.5 and 3.2.6), so the cost of such a system may not be justified.[38]

---

[35] For this reason the emissions under A/C use have recently been regulated. Starting with model year 2000, new cars and light-duty trucks will be tested on the SC03 cycle, which is designed to represent the effects of air conditioning (U.S. EPA, 1996a).

[36] Prof. Stedman suggested a strategy to determine which vehicles had air conditioners on in the summer: a second video camera which records whether the driver's side window is up. On hot days this could be a good predictor of whether the air conditioner is on (Slott, 1997).

[37] In our remote sensing study (Chapter 6) we measured mostly commuter vehicles and observed that a very large fraction only had one or two occupants. A possible strategy to screening out part of the effects of extra weight in remote sensing studies would be to use a second video camera and reject the measurements done on vehicles with high occupancy.

[38] The cost of a weight-in motion system for heavy-duty trucks was calculated to be about $20,000 per site for a state implementing 100 sites (U.S. DOT, 1997b). This cost will be certainly higher for a single portable system adapted to passenger cars and light-duty trucks.

▪ Large increases in aerodynamic drag due to roof racks or for high drag vehicles such as convertibles.[39] These will only be important at high speeds due to the dependence of the aerodynamic power dissipation term on the cube of the vehicle speed.[40]

    ▪ Effects of cross-winds on the aerodynamic drag coefficient. C_D generally increases when the effective wind is not in the same direction of vehicle travel (Barnard, 1996; SAE, 1996). This increase can reach 14% (20%) for cars (vans) (Barnard, 1996).[41]

    ▪ History effects over several seconds on the engine and the catalyst (An *et al.*, 1997; Nam and Ross, 1998). These appear because the engine-catalyst system can have some "memory" of past events, e.g. extra fuel may be left on the intake port from a recent commanded enrichment event, or the oxygen storage in the catalyst may have changed due to recent rich or lean operation.

3) <u>Emissions certification test cycles specify Specific Power directly</u>

A key fact that makes Specific Power very useful for emissions studies is that the driving cycles that are used for emissions testing and certification of passenger cars and light-duty trucks specify Specific Power vs. time directly. This due to the fact that all chassis dynamometer driving cycles used for emissions certification testing in the US, Europe, and Japan are defined as a speed vs. time trace (Bauer, 1996; U.S. EPA, 1996a). Acceleration is implicitly specified as well, since it is just the derivative of the speed vs. time curve. Since driving cycles do not include any simulation of roadway grade effects, the equation in section 3.1 implies that Specific Power is defined at each second for a given vehicle.[42, 43]

There is evidence that vehicle emission control strategies are optimized for the test cycles. Principal evidence is the threshold for commanded enrichment incorporated

---

[39] Typical drag coefficients for convertibles are on the range 0.5-0.7, as compared to 0.25-0.4 for normal cars (Bauer, 1996).

[40] Experimental values for C_D (Emmelman *et al.*, 1998) could be used in these cases.

[41] This increase reaches 60% for articulated heavy-duty trucks (Barnard, 1996).

[42] Chassis dynamometer cycles match the load encountered a vehicle on the road for a given speed and acceleration with simulated vehicle-specific loads for aerodynamic and rolling resistance and vehicle inertia (Haskew *et al.*, 1994).

[43] However significant differences in Specific Power can exist within the acceptable tolerances of the driving cycle, leading to significant differences in emissions (Webster *et al.*, 1996).

into the control strategies of vehicles, which starts to occur above the maximum Specific Power of the FTP certification cycle for vehicles with very different maximum rated Specific Powers (see sections 3.2.4 and 3.3.4). Another piece of evidence is the recent settlement in which seven heavy duty diesel engine manufacturers agreed to a penalty exceeding $1 billion for designing their emission control systems to pass the regulatory test for NO_x while not, according to the EPA, sufficiently reducing on highway emissions (U.S. EPA, 1998b).

In conclusion: Specific Power is directly measurable and is a good predictor of vehicle emissions. This predictive ability is demonstrated in section 3.2 by analyzing second-by-second data taken on test vehicles during chassis dynamometer testing. However, instantaneous vehicle emissions are not just a "state function" of Specific Power. Rather instantaneous Specific Power should be used as the main variable representing engine load in emission studies, although the history or statistics of Specific Power, or other additional input variables may be needed to properly describe or model all situations.

3.2. Analysis of Second-by-Second Emissions Data vs. Specific Power

3.2.1. Second-by-Second Emissions Data

Second-by-second emissions data from 68 vehicles of model years 1991-1996 recently tested on several driving cycles are publicly available (Liberty *et al.*, 1997).[44] These data include one second averages of vehicle speed, fuel economy, engine-out and tailpipe CO, HC, and NO_x emissions, catalyst and exhaust temperature, and engine speed. Very high power demands are included because the tests were designed to help quantify the emissions of current vehicles under aggressive driving conditions.

The analysis presented in the following sections is based on the use of these second-by-second data.[45, 46] The main objective of this analysis is to show that emissions are closely related to Specific Power, and that this relationship is stronger than that of other commonly used predictive parameters for vehicle emissions.

3.2.2. Variations of the Emissions Results of Different Driving Cycles vs. Specific Power

The relationship between the second-by-second CO, HC, and NO_x engine-out (uncatalyzed), and tailpipe (catalyzed) emissions and Specific Power for a recent production vehicle tested on a dynamometer driving cycle are shown in Figure 3-7. Specific Power was calculated with the equation given in section 3.1 from the one second average speed and a finite difference approximation of the acceleration. Additional graphs showing these same emissions vs. SP for two repetitions of four different driving cycles are included in Appendix B for reference.

---

[44] These emissions data were acquired as part of an EPA-industry effort to design the new regulations to limit emissions that occurred in driving modes not represented on the Federal Test Procedure driving cycle (FTP). These studies resulted in a redesign of the U.S. emission standards (U.S. EPA, 1996a), with two new driving cycles being required to limit emissions under aggressive driving (US06 cycle, shown in Figure 3-2) and with air conditioner use.

[45] A value of 0.0135 for C_r and 0.0005 for $(C_D*A)/m$ has been used for all vehicles in this section.

[46] An important limitation of this data set is the imprecision calculation of acceleration. Acceleration has been calculated as a centered finite difference derivative of speed. Using this procedure with 1 Hz data may "smooth out" significant changes in acceleration which happen on time scales shorter than 1 second. Driving cycle data acquired at 10 Hz instead of 1 Hz would be much more adequate for the purposes of this study. Unfortunately, and although the data in from SFTP program analyzed here were indeed acquired at 10 Hz (Haskew *et al.*, 1994), only the 1 Hz averaged data are available (Haskew, 1998). Two automobile manufacturers were contacted but were also unable to provide a data set of this kind taken at 10 Hz.

The dependence of second-by-second emissions, both engine-out and tailpipe, on instantaneous Specific Power is quite clear for this vehicle. Similar results were observed in 10 other vehicles studied in the same manner, with some differences of detail. The interpretation of the trends observed in these graphs are discussed below.
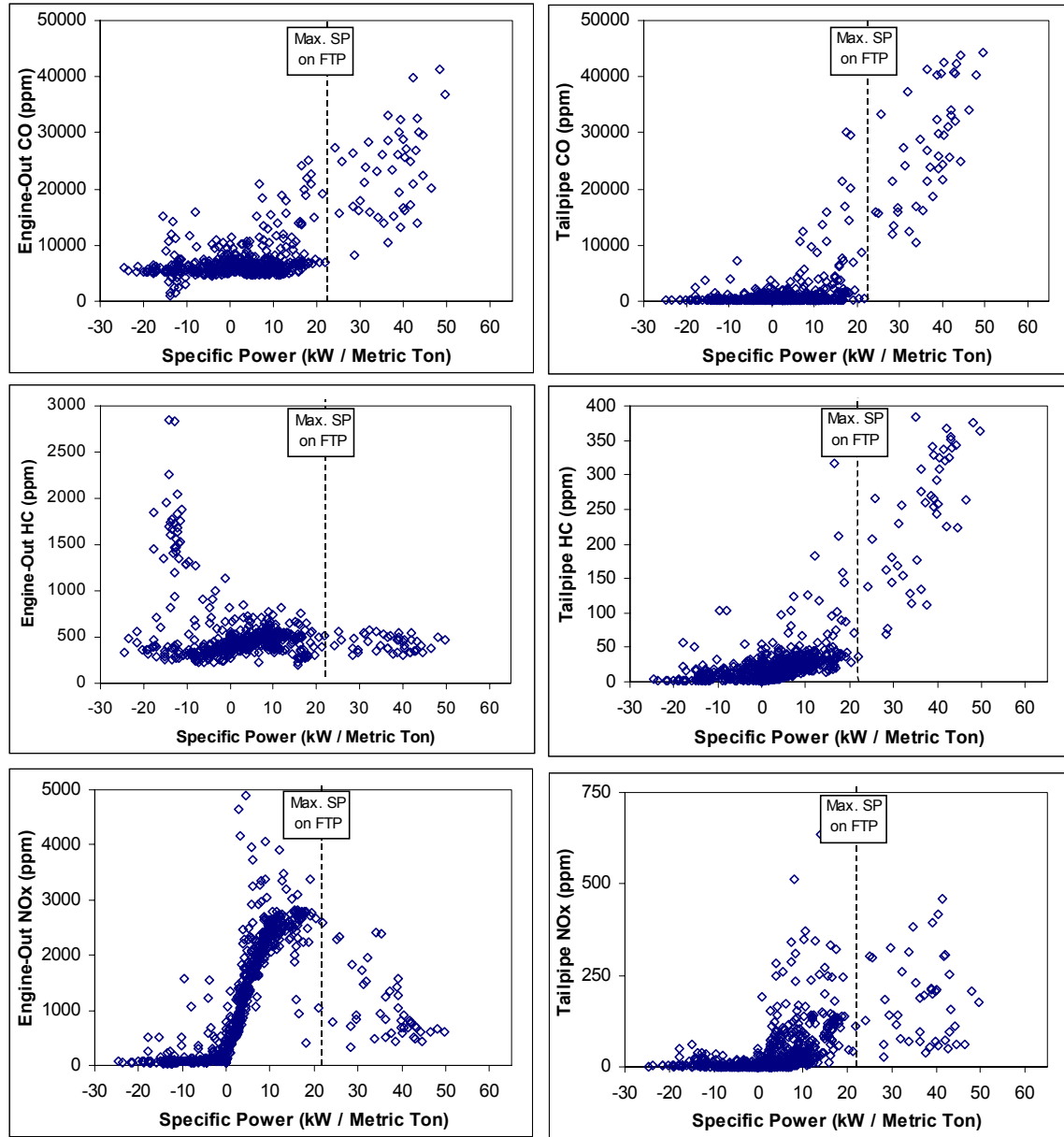
Figure 3-7: Second-by-second engine-out (left) and tailpipe (right) CO, HC, and NO$_x$ emissions vs. Specific Power for a 1994 Jeep Cherokee tested on the HL07 driving cycle

In order to facilitate the comparison of the different cycles, the emission results have been averaged for Specific Power bins for each driving cycle. The extent of the

scatter at each SP level can be observed in Figure 3-7 for one driving cycle and in Appendix B for all the driving cycles studied. Note that some of the differences in Appendix B between the results of the different cycles may be due to the low number of data points at a given SP or to the imprecision of the finite difference approximation to the acceleration from one second resolution speed data.

The total tailpipe carbon emissions (which are directly proportional to fuel consumption) vs. Specific Power for the same vehicle tested on four different driving cycles are shown in Figure 3-8. There is a strong relationship between fuel consumption and Specific Power, which is very similar for all of the driving cycles.
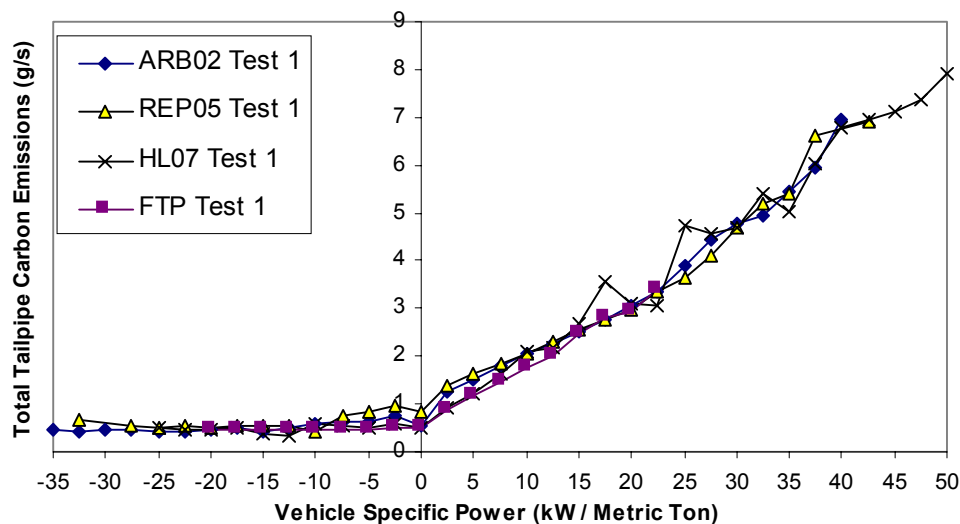
Figure 3-8: Total carbon tailpipe emissions binned by Specific Power ranges for a 1994 Jeep Cherokee for 4 driving cycles

The engine-out NO_x, CO, and HC emissions are shown in Figure 3-13, Figure 3-9, and Figure 3-11 respectively. Tailpipe NO_x, CO and HC emissions are shown in Figure 3-14, Figure 3-10, and Figure 3-12 respectively.[47]

The main features of these graphs are:

---

[47] These figures show the emissions in terms of concentration, which can easily be converted to grams per gallon of fuel (see Appendix A). The graphs of emission rates (grams/sec) vs. Specific Power show similar trends (not shown). Emissions in terms of concentration have been chosen are much less variable than emissions in grams/mile as driving conditions change (see section 4.5), and most likely future emissions models and studies will take advantage of this fact. They are also what remote sensing is able to measure, while g/mile emission require assumptions about fuel economy.

▪ Engine-out CO emissions stay at a value of about 0.6% for Specific Powers below the maximum FTP SP (~22 kW/Metric Ton). This levels are typical of stoichiometric combustion conditions (Heywood, 1988). Much larger CO emissions appear beyond the maximum FTP Specific Powers most likely due to the use of commanded enrichment.

▪ Engine-out HC emissions stay almost constant at about 500 ppm in all the cases presented here for all positive Specific Powers and driving cycles. These emissions do not increase appreciably during commanded enrichment situations. On the other hand, HC emissions increase for very negative SP in some cycles, during rapid or prolonged decelerations.[48]

▪ "Fuel cut-off" is a commonly used engine management strategy during decelerations to reduce HC emissions. Consequently, the fuel left on the engine manifold forms lean mixtures in the engine with poor combustion and high HC emissions (An *et al.*, 1997). "Manifold flash" happens when the throttle is suddenly closed and the liquid fuel present on the intake port vaporizes due to the drop in manifold pressure (Haskew *et al.*, 1994).[49]

▪ Engine-out NO_x emissions are low for negative Specific Powers due to the lower combustion temperatures, and increase rapidly with Specific Power up to about 2500 ppm.[50] NO_x concentrations decrease at Specific Powers larger than the maximum values on the FTP, due to commanded enrichment.

▪ Tailpipe emissions are also similarly clustered for the different driving cycles, with somewhat larger differences for NO_x emissions. Note that tailpipe HC emissions increase appreciably under commanded enrichment, even though engine-out HC

---

[48] An and Scora (An *et al.*, 1997) found a threshold on the rate of change of specific power (defined as 2*speed*acceleration) above which high HC emissions did not occur during rapid load reduction event in 15 test vehicles. This threshold is –50 mph^2/sec^2, or –10 kW/Metric Ton/second in metric units. It may be difficult to measure this parameter in remote sensing since it involves the derivative of the acceleration. These researchers also estimated that these emissions accounted for 25%-30% of the total HC on the MEC01 and US06 cycles.

[49] This discussion focuses on modern port fuel-injected vehicles. Earlier fuel delivery technologies such as throttle-body fuel injection or carburetors would produce higher HC emissions since there is more room for fuel accumulation due to the longer distance from the fuel introduction point to the engine cylinders, which leaves more room for fuel accumulation.

[50] This particular vehicle was not equipped with an Exhaust Gas Recirculation (EGR) system to reduce engine-out NOx emissions.

emissions did not. This is due to the loss of catalyst efficiency for HC under rich conditions.

The main purpose of these comparisons is that they show that emissions are very much related to Specific Power. In particular most of the transient high emissions occur at low or high values of SP. Although, as mentioned above, Specific Power does not capture all of the physics involved, this strong dependence can be exploited to interpret remote sensing measurements, to compare the emissions measurements under different driving conditions, or to model the effect of driving conditions on emissions. In particular it can be used to detect situations in which a properly functioning vehicle may have high emissions for a short period of time. These uses are further explored in sections 3.3 and 3.4.

Another conclusion of this analysis is that Specific Power can be used to compare the results of different driving cycles. Average cycle speed is sometimes used for this purpose (CARB, 1998a), but this is a poor procedure because cycles with the same average speed may have very different power conditions.

A caveat is in order at this point: these conclusions are based on the study of a few recent properly functioning vehicles. A systematic study of older vehicles and high emitters is necessary to verify the applicability of this result to the vehicle fleet.
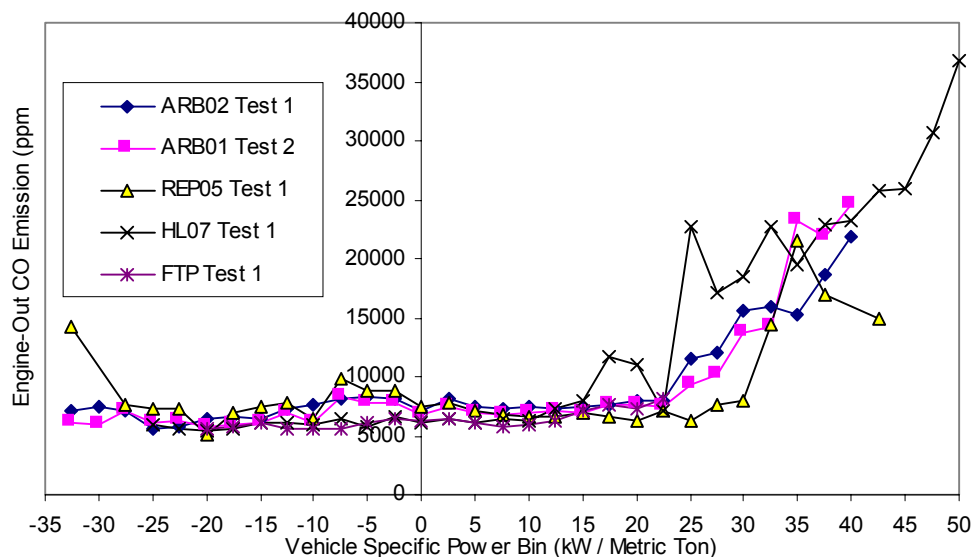
Figure 3-9: Engine-out CO emissions binned by Specific Power ranges for a 1994 Jeep Cherokee for 4 driving cycles
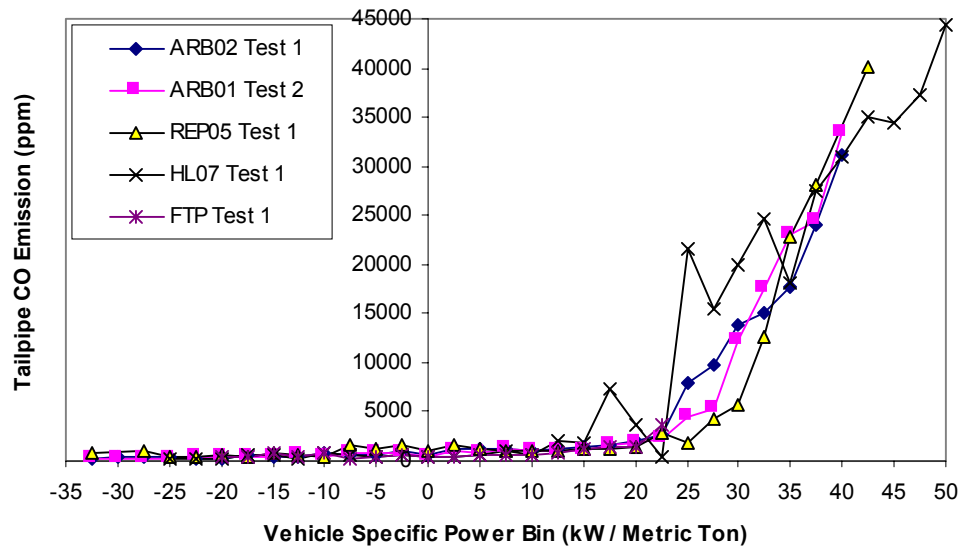
Figure 3-10: Tailpipe CO emissions binned by Specific Power ranges for a 1994 Jeep Cherokee for 4 driving cycles
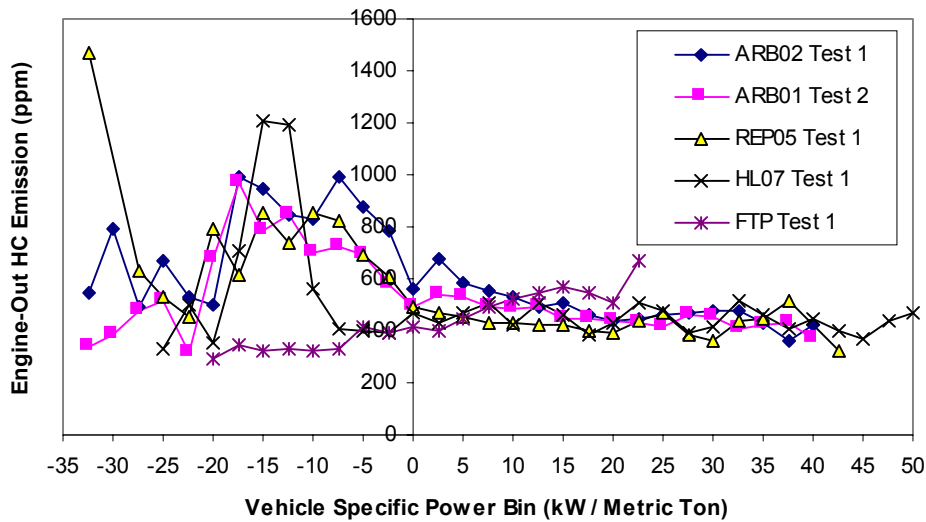
Figure 3-11: Engine-out HC emissions binned by Specific Power ranges for a 1994 Jeep Cherokee for 4 driving cycles
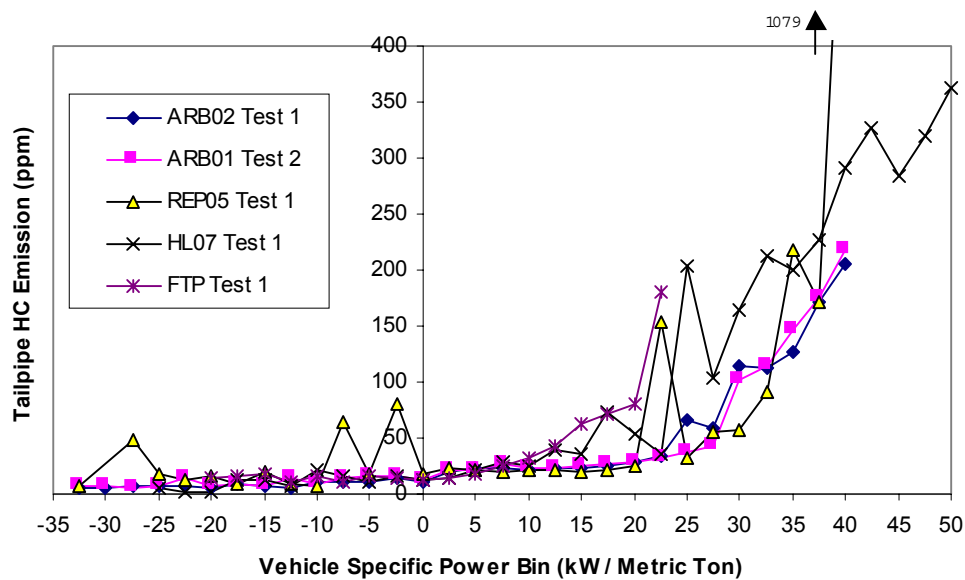
Figure 3-12: Tailpipe HC emissions binned by Specific Power ranges for a 1994 Jeep Cherokee for 4 driving cycles
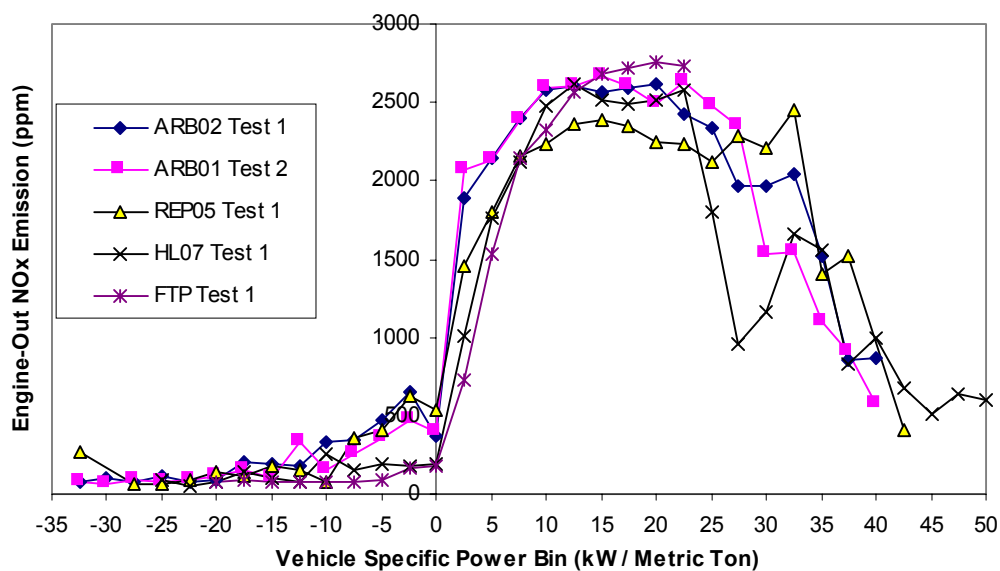
Figure 3-13: Engine-out NO$_x$ emissions binned by Specific Power ranges for a 1994 Jeep Cherokee for 4 driving cycles
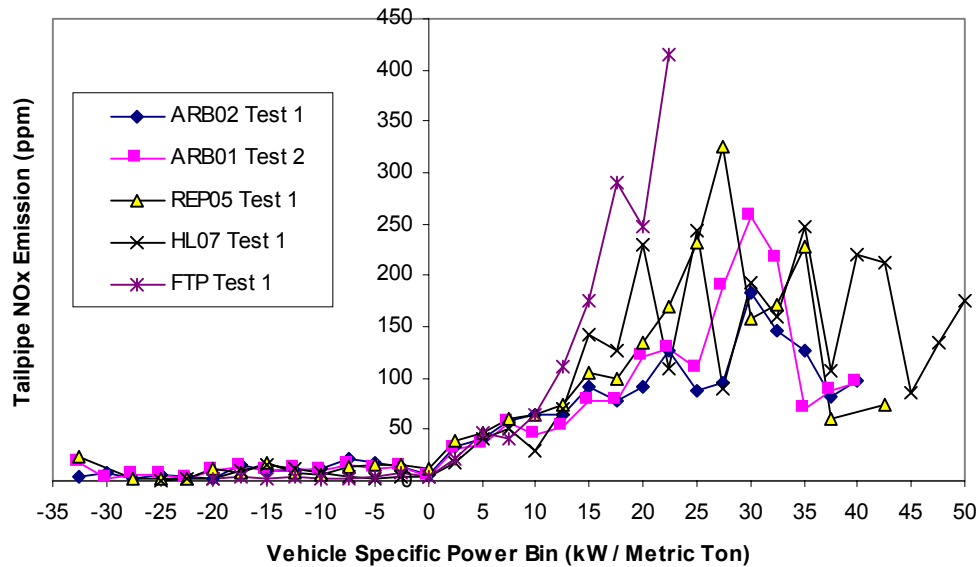
Figure 3-14: Tailpipe NO$_x$ emissions binned by Specific Power ranges for a 1994 Jeep Cherokee for 4 driving cycles

3.2.3. Specific Power vs. Speed and/or Acceleration

Several authors have studied the relationship of vehicle speed and acceleration with emissions measured by remote sensing (Todd *et al.*, 1995; Sjödin *et al.*, 1996; Popp *et al.*, 1998a; Walsh and Kite, 1998) or tried to use acceleration as a way to ascertain whether a vehicle may be in commanded enrichment (Kirschenmann *et al.*, 1996). Specific Power is a more adequate parameter than speed or acceleration since it is more directly related to the load on the vehicle's engine and thus to emissions.

To illustrate this point Figure 3-15 and Figure 3-16 show the variation of fuel consumption and engine-out NO$_x$ emissions with respect to acceleration and Specific Power for a 1994 light-duty truck tested on the FTP. The correlation is much stronger with Specific Power, showing a clearer trend and less scatter in the experimental measurements.
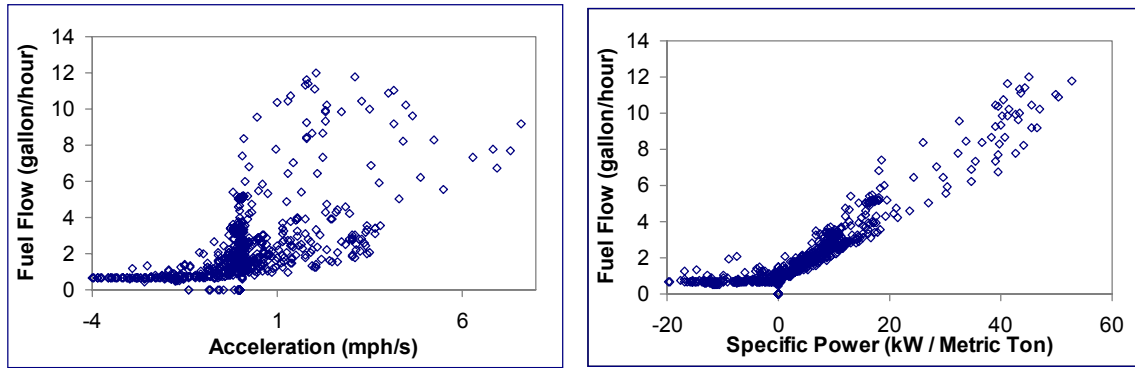
Figure 3-15: Fuel flow into the engine as a function of acceleration and Specific Power for a 1994 Jeep Cherokee tested on the FTP and HL07 driving cycles
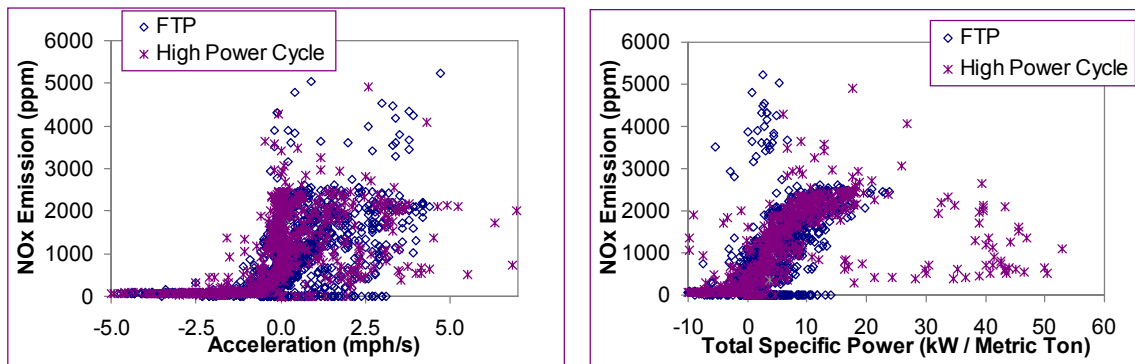
Figure 3-16: Second-by-second engine-out NO_x emissions vs. acceleration and Specific Power for a 1994 Jeep Cherokee tested on the FTP and HL07 driving cycles

Once the Specific Power of a given vehicle is known, speed and acceleration do not provide significant additional information with respect to emissions. This is demonstrated by studying the second-by-second engine-out NO_x emissions from the same vehicle tested on the FTP driving cycle. The contour plots of these emissions vs. Specific Power and acceleration, and SP and speed are shown in Figure 3-17. NO_x emissions show a clear trend with engine power, with a relatively constant emissions level for a given Specific Power, and very different emissions levels for given accelerations and/or speeds (moving horizontally on the graphs). For any constant Specific Power value, no emission changes are discernible in the graphs when speed or acceleration vary over their full range (moving vertically).
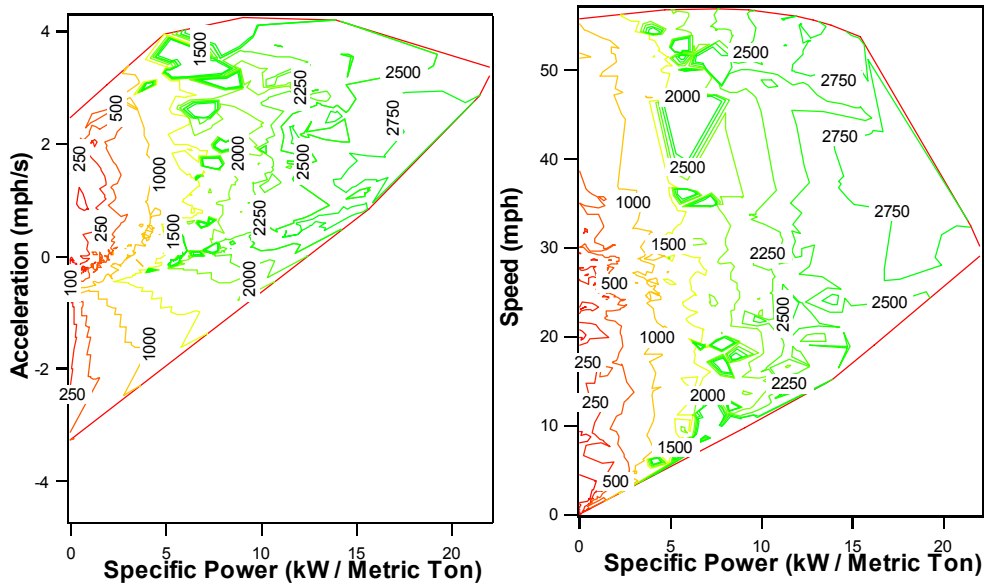
Figure 3-17: Contour plots of second-by-second engine-out NOx emissions for a 1993 Jeep Cherokee during the FTP cycle

This result is important since it indicates that a single parameter may be used to integrate most or all of the dependence of emissions on speed and acceleration (and grade). Two-dimensional regions on speed and acceleration maps contain the same information, but their determination and use is more complex, and the influence of roadway grade needs to be taken into account.

This conclusion is based on the study of a recent properly functioning vehicle, and is limited by the number of data points available on the speed-SP and acceleration-SP emission matrices. An systematic experimental exploration of these matrices, and data on other types of vehicles, specially high emitters, is necessary to verify the applicability of this result to the vehicle fleet.

3.2.4. Use of Specific Power to Predict Commanded Enrichment Situations

Tailpipe CO emissions of recent properly-functioning vehicles increase dramatically at very high engine powers due to the engine management strategy known as "commanded enrichment" (Haskew *et al.*, 1994). This strategy is used to avoid engine knock, maximize the torque output of the engine, and to protect the catalyst and exhaust valves from excessive temperatures. Commanded enrichment situations can result in CO emissions which are orders of magnitude higher than those under normal operation (see Figure 3-7). Enrichment events are estimated to occur in about 2% of in-use driving

(Pollack *et al.*, 1998) and to account for about 20% of the total CO emissions in a vehicle's lifetime (Ross *et al.*, 1998).

A reliable prediction of commanded enrichment situations from a directly measurable parameter is necessary for emissions modeling and remote sensing. Ripberger et al. (Ripberger *et al.*, 1996) proposed the use of speed and acceleration maps. An and Ross (An, 1996) employed Specific Power defined as 2*speed*acceleration.[51]

In this section, the use of the new definition of Specific Power for prediction of commanded enrichment is explored by analyzing the onset of enrichment[52] for six modern production vehicles (model years 92-94) from the SFTP data set (Liberty *et al.*, 1997).

Figure 3-18 shows the fraction of the time in each Specific Power bin during which each vehicle was running rich during the HL07 driving cycle.[53] Similarly, Figure 3-19 and Figure 3-20 show the same data, represented vs. total power and the fraction of maximum engine power respectively. Comparison of the three figures shows that Specific Power is the best predictor of the onset of commanded enrichment at high powers for all of the tested vehicles.
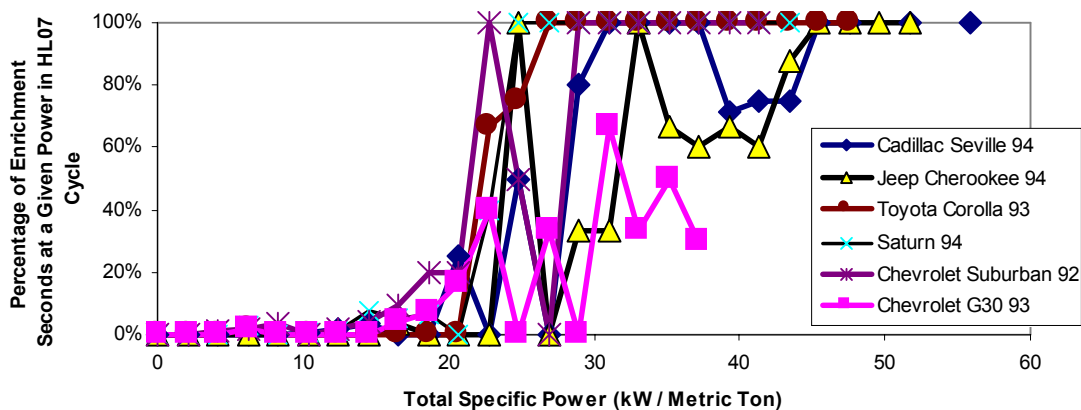
Figure 3-18: Percentage of the time at a given Specific Power level that the commanded enrichment strategy is used, for 6 vehicles tested on the HL07 cycle

---

[51] The difference in the relative values of specific power calculated with this definition and the one proposed in section 3.1 is significant, specially at higher speeds and when roadway grades are present (see Figure 3-3).

[52] This data set includes second-by-second air-to-fuel ratio. Enrichment was defined as A/F < 13 (stoichiometric conditions correspond to A/F ~ 14.6).

[53] This is the most aggressive driving cycle in the data set. Other cycles triggered commanded enrichment at slightly higher powers.

This onset occurs at Specific Powers around the maximum value for the FTP (~22 kW/Metric Ton), and at widely varying values of total power and fraction of available power. For example, the most powerful vehicle starts enriching at only 20% of the maximum available power. The likely explanation for this trends is that engine designers program the engine control system to use a stoichiometric air-fuel mixture for the range of powers tested on the FTP but permit enrichment to happen as soon as the power is larger than the maximum tested.
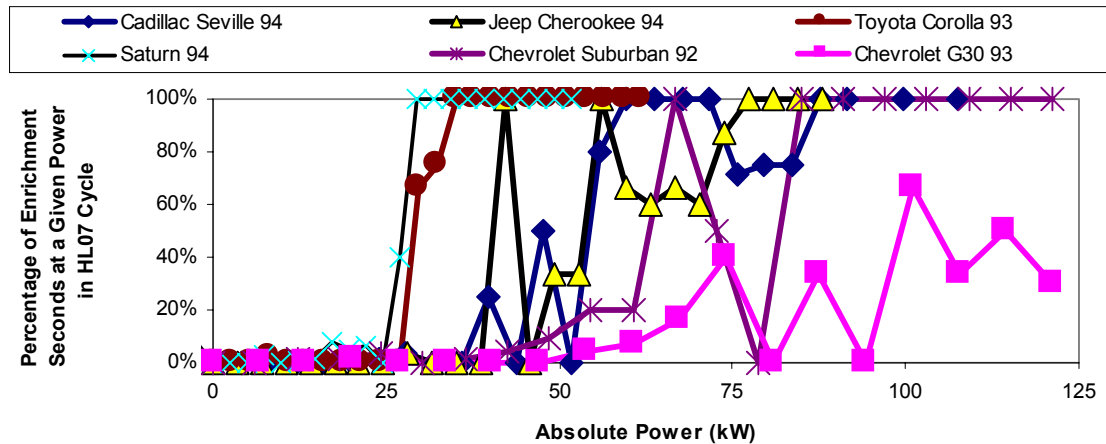
Figure 3-19: Percentage of the time at a <u>absolute power</u> level that the commanded enrichment strategy is used, for 6 vehicles tested on the HL07 cycle
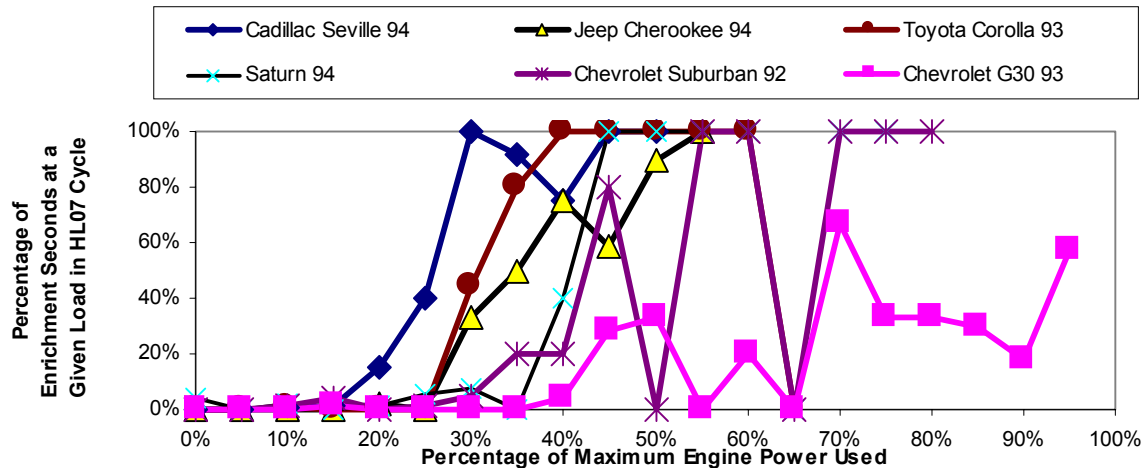
Figure 3-20: Percentage of the time at a <u>given percentage of the maximum engine power</u> level that the commanded enrichment strategy is used, for 6 vehicles tested on the HL07 cycle

Figure 3-21 shows the percentage of the total time that the same 6 vehicles of the previous figures were running rich, for each Specific Power and acceleration bin. As can

be seen in the figure, a criterion based on Specific Powers larger than the FTP maximum is able to predict most of the enrichment while one based on acceleration is not.[54, 55]
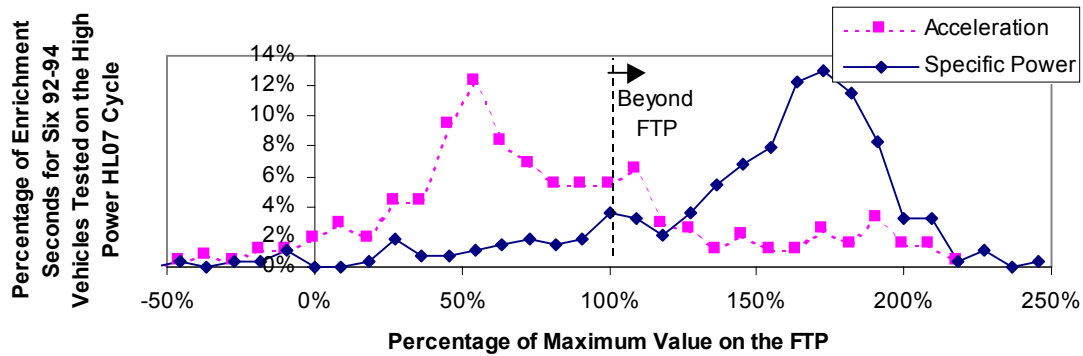
Figure 3-21: Percentage of the seconds with commanded enrichment vs. relative acceleration and Specific Power

---

[54] According to this figure some enrichment happens at Specific Powers below the FTP maximum. This may be real or may be an artifact due to imprecision in the estimation of the vehicle acceleration due to the low time resolution of the data set (1 second). A 10 Hz data set should be used for a finer assessment of this point.

[55] A criterion of acceleration < 40% of the FTP maximum would also work but would be much less selective. This is important e.g. in remote sensing situations where a large fraction of the data would need to be declared invalid.

3.2.5. Variation of the Emissions of Several Vehicles vs. Specific Power and Other Parameters

To compare the usefulness of several other parameters for emissions studies, the engine-out CO emissions of 6 different cars and light-duty trucks have been plotted vs. Specific Power, absolute power, fuel rate, and fuel rate per unit weight bins[56] in Figure 3-22, Figure 3-23, Figure 3-24, and Figure 3-25 . The relationship with Specific Power is seen to be much more consistent for the different vehicles than the other three parameters. The main reason for this may be that SP is the best predictor of the onset of commanded enrichment (see section 3.2.4).

A similar conclusion can be drawn for NO_x emissions (Figure 3-26 and Figure 3-27) and HC emissions. Thus the use of Specific Power instead of absolute power or fuel rate in emissions studies would be advantageous since this approach would exploit more of the constancy of the physical system.
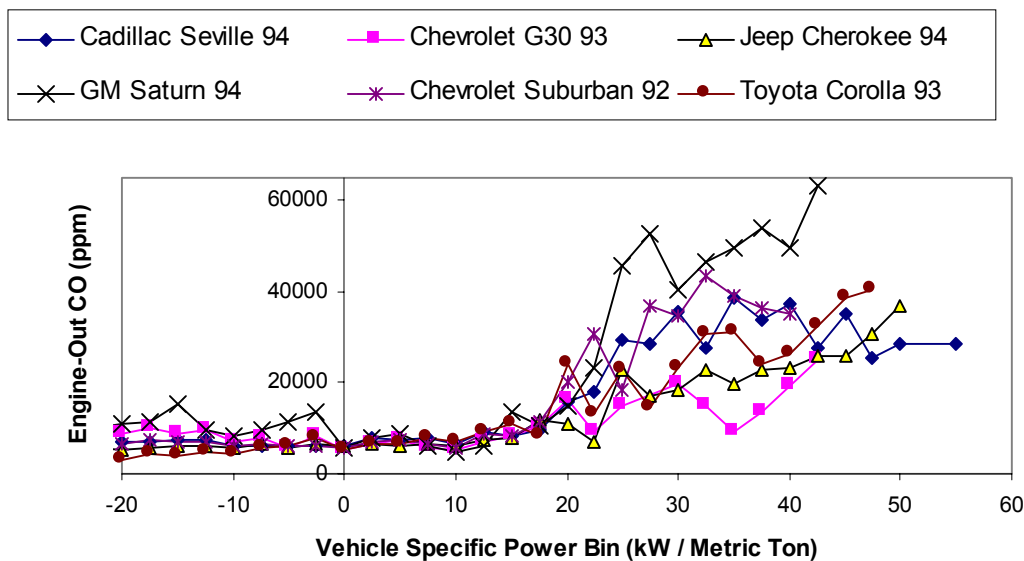
Figure 3-22: Engine-out CO emissions binned by Specific Power ranges for 6 vehicles tested on the HL07 driving cycle

---

[56] Fuel rate has been chosen because it is used as the main parameter of the most comprehensive modal emission model available (see section 3.4.3). Fuel rate per unit weight has been selected to compare with power per unit weight (Specific Power).
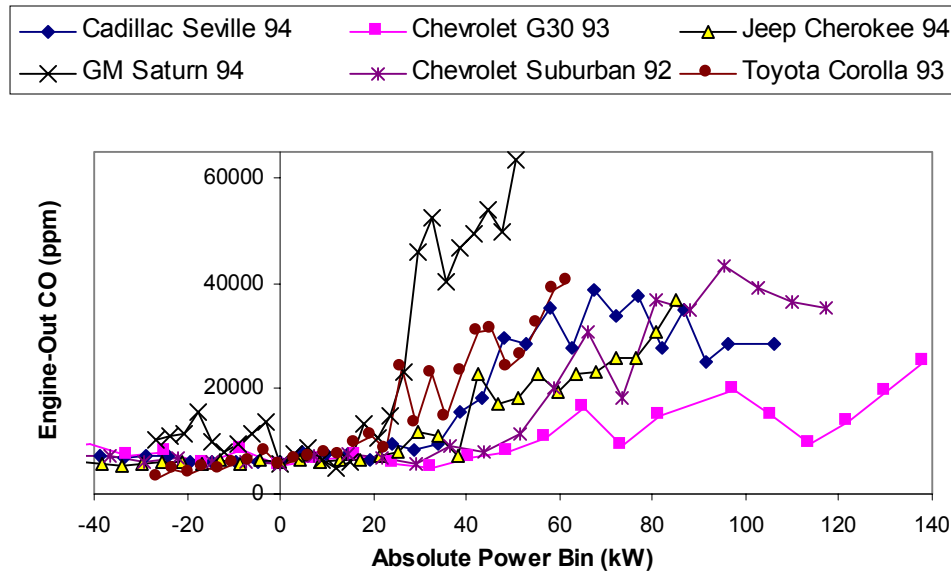
Figure 3-23: Engine-out CO emissions binned by absolute power ranges for 6 vehicles tested on the HL07 driving cycle

Figure 3-24: Engine-out CO emissions binned by fuel rate ranges for 6 vehicles tested on the HL07 driving cycle
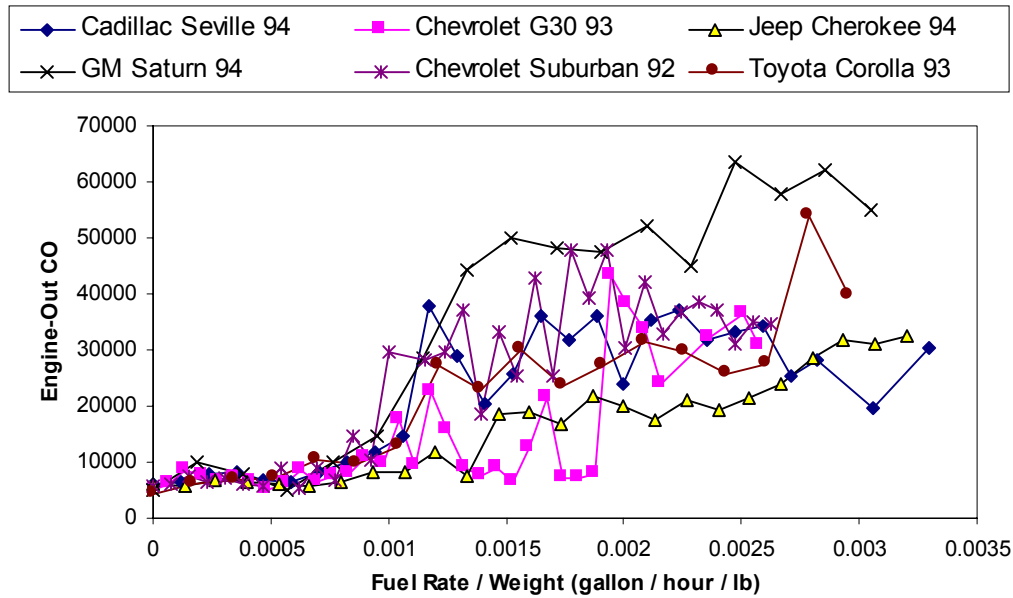
Figure 3-25: Engine-out CO emissions binned by <u>fuel rate per unit vehicle weight</u> ranges for 6 vehicles tested on the HL07 driving cycle
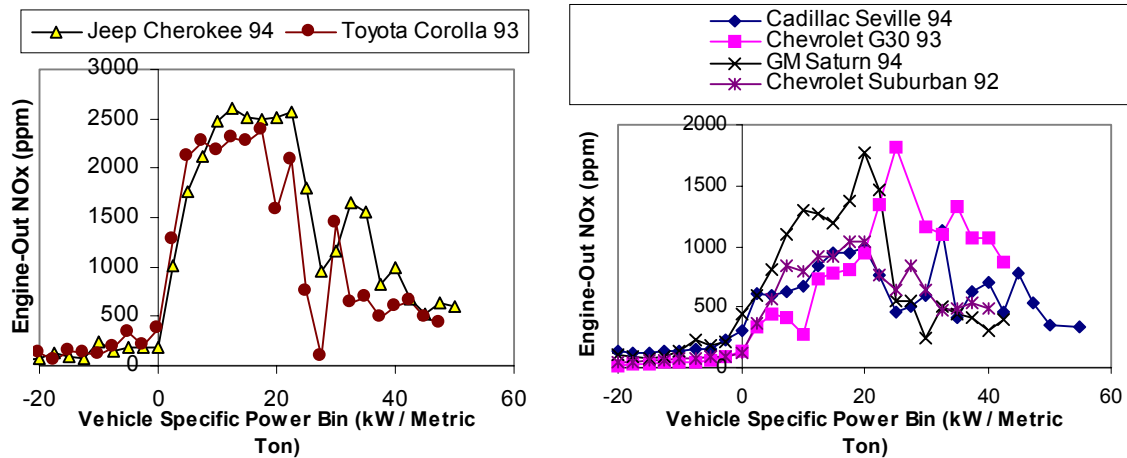
Figure 3-26: Engine-out NO$_x$ emissions binned by <u>Specific Power</u> ranges for 6 vehicles tested on the HL07 driving cycle (left: vehicles w/o EGR; right: vehicles with EGR)
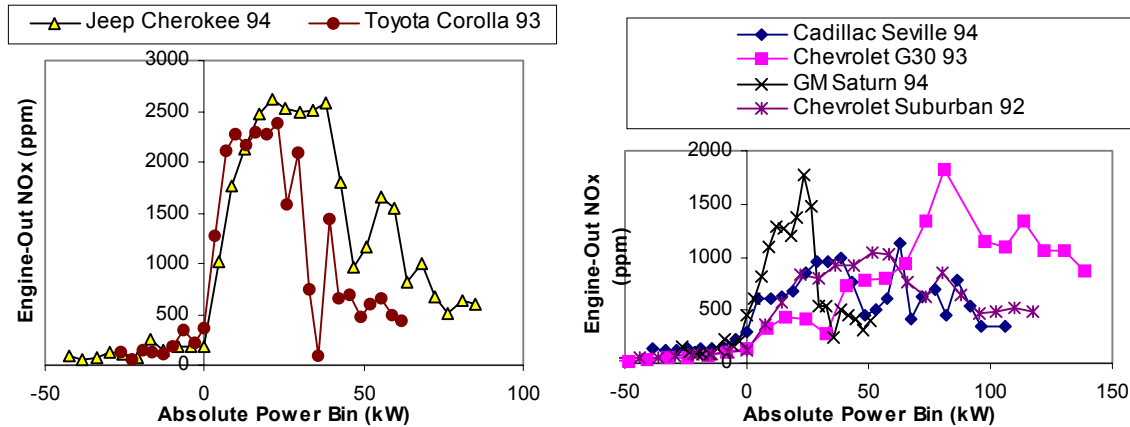
Figure 3-27: Engine-out NO$_x$ emissions binned by <u>absolute power</u> ranges for 6 vehicles tested on the HL07 driving cycle (left: vehicles w/o EGR; right: vehicles with EGR)

3.2.6. Effect of Payload Weight on Emissions[57]

For the same speed, acceleration, and grade, a relative change of 20% of the total vehicle mass from the basic test weight[58] (due to payload increase) can result in a ~0 to 20% change in total power.[59] Since emissions for a given vehicle physically depend on total engine power and not on Specific Power, and SP would be the same in both cases,[60] this could be a shortcoming for the uses of Specific Power proposed in sections 3.3 and 3.4.

We can estimate the maximum emissions impact of a 20% weight change by looking at the emissions generated with 20% more Specific Power in Figure 3-22 and

---

[57] EPA's MOBILE emissions model can theoretically account for this effect. According to M. Beardsley, from EPA's emission inventory group (Beardsley, 1998): "While the function is rarely used, MOBILE allows users to enter the percent of vehicles with "extra" load. This percentage is then used to apply a percentage increase in emissions to that percent of the fleet. This calculation has been in MOBILE for many years and will be continued in MOBILE6, but was not well documented originally and has not been updated at any time in the memory of current MOBILE staff. The MOBILE "extra load" factors (as listed in the model's block data) are based on dyno testing performed many years ago (probably in the late'70s) on vehicles over the FTP with an extra 500 lb load".

California's EMFAC model does not account for this effect (Long, 1998).

[58] Equal to the curb weight plus 300 lb (Haskew *et al.*, 1994).

[59] The change would be zero on the high speed limit when all the specific power is due to aerodynamic drag, since the absolute aerodynamic power does not depend on vehicle mass. The change will be equal to the change in vehicle mass at low speeds when aerodynamic drag is negligible and all terms of the SP equation are directly proportional to vehicle mass.

[60] If calculated from speed, acceleration, and grade with the same numerical coefficients in both cases, as it would be done during remote sensing measurements when weight information is not available.

Figure 3-26. The impact could be significant, especially if the additional power causes the vehicle to enter the region of commanded enrichment operation.

This issue has been further analyzed by looking at the second-by-second emissions from a Ford F250 light-duty truck tested on the SFTP program with two different payloads.[61] The first test was conducted with the curb weight plus 300 lbs., while the second test used one-half of the maximum payload. The increase in total weight between the tests was 35%.[62]

The engine-out and tailpipe CO, HC, and NO_x emissions for these tests binned by specific power are shown in Figure 3-28, Figure 3-29, and Figure 3-30 respectively.[63] The main difference between the emission curves is the extent of commanded enrichment, indicated by the high CO emissions at high Specific Powers. As shown in Figure 3-7, not all of the seconds in which a vehicle is above the maximum FTP Specific Powers result in commanded enrichment operation. The extra weight in this case results in more frequent enrichment at high Specific Powers and a slight displacement of the enrichment threshold to lower Specific Powers. The main features of the HC and NO_x curves are preserved.
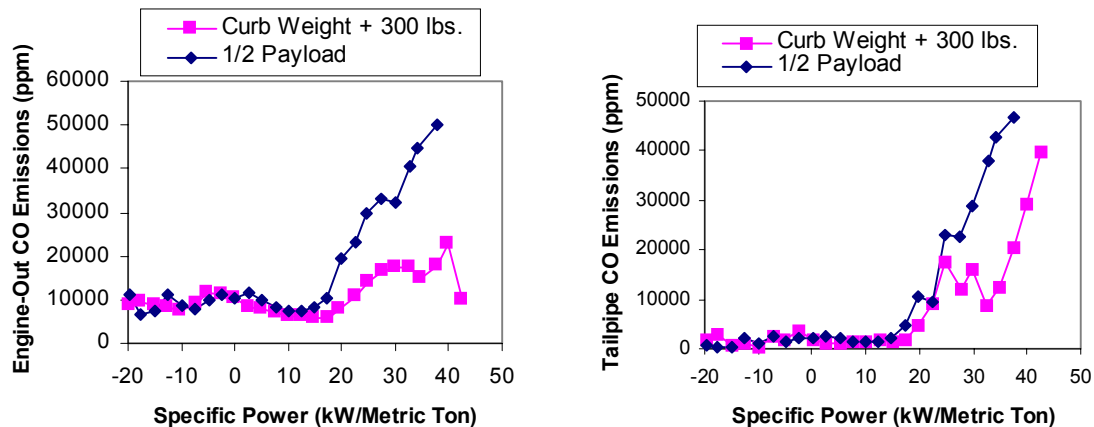
Figure 3-28: Engine-out and tailpipe CO emissions vs. Specific Power for a 1993 Ford 250 with two different weights

---

[61] Dynamometer load was not adjusted between the two tests. The driving cycle was the ARB02 cycle, developed by the California Air Resources Board (Haskew *et al.*, 1994).

[62] From 5000 lbs. to 6757 lbs. (2.27 to 3.06 Metric Tons).

[63] Specific Power has been calculated with the same coefficient values in both cases, in order to simulate its application in a remote sensing situation.
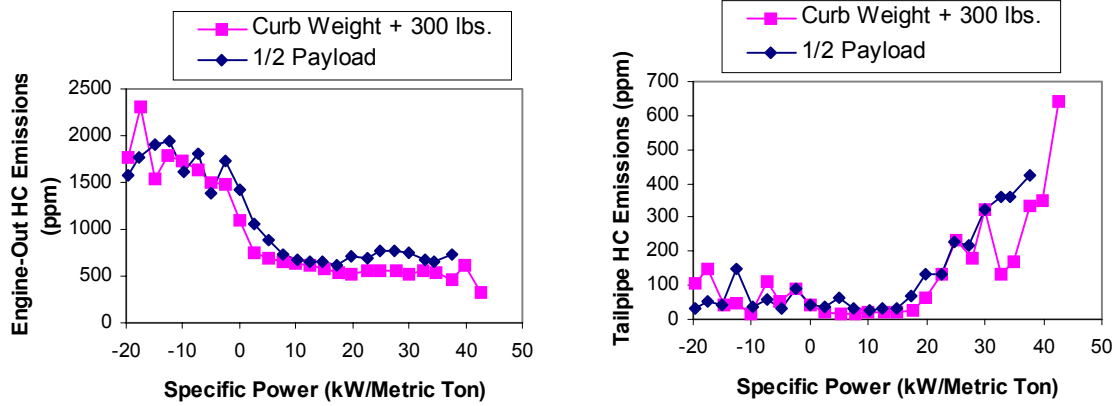
Figure 3-29: Engine-out and tailpipe HC emissions vs. Specific Power for a 1993 Ford 250 with two different weights
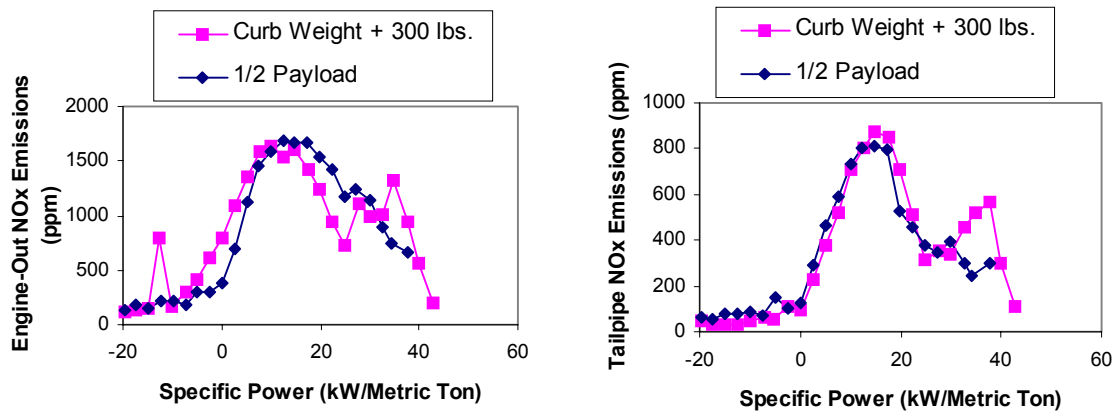
Figure 3-30: Engine-out and tailpipe NO$_x$ emissions vs. Specific Power for a 1993 Ford 250 with two different weights

3.3. Applications of Specific Power for Remote Sensing

3.3.1. Transient High Emissions and Remote Sensing

A potential application of remote sensing is as a "surveillance" component on inspection and maintenance programs, either to detect high emitters and direct them to a inspection and maintenance (I/M) programs, or to detect clean vehicles to exempt them from I/M testing. The attempts to design and implement these programs in practice have been hampered by the lack of a reliable method to screen out the occasional high emissions of properly functioning vehicles, that would lead to "false failures."[64, 65] This is the main reason why the U.S. EPA does not support the use of remote sensing to detect high emitters (Lorang, 1998).

An adequate method to screen out these transient high emissions in remote sensing measurements is needed. Some studies have tried to use speed and acceleration as a way to screen out these conditions (Todd *et al.*, 1995; Ripberger *et al.*, 1996; Walsh *et al.*, 1998). However, the power needed from an engine to accelerate a vehicle is influenced by the vehicle speed, the acceleration rate, and the roadway grade (see section 3.1). Thus, neither speed or acceleration, by itself, is a good measure of the load placed on the engine. Two-dimensional regions on speed and acceleration can be used in principle, but their determination and use is more complex, and a different map needs to be used for each roadway grade. In the next sections the application of Specific Power to this task is studied, based on the results of section 3.2.

Another remote sensing application is the evaluation of I/M programs (Zhang *et al.*, 1996b; Stedman *et al.*, 1997b; Stedman *et al.*, 1998). It could also benefit from a method to screen out transient high emissions, since these are normally not encountered during I/M testing.

Finally, a third use of remote sensing data is as in input in the calculation emission inventories (Singer *et al.*, 1996). In this case all of the data need to be taken into

---

[64] "False failures" occur when a vehicle which would have emissions lower than the applicable standard on the IM240 or FTP dynamometer tests is declared high emitter by a remote sensing surveillance program. "False passes" happen when a vehicle which would fail the dynamometer tests is declared a low emitter by remote sensing.

[65] Note that these transient high emissions captured by remote sensing are correct measurements of the actual emissions. They should be screened out because they are not indicative of a failure that could be repaired through an I/M program.

account, since the transient high emissions are real and can account for a significant fraction of the total emissions (An *et al.*, 1997; Ross *et al.*, 1998). A method to account for the effect of the variation of driving conditions on the inventory is described in section 3.4.2.

3.3.2. Analogies Between Second-by-Second Driving Cycle Data and Remote Sensing Data

In the following sections some conclusions are made about remote sensing measurements based on the results of second-by-second vehicle emission measurements on driving cycles presented in section 3.2. This assumes that second-by-second data and remote sensing measurements are analogous.

This analogy is clearly justified to the extent that dynamometer loads approximate road loads, since individual remote sensing measurements sample the instantaneous emissions with a time scale on the order of 0.5 seconds (see Figure 5-5).

For fleet averaged emissions, the rationale is the following: a second-by-second dynamometer data set represents the emissions of a vehicle under a distribution of operating conditions.[66] If remote sensing measurements of the same vehicle were performed, it is reasonable to assume that the range of emissions at each condition would be similar. E.g. if the remote sensing emissions of the same vehicle were plotted vs. Specific Power we would expect to have results such as those in Figure 3-7 for the second-by-second emissions and similar to Figure 3-8 to Figure 3-14 for binned data. Some preliminary evidence of this fact can be found by comparing the tailpipe CO emission of Figure 3-7 with Figure 3-31, which show similar characteristics even though they correspond to different vehicles..

Generalizing that idea, we can think of a given fleet[67] measured by remote sensing as a "composite vehicle," which, given a sufficient number of measurements, will produce stable curves of emissions vs. Specific Power such as those in Figure 3-8 to Figure 3-14. These curves may then be used to predict emissions under different conditions as described in section 3.3.6.

---

[66] Again note that we are explicitly excluding cold-start operation. The discussion refers to hot stabilized emissions only.

[67] Or subfleets such as 1990 light-duty trucks and TWC-equipped passenger cars.

3.3.3. Criteria for Interpreting and Screening Remote Sensing Emission Measurements

Variations in engine power demand are responsible for a significant part of the variability encountered in remote sensing measurements. Specific Power can be used to guide the interpretation and increase the usefulness of these measurements, by reducing the occurrence of "false failures" and "false passes."

Some rules for the interpretation of remote sensing measurements can be derived from the analysis in section 3.2:

- Vehicles with high CO emissions measured under Specific Powers beyond the FTP maximum (~22 kW/Metric Ton) are suspect of commanded enrichment[68] and should be rejected. Those with high CO readings and Specific Powers below the FTP maximum are likely to be real high emitters which are running with rich fuel-air mixtures. A similar criterion was recently was recently proposed by McClintock (1998). This criterion is a very effective way to screen out the high CO emissions associated with commanded enrichment operation. It has the potential to greatly reduce the associated erroneous high emitter identifications, as demonstrated in section 3.3.5.

  For example Walsh and Kite (Walsh *et al.*, 1998) recently estimated that up to 65% of the remotely sensed vehicles in their study with accelerations of 5-6 mph/sec were high CO emitters, when it is likely that most of them were simply under commanded enrichment.[69]

  Specific Power could also be used to determine the threshold for commanded enrichment for different vehicle models using large remote sensing data sets. This information would be useful for representing the effect of enrichment on emission models.

- HC measurements associated with negative Specific Powers should be rejected as well, since properly functioning vehicles may have high HC emission levels during strong decelerations.[70]

---

[68] See Figure 3-18 and Figure 3-21 in section 3.2.4.

[69] A vehicle with an acceleration of 5.5 mph/sec and a speed of 20 mph or larger will have an specific power larger than the FTP maximum.

[70] See section 3.2.2.

- NO$_x$ measurements for negative Specific Powers should be rejected as well. Under these conditions a vehicle with a broken catalyst may produce very low NO$_x$ emissions[71] due to low combustion temperatures. If load was not taken into account such a vehicle would be considered a low-NO$_x$ emitter incorrectly .

- Based on the limited data analyzed here, there is no reason to reject NO$_x$ measurements at high Specific Powers or CO measurements at negative SPs.

- Remote sensing measurements with high Specific Power (> 15 kW/Metric Ton), and with both low CO (< 0.1%) and low NO$_x$ (< 100 ppm) are a very strong indication of a properly functioning control system. The low CO emissions indicate that the commanded enrichment strategy is not being used and that the vehicle is not running rich for other reasons. Thus engine-out NO$_x$ emissions are necessarily high (see Figure 3-7 and Figure 3-13). The low tailpipe concentrations of NO$_x$ and CO indicate that the catalyst is being very effective for both pollutants. Vehicles with a remote sensing measurement that fulfills this requirement could be exempted from I/M testing for the current testing period without the need for a second measurement.[72, 73]

3.3.4. Verification of Commanded Enrichment Screening Using Specific Power

The criteria for commanded enrichment screening in remote sensing was verified experimentally based on several remote sensing measurements of a vehicle which had been recently verified to comply with the Ultra Low Emission Vehicle standards on the FTP cycle.[74] The CO emissions of this vehicle vs. Specific Power are shown in Figure 3-31. High CO emissions, indicating commanded enrichment, appear for Specific Power values slightly above the maximum FTP values.[75]

This result indicates that the screening criterion is necessary: otherwise a remote sensing program could classify this legally ultra-clean vehicle as a high CO emitter, if its

---

[71] See section 3.2.2.

[72] Low HC emissions should also be required.

[73] This conclusion should be confirmed by analyzing a data set with remote sensing and IM240 data on the same vehicles.

[74] This vehicle was made available to us during our measurement campaign at El Segundo, California (see Chapter 6) by an automobile manufacturer. The emission tests were performed by the California Air Resources Board.

[75] NO emissions for this vehicle are shown in 5.4.2, and did not increase for the highest specific powers. HC emissions also stayed at very low levels for all powers (not shown).

emissions happened to be measured under high Specific Power conditions. It also suggests that Specific Power can be calculated with sufficient accuracy based on real-world speed and acceleration measurements.
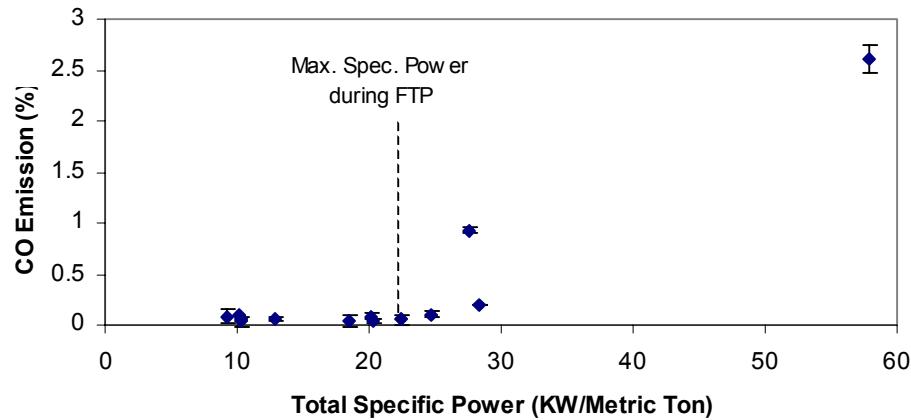
Figure 3-31: CO emission (measured by remote sensing) vs. Specific Power for a prototype Ultra Low Emissions Vehicle

3.3.5. False Failures Avoided by Specific Power Screening

The CO data from the remote sensing campaign at El Segundo, California (see Chapter 6) have been used for an evaluation of the false failure rate that can be avoided with the Specific Power screening criterion.

Figure 3-32 shows the CO remote sensing measurements vs. Specific Power for 540 vehicles measured during this campaign.[76] The vehicles with elevated CO readings for Specific Powers beyond the FTP maximum (~22 kW/Metric Ton) are suspect of commanded enrichment. Those with high CO readings at lower Specific Powers are likely to be real high emitters which are running with rich fuel-air mixtures.

If we define a high emitter cutpoint of 2% CO, 26% of the high CO emitters detected at this site (7 of 27) are suspect of commanded enrichment operation. This is a significant fraction whose elimination should add value to remote sensing measurements by allowing a more precise detection of the true high emitters.

---

[76] The vehicle in Figure 3-31 is not included in this figure.
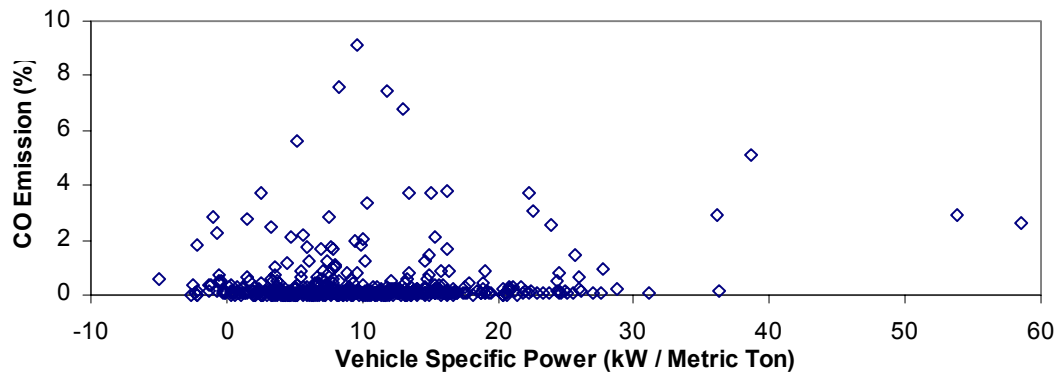
Figure 3-32: CO emission (measured by remote sensing) vs. Specific Power for 540 remote sensing measurements

3.3.6. Use of Specific Power to Compare Emissions Measured Under Different Conditions

A long standing problem in the on-road mobile source emissions field is how to compare the results of different emissions measurements, such as different driving cycles and remote sensing.

▪ Remote sensing studies have found that the average emissions levels measured in different sites in the same urban area are different (Walsh *et al.*, 1997). Part of this variability is attributed to the vehicle fleet while another part is attributed to differences in speed and acceleration distributions between the sites (Walsh *et al.*, 1998).[77]

▪ Remote sensing has been criticized for poor comparisons to driving cycle results (Welstand, 1997). However, remote sensing data cannot be expected to yield the same result as a cycle average data since the former represent only one vehicle operating condition while the latter includes emissions for a distribution of operating conditions. The use of Specific Power as an additional test variable permits a comparison of the results obtained by remote sensing and dynamometer tests.

Having a meaningful way to compare the emissions levels measured at different remote sensing sites and in different studies would be very useful (e.g. was the fleet in one study dirtier or just operating under higher powers?), and also in the design of remote

---

[77] This study did not account for effects of roadway grade.

sensing programs. Two strategies are explored in this section: comparing the curves of emissions vs. Specific Power; and using the Specific Power distributions to transform the results to the same basis.

Strategy I: Comparing the curves of Specific Power vs. emissions

Figure 3-33, Figure 3-34, and Figure 3-35 show the CO, NO_x, and HC emissions vs. VSP for 2 remote sensing studies in Chicago (Popp *et al.*, 1998a) and California (Chapter 6). Also shown are the data for second-by-second data for a 1994 passenger car tested on a driving cycle.[78] All of the data have been binned in by Specific Power. Both engine-out and tailpipe emissions are shown for the driving cycle data. The general trends of both remote sensing studies and the driving cycle data are similar.

The graphs make apparent that the remote sensing in California included higher powers than that in Chicago (as shown in Figure 3-4). E.g. comparing the average values of both data sets would give a difference of only 9% on the NO_x emissions, but the graph shows that the difference would be about 25% between 0 and 10 kW/Metric Ton.
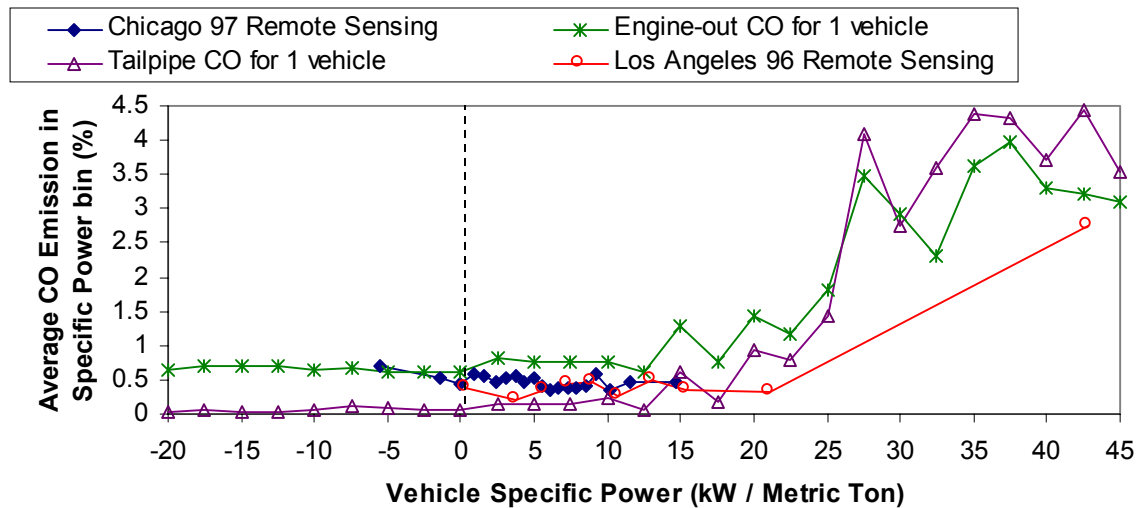
Figure 3-33: CO emissions vs. Specific Power for 2 remote sensing studies and engine-out and tailpipe second-by-second data for a vehicle on a driving cycle

---

[78] A 1994 Cadillac Seville tested on the SFTP program (Liberty *et al.*, 1997).
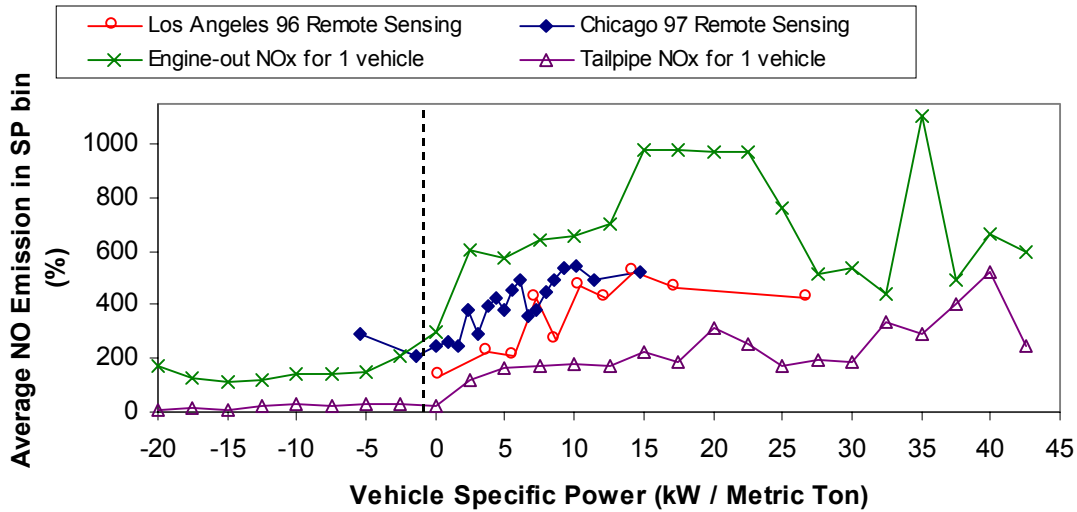
Figure 3-34: NOx emissions vs. Specific Power for 2 remote sensing studies and engine-out and tailpipe second-by-second data for a vehicle on a driving cycle
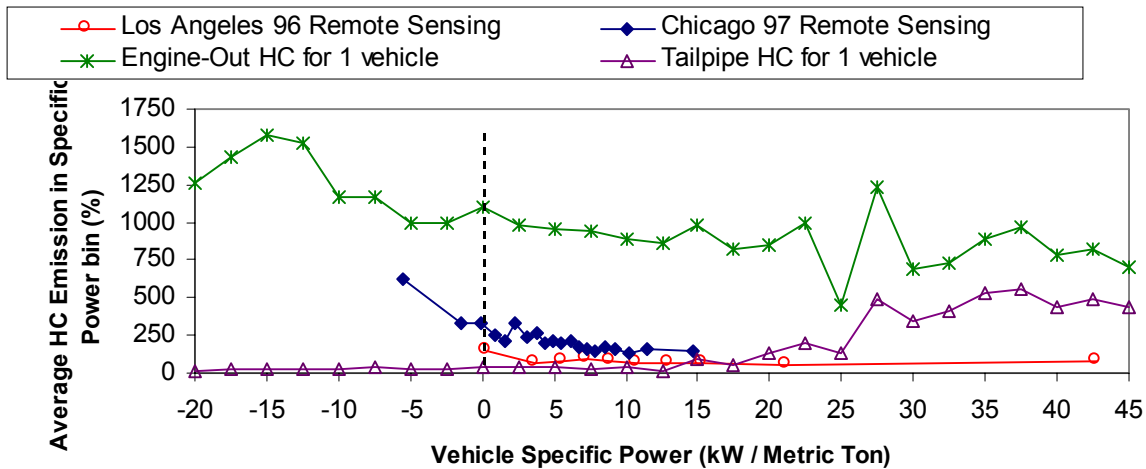
Figure 3-35: HC emissions vs. Specific Power for 2 remote sensing studies and engine-out and tailpipe second-by-second data for a vehicle on a driving cycle

The California fleet had lower emissions than the Chicago fleet at most powers. This is probably a consequence of the more stringent emission standards and the lower sulfur content of California's gasoline.[79]

---

[79] Sulfur is a mild catalyst poison, and lower gasoline sulfur contents result in lower CO, HC, and NO_x emissions (U.S. EPA, 1998d). The sulfur limit for California's gasoline at the time of the test was 30 ppm vs. an average of 300 nationwide (U.S. EPA, 1998d).

Referring to Figure 3-33 (CO emissions), the remote sensing study in Los Angeles included high Specific Power values that resulted in commanded enrichment operation, while the Chicago data set did not. If this difference in the Specific Power values between the two studies is not taken into account, any comparison of their results would be very misleading.

Under moderate Specific Powers,[80] both remote sensing studies are higher than the tailpipe emissions from the 1994 vehicle for all pollutants. This is not surprising since most vehicles in both remote sensing data sets are older than 1994 and may have been certified to less stringent standards and have undergone more in-use deterioration. For these reasons we would not expect their emissions to be as low as the tailpipe emissions of a 1994 properly functioning vehicle.

The remote sensing emissions are also lower than the engine-out emissions (for moderate Specific Powers). This is expected since the vast majority of the fleets in both remote sensing studies are equipped with functional three-way catalysts, and their emissions should be lower than engine-out values.[81]

These comparisons show that representing binned emissions data vs. Specific Power produces meaningful comparisons between the results of different studies and methods.

<u>Strategy II: Using the Specific Power distributions to put the results on the same basis</u>

Figure 3-36 shows an schematic representation of the proposed method for comparing emission data obtained under different conditions by considering the dependence of emissions on Specific Power:

■ First the emissions of data set "A"[82] are averaged in Specific Power bins.[83]

---

[80] The emissions at high Specific Powers are more variable between vehicles (e.g. Figure 3-22) and the particular vehicle selected here may not be a good representation of the average vehicle fleet.

[81] This vehicle used exhaust gas recirculation (EGR) to reduce engine-out NOx emissions. Engine-out emissions of vehicles without EGR have the same general shape vs. power but tend to be a factor of 2 higher (see Figure 3-26 and Figure 3-27).

[82] It would be advantageous to use the most extensive data set (both in number of data points and on the range of SP covered) for this purpose, since that will produce more stable emissions vs. SP curves.

[83] Using population deciles (taking e.g the 5% vehicles with the lowest Specific Power and averaging their emissions) may be more robust than using fixed Specific Power ranges (e.g. from 10 to 11 kW/Metric

- Then the emissions distribution of data set "A" corrected to the Specific Power conditions of data set "B" is calculated by multiplying the number of vehicles at a given Specific Power bin in data set "B" by the average emission level at that Specific Power level (calculated in the previous step from data set "A").

- An average emission level can now be calculated for data set "A" from this new distribution. The emission level obtained in this way represents what the vehicles in study "A" would have emitted under the power demand conditions of study "B."
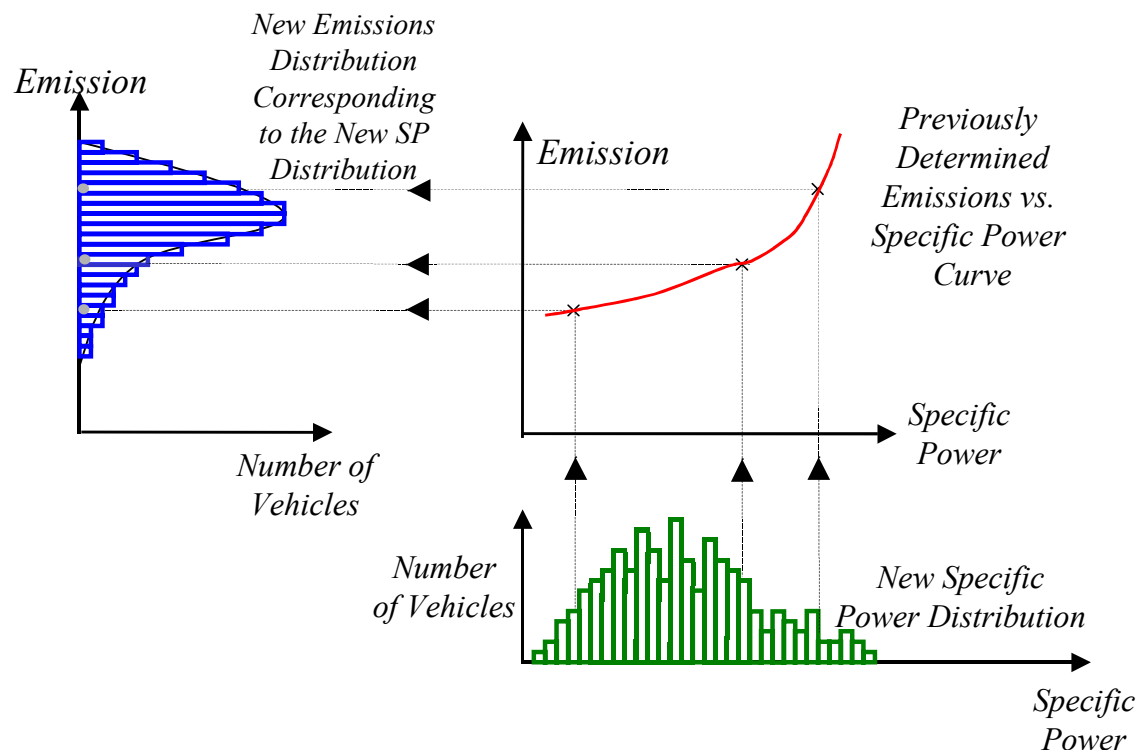
Figure 3-36: Schematic of the way to determine the emission distribution for new driving conditions

Using this strategy with remote sensing results (as "A") and the IM240 specific power distribution (as "B") would allow a direct comparison of remote sensing data with IM240 results.[84] This direct comparison would be very useful for the evaluation of inspection and maintenance programs.

Ton) for this purpose. The earlier procedure maintains the same number of vehicles in each bin and tends to produce more reliable trends.

[84] Provided that concentration data are acquired during IM240 testing. Otherwise fuel economy would be required to convert the remote sensing results in grams-per-gallon to grams-per-mile. Fuel economy data can be calculated from IM240 data by a carbon balance.

For example, if we wanted to compare an average CO result from Los Angeles (Figure 3-33) to the average result of some IM240 tests, this procedure would assign a zero weight to the high CO remote sensing levels at the highest Specific Power decile when calculating the remote sensing average .[85] This is appropriate because the high CO at high SP is caused by commanded enrichment events which rarely occur during an IM240 test. Not excluding them would make the on-road fleet appear dirtier than this same fleet would be on the IM240.

A remote sensing data set with repeated measurements on 2450 vehicles (Popp *et al.*, 1998a) has been analyzed in order to illustrate the soundness of this approach. The repeated measurements have been divided in two data sets, with the first measurement on each vehicle comprising the first data set and the second measurement comprising the second data set. Each vehicle was operating at a different Specific Power level in its two measurements (R^2=0.01 between SP_1 and SP_2). This is equivalent to measuring the same fleet at two different sites.
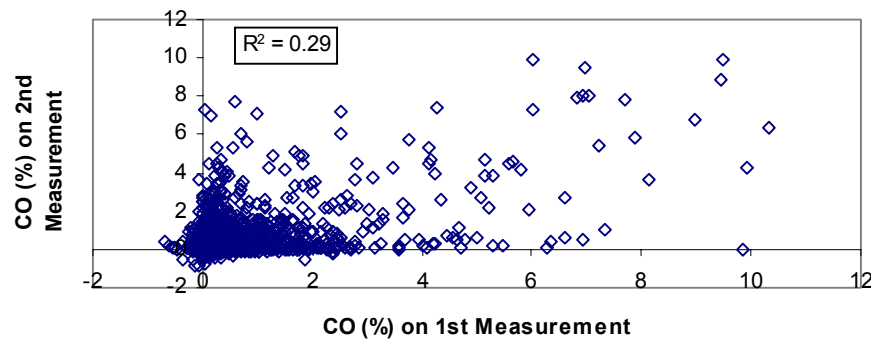
Figure 3-37: CO in the first measurement vs. the second measurement for the vehicles measured twice in the Chicago data set (Popp et al., 1998a)

The simple comparison of the first and second CO measurements for each vehicle (Figure 3-37) shows a lot of scatter, with an R^2 of 0.29, illustrating the typical variability of raw remote sensing measurements (Bishop *et al.*, 1996d; Stephens *et al.*, 1996a). However, when the emission measurements are binned by Specific Power the results of both data sets are very similar. The binned results for CO, HC, and NO_x are shown in Figure 3-38, Figure 3-39, and Figure 3-40 respectively.

---

[85] Since the maximum SP on the IM240 test is about 22 kW/Metric Ton.

This indicates that although the instantaneous emission of a single car may change appreciably from one site to another due to engine load changes and other factors, the fleet shows consistent emission trends.[86, 87] The conclusion is that the procedure outlined in Figure 3-36 could work well to compare the average emission levels measured by remote sensing at different sites.
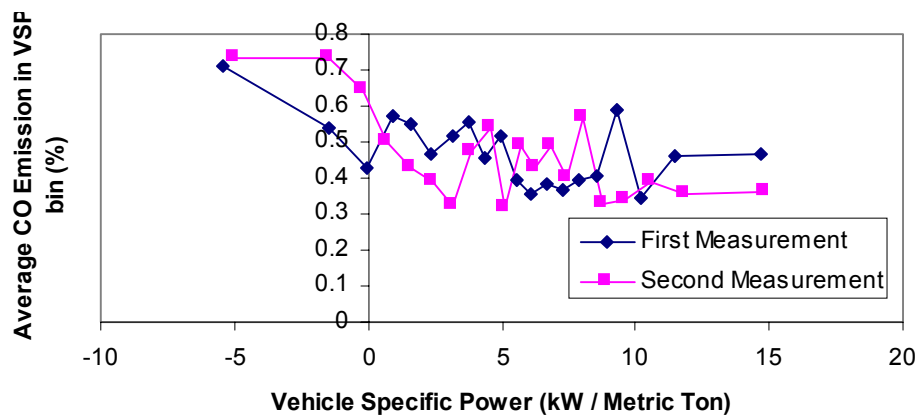
Figure 3-38: Average CO in each 5% Specific Power bin for the first and the second measurement for the vehicles measured twice in the Chicago data set (Popp et al., 1998a)
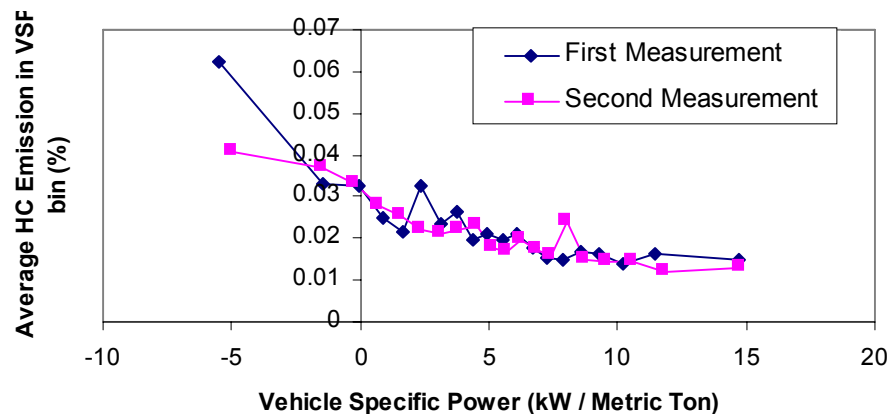
Figure 3-39: HC in each 5% Specific Power bin for the first and the second measurement for the vehicles measured twice in the Chicago data set (Popp et al., 1998a)

---

[86] The 95% confidence intervals of both data sets overlap for all 5% Specific Power bins and the three pollutants.

[87] The vehicle fleet could be thought of as a "composite car" characterized by its curves of emissions vs. Specific Power just as an individual vehicle is (see section 3.2.2).
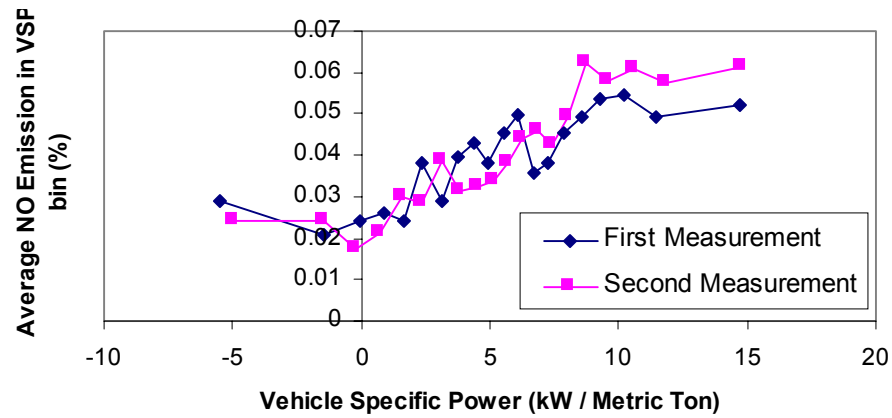
Figure 3-40: NO in each 5% Specific Power bin for the first and the second measurement for the vehicles measured twice in the Chicago data set (Popp et al., 1998a)

3.4. Applications of Specific Power for Emissions Modeling

3.4.1. Types of On-Road Vehicle Emissions Models

Two main types of models are used to predict emissions from on-road vehicles:

1) <u>Inventory models</u>, which are commonly used to predict the total emissions for a geographical region. Examples include California's EMFAC model and EPA's MOBILE model. The structure of the models is:[88]

Total Emissions = (Emission Rate) * (Vehicle Activity) * (Correction Factors)

The emission rates are generally expressed in grams-per-mile (gpm) and the activity data on vehicle-miles traveled[89] (U.S. EPA, 1993b; CARB, 1998a; Samaras and Ntziachristos, 1998). The correction factors account for effects such as average speed, ambient temperature, fuel changes, etc.

2) <u>Modal models</u>, which try to predict vehicle emissions in the microscale (second-by-second) based on operating parameters. Different model structures are used. These models can also be used to calculate emissions inventories (Barth *et al.*, 1998).

The advantages of using Specific Power in both types of models is studied in the next sections.

3.4.2. Use of Specific Power in Inventory Emissions Models

Emissions from on-road vehicles depend strongly on driving conditions. For this reason the results of several driving cycles are used to represent a variety of driving conditions in mobile source emission models:

- California's model (EMFAC) uses an interpolation of the results of 12 different driving cycles each with different average trip speeds to account for driving condition effects (Gammariello and Long, 1996). All of these "speed

---

[88] For hot stabilized emissions only. Cold start emissions are modeled differently and are not discussed here.

[89] Some researchers have proposed the use of emission rates in grams-per-gallon (gpg) of fuel, and activity data on gallons of fuel used (Singer *et al.*, 1996; Dreher *et al.*, 1998). The latter approach has the advantage of exploiting the smaller variability of gpg as compared to gpm emissions rates when driving conditions change, as shown in section 4.5 of this thesis. An additional benefit is that data on fuel sales is more readily available and more accurate than data on VMT (Singer *et al.*, 1996).

correction driving cycles" begin and end at idle, and the emissions of each cycle are more indicative of trips of certain average speed[90] than of emissions associated with instantaneous speed. A regression analysis of the results from the different cycles provides "speed correction factors," which are then applied to the basic vehicle emission rates to account for the variation of driving conditions. The speed correction factors used by the EMFAC model are shown in Figure 3-41 (CARB, 1998a).
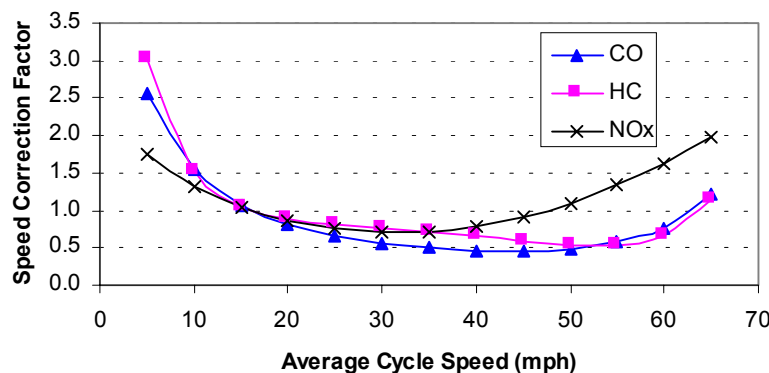
Figure 3-41: EMFAC speed correction factors vs. average cycle speed for the regulated pollutants

- EPA's model (MOBILE) uses the same approach (U.S. EPA, 1993b). The version currently under development (MOBILE6) will make use of several new "speed correction cycles." These cycles are chosen based on matching the joint distribution of speed and acceleration obtained from instrumented vehicle and "chase car" data (Carlson *et al.*, 1997).

- Current European inventory emissions models also use the same approach as EPA and CARB (Samaras *et al.*, 1998).

Using average trip speed to represent different driving conditions has an important limitation: trips with the same average speed may correspond to very different Specific Power distributions and emissions. For example a trip in which half of the time the vehicle is traveling at 60 mph and half is stopped would be assigned the same emission rates than a trip at a constant 30 mph speed.

---

[90] Defined as the distance traveled divided by the time spent in the driving cycle, including any stopped time.

It is suggested here that a better way to model the dependence of emissions on driving conditions would be to use correction factors based on distributions of Specific Power. This would also permit a seamless integration of the effect of grade on emissions.

The suggested procedure for implementing this correction is as follows:

1) The dependence of emissions vs. Specific Power can be determined from remote sensing and/or driving cycle data (e.g. Figure 3-14 and Figure 3-22 for driving cycles; Figure 3-38 for remote sensing).

2) The distribution of Specific Powers in the geographical area and roadway type of interest area can be obtained from instrumented vehicle and "chase car" studies (Carlson *et al.*, 1997).

3) Then the procedure outlined in Figure 3-36 can be used to relate the emissions measured on a given driving cycle or remote sensing site to the emissions that the fleet would produce with the measured distribution of Specific Powers.

3.4.3. Use of Specific Power in Modal Emissions Modeling

Modal emissions models attempt to predict the instantaneous vehicle emissions as a function of operating parameters.

Many different input variables have been used in them. Some of these models relate emissions directly to the joint distribution of speed and acceleration (Guensler *et al.*, 1997; West and McGill, 1997; Sturm *et al.*, 1998). Other modal models use diverse parameters non measurable from the roadside as surrogates for engine load. Examples include:

- Manifold vacuum and brake mean effective pressure (Koupal and German, 1995).

- Mass air flow, estimated from the total power and gear switch points (Ripberger *et al.*, 1998).

- Throttle position (Shih *et al.*, 1997).

- Fraction of available power being used (Guensler *et al.*, 1997).

- Fuel rate and the product of speed and acceleration (An *et al.*, 1997).

- Speed and the product of speed and acceleration (Sturm *et al.*, 1998).

- Fuel Rate. The most comprehensive physics-based modal emission model available, developed by the group at CE-CERT in U.C. Riverside, uses this parameter as the basis for emissions modeling (Barth *et al.*, 1997; Barth *et al.*, 1998; Nam *et al.*, 1998).

Some very promising recent modal models are based on neural networks (Long *et al.*, 1997; Atkinson *et al.*, 1998; Jesion *et al.*, 1998). The network is given a time series of a set of variables on a driving cycle and is then predicts what the emissions will be when given a new set of input variables. The input variables used so far include vehicle speed, engine speed, engine torque, and engine power demand.

Using Specific Powers instead of these diverse parameters cited above has two main two advantages: Specific Power is directly measurable in real-world conditions, and the dependence of emissions on SP is better than on the other measurable parameters (as discussed in sections 3.2.4 and 3.2.4).

Neural network-based models could also benefit from the benefits of Specific Power by using this parameter as an input variable. Models that use speed and acceleration as inputs would be simplified by using only 1 parameter instead of 2. Finally, those models that use non-measurable variables would benefit from switching to a variable with a strong correlation with emissions but which is directly measurable in the real world.

As mentioned above, it is not suggested here that instantaneous vehicle emissions are only a "state" function of Specific Power. For example commanded enrichment may or may not be used at the same Specific Power level (see Figure 3-7), and history effects over several seconds may be important for the engine and the catalyst (An *et al.*, 1997; Nam *et al.*, 1998). Rather the conclusion of this study is that instantaneous SP should be used as the main variable representing engine load, although the history of SP or other additional input variables may be needed to properly model all situations.

3.5. Conclusions

The main results of the study in this chapter are:

- Specific Power (SP), defined as the total tractive power per unit weight for a given vehicle, can be calculated with good approximation from measurements of vehicle speed, acceleration, and roadway grade and estimates of aerodynamic and rolling resistance.

- Emissions have a strong dependence on Specific Power. In particular Specific Power is the best predictor of commanded enrichment in recent production vehicles, which start to enrich at Specific Powers slightly above the maximum value of this parameter on the FTP driving cycle.

- Once Specific Power is known, speed and acceleration do not provide additional information with respect to emissions.

- Specific Power distributions or curves of emissions vs. Specific Power can be used to relate the emissions produced on different driving cycles or at different remote sensing sites.

- The Specific Power that is relevant for remote sensing is that of the instant in which the emissions which are leaving the tailpipe were generated in the engine. This means that the speed and acceleration measurements should be done between 5 and 20 meters before the point where emissions are measured (for positive SPs).

- Specific Power can be used to screen out remote sensing measurements under conditions that lead to transient high emissions in properly functioning vehicles, since these emissions may not be repairable through an inspection and maintenance program. These include high CO and HC emissions due to commanded enrichment and high HC emissions during strong or prolonged decelerations. Emissions inventories should not screen out these high readings since they are correct measurements of real phenomena that must be accounted for in an inventory.

- Specific Power could be used to determine the threshold for commanded enrichment for different vehicle models using large remote sensing data sets.

- Low NO_x emissions in remote sensing situations when the vehicle is under very low or negative Specific Power should also be screened out for I/M purposes. Under these conditions a vehicle with a broken catalyst would have very low tailpipe NO_x emissions due to low NO_x production in the engine.

- Low NO_x, CO, and HC in a remote sensing measurement under high Specific Power is a strong indication that the emission control system of the vehicle is working properly.

- Emissions models can benefit from using Specific Power as the main parameter to represent load since this parameter has a strong relationship with emissions and is directly measurable in the real world.

  - Inventory emissions models can benefit from the use of Specific Power-based correction factors instead of speed-correction factors to represent the effect of different driving conditions on warmed-up emissions.

  - Modal emissions models can also be improved and/or simplified by using Specific Power as the main load surrogate, in order to take advantage of the good relationship between SP and emissions.

- An additional benefit of the use of Specific Power in the different sub-fields would be the use of a common parameter to represent load on emission studies performed with different methods, such as dynamometers tests, remote sensing, and emissions models. Such "common language" would allow a much easier and more detailed comparison of the results of the different methods.

- The main limitation of the new definition of Specific Power presented here is that it cannot account for the emission impact of large increases in vehicle weight due to payload, and of non-tractive power use such as for air conditioning operation. Some strategies to deal with these problems are suggested. Further research is needed in these areas.

Chapter 4. Analysis of Remote Sensing Measurements

4.1. Introduction

Remote sensing of on-road vehicle emissions was pioneered by Don Stedman and Gary Bishop of the University of Denver in 1987 (Bishop *et al.*, 1989). Since then several other groups and companies have developed and used remote sensing instruments, and remote sensing measurements have been made for millions of vehicles. However, some basic aspects of the measurements have not been studied or documented.

This chapter presents analyses of a number of practical issues associated with remote sensing measurements. These are of general applicability and are not restricted to remote sensing with the TILDAS technique. Section 4.2 deals with the fluid mechanical aspects of remote sensing measurements, including the interference between the exhaust of two vehicles measured sequentially. Section 4.3 introduces the concept of plume capture and some models and experimental data for its quantification. Section 4.4 analyzes the variation of remote sensing noise with plume capture and emission level. Section 4.5 introduces the issues associated with the residence time of the exhaust gases in the vehicle, and presents a model for its quantification. Section 4.6 shows the advantage of using grams-per-gallon emission factors because of their lower variability as compared to grams-per-mile emissions factors. The need to include the relative fuel economy when using remote sensing data to compile emission inventories is demonstrated in section 4.7. Finally section 4.8 summarizes the conclusions of this chapter.

4.2. Fluid Mechanical Aspects of On-Road Remote Sensing

4.2.1. Automobile Wake Flow Patterns

Remote sensing of automobile emissions is carried out by passing a light beam through the vehicle exhaust as these gases are being transported and diluted by the vehicle wake, as shown in Figure 2-6. This section introduces the main characteristics of automobile flows.

The flow in the wake of an automobile is very complex and unsteady, characterized by a large separated region (Hucho, 1993). These flow patterns influence of fuel consumption associated with aerodynamic drag, and for the lateral and vertical aerodynamic forces on the vehicle which affect its driveability. For these reasons they have been intensively studied both experimentally in wind tunnels (Ahmed and Baumert, 1979; Hucho, 1993) and with computational fluid dynamics codes (Kobayashi and Kitoh, 1992; Spragle *et al.*, 1993; Johnson and Tezduyar, 1996).
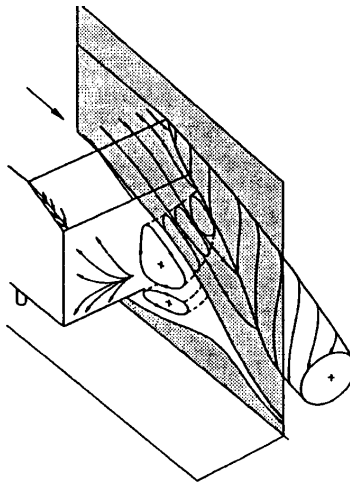
Figure 4-1: Schematic representation of the flow patterns in the wake of an automobile (Hucho, 1993)

The details of the flow patterns depend critically on the vehicle shape and specially on the shape of the rear end of the vehicle. Minor changes in design can lead to completely new flow patterns, as can speed changes for a given vehicle shape (Ahmed *et al.*, 1979; Hucho, 1993).

The main features of the wake flow of an automobile highlighted by these studies are a large separated region or "bubble" and, depending on the rear shape, two

longitudinal counterrotating vortices as shown in Figure 4-1. The variation of the flow patters with vehicle rear shape is illustrated by Figure 4-2.

The computed air speed vectors from a recent supercomputer study[91] in a plane behind a car[92] traveling at 55 mph on a plane perpendicular to the vehicle velocity and ¼ car length after the vehicle are shown in Figure 4-3. This computation illustrates the strength of the counterrotating vortices and the large shear near the tailpipe height, which will lead to very rapid mixing of the exhaust leaving the tailpipe.
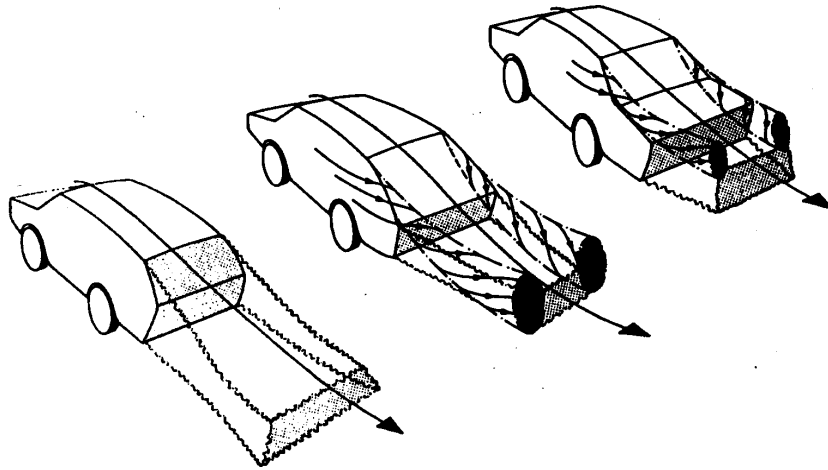
Figure 4-2: Flow patterns in the wake of 3 typical automobile rear-end shapes (Hucho, 1998)

Figure 4-3: Computed speed vectors at a cross section normal to the vehicle velocity at ¼ car lengths behind the automobile (Johnson et al., 1996)

---

[91] These are steady-state time-averaged results computed using the Reynolds-averaged equations and a turbulence model.

[92] Modeled after a Saturn SL2, which is closer to the rightmost shape in Figure 4-2.

Tailpipe locations and orientations vary widely from vehicle to vehicle, and in general the tailpipe flow may be "captured" and recirculate in the bubble behind the vehicle, interact with the vortex pattern leading to very fast dispersion, or flow almost horizontally near the road surface. Higher vehicle speeds create a larger bubble and a stronger vortex pattern (Hucho, 1998), leading to enhanced exhaust dispersion (Eskridge, 1991). If we add the unsteadiness of the flow and (sometimes) the presence of ambient wind, the variability in plume dispersion is so large as to make the exhaust flow pattern almost random. This was verified by observing the dispersion patterns of a large number of recently started vehicles under low ambient temperature conditions, when the exhaust water vapor condenses forming a visible plume. It was concluded that little information of use to remote sensing can be derived from a detailed study of this topic from a fluid mechanical point of view, such as with CFD models or wind-tunnel studies. A statistical point of view has been adopted instead as described in section 4.3.

4.2.2. Geometry, Time-Scales, and Physical Effects for Automobile Remote Sensing

The main characteristics of the geometry of the automobile exhaust systems and the flow out and around them are important in the selection of some operating parameters for remote sensing measurements, in particular the height of the light beam and the data acquisition rate.

The exact height, size position, and direction of automobile tailpipes varies with each specific vehicle model. Nevertheless most automobiles have a tailpipe about 5 cm (2 in) in diameter located about 29 cm (11 ½ in) above the road. Light-duty trucks tend to have larger tailpipes, of about 6 cm (2.4 in) in diameter and located about 35 cm (13.8 in) above the road. For the remote sensing study presented in Chapter 6 and Chapter 8 the laser beam was located at a height of about 31 cm (12 in) as a compromise between automobiles and light-duty trucks.[93]

The time scales of the flow around a vehicle and of the exhaust leaving the tailpipe can be calculated as:

$$\text{Time Scale} = \frac{\text{Length Scale}}{\text{Velocity Scale}}$$

---

[93] A high precision in fixing this parameter experimentally is not possible, since road curvature effects change the height even for different passes of the same vehicle.

The length and velocity scales of interest are depicted in Figure 4-4. The exit speed of the exhaust gases leaving the tailpipe (relative to the moving vehicle) can be estimated from the tailpipe diameter and the fuel consumption.[94]
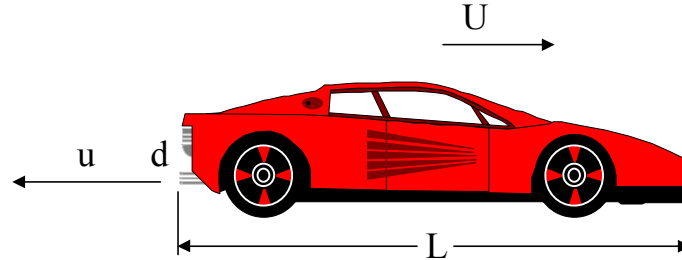
Figure 4-4: Schematic of the important quantities for determination of flow time-scales

The results of this time scale analysis are shown in Table 4-1. The time scales of the tailpipe jet flow are an order of magnitude smaller than those of the flow around the car body. From the values in the table it can be estimated that 100Hz is an appropriate data acquisition rate. This permits approximately 50 data samples of the exhaust plume based on the time scale of the flow around the car. The TILDAS system used in this thesis can achieve data rates exceeding 200 Hz. Data acquisition rates of 80 and 60 Hz were used for the automobile measurements after experimentally verifying that higher rates resulted in higher noise,[95] probably arising from instabilities of the non-linear least squares fitting procedure (section 5.3). A data rate of about 30 Hz was used for the heavy-duty truck measurements due to the much slower decay of the plumes of these vehicles (section 4.3.7).

	15 mph	60 mph
Time Scale of Flow Around Car	500 ms	110 ms
Time Scale of Tailpipe Exit Flow	50 ms	10 ms

Table 4-1: Time scales relevant to remote sensing

Finally some characteristics of the tailpipe flow can be estimated from non-dimensional fluid flow parameters (Batchelor, 1973).

The Reynolds number for the tailpipe jet flow at 15 mph would be:

---

[94] More precise estimates could be derived from second by second driving cycle data such as those used in section 4.3.3. However only an order of magnitude estimate is needed here.

[95] Beyond the expected increase with the inverse of the square root of the averaging time (Zahniser, 1998).

$$\text{Re} = \frac{\text{inertial effects}}{\text{viscous effects}} = \frac{\rho \cdot U \cdot L}{\mu} = \frac{1.25 \, \text{kg/m}^3 \cdot 1 \, \text{m/s} \cdot 5 \, \text{cm}}{1.7 \cdot 10^{-5} \, \text{N} \cdot \text{s/m}^2} \cong 3{,}670$$

which is about twice as high as that of transition to turbulence. Re is larger at higher speeds, thus the tailpipe flow is always turbulent for the conditions of interest to remote sensing.

Since the exhaust gases leaving the tailpipe can have elevated temperatures, it is important to determine if buoyant effects will play an important role in determining the flow pattern. If buoyant effects were dominant the remote sensing light beam might need to be elevated above tailpipe height for optimum plume capture.

The Froude number represents the ratio of inertial forces to buoyancy on a given flow. If $\text{Fr} \ll 1$, the flow is dominated by buoyancy, if $\text{Fr} \gg 1$, the flow is dominated by inertial forces, and if $\text{Fr} \sim 1$, both effects are important. We can calculate a typical value for the tailpipe flow at 15mph as :

$$\text{Fr} = \frac{\text{inertial force}}{\text{buoyancy force}} = \frac{U^2/L}{g \cdot \Delta\rho/\rho} = \frac{1.25 \, \text{kg/m}^3 \cdot (1\text{m/s})^2 / 5\text{cm}}{9.8\text{m/s}^2 \cdot 0.25} \cong 10$$

The value at 60 mph is about 125. This indicates that buoyant effects are not dominant for the tailpipe jet flow of a moving vehicle except at very low speeds, a conclusion confirmed by experimental observation of tailpipe plumes.

4.2.3. Interference between the Exhaust of Two Vehicles

Several remote sensing studies have reported interferences between the measurement of the emissions of two consecutive vehicles when the separation between them is smaller than four seconds (Glover and Clemens, 1991; Stephens *et al.*, 1991; HES, 1992). Bishop et al. (Bishop *et al.*, 1994) measured the emissions of vehicles across two lanes of traffic in a tunnel and found that under these conditions the time needed between two measurements to avoid interference was 1.7 ± 0.17 seconds, or 45 meters at 60 mph.

When performing remote sensing measurements the column density found before the vehicle is subtracted from the measurements taken on the wake of the vehicle (section 5.3). Thus a background level which is constant before and after the vehicle can be subtracted without causing an error. Interference is most apparent when a low emitting

vehicle follows a high emitter, since the large amount of the pollutant left behind by the high emitter may not be distributed uniformly and can confound the background subtraction process.[96] If these occurrences were not screened out a bias may be introduced in remote sensing data sets acquired at high traffic density sites. Normally this is dealt with by using a software trap which rejects the measurement if the standard deviation of the linear fit (section 5.3) exceeds a certain threshold, e.g. 20% for the University of Denver instrument (Bishop *et al.*, 1989; Stephens *et al.*, 1991).

These interferences have been observed in some of the TILDAS NO measurements. Since we subtract[97] an average spectra taken before the car from those taken after the car, the situation described above could result in "negative absorption lines." This is shown in Figure 4-5 for a measurement taken in the remote sensing campaign in California (Chapter 6). The two NO transitions are reversed (compare to Figure 5-4), indicating that the interference from the previous vehicle was important. Measurements with this characteristic have been systematically rejected.
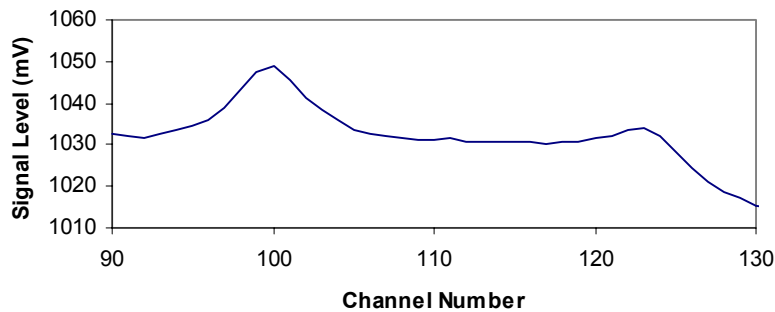
Figure 4-5: Remote sensing spectra of NO showing the negative peaks due to interference with the exhaust of the previous vehicle

---

[96] This situation would result in a lower (even negative) measurement than the real emission level of the second vehicle.

[97] Actually a ratio is used since this is the correct procedure according to Beer's law (see section 2.1.1).

4.3. Variations in Plume Capture

The amount of gases that is traversed by the light beam in a remote sensing measurement is highly variable due to the dispersion of the exhaust in the highly turbulent vehicle wake (see section 4.2.1) and to the variation in the amount of exhaust gases produced with power demand.

In this section the strength of plume capture in remote sensing measurements is analyzed. First some parameters to represent plume capture are defined, then some simple models for plume capture presented, and finally experimental data for automobile and heavy-duty truck measurements are reported.

4.3.1. Parameters to Represent the Strength of Plume Capture

The strength of the column density signals measured by remote sensing depend on several factors such as dispersion on the wake of the vehicle and the amount of gases being exhausted through the tailpipe. The CO_2 column density is generally used as a measure of plume capture, since its amount varies much less than those of the other species measured and is proportional to fuel use.[98] The possible definitions of this parameter, and its trends with remote sensing variables are analyzed in this section.

Figure 4-6 shows the variation of the CO_2 column density signal vs. time for a typical automobile remote sensing measurement.[99] The signal commonly starts with a large spike as the laser beam intersects the relatively undiluted exhaust, with a duration of the order of 150 msec. Then the plume decays to lower values returning to the background concentration in a few seconds.

We define here two parameters to quantify the strength of plume capture: the maximum CO_2 column density observed and the time-integral of the CO_2 signal. Both are schematically represented in the figure. Only CO_2 signals larger than a minimum value of 1,000 ppm-m are included in the determination of those two parameters.

---

[98] The column density of total carbon (CO_2+CO+n*HC), where n is the assumed HC molecular weight, could be a better measure since it normalizes the plume capture to fuel consumption. The error by using CO_2 only is small for most vehicles (~3% on average), however. This approach has not been implemented here.

[99] The background CO_2 column density has been spectrally subtracted as described in section 5.3.
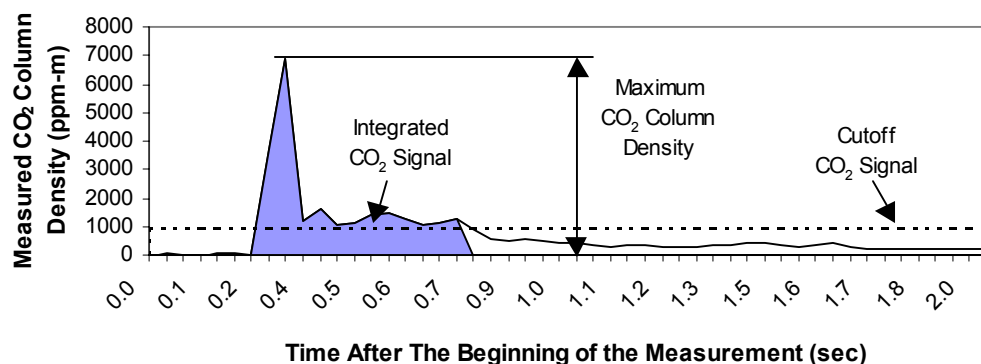
Figure 4-6: Schematic of a remote sensing plume signal vs. time, with the definitions of the parameters used to describe plume capture

The time-integral of CO_2 is in principle a better measure of plume capture, since this parameter has a stronger relationship with the signal-to-noise ratio of the remote sensing measurement.[100] The maximum CO_2 column density is inherently more affected by the details of the local dispersion and therefore more random. However, it has been retained for this analysis for two reasons: first, its modeling is much more straightforward than that of the time-integral of CO_2 column density. Second, all of the groups which have performed a significant number of remote sensing measurements (Prof. Stedman's group at the University of Denver, Remote Sensing Technologies, and Hughes "Smog Dog") group use the maximum CO_2 as a the variable representing the strength of plume capture.[101] Sections 4.3.4 and 4.3.7 shows the experimental distributions of both parameters.

---

[100] The emission index is calculated from the regression of the NO column density vs. the CO_2 column density (Figure 5-6). The uncertainty of the slope returned by this regression analysis is more dependent on the total CO_2 (the number of points entering the analysis and their individual signal-to-noise ratios) than on the signal-to-noise ratio for the one point with the largest CO_2 signal. This consideration is applicable to all remote sensors, independent of the technology used.

[101] For Prof. Stedman's group and Hughes "Smog Dog" this was observed in some of their data files that they made available to us. For Remote Sensing Technologies (RSTi) it was observed in the description of their datafiles by Walsh and Gertler (Walsh *et al.*, 1997).

4.3.2. Expected CO_2 Column Density in Automobile Remote Sensing: Fluid Mechanical Model

The flow of the gases exiting the tailpipe is an axial jet in a rather complicated bluff-body wake, which normally features a recirculation zone attached to the vehicle near the tailpipe (see section 4.2.1).

As a first approximation to estimate the signal levels that can be expected on remote sensing an unperturbed axial jet can be assumed. A visualization of such a jet is shown in Figure 4-7 (Kurima *et al.*, 1994). A general characteristic of these jets is the existence of a "potential core" which lasts a few nozzle diameters (Beer and Chigier, 1972) where the jet has not mixed with the surrounding fluid.
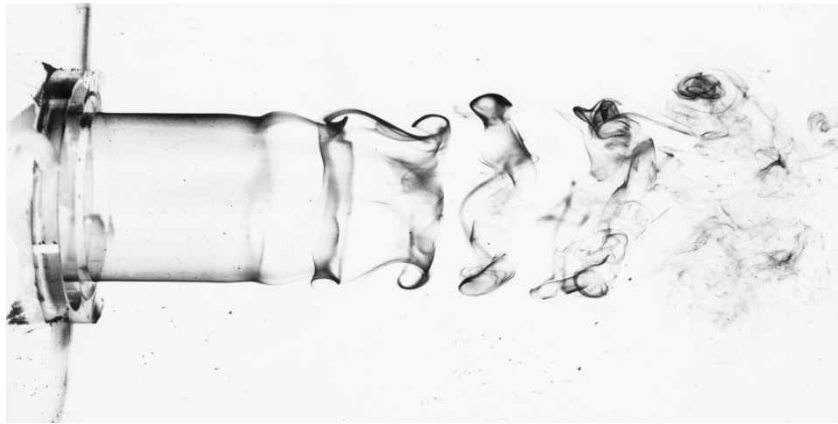
Figure 4-7: Visualization of an axisymmetric jet showing the potential core and the jet breakup and mixing region

A remote sensing system such as the TILDAS instrument described in section 5.2 sends a light beam across the road to a retro-reflector which then returns the beam to an optical detector. Under ideal conditions both the outgoing and the incoming light beams would traverse the undiluted exhaust for a distance of 2 tailpipe diameters, as shown in Figure 4-8. This is what we call the "direct hit" model.

The tailpipe diameter of a typical automobile is 2 inches or 5 cm and the exhaust CO_2 concentration is about 13.4% for stoichiometric combustion. This yields a "direct hit" signal strength of 13,400 ppm-m. The signal strengths observed in the real world are of this order. Signal strengths lower than 1,000 ppm-m CO_2 are rejected as too low for good signal-to-noise ratio.
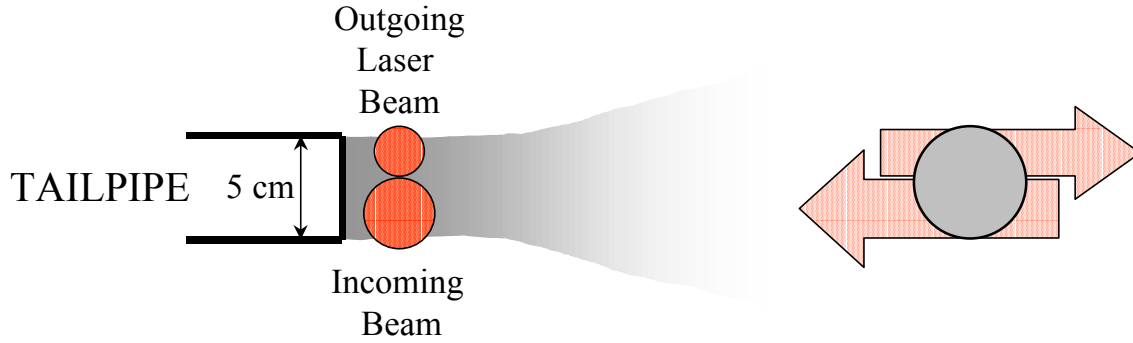
Figure 4-8: Schematic diagram of the TDL laser beam traversing the exhaust jet

4.3.3. Expected CO_2 Column Density in Automobile Remote Sensing: Cylindrical Exhaust Model

A more realistic and flexible model to quantify the CO_2 column density that takes into account the instantaneous fuel economy can be derived in the following way:

Let's assume that the exhaust plume leaving the tailpipe is a cylinder whose cross-sectional area is determined by the exhaust flow rate in the following way:

$$A = \frac{\text{Exhaust Volumetric Flow Rate}\,(m^3/s)}{\text{Vehicle Speed}\,(m/s)}$$

Then, calling D the plume diameter, a "direct hit" of such a cylinder will result in a CO_2 column density of:

$$CO_2 \text{ Column Density} = 2 \cdot D(m) \cdot (CO_2 \text{ concentration}) =$$

$$= 2 \cdot D \cdot 134{,}000\,\text{ppm} = 268{,}000 \cdot \sqrt{\frac{4 \cdot A}{\pi}} \quad \text{ppm} - m$$

This expression can be evaluated numerically using the second-by-second data of a modern vehicle in a driving cycle from the SFTP program (Liberty *et al.*, 1997). The distribution of maximum column densities predicted by this model for one vehicle[102] is shown in Figure 4-9. The values predicted by the model are centered between 10,000 and 20,000 ppm-m, with a long tail up to 40,000 ppm-m.

---

[102] See section 4.5 for the details on the calculation of the exhaust mass flow and temperature.

The variation of the model results vs. vehicle speed and specific power[103] are shown in Figure 4-10. Although with significant larger scatter, the predicted maximum CO_2 column density decreases with vehicle speed and increases with vehicle specific power.[104]
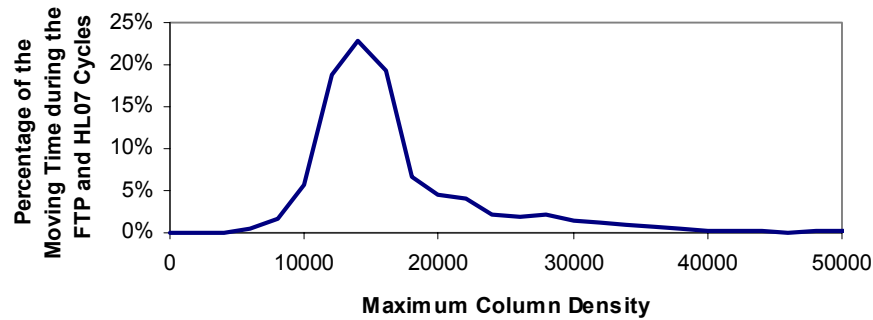
Figure 4-9: Distribution of expected maximum CO_2 column densities for the second-by-second data of a 1994 Jeep Cherokee tested on the FTP and HL07 driving cycles
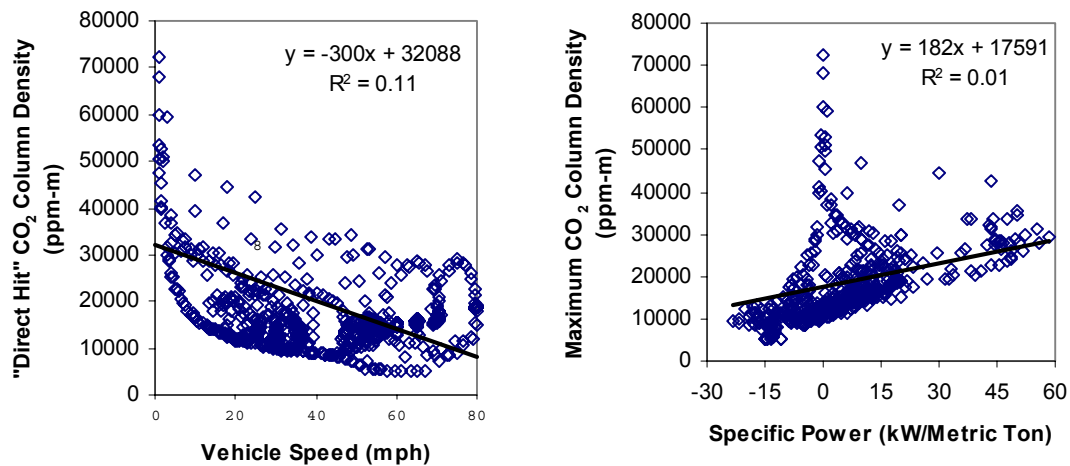
Figure 4-10: Variation of the expected maximum CO_2 column densities vs. speed and specific power for the second-by-second data of a 1994 Jeep Cherokee tested on the HL07 driving cycle

---

[103] Specific power is the instantaneous engine power per unit mass of the vehicle. It is defined in section 3.1.1.

[104] This is the same as saying that, according to the model, the exhaust gas volume per unit distance tends to decrease with speed and to increase with specific power.

4.3.4. Experimental Distribution of Plume Capture

A remote sensing campaign involving the measurement of emissions from about 1,500 cars and light-duty trucks was carried out in the Los Angeles area in Nov. 1996 (as described in Chapter 6). The distributions of the plume capture parameters for this study are presented below.

A scatter plot of two plume capture parameters defined in section 4.3.1, the maximum CO_2 and the time-integrated CO_2 observed for each vehicle is shown in Figure 4-11. The two parameters are correlated but with a large scatter.
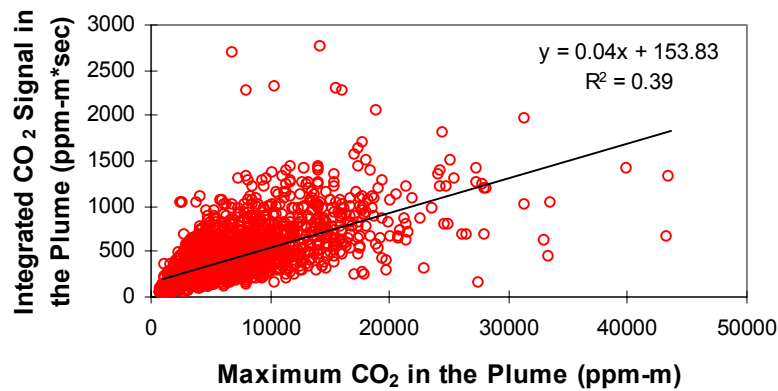
Figure 4-11: Scatter plot of the two plume capture parameters

Parameter	Integrated CO₂ Signal (ppm-m*second)	Highest CO₂ Column Density (80 Hz data)	Highest CO₂ Column Density (60 Hz data)
Number of Vehicles	1528	551	977
Average	459	9185	7356
Standard Deviation	337	5972	5248
Maximum	2730	43416	43684
Minimum	17	1072	1072
Max/Min	163	41	41
Skewness	1.5	1.3	1.8

Table 4-2: Statistics of the distributions of the parameters measuring plume capture[105]

---

[105] Only the measurements for which the CO_2 signal was larger than a minimum of 1,000 ppm are included.

The statistics of both parameters are presented in Table 4-2. We acquired data at two different rates (60 Hz and 80 Hz) which yielded slightly different statistics.[106] The maximum values observed are of the order of the maximum results of the model in section 4.3.3, while the experimental average is about one-half of the expected values from the models in sections 4.3.2 and 4.3.3.
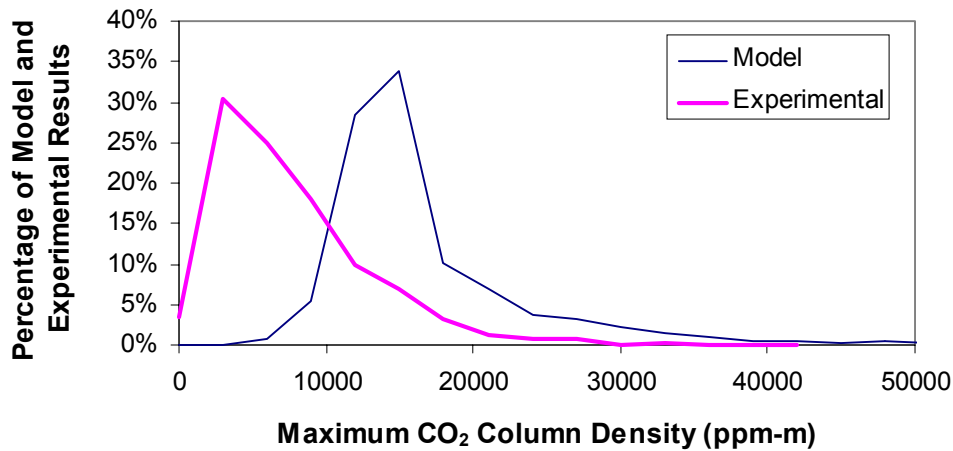
Figure 4-12: Histogram of maximum CO$_2$ column densities observed experimentally, compared to the results of the model in section 4.3.3
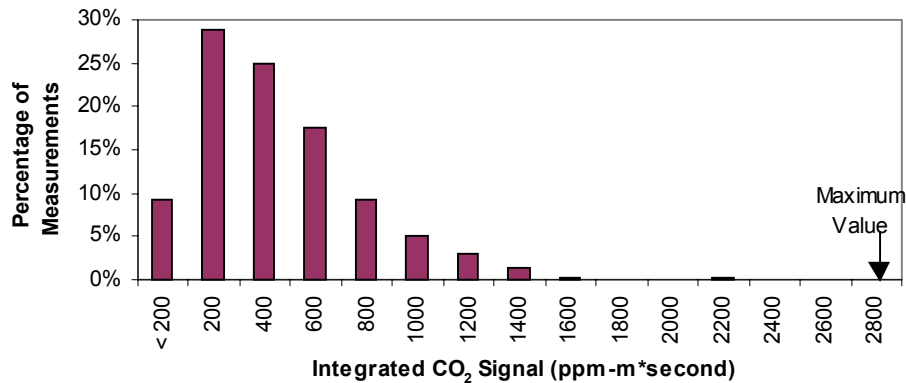
Figure 4-13: Histogram of integrated CO$_2$ signal levels observed

The distributions of both parameters are shown in Figure 4-12 and Figure 4-13. Both parameters have similarly skewed distributions. The experimental distribution of maximum plume capture is of the same order but is shifted to lower values than the

---

[106] The higher rate (80 Hz) resulted in slightly higher values since it was better able to capture transient spikes.

model results, most likely due to dispersion of the exhaust in the automobile wake and variations in tailpipe height.

4.3.5. Variation of Plume Capture with Vehicle Speed, Acceleration, and Specific Power for One Vehicle

It is interesting to study the variation of plume capture vs. speed, acceleration, and specific power, since dispersion increases with vehicle speed, while the amount of gases generated per unit distance increases with specific power and decreases with speed (see Figure 4-10). Figure 4-15 and Figure 4-14 show the variation of the plume capture parameters vs. speed, acceleration, and specific power for a single car (a prototype ULEV) that was measured repeatedly at the same location.[107]

The trends observed in the figures can be explained by the trends of exhaust volume per unit distance (modeled in section 4.3.3) plus the effect of dispersion, which increases with increasing vehicle speed but is mostly unrelated to acceleration or specific power at a constant speed[108, 109]. First, plume capture decreases with vehicle speed (leftmost graph), which agrees with both the trend of the model of exhaust volume per unit distance and with the increase of dispersion with speed.

Second, the model predicts that plume capture should increase with increased exhaust mass flow rate, which is larger for larger specific powers. But since specific power is correlated with speed,[110] and speed increases dispersion and lowers plume capture, no effect is seen (rightmost graph). Acceleration (center graph) is strongly correlated with power but not with dispersion, and a trend of larger plume capture with larger acceleration is seen (second graph).

---

[107] The NO remote sensing measurements of this car are presented in section 5.4.2 and the CO measurements are in section 3.3.4.

[108] It may be related to specific power by the correlation of this parameter with speed, see Figure 6-9.

[109] The results of the time-integrated CO_2 signal are considered more meaningful since the maximum CO_2 signal is more influenced by the details of local dispersion and is inherently more random. In addition the former parameter has a better relationship with the signal-to-noise ratio of the remote sensing measurement as explained above.

[110] See Figure 6-9 for a scatter plot of these 2 parameters for a vehicle fleet. The correlation is also present for this vehicle (not shown).
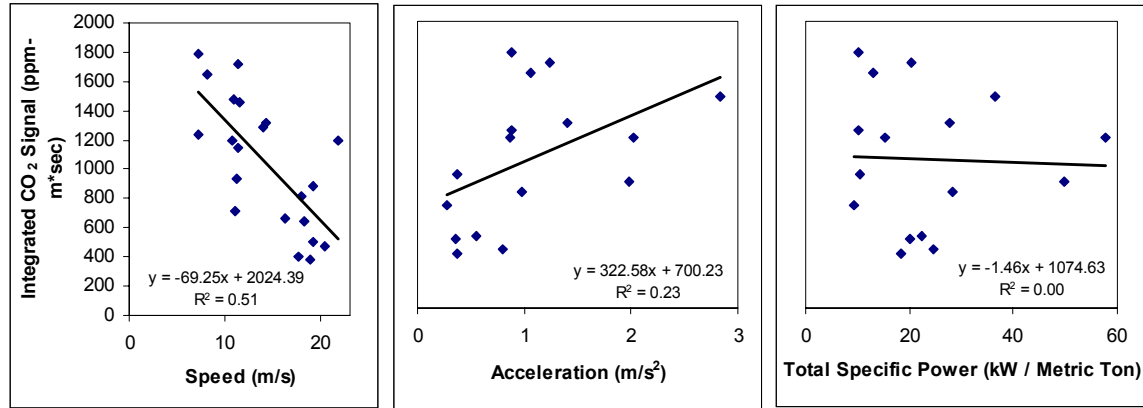
Figure 4-14: Effect of speed, acceleration, and specific power on the <u>time-integrated CO_2 signal</u> for a single car measured repeatedly on the same location
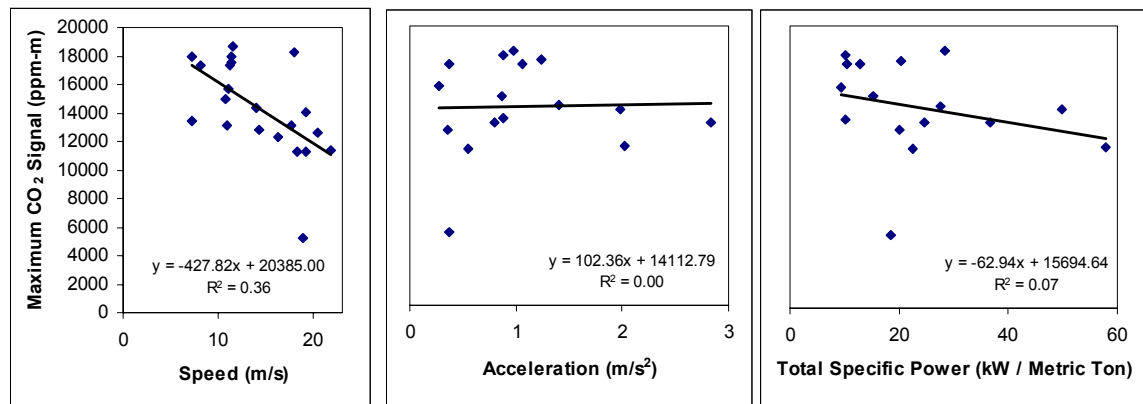
Figure 4-15: Effect of speed, acceleration, and specific power on the <u>maximum CO_2 signal</u> for a single car measured repeatedly on the same location

4.3.6. Variation of Plume Capture with Vehicle Speed, Acceleration, and Specific Power for a Vehicle Fleet

The same graphs (plume capture vs. speed, acceleration, and specific power) for all the vehicle fleet that we measured at El Segundo are shown in Figure 4-16, Figure 4-17, and Figure 4-18. The same trends observed in Figure 4-14 for the prototype ULEV appear in the regression equations, but with much more scatter. This indicates that the differences in dispersion between different vehicles are dominant,[111] which can be explained by the critical dependence of the wake flow patters on vehicle shape and speed and tailpipe location (section 4.2.1).

---

[111] Changes in local dispersion due to strong winds may also cause large variability in plume capture. However during our measurement campaign at El Segundo no significant wind was present.

As in the case of the ULEV data, plume capture increases with acceleration, indicating that higher power conditions yield better signal levels for remote sensing measurements. To separate the effect of power and speed plume capture has been plotted vs. specific power at a constant speed in Figure 4-19. A positive correlation between both parameters is observed as expected. This result explains the observations of Verdegem (1997) and Walsh and Kite (1998), who reported that performing remote sensing on a site where vehicles were decelerating produced significantly fewer valid readings than at a site where vehicles were under acceleration.
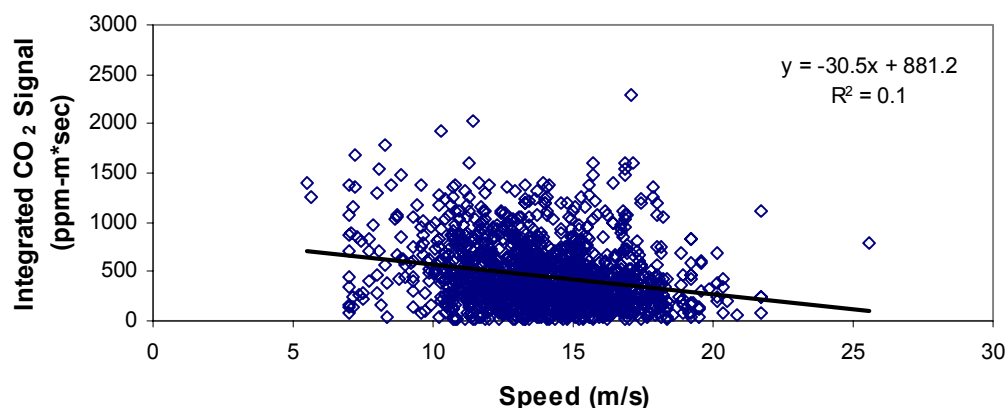
Figure 4-16: Time-integrated CO$_2$ signal vs. vehicle speed
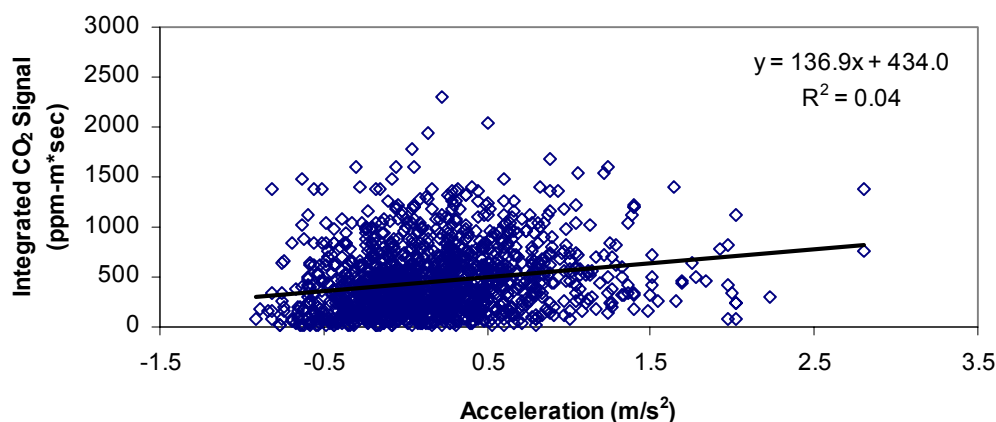
Figure 4-17: Time-integrated CO$_2$ signal vs. vehicle acceleration
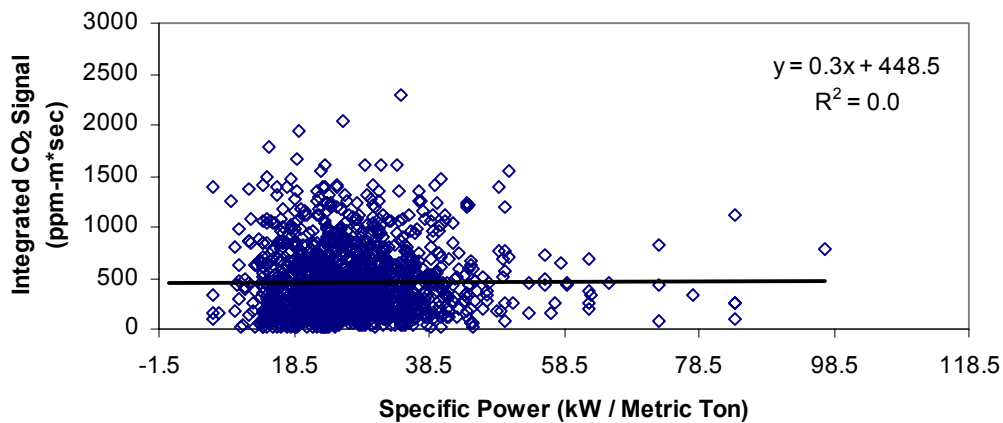
Figure 4-18: Time-integrated CO_2 signal vs. vehicle specific power
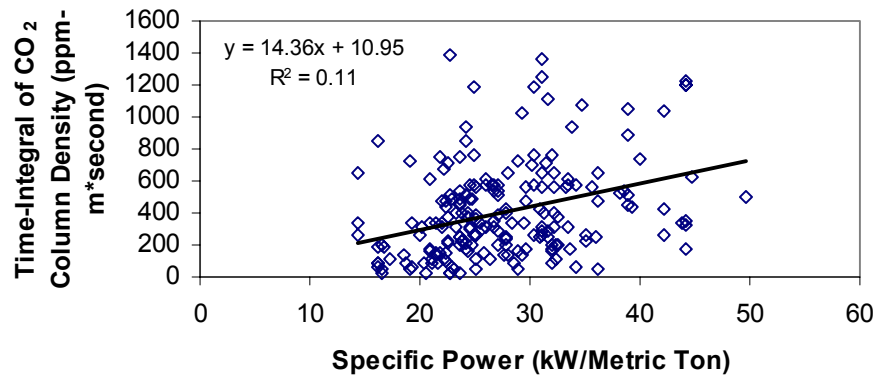
Figure 4-19: Time-integrated CO2 signal vs. specific power at a constant speed[112]

4.3.7. Plume Capture in the Heavy Duty Diesel Truck Measurements

The maximum CO_2 signal levels for heavy-duty diesel trucks observed during the experiments described in Chapter 7 are similar to those observed in the automobile measurements. A comparison of the distribution of the maximum CO_2 signal for the two data sets is shown in Figure 4-20. This comparative result is reasonable since heavy-duty trucks have about twice as large exhaust pipe diameters and about one-half the CO_2 concentration than automobiles, which would result in the same signal level according to the "direct-hit" model (section 4.3.2).

---

[112] The vehicles in this figure have speeds between 14 and 15 m/s.

The duration of the elevated CO_2 signal, however, is much larger in the case of the heavy-duty trucks as compared to the automobiles. Most automobile plumes last only 0.25-0.5 seconds, while most heavy-duty truck plumes last[113] more than the 2 seconds for which we acquired data. This is reflected in the values of the time-integrated CO_2 signal, which is about twice as large as that for automobiles on average. The fuel economy of a heavy-duty truck is about one-fourth of that of a typical automobile,[114] so about four times the amount of CO_2 is be emitted by a heavy-duty truck as compared to an automobile. The reason that the time integrated signal is only about a factor of 2 larger probably lies with the faster dispersion of the truck plume since in this configuration the exhaust jet meets a perpendicular air flow and mixes with ambient air faster than in the automobile case (Chen *et al.*, 1996).
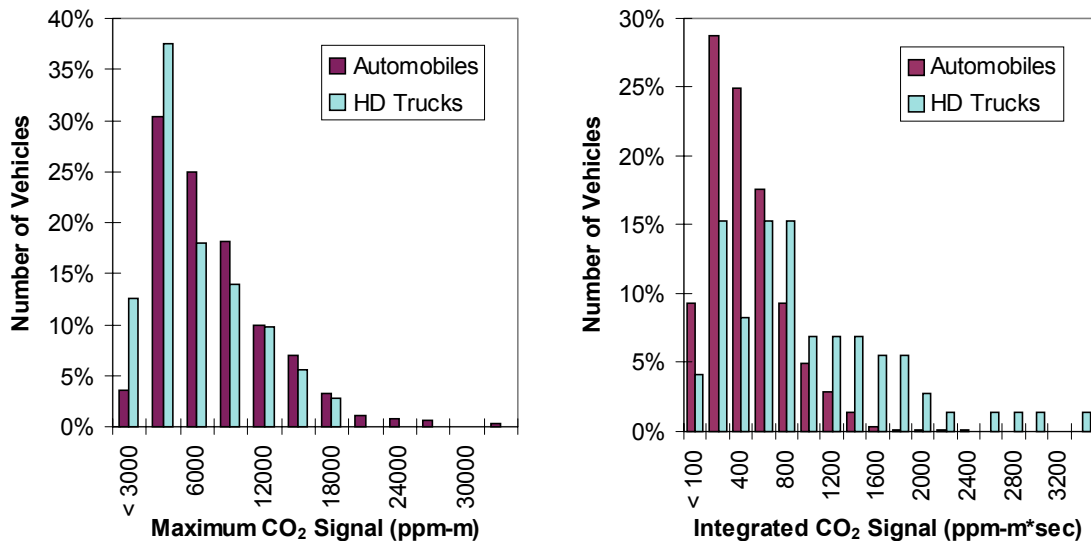
Figure 4-20: Histogram of maximum column densities observed on individual automobile and heavy-duty truck remote sensing measurements

---

[113] The duration of the plume is defined here as the time that the signal stays above the minimum signal level of 1,000 ppm CO_2.

[114] About 6 mpg (Berges *et al.*, 1993; Brown, 1997) vs. about 25 mpg.

4.4. Variations of the Precision of Remote Sensing Measurements

It is important to distinguish between the detection limit and the measurement precision of a remote sensing reading. The detection limit for NO, for example, is the measurement precision in the limit of low NO column density. In this limit, the dominant noise source is the detection of the NO absorption features. At higher column densities, the quantification of the NO absorption depth will no longer be the dominant source of noise. Other potential noise sources include laser line width variation, noise in the measurement of the laser intensity returned to the detector, variation of the background NO concentration in the optical path and variation in the plume temperature or pressure. Typically these effects limit the instrument to a precision of approximately 2-3% in the measurement of the NO column density even for very high NO concentrations. In addition there is a similar level of noise in the measurement of the carbon dioxide column density. Both noise sources contribute to the total noise in the NO emission index since the index is calculated as the ratio of the two column densities.

This is highlighted in Figure 4-21 where the NO column density is plotted versus the CO_2 column density for two hypothetical measurements (error bars not to scale). As in Figure 5-6, the emission index would be the slope of a line going from the origin to the data point in each case. As it can be seen, at low NO/CO_2 ratios the noise in the NO column density measurement dominates the noise in the NO/CO_2 measurement. The measurement precision will equal the detection limit in this case. In contrast, at high NO/CO_2 ratios the noise in the measurement of the CO_2 column density becomes dominant. For example, if we measure a car which is emitting 3,000 ppm NO, the noise in the NO channel (a few ppm NO) is negligible compared to the noise from the CO_2 channel and other sources, which is equivalent to about 2.5% of 3,000 ppm, or 75 ppm NO. In this case the measurement precision is much larger than the detection limit.
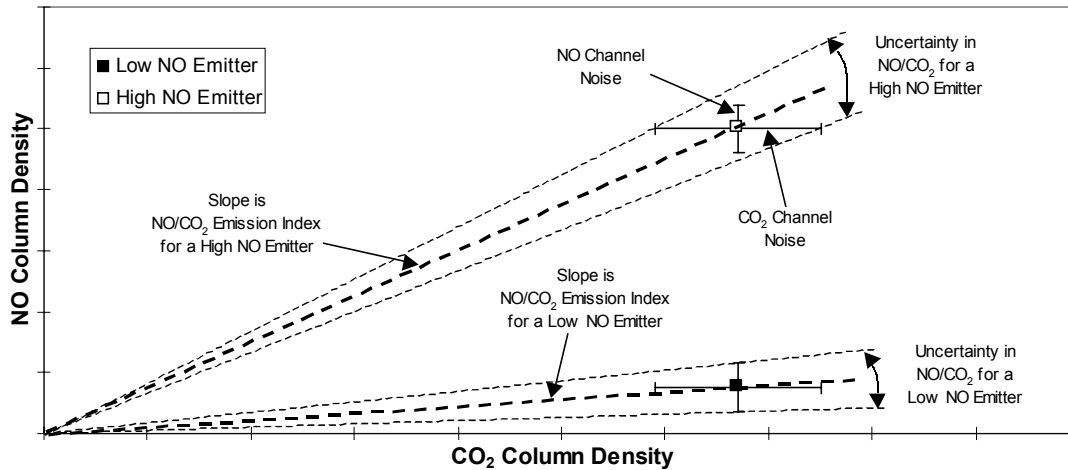
Figure 4-21: Effect of the noise in the NO and CO_2 channels on the NO/CO_2 ratio measurement

A final point is that the measurement precision is also dependent on how well the exhaust plume from the vehicle overlaps with the path of the laser light. Since the noise in the CO_2 and NO column densities is basically independent of the total column density being measured, a lower amount of both gases will result in more measurement uncertainty. In other words, the signal-to-noise ratio is larger for a larger signal since the noise is about constant. This is shown in Figure 4-22.

For this reason it is preferable to choose remote sensing sites where the vehicles are under significant load, since they will generate a larger volume of exhaust gases which increases the probability of having a larger signal . This has been observed experimentally in this study (as described in section 4.3.5 and 4.3.6).

But even at a single site each vehicle will be measured with a different precision. The distribution of the signal strengths obtained from remote sensing of 1,500 vehicles in California (Chapter 6) was shown in Figure 4-12. We can see from that figure that a wide range of signal strengths are observed for different vehicles driving through the same remote sensing site.
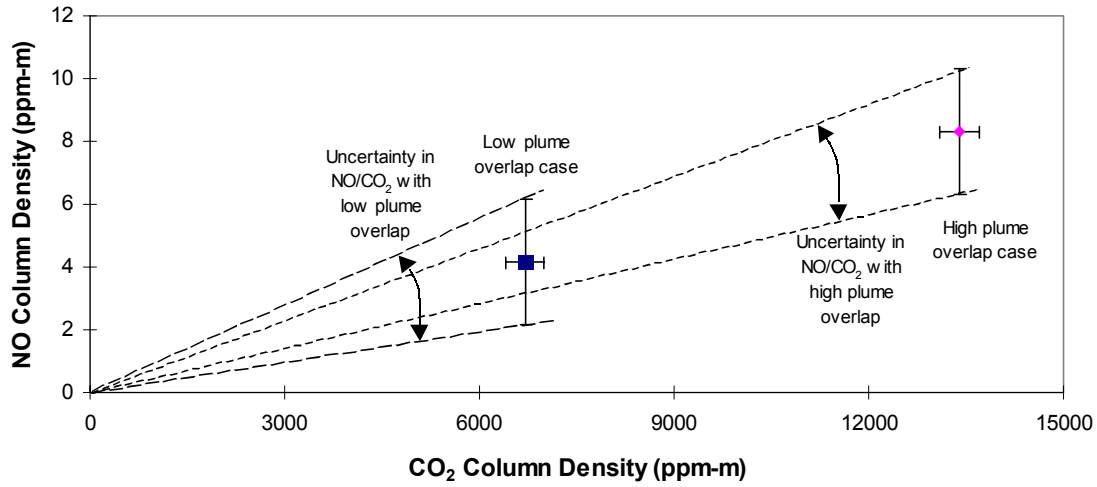
Figure 4-22: Effect of Plume Overlap in the NO/CO₂ Measurement Noise

The expected noise in the NO measurement has been estimated as a function of NO concentration and CO_2 column density from the propagation of errors in a ratio (Harris, 1987):

$$\text{if } R = \frac{NO}{CO_2} \Rightarrow \sigma_R (\%) = \sqrt{\sigma_{NO}^2 (\%) + \sigma_{CO_2}^2 (\%)}$$

$$\text{then } [NO \text{ noise}] = \sigma_R (\%) * [NO \text{ Emission}]$$

Those operations have been performed for the NO emission levels and CO_2 column densities of the California remote sensing data set (Chapter 6). The results are shown in Figure 4-23 and Figure 4-24.
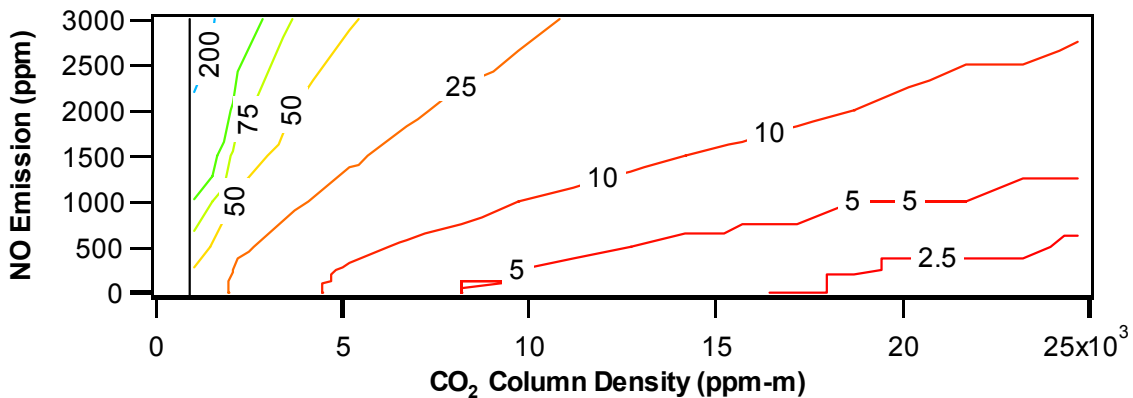
Figure 4-23: Average noise in the returned NO concentration (ppm) as a function of CO₂ column density and NO emission level
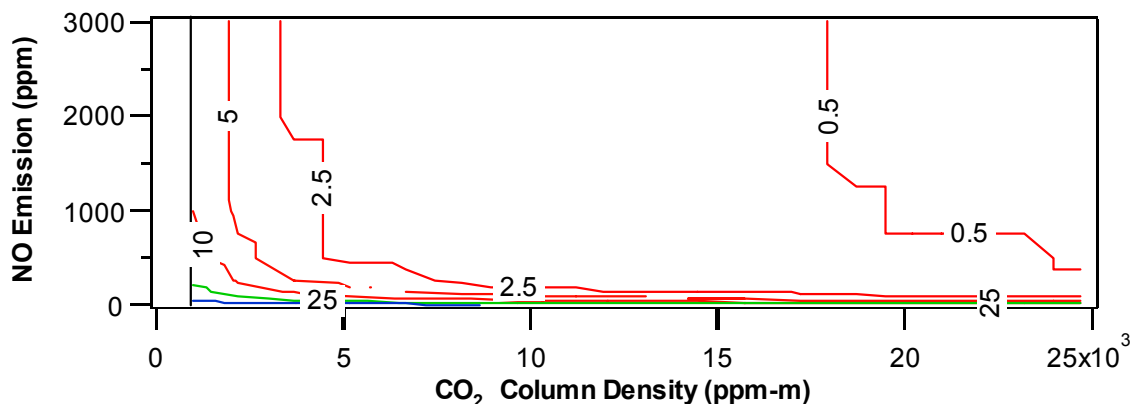
Figure 4-24: Average noise in the returned NO concentration (% of NO concentration) as a function of CO₂ column density and NO emission level

Figure 4-25 shows the location of the 1473 vehicles whose NO emissions we measured in California (Chapter 6) on the map of Figure 4-23. Clearly the range of measurement precisions for the different vehicles spans a factor of 50 in ppm units, from about 1 ppm for low emitters with high signal to more than a 100 ppm for high emitters with high signal.

The stated precision of the TILDAS instrument (3 ppm NO) corresponds to a "direct hit"[115] of about 13,400 ppm-m CO_2 and very low NO, while the fleet average precision (5 ppm NO) corresponds to the level of noise at the average plume capture level of about 8,000 ppm-m CO_2 [116] and low NO.
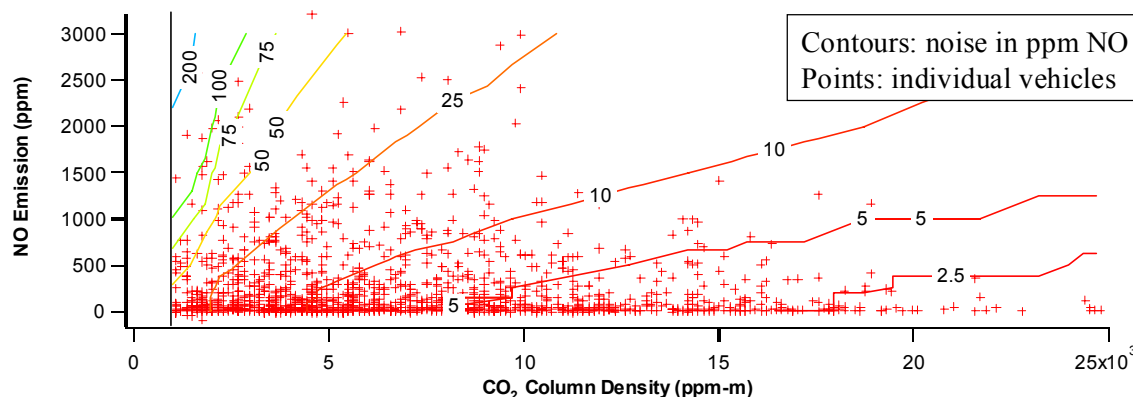
Figure 4-25: Location of the 1473 vehicles measured in California in the map of Figure 4-23

---

[115] See section 4.3.2.

[116] See Table 4-2

The points illustrated in this section are applicable to all remote sensing instruments independent of the particular spectroscopic technology being used.

4.5. Residence Time in the Exhaust System

There is some time delay from the instant at which the pollutants are made inside the engine during combustion and the instant when those exhaust gases leave the vehicle tailpipe. This delay is important with respect to the usefulness of the vehicle speed and acceleration measurements taken simultaneously with remote sensing measurements. The location of interest correspond to the vehicle position at the instant when the exhaust gases which are leaving the tailpipe in the line of sight of the remote sensor were made in the engine. That was the moment that produced the measured exhaust gas and in which the engine supplied the instantaneous power demand reflected in the vehicle speed and acceleration measurements.

We have estimated this delay and distance with a simple model of the exhaust process using second-by-second data from the Supplemental FTP program to obtain the distribution of actual values under normal operation.

The distance traveled by the vehicle while the exhaust gases flow from the engine to the tailpipe is:

Distance = (Vehicle Speed) * (Gas Residence Time)

And the gas residence time can be calculated using a simple plug-flow model as:

$$\text{Gas Residence Time} = \frac{\text{Volume of the Exhaust System}}{\text{Exhaust Flow Rate}}$$

Second-by-second data of speed, flow rate, and engine-out and catalyst temperature for many recent production vehicles tested on different driving cycles are publicly available from the Supplemental FTP research program (Liberty *et al.*, 1997). These data can be used to compute the results of the model above for the actual operating conditions that a vehicle is likely to encounter. The instantaneous flow rate has been calculated as:

Flow Rate = (Standard Flow Rate) * (Average Exhaust Temperature)

Since significant cooling takes place on the exhaust system (e.g. compare Figure 5-12 and Figure 5-13) and tailpipe exit temperature is not available from the SFTP data set, the average exhaust temperature has been estimated by averaging the engine-out

temperature at each point with a regression to the temperature vs. speed data of Figure 5-13.

These computations have been performed here for a 1994 Jeep Cherokee tested on the FTP and HL07[117] driving cycles. To estimate the exhaust system volume of the Jeep Cherokee, we modeled the exhaust system of this vehicle as a straight pipe of 6 cm in diameter and about 3.5 meters of length. Catalyst and muffler volumes are 4.5 and 16.2 liters, based on external measurements on one such vehicle. These estimates yield a total volume of 31 liters for the exhaust system.

The distributions of residence times in the exhaust system and distance traveled during that residence time are shown in Figure 4-26 for this vehicle and test cycles. It can be observed that the residence time varies between about 0.1 and 4 seconds and the distance traveled during this interval is between 0.1 and 25 meters most of the time. High power demand conditions such as those in the HL07 cycle result in shorter residence times and smaller distances traveled.
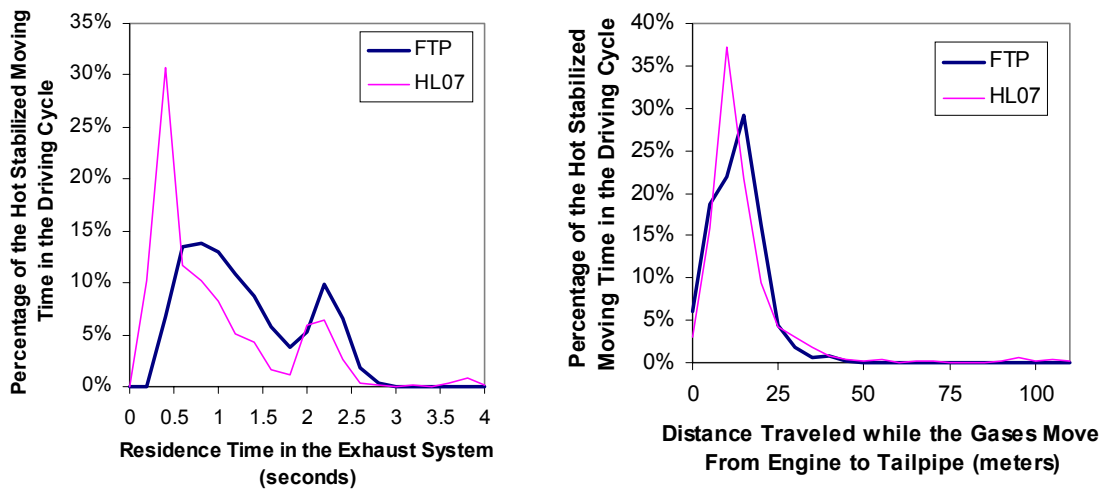
Figure 4-26: Distribution of residence times of the exhaust gases from the engine to the tailpipe, and of distance traveled during that period for a 1994 Jeep Cherokee during the FTP and HL07 driving cycles

In our model this distance is influenced by three basic factors: exhaust flow rate and temperature, which determine residence time, and vehicle speed, which determines the distance traveled during that time. Exhaust mass flow rate is closely related with

---

[117] A high power driving cycle (Haskew *et al.*, 1994).

specific power.[118] The volumetric flow of exhaust is proportional to the exhaust mass flow and to the exhaust temperature, which also increases with specific power.[119] Thus it is logical to analyze the variation of the distance vs. specific power and vehicle speed.

The scatter plots of the distance traveled vs. specific power and speed are shown in Figure 4-27 and Figure 4-28 respectively. The relationship is much better with specific power than with vehicle speed, but significant scatter appears on both plots, indicating that neither parameter is dominant.

To show simultaneously the dependence of the distance traveled during the exhaust residence time on specific power and vehicle speed, a contour plot of distance traveled by the vehicle vs. both parameters is shown in Figure 4-29. High powers at low speed can result in very short distances while very low powers at high speed yield very long distances. For the positive powers which are most interesting for remote sensing,[120] this distance varies from 0.1 to 25 meters.
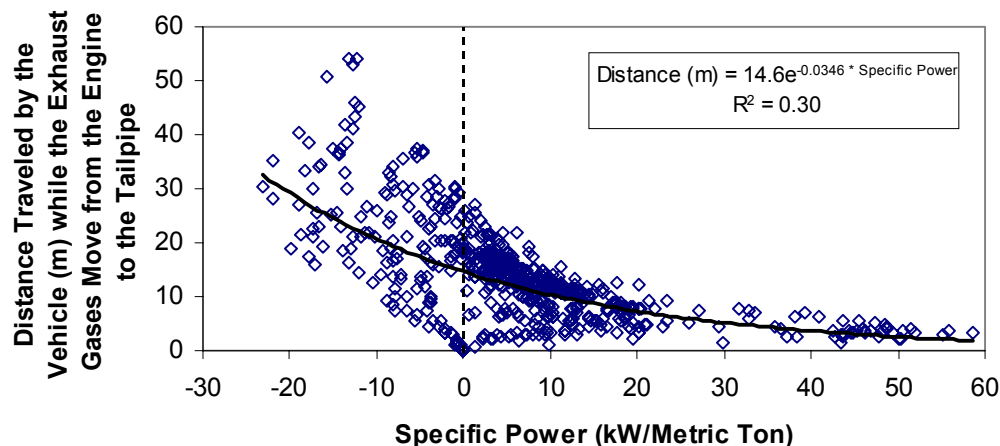
Figure 4-27: <u>Distance traveled</u> by a 1994 Jeep Cherokee while the exhaust gases move from the engine to the tailpipe <u>vs. specific power</u> (HL07 cycle)

---

[118] See section 3.1.1 for the definition of this specific power, and Figure 3-8 and Figure 3-15 for the relationship between specific power and fuel flow. Exhaust mass flow equals EMF=(fuel flow)*(1+A/F) where A/F is the air to fuel ratio. Since A/F is maintained at stoichiometric most of the time a very good relationship exists between exhaust mass flow and specific power.

[119] See the temperature variations in Figure 5-12 as the vehicle accelerates, cruises, and decelerates, and in Figure 5-13 vs. speed.

[120] As concluded in section 3.2.2.
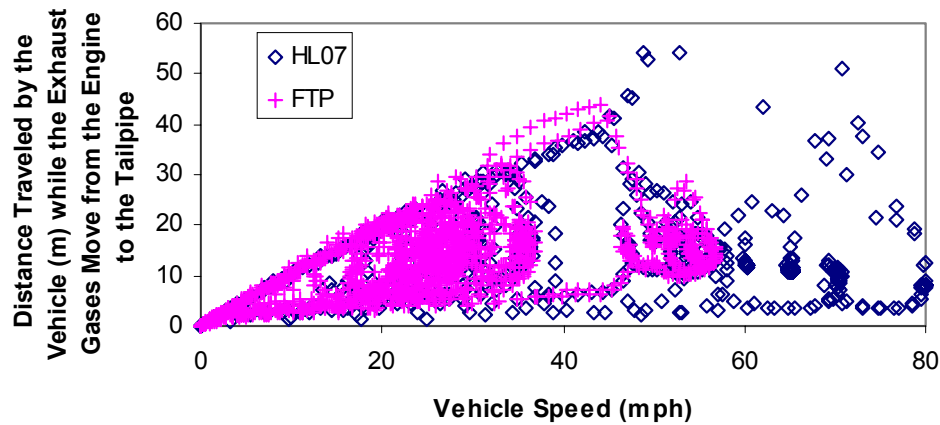
Figure 4-28: <u>Distance traveled</u> by a 1994 Jeep Cherokee while the exhaust gases move from the engine to the tailpipe <u>vs. vehicle speed (FTP and HL07 cycles)</u>
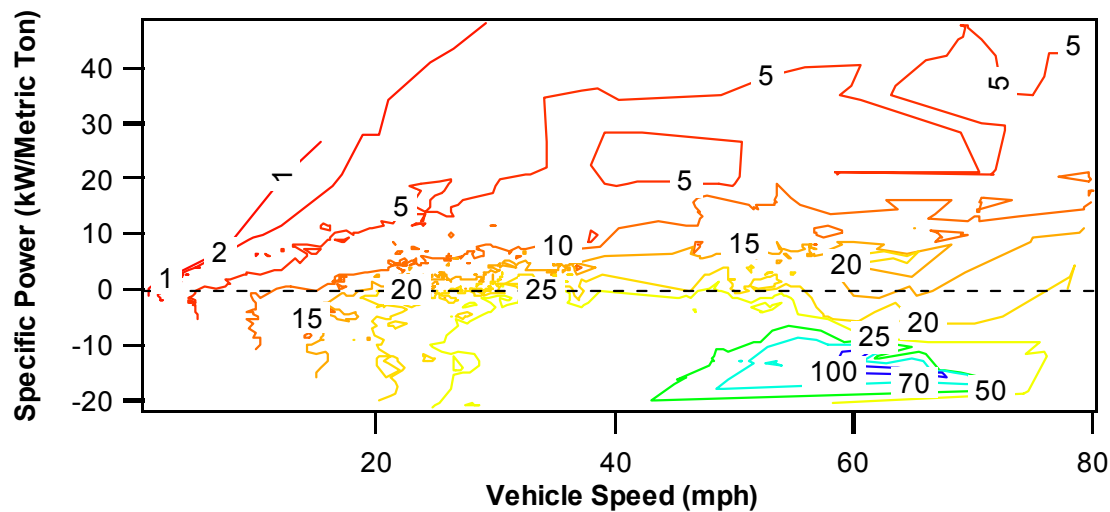
Figure 4-29: Contour plot of the estimated distance traveled by a 1994 Jeep Cherokee while the exhaust travels from engine to tailpipe for (FTP and HL07 cycles)

In conclusion, and although the model presented here is limited by the approximations in the calculation of average exhaust temperatures and because it has been computed for only one vehicle, it illustrates the main issues and the strategy to deal with them:

- The location of interest for the speed and acceleration measurements for remote sensing measurements is that where the exhaust which is leaving the tailpipe was generated in the engine.

- This distance has been estimated to vary between 0.1 and 25 meters for one modern production vehicle tested on two driving cycles, with a strong dependence on vehicle speed and specific power.

- An array of low-cost diodes[121] could be used to determine the speed and specific power profile of each vehicle as it approaches the remote sensor. An algorithm could use an generalized version of Figure 4-29 to determine the location of interest for the speed and acceleration measurements.

- Alternatively, and based on this limited data, speed and acceleration should be measured between 0 and 25 meters to minimize errors associated with this delay. However, based on Figure 4-29, this approach may not be sufficient for all conditions.

---

[121] Such as those described in section 6.2.4.

4.6. Grams-per-mile vs. Grams per Gallon Emission Factors

Remote sensing data can be readily used in emission inventories. One alternative is to convert the concentration results to grams-per-mile (gpm) of each pollutant using the estimated fuel economy.[122] Once the gpm have been determined, they can be combined with estimates of vehicle activity to produce emission inventories.

Another alternative is to convert the pollutant/carbon ratios into grams-per-gallon (gpg) of fuel. These can be combined with fuel sales data to determine the total amount of emissions in a given area (Singer *et al.*, 1996).

Both units are related by the instantaneous fuel economy:

$$\frac{\text{Grams Emitted}}{\text{Miles Traveled}} = \frac{\dfrac{\text{Grams Emitted}}{\text{Gallon of Fuel}}}{\dfrac{\text{Miles Traveled}}{\text{Gallon of Fuel}}} \qquad \text{or} \qquad \text{gpm} = \frac{\text{gpg}}{\text{mpg}}$$

An advantage of the later procedure is that emission rates in gpg vary much less than emission rates in gpm with driving conditions. Pierson et al. (Pierson *et al.*, 1996) reported that in a tunnel study the effect of roadway grade on gram-per-mile emission was substantial while fuel-specific emissions were almost independent of roadway grade.[123]

The variability of gpg vs. gpm emissions has been explored further here by analyzing second by second emission data for a 1993 Toyota Corolla tested on the HL07 high power cycle during the SFTP program (Liberty *et al.*, 1997).

The emission rates of NO_x in gpg and gpm vs. time along the driving cycle are presented in Figure 4-30. The gpm emissions are much more variable (i.e. the ratio of the peak to the average value), while gpg emissions exhibit much more constant values. This indicates that most of the spikes in the gpm emissions are due to large variations of the instantaneous fuel economy (mpg), and that changes due to the amount of NO_x produced per unit fuel (gpg) are much smaller.

---

[122] This has been done in Chapter 6 of this thesis for NO and Chapter 8 for N_2O.

[123] For both light-duty and heavy-duty vehicles, with the exception of light-duty NO_x which increased by a factor of 1.4 from downhill to uphill.
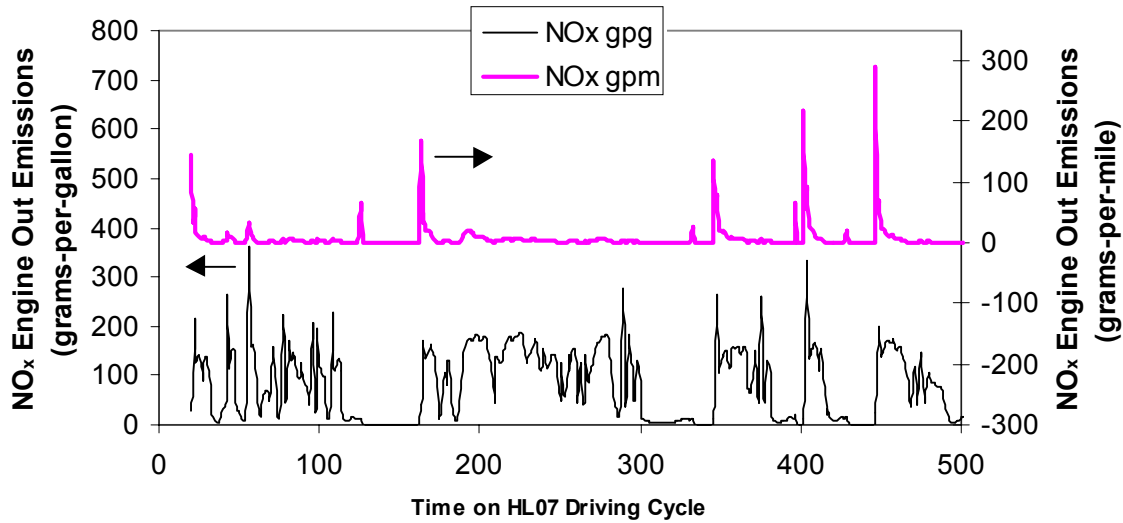
Figure 4-30: Engine out emission rates of NO_x (gpg and gpm) during the HL07 cycle for a 1993 Toyota Corolla

Some statistics of the distributions of the emission rates of CO and NO_x in gpm and gpg for this vehicle and driving cycle are presented in Table 4-3, while their distributions are compared in Figure 4-31 and Figure 4-32.

The statistics and the distributions show again that the emissions in gpg are much more constant along the driving cycle that those in gpm. The ratio of the maximum to the average value is an order of magnitude larger for CO and NO_x gpm emissions than for the gpg emissions, while the ratio of the maximum to the minimum value is 2 orders of magnitude larger.

	CO gpm	NO_x gpm	CO gpg	NO_x gpg
Average	45	7	399	97
Maximum	2267	384	2342	512
Minimum	0.5	0.01	46.3	0.6
Skewness	9.0	10.3	3.0	0.4
Max./Min.	4899	67373	51	898
Max./Avg.	51	55	6	5
Min./Avg.	1.0%	0.08%	12%	0.6%

Table 4-3: Statistics of the distributions of engine out CO and NO_x emissions during the HL07 cycle for a 1993 Toyota Corolla

The conclusion that the emission rates in gpg are an inherently more constant parameter than the gpm emissions. This is a clear advantage of emissions inventories based on gpg emissions.
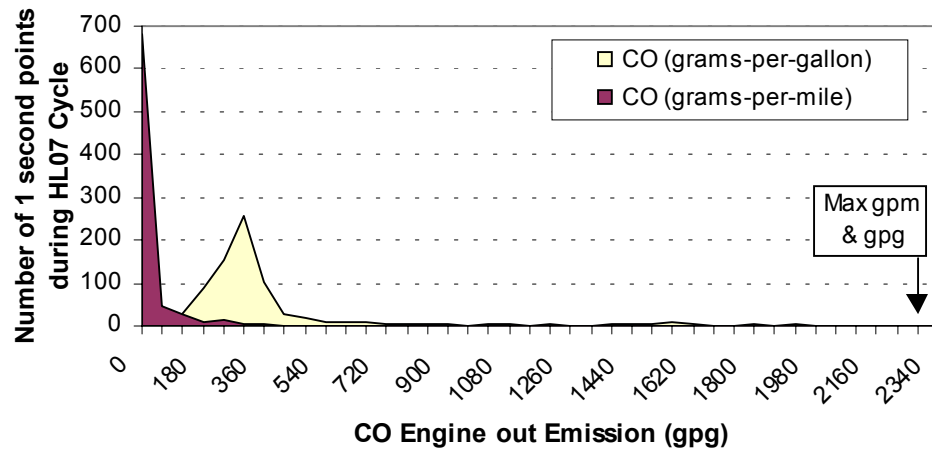
Figure 4-31: Distribution of engine out CO emissions during the HL07 driving cycle for a 1993 Toyota Corolla
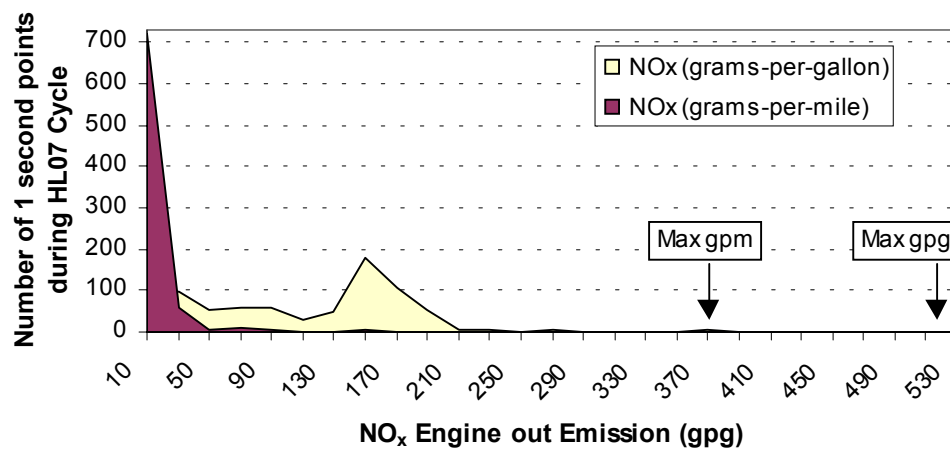
Figure 4-32: Distribution of engine out NO_x emissions during the HL07 driving cycle for a 1993 Toyota Corolla

4.7. The Need to Factor In Relative Fuel Economy

Even though remote sensors measure the emissions directly in grams of pollutant per gallon of fuel, there is a danger of introducing a bias when the concentration (which is equivalent to grams-per-gallon, or gpg) of each vehicle are directly averaged to produce an average concentration or gpg value for the fleet, as pointed out by Singer and Harley (1996). This bias can appear if there is a correlation between emissions and fuel economy.

To simplify, let's assume the following: a remote sensor measures the emissions of two vehicles which emit a constant rate of NO in gpg. Vehicles A and B have emission rates of 10 and 100 gpg NO and fuel economies of 30 and 20 mpg respectively, and they both travel the same distance. If the NO emissions of both vehicles are measured by a remote sensor and averaged to calculate a fleet average gpg value we obtain:

$$\text{Fleet Average NO (gpg)} = \frac{\text{NO Vehicle A (gpg)} + \text{NO Vehicle B (gpg)}}{2} = \frac{10 + 100}{2} = 55 \text{ gpg}$$

while the true emission rate is:

$$\text{Fleet Average NO (gpg)} = \frac{\text{NO Vehicle A (grams)} + \text{NO Vehicle B (grams)}}{\text{Fuel Vehicle A (gallons)} + \text{Fuel Vehicle B (gallons)}} =$$

$$= \frac{\dfrac{NO_A (gpg)}{FE_A (mpg)} * miles_A + \dfrac{NO_B (gpg)}{FE_B (mpg)} * miles_B}{\dfrac{miles_A}{FE_A (mpg)} + \dfrac{miles_B}{FE_B (mpg)}} = \frac{\dfrac{10}{30} * 1 + \dfrac{100}{20} * 1}{\dfrac{1}{30} + \dfrac{1}{20}} = 64 \text{ gpg}$$

or an error of -14% if the different fuel economy is not taken into account.

If emission rates and fuel economies were uncorrelated, this effect would average out. In the real-world however, this is never the case. Light-duty trucks are certified to more lenient emission standards than passenger cars[124] and do show higher average exhaust concentrations (see Figure 6-32 and Figure 8-11), and also have lower fuel economy (Heavenrich and Hellman, 1996). High CO and HC emitters also have lower

---

[124] This will change in California in the next decade. The California Air Resources Board recently approved a regulation package that requires light-duty trucks up to 8,500 lbs. gross vehicle weight to pass the same emission standards of passenger cars by 2007 (CARB, 1998b).

fuel economy since part of the energy of the fuel is escaping with these incomplete combustion products. Also older vehicles have higher average pollutant concentrations (see Figure 6-32) and lower average fuel economy (Heavenrich *et al.*, 1996).

Thus the fuel economy is still necessary to determine emission factors and calculate emission inventories. When this effect is taken into account for the calculation of emission factors from the remote sensing data set obtained with the TILDAS remote sensor in California (Chapter 6 and Chapter 8) the average NO emission increases by 2.5%, with respect to averaging the concentration results. This is a small effect in this case because the fuel economies of the model years with strongest presence are not very different, but could be larger for other data sets acquired in other locations.

4.8. Conclusions of the Analysis of Remote Sensing Measurements

The main conclusions of this chapter are:

- Detailed fluid mechanical studies (e.g. by CFD or in a wind tunnel) of the dispersion of the exhaust gases in the wake of a vehicle would not yield useful information for remote sensing. This is due to the fact that flow pattern of the exhaust gases leaving an on-road vehicle is highly turbulent and unsteady, and highly dependent on the vehicle shape and speed.

- We define plume capture as the column density of CO_2 observed in an individual remote sensing measurement. We propose a simple model for this parameter based on second-by-second driving cycle data. Plume capture levels observed experimentally are lower than the results of the model due to larger exhaust dispersion. Plume capture in the experiments decreases with vehicle speed and increases with specific power at constant speed, in agreement with the model results.

- Plume capture in the heavy-duty diesel truck measurements was about twice as large than on the automobile measurements, which can be explained by four times more CO_2 flow and twice as strong dispersion.

- The noise in the remote sensing measurements depends both on plume capture and on the level of the pollutant measured. High plume captures and low pollutant concentrations yield the best precision while low plume captures and high pollutant concentrations result in lower absolute precision. These effects should be taken into account when using remote sensing measurements for the detection of low and/or high emitters.

- The location of interest for the speed and acceleration measurements for remote sensing measurements is the vehicle position where the measured exhaust leaving the tailpipe was generated in the engine. This distance has been estimated to vary between 0.1 and 25 meters for one vehicle, with a strong dependence on vehicle speed and specific power. It is suggested that an array of low-cost diodes be used to determine the speed and specific power profile of each vehicle as it approaches the remote sensor.

- Grams-per-gallon emission factors are one to two orders of magnitude more constant that grams-per-mile emission factors for a modern production vehicle. It is suggested that gpg emission factors should be used in emission inventories and models.

- The relative fuel economy of the different vehicles should be taken into account when compiling fleet emission factors from remote sensing measurements.

Chapter 5. The TILDAS Remote Sensor

5.1. Introduction

Current remote sensors are limited in sensitivity and range. The use of tunable infrared laser differential absorption spectroscopy (TILDAS)[125] in remote sensing can help overcome those limitations. In this study a TILDAS instrument has been adapted for use as a remote sensor of vehicle emissions. Tunable diode lasers have very high spectral resolution, allowing the monitoring of individual absorption lines. This results in very high sensitivity and chemical specificity. The high sensitivity of the technique was demonstrated by measuring the emissions of an Ultra Low Emission Vehicle (ULEV). This technique has the unique ability to remotely sense minor species of interest in automotive exhaust such as NO_2, NH_3, N_2O, formaldehyde, and other small hydrocarbons. A very long path length is achievable with this technique due to the coherent nature of laser radiation, which allows much more flexible deployment. This TILDAS remote sensor was used to measure the NO_x and N_2O emissions of passenger cars and light-duty trucks (as described in Chapter 6 and Chapter 8), and of heavy-duty diesel trucks (Chapter 7).

This chapter is organized as follows: section 5.2 presents the optical design of the instrument. The data analysis and processing techniques are reviewed in section 5.3. The accuracy and sensitivity demonstrated with this instrument in real-world measurements are reviewed in section 5.4. Section 5.5 summarizes the advantages of the TILDAS technology over the commonly used NDIR technology for on-road remote sensing. The effects of elevated exhaust temperatures on TILDAS remote sensing measurements and the strategies to deal with these effects are reviewed in section 5.6. The determination of gas temperature from TILDAS remote sensing spectra is demonstrated in section 5.7. Finally, section 5.8 presents the conclusions of this chapter.

---

[125] Also known as Tunable Diode Laser (TDL) spectroscopy and Tunable Diode Laser Absorption Spectroscopy (TDLAS).

5.2. Optical layout of the instrument

The TILDAS instrument used in this study measures vehicle pollutant emissions by sending two overlapping infrared laser beams across the roadway through the exhaust plumes of passing vehicles. The lasers simultaneously measure NO and CO_2 emissions with high detection sensitivity and high temporal resolution. The two color spectrometer co-aligns two diode laser beams using a beam splitter (see Figure 5-1). The two beams therefore travel the same path and sample identical portions of the exhaust plume. Both lasers are monitored by the same detector upon returning to the optical table. Their signals are distinguished by rapid temporal multiplexing of the lasers so that only one laser is turned on at any given instant. This two-color across-road instrument was constructed with support from the NASA Atmospheric Effects of Aircraft Program (AEAP) for jet aircraft engine exhaust emission measurements (Wormhoudt *et al.*, 1994; Wormhoudt *et al.*, 1995).
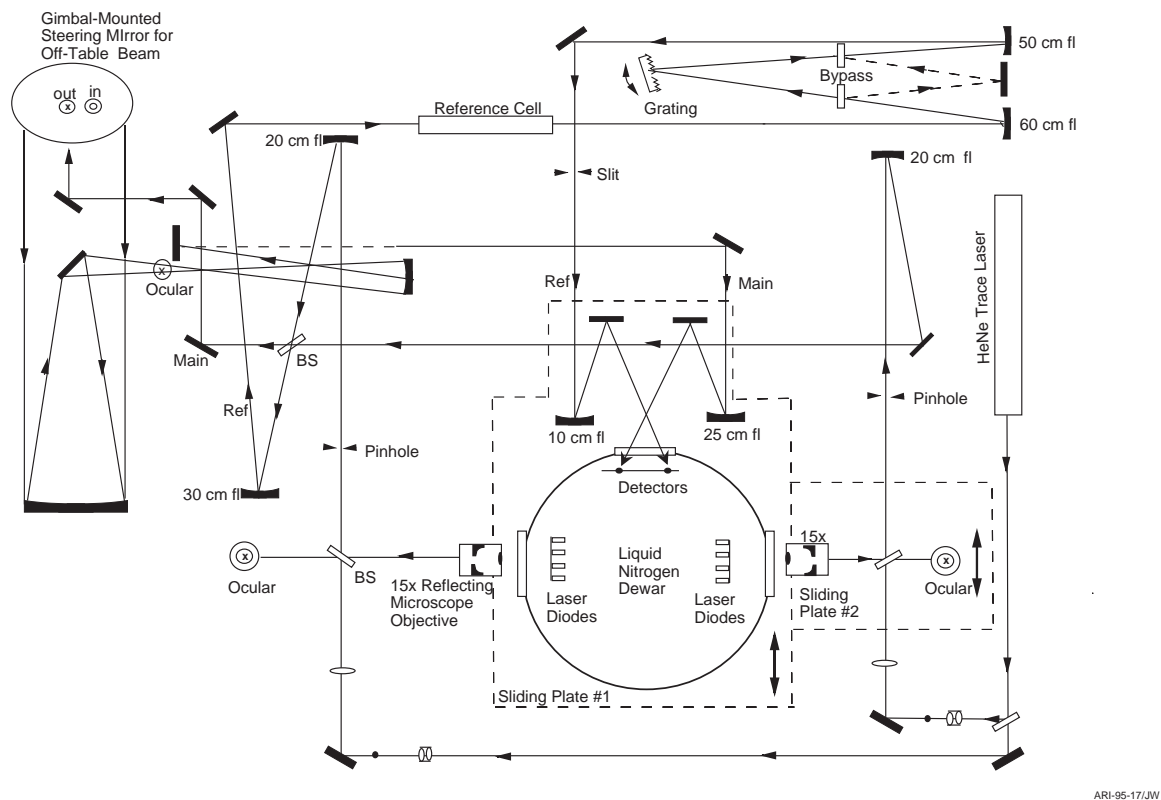
Figure 5-1: Optical layout of the TILDAS dual laser instrument

The optical module of the instrument is shown in Figure 5-1. It is designed to be compact, a design which is facilitated by using a liquid nitrogen dewar that contains the

two laser diodes and the two detector diodes. This dewar offers an excellent alternative to systems with separate detector dewars and helium refrigerator cold heads, especially for field applications.

Infrared light from each of the laser diodes in the dewar is collected by a reflective microscope objective (15x) and focused onto a 200 micron pinhole, which defines the input aperture. This pinhole is used only during alignment, so it is mounted on a removable, kinematically indexed base. The microscope objective is mounted on an X-Y-Z translator to allow accurate focusing into the fixed aperture. Past the input apertures, the two infrared beams are collimated and combined on the main beam splitter. One leg of the beam splitter (the "reference leg") is directed through a gas calibration cell and onto a detector. Light passing through this cell has strong absorption features that are used to identify and lock the spectral line positions. The reference leg also passes through a grating monochromator before being focused onto the detector. The monochromator is useful for identifying the wavelength of the diode during setup of the instrument.

The "signal leg" is directed to a pair of flat mirrors and onto a large gimbal-mounted steering mirror which directs the beam off the table and across the roadway to a corner cube retroreflector. The return beam is collected by the large steering mirror and a curved mirror of similar diameter, passed through several more flat mirrors and finally focused onto the signal beam detector. An ocular can be dropped into the path of the return beam allowing one to observe and optimize the aiming of the outgoing signal beam. While viewing through this ocular the operator can simultaneously adjust the gimbal-mounted steering mirror to place the image of the corner cube over the ocular's cross hairs. Under many conditions, scattered light from the HeNe "trace laser" (see below) can be seen on the corner cube's gold surface showing the precise location of the optical beam at the corner cube.

A parallel visible optical system is employed for alignment and setup. A red HeNe "trace" laser beam passes through a dichroic beamsplitter and is coaligned with the infrared beam. Coalignment is guaranteed by focusing the beam through the input aperture. The trace beam is an indispensable aid for alignment of the optical system. In addition, the trace beam is used to accurately calibrate the monochromator, via higher order diffraction. The fourth port of the dichroic beamsplitter can be used to visibly observe the laser diode. An eyepiece mounted at the position conjugate to the pinhole forms an effective microscope for viewing the laser diode.

5.3. Data Processing and Analysis Techniques

Our data acquisition method is an advanced form of sweep integration which is carried out by a software package developed at Aerodyne Research. This software uses commercially available data acquisition boards to control and monitor the diode lasers. The software sweeps the laser frequency over the full infrared transition or group of transitions, then integrates the area under the transitions using nonlinear least squares fitting to the known spectral line shapes and positions. We do not generally use frequency modulation (FM) techniques because we prefer the clear connection between the direct absorption spectrum and the species' concentration. This data acquisition approach is highly flexible and can be used for many different applications.

There are several advantages to this sweep integration approach. First, absolute species concentrations are returned from the nonlinear least squares fits so that external calibration is not required. The species concentrations are tied to the absolute spectroscopic data found in the HITRAN data base (Rothman *et al.*, 1998). Second, the line shape functions are known from theory and can be precisely calculated, as described in section 2.1.3. Finally, this detailed understanding of the expected line shapes and positions allows one to easily monitor complex and overlapping spectral features. We call this "fingerprint fitting." This is important because monitoring several transitions for one species can enhance sensitivity and is sometimes necessary - especially for larger molecules.[126] In addition, fingerprint fitting allows one to monitor multiple species simultaneously, since we can use overlapping lines, and it even allows one to fit unknown lines which overlap the desired spectrum as a method of removing background absorption from unknown species. This feature is particularly useful in the present application to the analysis of overlapping N_2O and CO_2 lines at atmospheric pressure.

The details of the data acquisition process can be divided into several tasks which we will discuss separately:

- The software creates a waveform which is used to modulate the frequency of the laser or lasers.

- The output of the infrared detectors are recorded as a function of time and this data is stored in the computer's extended memory.

---

[126] E.g. the overlapping CO_2 and N_2O transitions in Figure 5-4, and the 24 overlapping NO_2 transitions in Figure 7-10.

- The program divides the data in extended memory into individual sweeps and averages the individual sweeps to produce one resultant spectrum for each laser.

- The resultant spectra are analyzed spectroscopically to determine the concentrations or column densities of any species which absorb in that spectral window.

- The column densities are displayed to the operator, saved to disk and analyzed to provide emission indices for each of the pollutant species.

The modulation waveform

In the experiments the laser temperature is held constant while the current through each laser is modulated with a computer-generated saw tooth to sweep the output frequency across the infrared transition. The temperature and base current of each laser diode are fixed by a dual laser controller (Laser Photonics, Inc.). Typical modulation waveforms are shown in Figure 5-2. The current is varied linearly for a given time period, which causes a variation of the frequency of the laser light that the diode emits. Then the current is lowered to a much lower value which is below the threshold for laser emission. This provides a measurement of detector output in the absence of laser light. Each laser is below its light emission threshold while the other is swept. Both lasers are below threshold at the end of the scan.
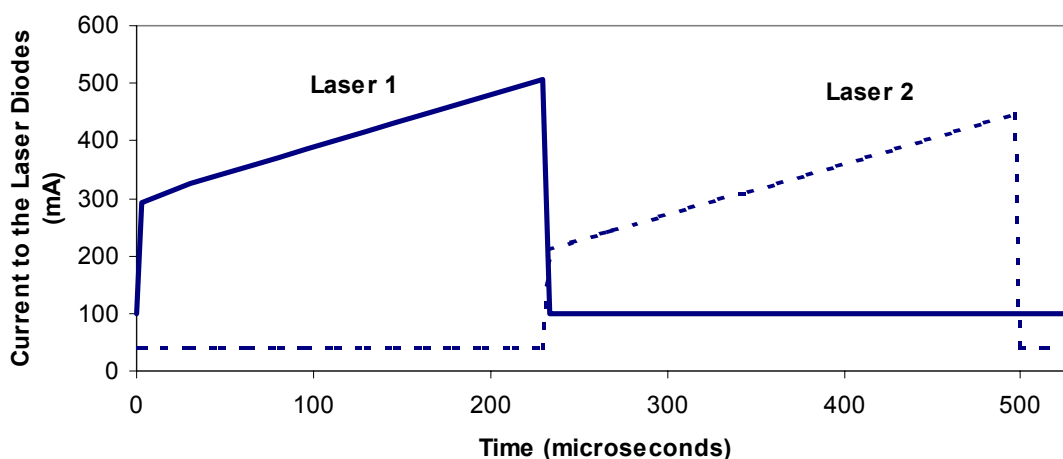
Figure 5-2: Sawtooth current input used to modulate the diode laser frequency

The digital waveform is converted to an analog voltage at a rate of 300 kHz using a 12 bit digital to analog converter (Scientific Solutions, Lab Maser AD). Typically 150 points are used to represent the waveforms so that each frequency sweep is 500 μs in duration.

The infrared detector output

The detector output voltage is sampled by an analog-to digital converter using the same data acquisition board. The individual spectra are automatically transferred to the computer's extended memory using direct memory access.

The averaged spectra

The spectra are coaveraged using assembly language averaging routines in order to maintain a 100% duty cycle. For automotive exhaust measurements, the averaging time is typically set to about 10 ms in order to be able to resolve temporal structure in the exhaust plume (as determined in section 4.2.2). The measurement cycle is triggered by a vehicle blocking the optical path. Usually, the laser beam height is chosen to be about 29 cm which is a typical tailpipe height. In fact, the measurement process actually begins before the vehicle blocks the laser beams since the instrument acquires background spectra continuously while waiting for the next vehicle. The exhaust plume spectra are each divided by the most recent background spectrum in order to eliminate the effects of background absorption and to improve sensitivity. This is especially important for carbon dioxide whose background column density in a 20 meter path (~7,000 ppm-meters) is nearly as large as the initial column density observed in the exhaust plume with optimal overlap of laser and plume (~13,000 ppm-meters).

A pair of background corrected spectra are shown in Figure 5-4. We obtained these spectra during field experiments in the Los Angeles area (see Chapter 6). These spectra were obtained during the 12.5 ms time slice corresponding to maximum absorption for a plume with an NO concentration of 1400 ppm and an N_2O concentration of 240 ppm. The scan time for each laser was 250 μs, therefore, the laser scans were essentially simultaneous. Twenty-five scans of each laser were co-averaged to give a column density for each species every 12.5 ms. Nitric oxide was measured by recording the change in absorption of individual rotational-vibrational lines at a frequency around 1903 cm^{-1} (5.25 μm). The diode laser was scanned over a spectral region of 1cm^{-1} by varying the laser current in order to obtain a baseline on either side of a pair of spectral

lines. The laser was turned off at the end of each scan to obtain the total laser intensity during the scan. This is particularly important for open path monitoring through a turbulent atmosphere where the collected laser intensity varies significantly from scan to scan. Carbon dioxide was monitored using a pair of rovibrational lines at 2243 cm^{-1} (4.45 μm). A pair of nitrous oxide (N_2O) absorption lines were present in the CO_2 scan region and were used to obtain a measurement of the N_2O column density.

<u>Spectral Analysis</u>

The resultant spectra were analyzed in real-time using the Levenberg-Marquardt non-linear least-squares method (Press *et al.*, 1992) to obtain the best fit to the Voigt line shape and a baseline polynomial. Figure 5-4 shows the observed spectra, the fits to the observed spectra and the least squares fit determination of the unabsorbed laser intensity. The average NO, N_2O and CO_2 column densities in the laser beam were calculated from the measured fractional absorption using the tabulated line strengths and pressure broadening coefficients from the HITRAN data base (Rothman *et al.*, 1998) and the improved broadening coefficients for NO (Appendix C). The software will fit up to four species simultaneously using up to 45 individual spectral lines per species.
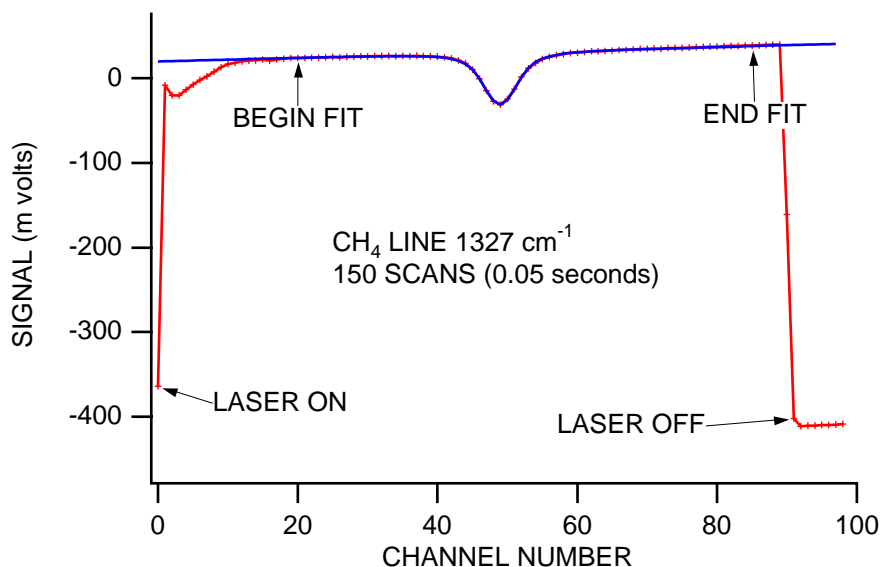
Figure 5-3: Methane spectrum obtained with a TILDAS spectrometer

Figure 5-3 shows a simple methane spectrum obtained using this approach. At the beginning of the scan the software turns the laser on and its frequency is swept across the desired transition frequency. At the end of the scan the laser current is dropped below

threshold to determine the detector voltage corresponding to the absence of laser light. The sweep rate is 2 kHz per spectrum. Spectra are co-averaged (in this case for 50 ms) using assembly language averaging routines maintaining a 100% duty cycle. The resultant spectrum is fit to a Voigt line shape function which is determined as a function of the pressure and temperature of the gas along the beam path. The baseline is treated as a slowly varying polynomial, typically of third order.
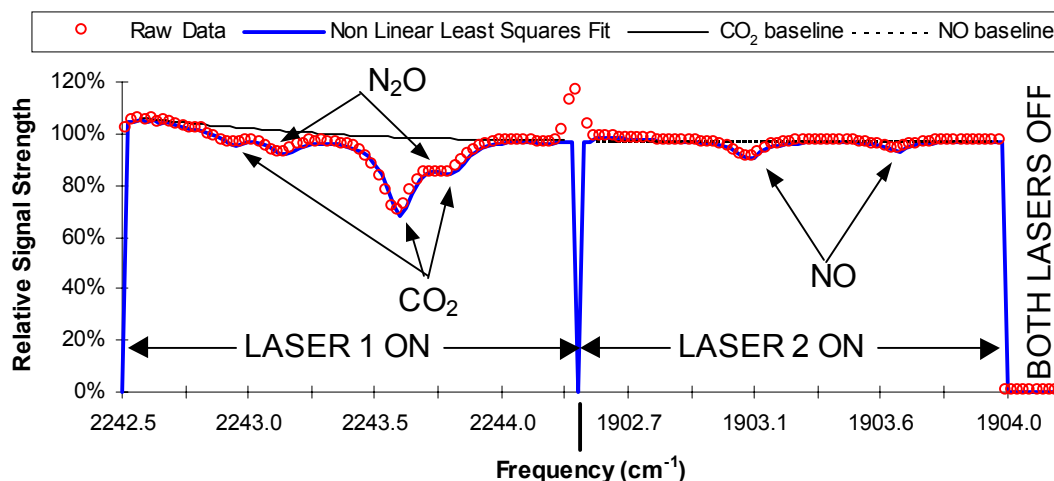
Figure 5-4: Two laser combined frequency scan[127]

The spectral analysis assumes that the plume temperature and pressure are equal to the ambient temperature and pressure since the plume rapidly equilibrates with the surroundings. The assumption regarding the plume pressure is undoubtedly sound. However, spectra acquired from portions of the plume very near the tail pipe exit point might have elevated temperatures. If this were the case, we would expect to see systematic deviations in plots of [NO] versus [CO_2]. This effect appears to be small since for light duty vehicles, and important at the beginning of heavy-duty truck plumes (section 5.6.2). Plume temperature can be determined from the observed spectrum, since the dependence of the spectral line widths and relative spectral intensities with temperature is well known (section 2.1.5). This approach has been demonstrated in this study as described in section 5.7.

Although, the frequency scale in Figure 5-4 is depicted as linear, the tuning rates of the lasers are not actually linear because of the thermal tuning induced by dropping the

---

[127] The background absorption in the optical path has been removed by dividing the observed spectra by background spectra.

lasers below threshold. Hence, the tuning rates of the lasers are greatest at the beginning of each sweep and decrease with time becoming linear asymptotically. For the spectra shown in Figure 5-4, the effect is subtle. The software accounts for the nonlinearity even in extreme cases. The expression used to describe the tuning rate is:

$$T = C_1 + C_2 \exp(-C_3 t) \tag{2}$$

where T is the laser tuning rate, t is time since the laser was turned on and the C_i are free parameters describing the tuning rate which are determined using reference spectra in a separate automated analysis.

Typically, plume spectra are acquired for approximately one half second at a rate of 80-100 Hz. The spectra are stored in computer memory and analyzed immediately after the measurement. The analysis requires approximately one second with a 133 MHz Pentium processor. Thus, the current TILDAS system is capable of measuring a vehicle every 1.5 seconds. This time interval would be reduced by using a faster processor. However, it is not be desirable to measure vehicles which are less about 2 seconds apart, since the emissions from the first vehicle can contaminate the background of the second vehicle making the measurement less reliable (section 4.2.3).
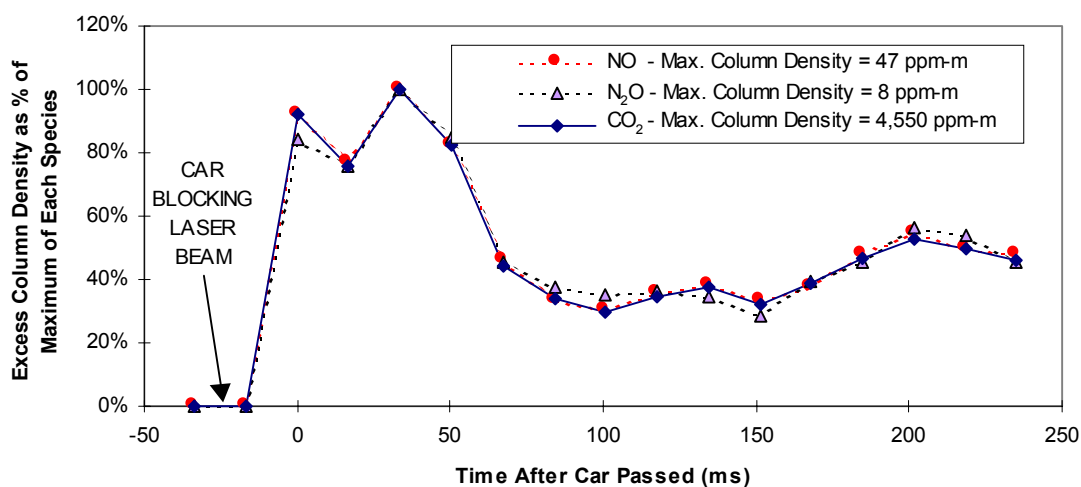
Figure 5-5: Column densities of NO, N_2O and CO_2 in the wake of a vehicle as a function of time.

Figure 5-5 shows the column densities of NO, CO_2, and N_2O measured in the wake of a vehicle as a function of time after the vehicle passed. In this case the spectra were acquired at a data rate of 80 samples per second. The correlation of the three species

is remarkably good. Measurements performed on vehicles traveling with speeds up to 70 mph have shown very good correlation of the time traces of NO and CO_2 and very stable NO/CO_2 ratios.

Calculation of Emission Indices

The data processing software uses a linear regression algorithm to determine the NO and N_2O exhaust concentrations for each vehicle. Every point for which the CO_2 column density is larger than a minimum of 1000 ppm-m is used in this algorithm. This is shown in Figure 5-6 for the data from Figure 5-5. The high correlation between the time dependence of the column densities in Figure 5-5 is reflected in the very high values for R^2 from the regression analysis shown in Figure 5-6.
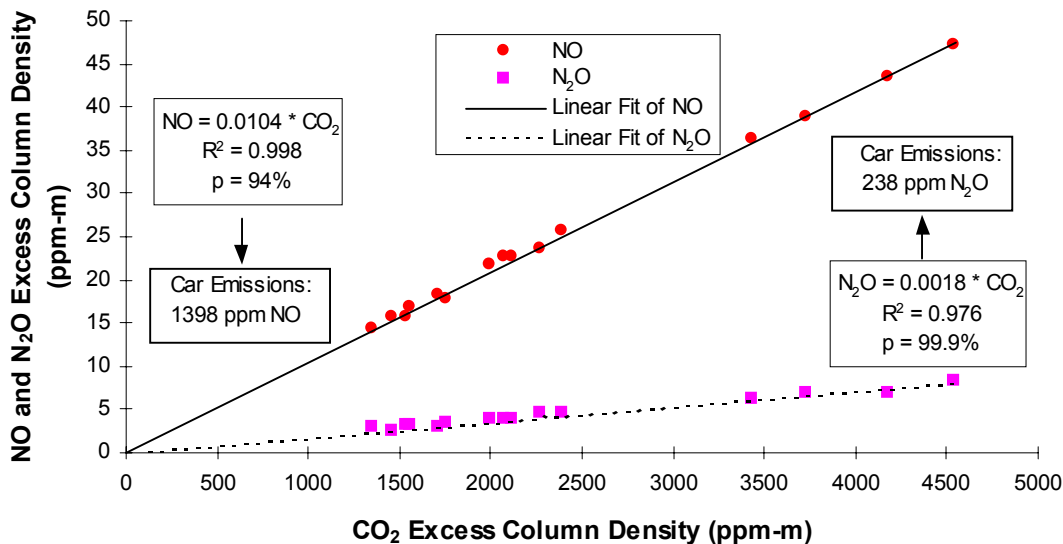
Figure 5-6: Regression analysis to determine NO and N_2O emission indices

5.4. Sensitivity and Accuracy of the TILDAS Remote Sensor

5.4.1. Estimation of the instrumental precision in the field

The TILDAS instrument detection limit for NO has been estimated from the noise levels observed during open path field tests performed in the absence of a vehicle. Each measurement was performed for 100 ms to simulate the plume duration of actual on-road exhaust measurements. The observed NO column densities were converted to exhaust mixing ratios using a value of the CO_2 column density (13,000 ppm-meters) which corresponds to ideal overlap of laser beam and exhaust plume. These tests returned an NO column density near zero with a standard deviation equivalent to an exhaust mixing ratio of ~3 ppm. We therefore report the ideal 3σ detection limit as ~9 ppm NO. Experimental confirmation of this detection limit has been obtained by repeated measurements on an ultra low emission vehicle (ULEV) as is described below. The result for N_2O was 2 ppm, or ~6 ppm for the ideal 3σ detection limit.

This level of sensitivity is the best that has been demonstrated for any NO remote sensor, with an improvement in the detection limit by a factor of approximately 100 over the two widely employed commercial techniques (Jack *et al.*, 1995; Zhang *et al.*, 1996a), and by a factor of 4 to 7 over the most precise UV instrument (Jack *et al.*, 1995; Zhang *et al.*, 1996a; Popp *et al.*, 1997).

This high sensitivity enables the TILDAS technique to measure the NO emissions from even the cleanest vehicles on the road. For example, average signal-to-noise ratios (SNR) of the NO measurement for an ultra-low emissions vehicle (ULEV)[128] would be about 28, when generally a SNR of 3 is the minimum for a good measurement. A vehicle complying with the most stringent regulation ever proposed for light-duty vehicle NO_x, California's proposed Super Ultra Low Emission Vehicle regulation (SULEV, as defined in CARB, 1998c), would still be marginally measurable with TILDAS (SNR of 3).[129]

---

[128] ULEV is a California emission standard. A fuel economy of 30 mpg has been assumed.

[129] Assuming a fuel economy of 30 mpg.

5.4.2. Measurement of the NO Emissions from a Prototype Ultra Low Emissions Vehicle (ULEV)

During the field campaign in the Los Angeles area (see Chapter 6), we performed an experiment which highlights the sensitivity of the TILDAS instrument. The emissions of a prototype Ultra Low Emission Vehicle were measured using the TILDAS remote sensor. This ULEV was made available to us by an automobile manufacturer. This vehicle has been verified by the California Air Resource Board as easily meeting the ULEV emission standard of 0.2 grams per mile, which corresponds to an average exhaust concentration of 85 ppm NO.[130] The NO_x emission rate of this vehicle on the Federal Test Procedure (FTP) emissions certification cycle was 0.054 grams per mile which corresponds to an average exhaust concentration of 28 ppm NO. We measured the NO emissions of this vehicle 21 times under a wide variety of driving conditions and always found its emissions to be below the average ULEV emission standard.
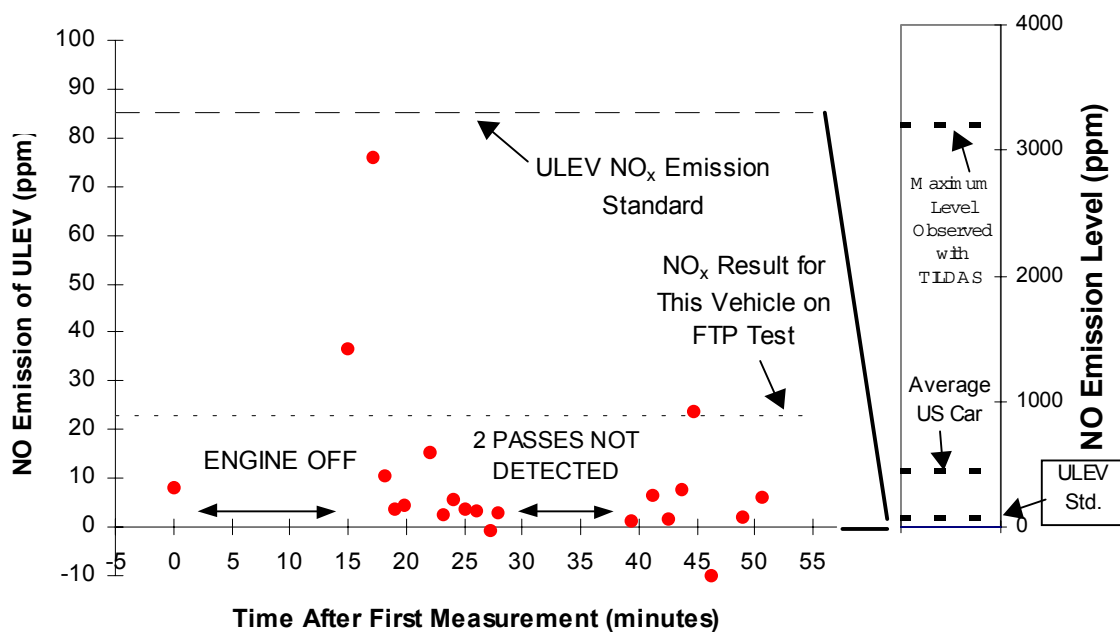
Figure 5-7: NO emissions of the Ultra Low Emission Vehicle vs. time.

These measurements are plotted in Figure 5-7 as a function of time, together with a comparison to the full range of NO levels which can be found in light-duty vehicle

---

[130] Assuming a fuel economy of 30 mpg.

exhaust. This overview of NO emissions is plotted on the right axis, beginning with the ULEV standard (114 ppm) and extending through the average U.S. car (U.S. EPA, 1995a), and on to an extreme NO emission level which exceeds 3000 ppm.

The rest of the figure is referred to the left axis which spans only the ULEV range (0-100 ppm). In this part of the figure we plot our measurements of the prototype ULEV. We obtained a mean emission reading of 10 ppm NO, a standard deviation of 18 ppm, and a maximum of 76 ppm. This is consistent with the FTP result. This is the first time that such low emission levels have been successfully measured by remote sensing. We observed two relatively high NO readings taken shortly after the engine had been off for 15 minutes. We attribute these high readings to a colder catalyst.[131]

The variation in the 21 measurements is a combination of instrumental noise and actual variation in the emissions of the vehicle. There are three points which are significantly higher than the rest and which clearly indicate increased NO emissions. If we ignore these three measurements (each of which is greater than 20 ppm), we can use the remaining 18 points to estimate an upper limit to the noise in our emission measurement. These 18 points average 4 ppm of NO with a standard deviation of 5 ppm. This is an upper limit to the instrumental noise for low NO emissions and is consistent with the 3 ppm value for the instrumental noise reported above since it is likely that some of the noise in the 18 ULEV emission measurements is due to actual emission variation. The same estimation procedure yielded an N_2O noise level of 3.5 ppm for this vehicle, which is again higher than the ideal sensitivity for the same reasons as for NO.

5.4.3. Accuracy of the NO Remote Sensor

The absolute accuracy of the TILDAS instrument is limited by the accuracy of the spectral line parameters from the HITRAN database, which depends on the particular absorption transitions being used. For the NO transitions shown in Figure 5-4, this accuracy is estimated at 2%,[132] while for the CO_2 transitions in the same figure it is better than 5%. If necessary, better measurements of the absorption parameters can be done with this system given its very high spectral resolution (Nelson and Zahniser, 1994; Shorter *et al.*, 1997). Because the accuracy of the instrument is tied to known invariant

---

[131] No effect of acceleration or specific power on NO emissions was observed for this vehicle.

[132] After the corrections reported in section Appendix C.

physical properties, it does not need periodic calibrations. This is a significant advantage for field measurements using the TILDAS technique.

This accuracy was verified by comparing the TILDAS NO_x/CO_2 measurements with those of the on-board instrumentation of the EPA heavy-duty diesel truck, as shown in Figure 7-5. The average of the TILDAS measurements was 99% $\pm$ 4.7%, which indicates that the TILDAS instrument is accurate within the experimental uncertainty.

The precision of these measurements is not as good as the one reported in sections 5.4.1 and 5.4.2 for two main reasons:

- Variation of the emission ratios of the EPA instrumented truck within the same measurement.

- The fact that remote sensing precision is lower for any technique when measuring high pollutant concentrations, as explained in section 4.4.

5.5. Advantages of the TILDAS vs. NDIR Remote Sensing

5.5.1. Frequency Resolution and Information Content

Most of the instruments used for remote sensing of on-road vehicle emissions are based on non-dispersive infrared (NDIR) technology[133] (Bishop *et al.*, 1989; Stephens *et al.*, 1991; Jack *et al.*, 1995). As described in section 2.2.3, the NDIR technique uses a broad band infrared source and a band pass filter to measure changes of total transmission in a given spectral region. This is depicted in the bottom part of Figure 5-8. Only the change in the total transmission in this frequency region is measured (a single number for every instant in time). Interfering species may absorb light in the same region and confound the measurement.
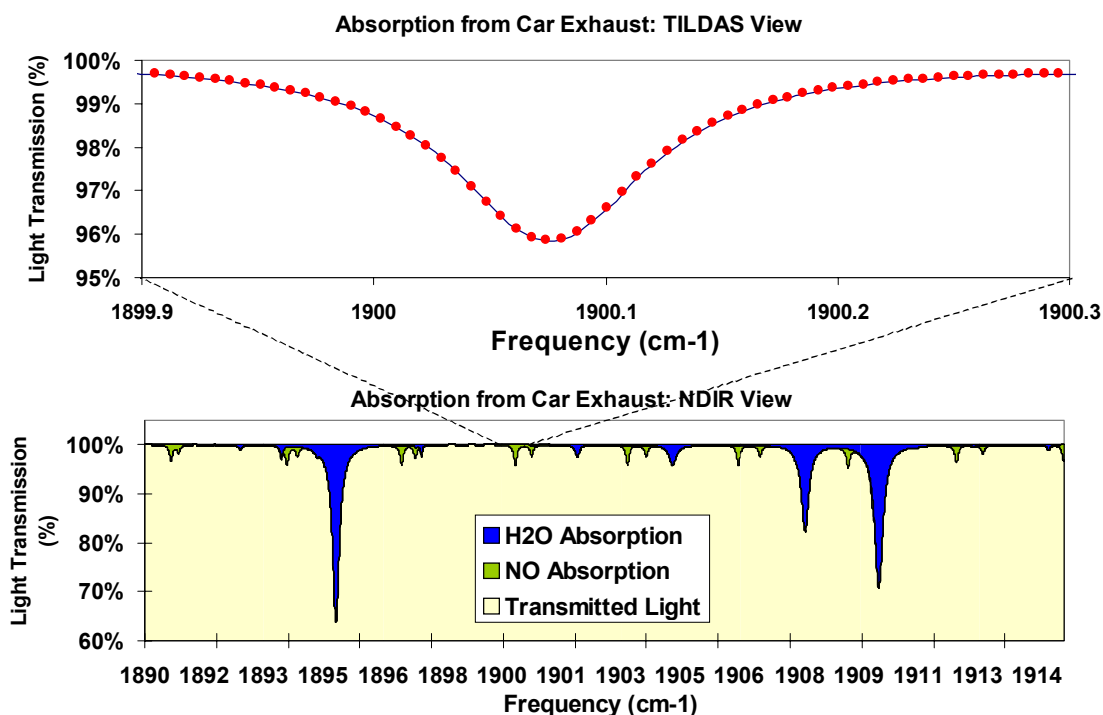
Figure 5-8: Comparison of the TILDAS and NDIR spectral views of the NO absorption lines around 1900 cm^{-1}

TILDAS (top of Figure 5-8) takes advantage of its very high spectral resolution to focus on an individual absorption feature of a species of interest. This greatly reduces the

---

[133] One remote sensor uses non-dispersive ultraviolet technology (NDUV, Zhang *et al.*, 1996a). This technology is analogous to NDIR except that it operates in the UV. All the points in this discussion apply equally well to both NDIR and NDUV.

possibility of interference from other chemical species. An additional advantage is that TILDAS provides much more information in each measurement than NDIR does: dozens of transmission vs. frequency data points versus only one total transmission for the whole filtered spectral region. For both of these reasons TILDAS is able to achieve greater precision than NDIR is (5 ppm vs. 300 ppm for NO, respectively).

A new NO remote sensor based on ultraviolet (UV) spectroscopy (Popp *et al.*, 1997) achieved much higher precision[134] than its NDUV predecessor (Zhang *et al.*, 1996a) by using a technique conceptually similar to TILDAS. In this instrument the UV beam is diffracted in a grating and sent to an array of detectors so a curve of transmission vs. frequency is obtained. This approach shares part of the two main advantages of TILDAS: the effect of interferences can be greatly reduced and the amount of information in each measurement is increased.

5.5.2. Long Optical Path

A long pathlength is of interest for remote sensing since it would allow greater flexibility in the placement of the sensors (e.g. across multilane highways). Some studies also suggest that drivers change their behavior while driving in front of a remote sensor. Walsh and Gertler (Walsh *et al.*, 1997) found that for those light-duty vehicles with one high and one low remote sensing measurement, the first measurement was the high one on 60% of the cases. They suggest that motorists may have been aware of the remote sensing device after the first pass and may have altered their driving in response. A longer pathlength could avoid this problem since the instrument would be less visible. It would also diminish associated concerns of motorist and operator safety which greatly limit site selection (Walsh *et al.*, 1997), and vandalism of unmanned remote sensors.

NDIR-based instruments are very limited in this respect due to the angular dispersion of their non-laser light, and because the absorption due to background CO_2 decreases the signal-to-noise ratio of their CO_2 measurement (HES, 1992). The longest pathlengths reported with this type of instruments are 40 to 50 ft (12m) (HES, 1992; Stedman *et al.*, 1994). Bishop and Stedman (Bishop *et al.*, 1996c) report in a recent description of their NDIR-UV instrument that "the system is designed to operate on a single lane road. […] Multiple lane operation has been reported but is not recommended."

---

[134] About 20 ppm NO vs. 300 ppm NO.

The TILDAS instrument allows for much longer pathlengths than NDIR instruments due to the coherence of laser light. In order to test the practical pathlength limits of the TILDAS technique we decided to attempt the measurement of NO/CO$_2$ emission ratios with as long a pathlength as practically possible.

We performed an experiment on road I-54, a four-lane road in Research Triangle Park, NC during the experimental campaign described in Chapter 7. The experimental setup is shown in Figure 5-9. The total optical pathlength in this configuration was 88 meters (289 ft), more than 5 times longer than the 50 feet reported for NDIR-based instruments. The horizontal distance between the TILDAS instrument and the base of the retro-reflector was 37 meters (120 ft).
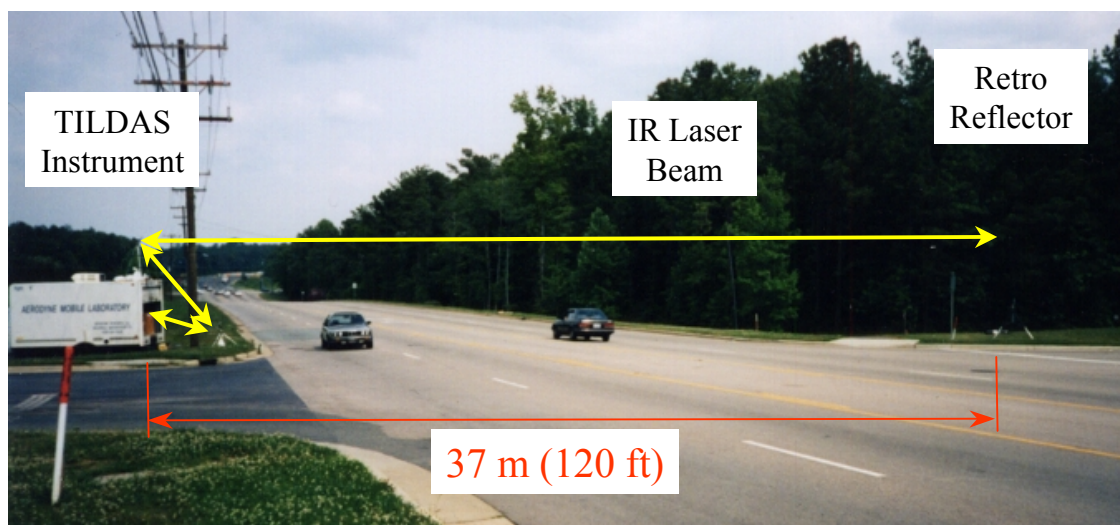
Figure 5-9: Setup of the TILDAS instrument with a very long pathlength

The results of one of these measurements are shown in Figure 5-10 and Figure 5-11 in the same format of Figure 5-5 and Figure 5-6. The longer pathlength did decrease the signal-to-noise ratio (SNR) of the measurements somewhat, however, the correlation of the NO and CO$_2$ traces is still excellent. As mentioned in section 7.2.3, some of this loss of SNR was due to the available optics being smaller than should be used with this very long path.
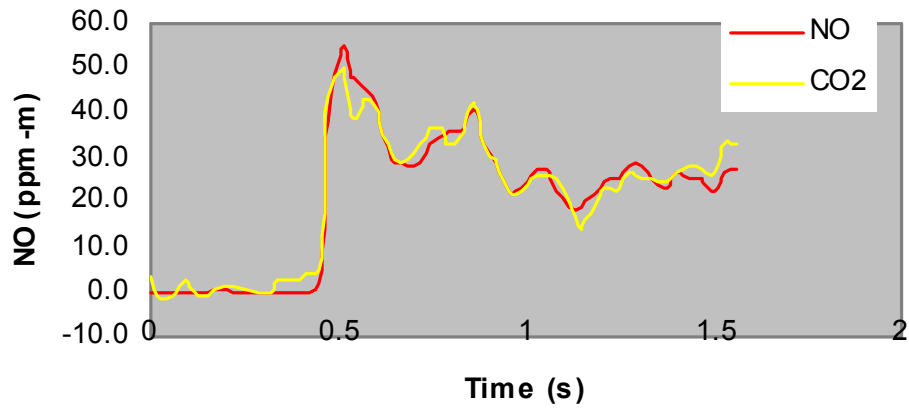
Figure 5-10: NO and CO$_2$ vs. time in a measurement of the EPA instrumented truck across road I-54
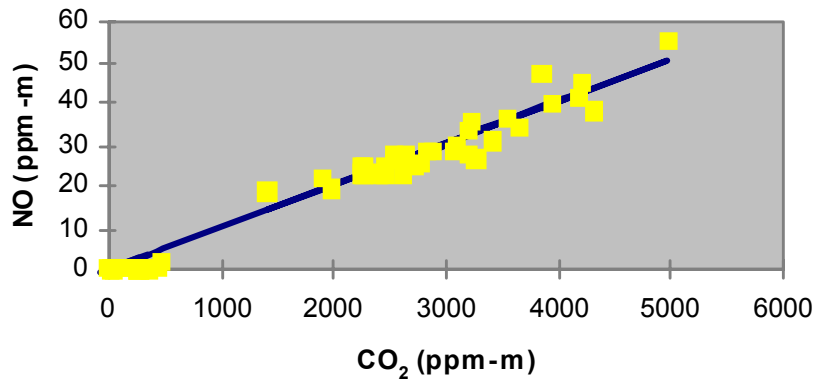
Figure 5-11: NO vs.CO$_2$ for each data point in time for a measurement of the EPA instrumented truck across road I-54

5.6. Effects of Exhaust Temperature on TILDAS Remote Sensing Measurements

5.6.1. Expected Gas Temperatures

Exhaust temperatures can be of importance for some remote sensing techniques, including TILDAS, since the absorption properties of gases are a function of temperature (see 2.1.5).

To provide an estimate of the range of exhaust temperatures that can be encountered, Figure 5-12 presents the engine-out and catalyst temperatures for a 1994 vehicle during the FTP dynamometer cycle. Engine-out and catalyst temperatures under warmed up operation range from about 480 to 630°C.
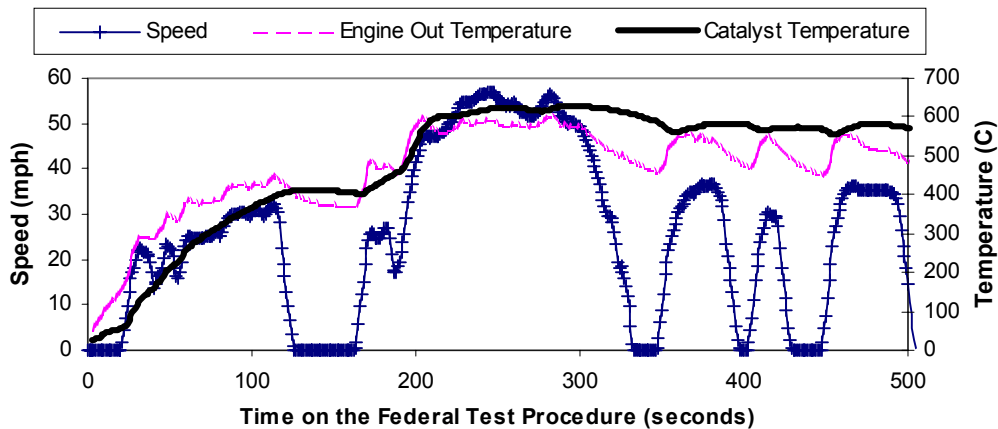
Figure 5-12: Speed, engine-out temperature, and catalyst temperature for a 1994 Jeep Cherokee tested on the Federal Test Procedure[135]

Significant heat transfer does occur in the exhaust system, so the temperature at the tailpipe will be lower than those in the previous figure. To evaluate that effect a thermocouple was placed on a vehicle tailpipe[136] as it was driven in the Boston area. The results are shown in Figure 5-13, which shows lower temperatures than the previous figure, between about 50 and 220°C.

---

[135] From the data of the Supplemental FTP program (Liberty *et al.*, 1997).

[136] A 1994 Mitsubishi Expo.

The temperatures of the exhaust gases as they are traversed by the remote sensing light beam will be even lower, due to the rapid mixing with ambient air in the highly turbulent vehicle wake (section 4.2.1).
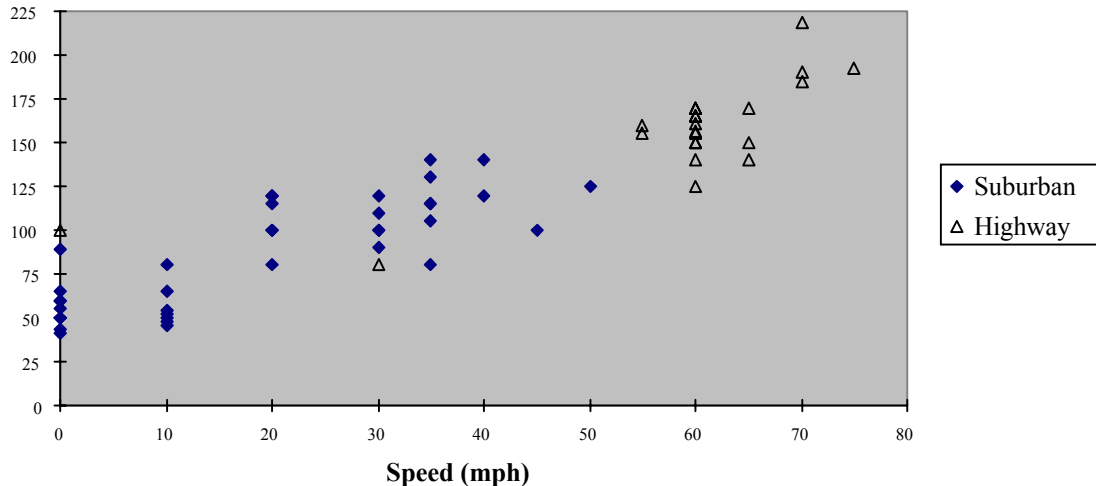
Figure 5-13: Exhaust temperature measured with a thermocouple at the tailpipe vs. vehicle speed for a vehicle driven in the Boston area

5.6.2. Effect of Temperature on the TILDAS Remote Sensing Measurements

For the TILDAS technique, high exhaust temperatures could confound the measurement due to different dependence of the absorption lines of the different species measured on temperature, as shown in Figure 5-14. The importance of this effect depends on which absorption lines are selected for each species (section 2.1.5). This effect is readily detectable and can be removed, as described below. On the experimental campaign for automobiles and light-duty trucks carried out in the Los Angeles area (Chapter 6) this effect was small except for some of the vehicles measured at the highest powers.

Temperature effects on the NO/CO_2 measurements were more important for the heavy-duty diesel truck measurements described in Chapter 7. Figure 5-15 shows the results of a measurement of NO and CO_2 taken across the exhaust of the EPA heavy-duty truck on July 16, 97. The time trace of both species rises sharply when the laser light first intersects with the exhaust plume, and remains well above background levels for several seconds.
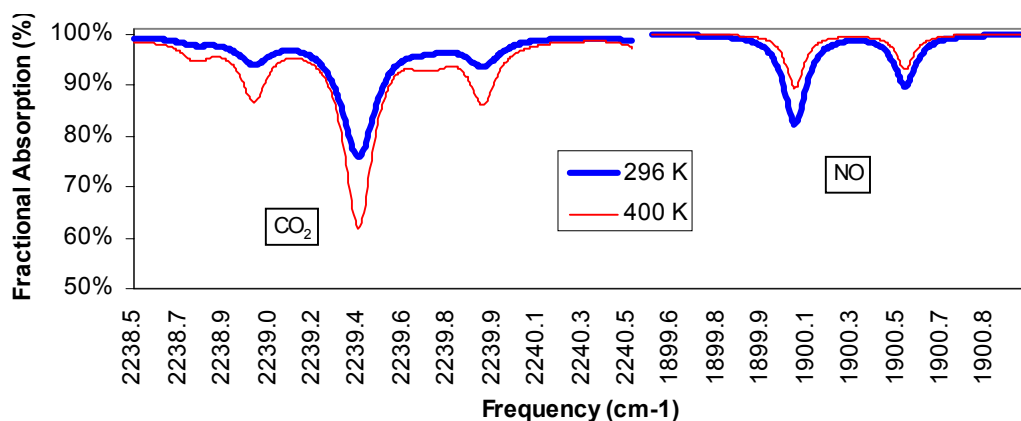
Figure 5-14: Effect of temperature on some CO_2 and NO transitions

In about half of the measurements performed on heavy-duty trucks a systematic deviation is apparent on the first few points of the plume.[137] This is especially obvious on the NO vs. CO_2 plot, in which most of the points fall on a well defined line but the two highest points and two lower points fall below the line.
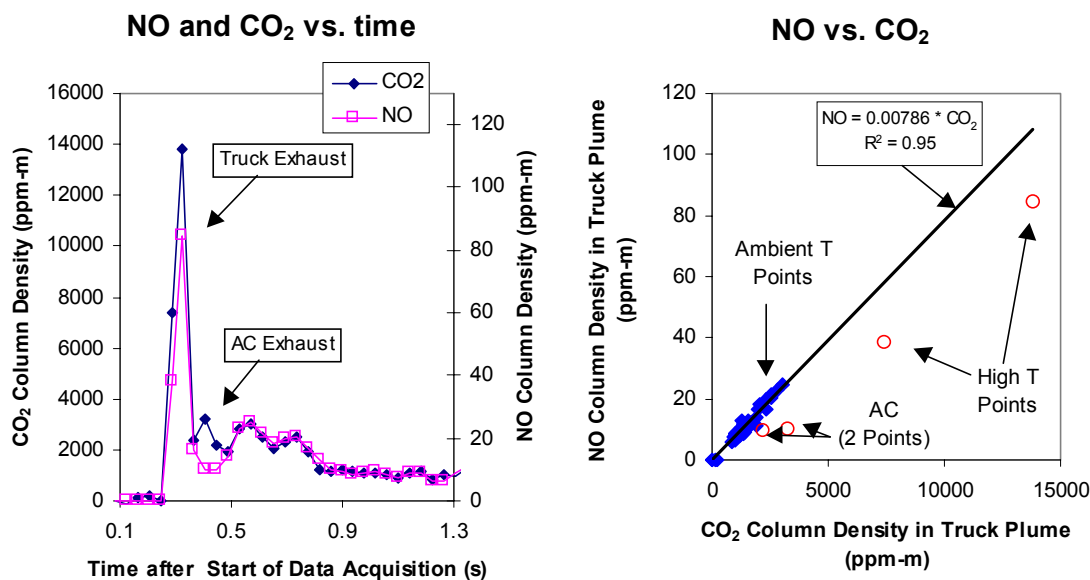
Figure 5-15: NO and CO_2 vs. time, and NO vs. CO_2 for a remote sensing measurement

---

[137] These figures can be compared with Figure 5-5 and Figure 5-6 which represent a remote sensing measurement for an passenger car in the same way and which do not show this effect.

The fact that the first two points of the plume measurement have a lower NO/CO_2 ratio than the subsequent measurements is attributed to the higher initial temperature of the plume before it has mixed with the surrounding air. Given the specific absorption lines used in this study, this higher temperature causes a lower apparent NO/CO_2 ratio measurement than is real. The other two points with a low NO/CO_2 ratio most likely correspond to the exhaust of a secondary diesel engine that powers the air-conditioning system for the instruments in the EPA trailer.[138]

There are two alternatives[139] for correcting the effect of high exhaust temperatures on the determination of the NO/CO_2 ratio:

- Remove the points with high temperature from the linear regression. The relative positions on the NO vs. CO_2 plot are always a clear indication of which points should be removed.

- Estimate the temperature of every point from the recorded absorption spectra and use the temperature measurement to correct the NO/CO_2 measurement

The procedure followed in this case was to remove the points for which high temperature was observed, based on the NO vs. CO_2 plots such as Figure 5-15 (right). This affected about half of the recorded plumes,[140] with 1 to 3 data points being affected in those plumes. These points are always located at the beginning of the plume, as would be expected since that is the location where the high temperature exhaust jet has not had time to mix thoroughly with ambient air.

---

[138] This secondary engine had a fuel consumption of about 1/10th of the truck engine, with lower NO/CO_2 ratios than the main engine. Its exhaust pipe was located at about the same height, which caused the TILDAS instrument to measure its exhaust as well. The points which are susceptible to contain a high proportion of this AC engine exhaust can be determined by their systematically lower NO/CO_2 ratios and by the time separation with the main plume (which can be compared to the time derived by dividing the distance between both exhaust pipes by the truck speed). These points have been manually eliminated from the data used to compare the TILDAS vs. the instrumented truck data (Figure 7-5 in section 7.3.1).

[139] Another alternative would be to choose absorption lines that have similar temperature dependence so most of the effect is canceled. We explored this strategy and concluded that it was not practical for the NO/CO2 remote sensing study, because the suitable absorption lines for remote sensing were very limited. The NO/NO2 remote sensing study naturally had this property (see section 7.3.4). Studies measuring absorption under low-pressure have many more absorption lines available to them, due to the much smaller line widths at low pressure, and could probably implement this strategy effectively.

[140] For the heavy-duty truck measurements only.

The estimation of gas temperature from its effect on the shape of absorption spectra has also been successfully achieved for some of the experimental data obtained in this study. The details of the temperature estimation procedure are given in section 5.7.

5.7. Determination of Gas Temperature from TILDAS Remote Sensing Spectra

5.7.1. Motivation

It was shown in section 5.6.2 that the effect of high exhaust temperatures can be important for the NO/CO_2 remote sensing measurement, specially for heavy-duty diesel trucks. This problem can be reliably detected by looking at deviations in the linear regression fit (Figure 5-15) and those points can be eliminated. That approach has been implemented in for the data presented here.

However, a more direct approach would be to determine the gas temperature[141] from the recorded spectra, since both line strength and line width are known functions of temperature. Once gas temperature is known, the data points with elevated temperatures can be screened out automatically. Alternatively, the temperature measurement can be used to correct for the temperature effect and the data points can be included in the regression analysis for determining the NO/CO_2 ratio for a given vehicle (Figure 5-15-right).

5.7.2. Previous Work on Gas Temperature Measurement using Absorption Spectroscopy

The application of laser techniques to the measurement of temperature and other scalars has been pioneered by researchers in combustion and supersonic flow diagnostics, due to these fields' need for precise, fast, and non-intrusive measurements. Eckbreth (Eckbreth, 1981) reviews the early efforts of temperature measurement using non-absorption laser techniques such as Raman scattering, Rayleigh scattering, and laser-induced fluorescence (LIF).

Temperature measurements in combustion systems using the diode-laser absorption technique have been pioneered by the Hanson research group at Stanford University (Chang *et al.*, 1991; Arroyo and Hanson, 1993; Philippe and Hanson, 1993; Arroyo *et al.*, 1994; Baer *et al.*, 1994; Baer *et al.*, 1996; Nagali *et al.*, 1997; Mihalcea *et*

---

[141] In this section we use "exhaust temperature" to refer to the temperature of the undiluted exhaust gases as they leave the vehicle's tailpipe. "Gas temperature" refers to the temperature of the exhaust as it is being diluted with ambient air after leaving the tailpipe.

al., 1998), and also pursued by other groups (Allen and Kessler, 1996; Mohamed *et al.*, 1996). This efforts are summarized in the recent review by Allen (Allen, 1998).

Three basic approaches have been used in those studies in which temperature is determined:

- from the ratio of the integrated absorption of 2 absorption lines (Chang *et al.*, 1991; Arroyo *et al.*, 1993; Arroyo *et al.*, 1994; Baer *et al.*, 1994; Allen *et al.*, 1996; Baer *et al.*, 1996; Mihalcea *et al.*, 1998)

- from the ratio of peak absorption of 2 absorption lines (Baer *et al.*, 1996; Nagali *et al.*, 1997)

- from a non-linear least-squares fit to the frequency vs. absorption data (Philippe *et al.*, 1993; Mohamed *et al.*, 1996)

Sensitivities of up to 2 degrees K at ambient temperatures have been reported with the first technique (Baer *et al.*, 1994). In general the achievable sensitivity will be different for each combination of diode laser power, detector characteristics, absorption lines used, measured temperatures, averaging time, and species column density observed. However, this result indicates that measuring temperature from remote sensing spectra is feasible in principle.

A variant of the first two approaches was tried in this study but was found to not give adequate performance. I believe this is due to the uncertainty in the baseline laser intensity for the pressure broadened absorption lines used in this study. Nagali and Hanson reported a similar problem which they solved by using an additional laser diode to determine the baseline intensity (Nagali *et al.*, 1997).

A variant of the third approach was determined to be the most feasible option for this study for 2 reasons:

- Using the full frequency vs. absorption data makes use of the most information content of the three approaches.

- An additional laser channel may allow the use of the peak-absorption ratio technique of Nagali and Hanson (Nagali *et al.*, 1997). However, such a channel is not available in the instrument used in this study, and any future channels will be preferentially devoted to the measurement of additional species rather than exhaust temperature.

The application of this approach to TILDAS remote sensing spectra is described in the following sections.

5.7.3. Feasibility of Obtaining Temperature from TILDAS Remote Sensing Spectra

A numerical experiment was performed in order to test the feasibility of measuring the temperature of the exhaust gases with the shape variations of the absorption spectra. A NO spectra with 40 ppm-m (corresponding to about 400-800 ppm NO in the exhaust of an automobile with typical plume overlaps) was simulated at 400K using the ATMTRANS software described above. Then the spectra was fit by the TDL software with different assumed fixed temperatures. The minimum chi-square error returned by the fit is shown in Figure 5-16.

The chi-square is indeed minimized for a temperature of 403K. This result indicates that the TDL software is capable in principle of determining the temperature of the gases which cause the absorption features measured.
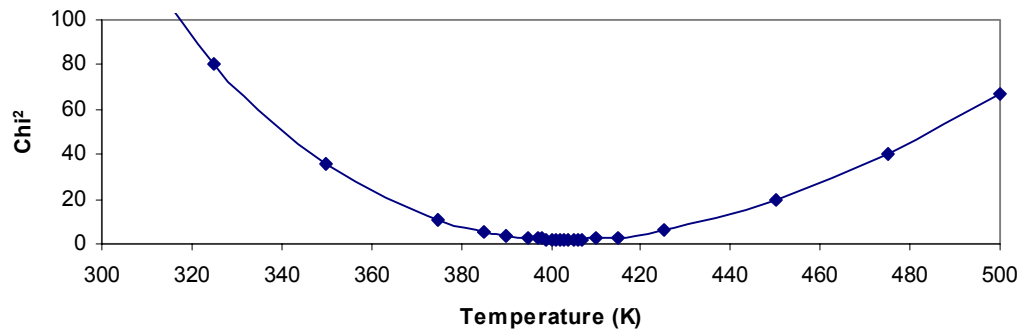
Figure 5-16: Chi-square returned by the spectra fitting program vs. assumed temperature

It was observed that the precision of the returned temperature depended very strongly on the NO column density in the analyzed spectra. Spectra with strong absorption features yielded highly precise temperature estimates while spectra with weaker absorption produced noisier results.

This issue was explored by creating a series of simulated spectra at 6 different column densities and adding 5 different white (Gaussian) noise simulations with a root-mean-square value of $3*10^{-4}$ fractional absorption, which is an upper limit of what was

observed in the experiments. The TDL software was then used to determined the temperature that provided the best fit to these synthetic spectra, and the rms noise of the temperature estimates was determined as the standard deviation of the 5 returned temperatures at each column density.

The results of this procedure are shown in Figure 5-17. The noise in the temperature estimate remains very small for column densities larger than about 15 ppm-m, increasing very rapidly for lower values.

The plot shows RMS Noise in Temperature Estimation (K) on the y-axis (0 to 50) vs NO Column Density (ppm-m) on the x-axis (0 to 120). The fitted curve is labeled:

RMS Noise in T Estimation = $85.381(\text{NO Column Density})^{-0.9298}$

$R^2 = 0.99$
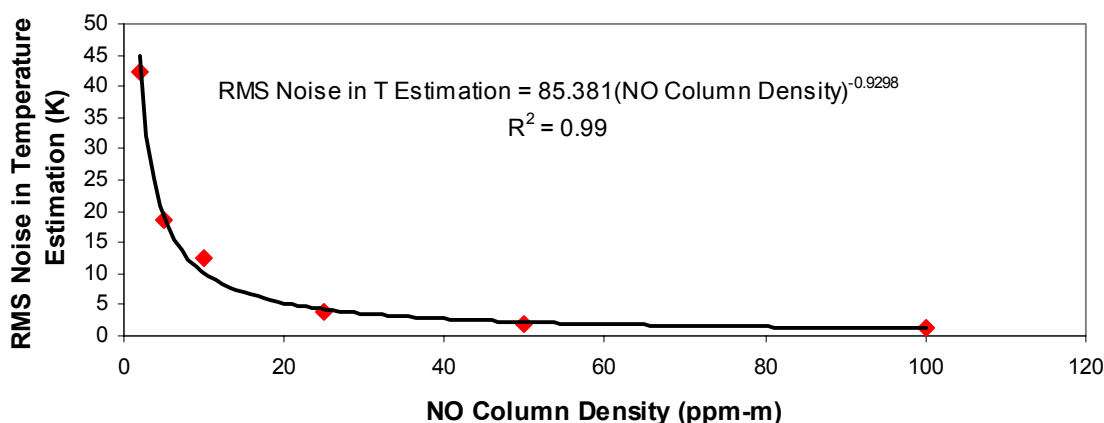
Figure 5-17: RMS error in the estimation of the gas temperature from NO spectra vs. NO column density

5.7.4. Application of the Estimation Procedure to a Heavy-Duty Diesel Truck Plume

Figure 5-18 shows the estimated gas temperatures for the EPA diesel truck plume shown in Figure 5-15. Also shown are the bounds of the 95% confidence interval for the noise in the estimation of temperature, based on the observed NO column density and the results in Figure 5-17. These results indicate that the first 3 points on the plume have temperatures which are significantly different from ambient, while the rest of the plume does not. This is consistent with the deviations on the NO/CO_2 ratio shown in Figure 5-15.
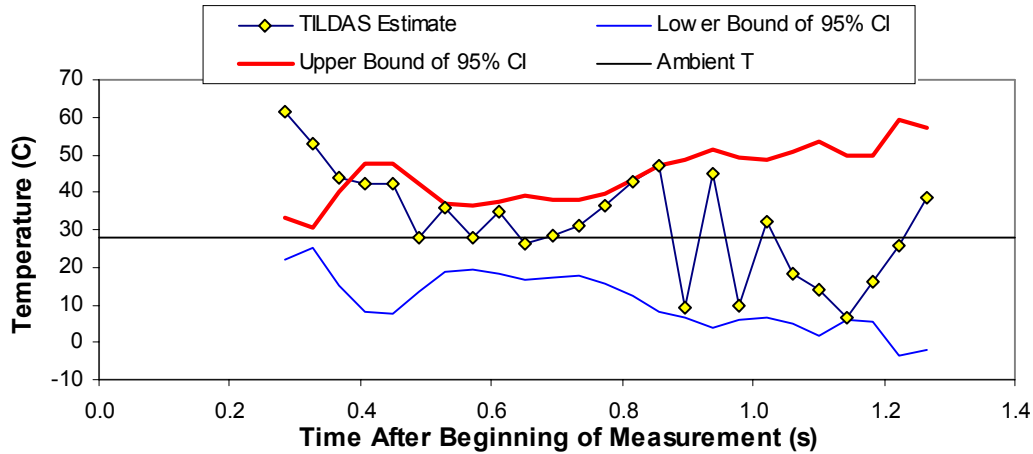
Figure 5-18: TILDAS estimate of temperature for the plume in Figure 5-15 and confidence intervals for the noise based on Figure 5-17

The maximum NO column density on a measurement depends on the NO emission level and on how well the laser beam and the exhaust plume overlap. The later effect is best expressed by the CO_2 column density (see section 4.3.4). The estimate of the 95% confidence interval of the noise in the estimation of temperature is shown in Figure 5-19 as a function of these two parameters.
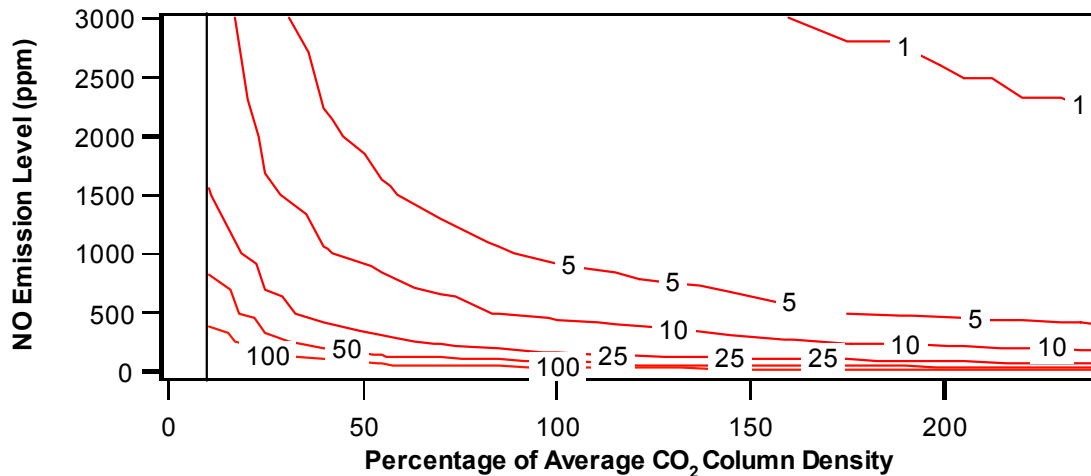
Figure 5-19: 95% confidence interval of the error in the estimation of temperature (K) from remote sensing NO spectra, vs. NO emission level and plume capture

Figure 5-19 indicates that the determination of the gas temperature from NO spectra will be viable with good sensitivity for vehicles with high NO emissions and good plume captures.[142]

5.7.5. Computational Strategy

As explained above the method chosen for the measurement of temperature from remote sensing spectra is the minimization of the χ^2 residual between the experimental and the simulated spectra. The computational implementation of this strategy needs some attention in order to provide the best accuracy without taxing excessively the time required for analyzing each individual remote sensing measurement.

Mohamed et al. (Mohamed *et al.*, 1996) implemented a least-squares fit that returned simultaneously column densities and temperature. They report large variations in the concentration and temperature returned from the fit due to the coupling between both parameters (Mohamed *et al.*, 1996). Such an approach may also require a large number of iterations as compared to only obtaining column densities only, therefore increasing the time needed to analyze each measurement and thus decreasing the productivity of the remote sensor.

Philippe and Hanson (Philippe *et al.*, 1993) calculated the spectral profiles for tabulated values of pressure and temperature and computed the value of χ^2 for each tabulated value, choosing the P and T that produced the lowest χ^2. This approach, while more robust than that of Mohamed et al., remains very computationally intensive.

A different strategy is proposed here to avoid the coupling reported by Mohamed et al. and maintain low computational requirements. It was observed during this study that the shapes of the χ^2 vs. temperature curves (such as that in Figure 5-16) can be approximated by a second-order polynomial with excellent precision. The gas temperature can be obtained economically by taking advantage of this property: the residual is calculated at three fixed temperatures and the minimum of the parabola which fits those 3 points is taken as the measured temperature. This procedure was found to

---

[142] A possibly more sensitive alternative would be to use the CO_2 spectra instead of the NO spectra to determine temperature, since some of the CO_2 lines used are slightly more sensitive to temperature that the NO lines used here. This approach was tried but yielded unsatisfactory results, possibly due to inaccurate parameters for the absorption lines used. Further research on this possibility is needed.

consistently return temperatures within a few K of the true minimum, and only requires running the fitting program 4 times.

5.8. Conclusions on TILDAS Remote Sensing

A TILDAS instrument has been modified for use as a remote sensor of vehicle emissions. The current instrument operates two diode lasers in two different frequency regions. The sensitivity of the instrument is 3 ppm NO and 2 ppm N_2O under ideal conditions. This has been demonstrated by measurements on an Ultra Low Emission vehicle.

The main advantages of the TILDAS technique for its application to remote sensing of vehicle emissions are:

- The high sensitivity of the technique, which allows the measurement of the emissions from even the cleanest vehicles.

- The unique ability of this technique to remotely sense minor species of interest in automotive exhaust such as NO_2, NH_3, N_2O, and formaldehyde.

- The absence of interferences from other gases or particulates in the vehicle exhaust or in ambient air, or from infrared emission from the vehicle or the exhaust, due to the its very high spectral resolution and fast time response.

- The higher information content of the technique with respect to NDIR or NDUV make it more robust against anoumalous effects such as interferences from the exhaust of previous vehicles, vibrations, etc.

- The absolute nature of this technique, which makes repeated calibrations unnecessary. Other techniques require frequent field calibration to resist inherent drifts.

- The longer path length achievable with this technique with only minor degradation of sensitivity, due to the coherent nature of laser radiation. Measurements of NO/CO_2 ratios over a total pathlength of 88 meters (289 ft) have been demonstrated, as described in section 7.3.

- This fact eliminates the need for constricting the traffic, alleviates safety concerns, and provides much more freedom in choosing remote sensing sites. The authors of the Texas Remote Sensing Feasibility study (Walsh *et al.*, 1997) conclude that finding adequate sites was very difficult in some urban areas.

- The Texas study also found that for repeated measurements in the same location, the first reading was higher 60% of the time, which they attribute to changes on driving behavior after noticing the presence of the remote sensor. The longer paths achievable with TILDAS would allow the instrument to be hidden from motorists, eliminating this potential source of measurement bias.

- Exhaust gases may have elevated temperatures as they leave the tailpipe, and quickly cool down as they mix with ambient air. Little effect was observed in the automobile measurements, while significant effects appeared in the heavy-duty diesel truck measurements. A numerical optimization scheme was successfully developed to allow the estimation of the gas temperatures from the remote sensing spectra.

Chapter 6. Remote Sensing of NO Emissions from Automobiles and Light-Duty Trucks

6.1. Introduction

NO_x[143] emissions from passenger cars and light-duty trucks are very important due to their contribution to photochemical smog formation and other environmental problems (NRC, 1991; Sawyer *et al.*, 1998a). NO_x is formed during combustion in the engine cylinder. Larger amounts are formed with higher combustion temperatures and lean mixtures (excess air), while rich mixtures inhibit NO_x formation (Heywood, 1988). Three-way catalysts reduce NO_x to molecular nitrogen with an efficiency of about 90%, but are only effective with stoichiometric or fuel-rich gases, and above a minimum operating temperature (Kummer, 1980; Koltsakis *et al.*, 1997).

A high-precision, highly specific TILDAS remote sensor was developed in this study as described in Chapter 5. This chapter presents the results of a NO remote sensing campaign performed using the TILDAS instrument in El Segundo, California, from November 13 through November 22, 1996. During this period the TILDAS instrument was used to obtain NO emission measurements for 1473 passing vehicles. N_2O emission data were obtained coincident with the NO emission data. The N_2O emission results are reported in Chapter 8.

This chapter is organized as follows: section 6.2 introduces the details of the experimental campaign. Section 6.3 shows the results of the non-emission measurements. Section 6.4 contains the analyses of the NO remote sensing results. Finally, section 6.5 presents the conclusions of this study.

---

[143] NO_x is the sum of NO and NO_2. More than 98% of the NO_x emitted from spark-ignition (gasoline) engines is in the form of NO.

6.2. Experimental

6.2.1. Experimental Site Description

The measurements were performed at Hughes Way in El Segundo, an urban street with a 4% uphill grade and a central divider. The location of the site within El Segundo is shown in Figure 6-1. The layout of the field site is given in Figure 6-2. Hughes Way is an access road to a large business facility. A traffic light was located about 100 meters before the remote sensing site. Some of the vehicles that were measured had stopped at this traffic light, but others had not. This location was chosen with the intention of minimizing cold start operation and ensuring high engine loads that were expected to yield larger NO emissions.

Figure 6-1: Location of the remote sensing site at El Segundo[144]

6.2.2. Likelihood of Vehicles in Cold Start Driving Through the Site

Modern vehicles have higher emissions when they have been recently started, due to low catalyst activity at low temperatures and to "cold start enrichment." It is important to be able to exclude recently started vehicles from remote sensing studies because properly functioning vehicles may appear to be super-emitters under these conditions.

---

[144] "CS": closest shop; "CR": closest restaurant.
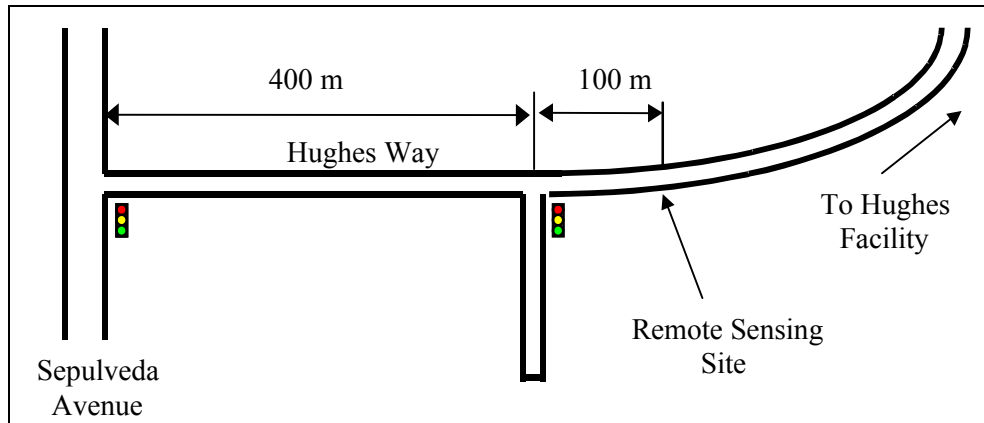
Figure 6-2: Characteristics of the Hughes Way remote sensing site at El Segundo

Some remote sensing studies have been carried out on highway off-ramps located far enough from the previous entrance to exclude recently started vehicles (Zhang *et al.*, 1993; Zhang *et al.*, 1996a). This was not possible in this study due to local constraints on site selection. However, the measurement location in this study was selected to make cold starts highly unlikely. We were set up at the entrance of a large Hughes business facility, and we measured the emissions of the vehicles of Hughes employees and visitors to the facility. El Segundo has a population of about 15,000 people, while about 150,000 people work in the city. Since a vehicle needs to travel only about 120 seconds[145] to be fully warmed up, and about 60% of the vehicles we measured were those of commuters coming to work in the morning from mostly other cities, they should have been fully warmed-up.

For the afternoon vehicles (40%), there could be a possibility of cold starts when some drivers were returning from lunch at local restaurants. The location of the closest places where a vehicle could have been stopped is shown in Figure 6-1. Since the closest restaurant was 1400 m from the measurement site, and the closest place were a vehicle could have been stopped was about 1200 meters from the site, the vehicles would require at least 2 to 3 minutes of travel to reach the remote sensing site (Sorbo, 1997). This would make cold start operation very unlikely.

Very few vehicles[146] came from a small business facility located at the last traffic light in Figure 6-2.[147] Those vehicles may have been in cold or hot start, depending on the

---

[145] Based on the data from the SFTP research program (Haskew *et al.*, 1994; Liberty *et al.*, 1997). This assumes driving conditions similar to those at the beginning of the Federal Test Procedure (FTP) dynamometer driving cycle.

[146] A rough estimate is that we obtained remote sensing measurements on about 10 such vehicles.

length of time that they had been parked. Unfortunately, there is no way to determine which vehicles were those in order to eliminate them from the emission data, but their impact on the results should have been small owing to their small number.

6.2.3. Instrumentation

We employed our two-laser TILDAS apparatus to simultaneously measure NO, N_2O, and CO_2 column densities with high detection sensitivity and high temporal resolution. The heart of the TILDAS instrument is a pair of infrared diode lasers, whose frequency of emission can be varied by changing the electrical current through each diode. The laser frequencies were tuned across known absorption lines of NO, CO_2 and N_2O, and the strength of the absorption was related to the column densities of the species in the absorption path. The species concentrations in the exhaust can be calculated from the ratio of the measured column densities, as summarized in section 2.2.2. Further details of the TILDAS instrument and its application to remote sensing measurements have been described in Chapter 5.
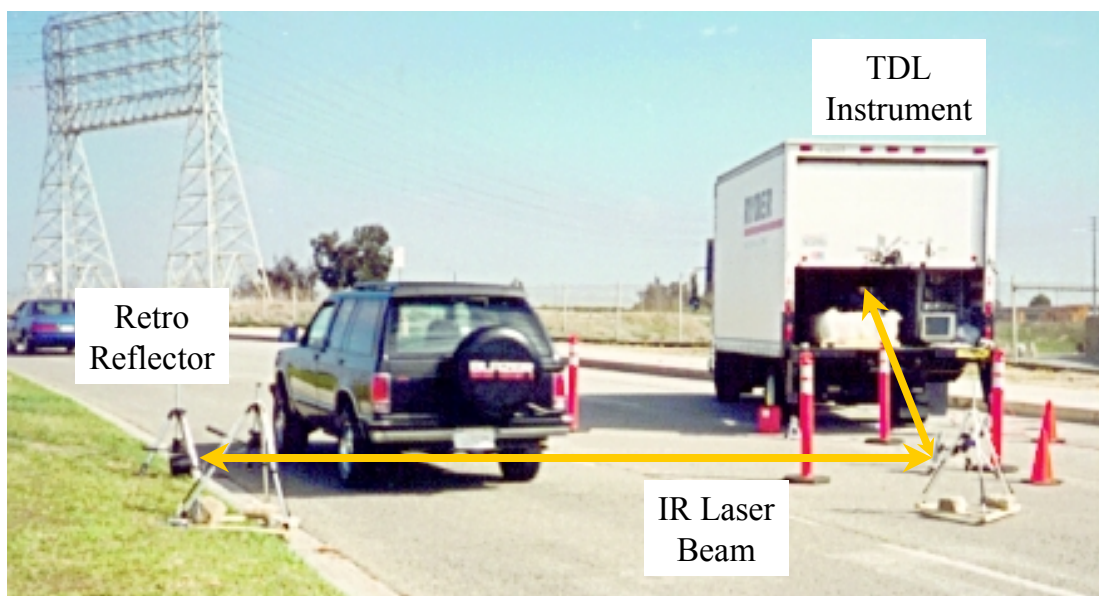
Figure 6-3: Photograph of the experimental setup at El Segundo

The precision of the instrument for low NO emitters was determined to be about 3 ppm of the vehicle exhaust for optimal overlap of the laser with a vehicle plume (as defined in section 4.3.4). This translates to an ideal 3σ detection limit of 9 ppm (section

---

[147] Most of the vehicles leaving that facility headed back to Sepulveda Ave. and did not drive through the remote sensing site.

5.6). In this study the average plume capture was about 3/5 of the optimal value which increased the average noise in the system from 3 ppm to 5 ppm, which is still excellent.

The experimental setup is shown in Figure 6-3 and Figure 6-4. The TILDAS instrument was located inside a truck parked in the rightmost lane behind the traffic cones. The combined laser beams from the TILDAS instrument were sent to a turning mirror and then to a corner cube retroreflector. The total optical path length (to the retroreflector and back) of the TILDAS laser was 36 meters.
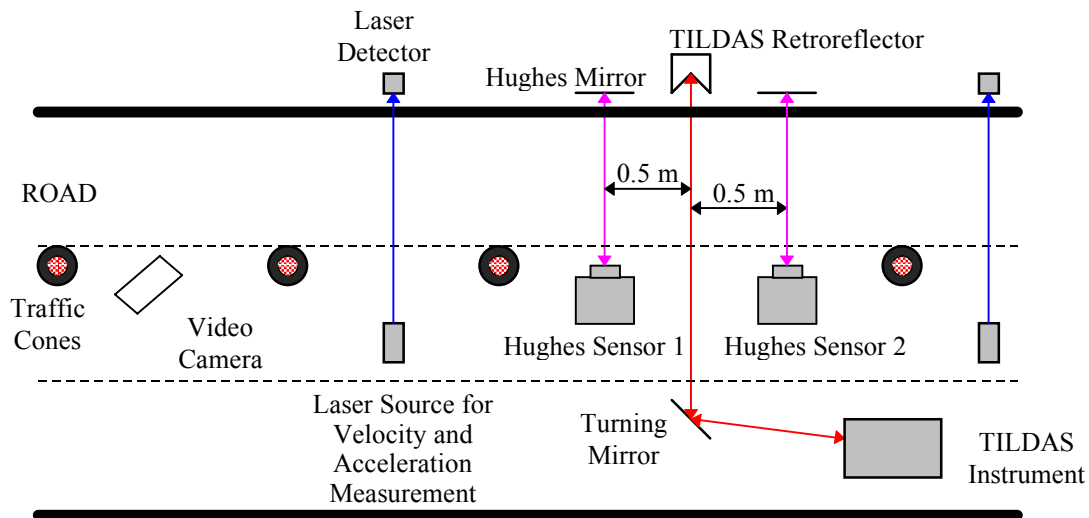
Figure 6-4: Field instrumentation arrangement

To provide a context for the interpretation of vehicle NO emissions, the NO measurements were supplemented with simultaneous measurement of vehicle speed, acceleration, and CO and HC emissions. On each side of the TILDAS optical path were set up one of a pair of Hughes "Smog Dog" remote sensors for CO and HC measurement (Jack *et al.*, 1995). Two diode-laser instruments for speed and acceleration measurement were set up before the TILDAS laser beam. Because of the range limitation of the Hughes "Smog Dog" instrument, the three-lane roadway was "coned down" to one lane of traffic.

We used a video camcorder to record images of the vehicle license plate and a custom-built computer based optical system to measure and record vehicle speed and

acceleration data. Vehicle make, model year and identification number (VIN) were retrieved from the California Department of Motor Vehicles (DMV) from the recorded license plate data.

6.2.4. Vehicle Speed and Acceleration Measurement

A low-cost, laser diode-based instrument was developed by EMDOT Corporation to provide an accurate means of measuring vehicle speed and acceleration that would be compatible with the remote sensing field environment. This instrument timed with microsecond accuracy the interruption of two light beams directed perpendicularly across the vehicle path from two roadside sources onto two photo detectors on the opposite side of the road. The two stations were separated by about 10 meters. The two station setup provided the necessary information needed to calculate the speed and a constant rate of acceleration for the vehicle between the two stations.

The precision of the speed and acceleration data are estimated[148] to be 0.033 m/s (0.07 mph) and 0.05 m/s^2 (0.11 mph/s), respectively. This represents a fractional accuracy of 0.2% of the range of velocities and of 1.3% of the range of accelerations observed in this study.

The average speed of the vehicles with valid NO emission measurements was 13.9 m/s $\pm$ 2.6 m/s (31.1 $\pm$ 5.8 mph). The average acceleration was 0.59 m/s^2 $\pm$ 0.49 m/s^2 (1.32 $\pm$ 1.10 mph/s). This includes the effect of roadway grade since the forces due to acceleration and grade are indistinguishable. Two-thirds of the average acceleration was due to the 4% road grade, which contributes 0.4 m/s^2.

6.2.5. License Plate Data Acquisition

The last component of the remote sensing data acquisition system was the license plate imaging equipment. In order to obtain vehicle information such as model year, make, vehicle identification number (VIN), etc. from a source such as the California Department of Motor Vehicles (DMV), it was necessary to obtain a readable image of each vehicle's license plate as it passed through the emissions measurement station. In addition, each license plate image required a time stamp that was synchronized with the TILDAS instrument clock. This was necessary so that the corresponding license plate

---

[148] The precision of these measurements was estimated from the calculated length of those vehicles that were measured more than once.

numbers and emissions measurements could be matched during the data analysis phase of the program.

Capturing of the license plate images was accomplished though the use of a video camcorder (camera/recorder) equipped with a telephoto lens. The video camcorder was tripod mounted and placed approximately 30 feet upstream with respect to the direction of traffic flow from the location of the TILDAS beam. The camera zoom and focus were then adjusted so that the license plate image was in focus and large enough to be resolved clearly as the vehicle passed through the TILDAS beam path. The camera shutter speed was set at 1/500th of a second to prevent blurring of the license plate image as the vehicle moved through the focal field. The camera was then set to run continuously, with a new tape being inserted every two hours.

This approach worked well for the limited number of vehicles we measured. We were able to successfully read more than 90% of the vehicles plates recorded by manually reading the video data from a television screen and entering the license plate and time stamp data into a computerized data file. Although this was a time consuming process, it yielded a substantially higher success rate than had been reported for some automated license plate reading systems operating under similar field conditions.[149] In all, we recorded several thousand unique plates, 1260 of which had valid corresponding NO emissions measurements. With the assistance of the Mobile Sources Review Committee of the SCAQMD, we were able pass these license plate numbers to the California DMV, which in turn provided us with information on the corresponding vehicles including model year, make, body type and VIN. The DMV sent back records on 95% of the submitted plates.

6.2.6. Decoding of Vehicle Information from the Vehicle Identification Numbers

The Vehicle Identification Number (VIN) of automobiles and light-duty trucks contain encoded information about a number of vehicle characteristics, including the vehicle emission control system. The VINs from all the vehicles for whom we had both emissions and license plate data were decoded using a proprietary computer program developed by Radian International[150] (DeFries, 1997). The vehicle information obtained

---

[149] E.g. the success rate for the automated system used by Hughes "Smog Dog" during this study was around 55%.

[150] Version 9602 of the Radian VIN decoder.

by decoding the VINs is summarized in Table 6-1. About 10% of the VINs supplied by the California DMV contained errors and could not be decoded.

FIELD	Meaning
YEAR	Model Year
MAKE	Vehicle Make
SERIES	Vehicle Model
BODY	Body Style
DISP	Engine Displacement
UN	Units for Displacement (cubic inches/liters)
CYL	Cylinder Configuration
ASP	Aspiration (Normal/Turbocharged/Supercharged)
IND	Fuel Induction (Carburetted/Fuel Injected/Diesel/CNG/LPG)
AIR	Air Injection Reactor
EVP	Evaporative Emissions Controls
OXY	Oxidation (Two-way) Catalyst
TWC	Three Way Catalyst
EGR	Exhaust Gas Recirculation
CLL	Closed Loop Combustion Control
PCV	Positive Crankcase Ventilation
TAC	Thermostatic Air Cleaner
MANUFACTURER	
CNTRY	Country of Manufacture
TYPE	Vehicle Type (CAR/MPV/TRK/Other)
GVWR	Gross Vehicle Weight Rating (pounds)

Table 6-1: Summary of the output parameters provided by the Radian VIN decoder for every vehicle

Some of this information was already available to us from the DMV records (model year, make, manufacturer, and some information on body type), but most of it was not.

The TYPE field permitted to distinguish between vehicles subject to the passenger car and the light duty truck emission standards (DeFries, 1997; Good, 1998). Only vehicles classified as "CAR" were subject to the passenger car standards, while vehicles classified as "TRK," "MPV" (multi-purpose vehicle), "VAN," and "BUS" were subject to the light-duty truck standards. Vehicles classified as "INC" (incomplete) could be subject to either standards.

6.2.7. CO and HC Remote Sensing

As mentioned above, during our two days of measurements at El Segundo a pair of non-dispersive infrared (NDIR) "Smog Dog" remote sensors from Hughes SBRC (Jack *et al.*, 1995) were used to measure CO and HC emissions simultaneously with our NO emission measurement. The two Hughes instruments were located 0.5 meters before and after the TILDAS laser path, as indicated in Figure 6-4.

The detection limits for this system were 200 ppm for CO and 30 ppm for HC (Jack *et al.*, 1995). These systems also included and NO emission channel by a non-dispersive infrared method with a stated detection limit of 500 ppm of the exhaust (Jack *et al.*, 1995). NO data were acquired but Hughes did not authorize us to present the results.

6.3. Results of the Non-Emission Measurements

6.3.1. Vehicle Statistics

The vehicle statistics for this remote sensing campaign are summarized in Table 6-2, including the losses from each step to the next. The TILDAS remote sensor worked extremely well, providing valid NO data from 96.4% of the vehicles that triggered data acquisition and for which enough overlap of the plume and the laser beam occurred. Successive small losses in license plate capture, data recovery from DMV, and VIN decoding ranged on 5-10% of the vehicles each.

	Number of Vehicles	Percentage of TILDAS triggers	Percentage of Category Above	Relative Loss in Step	Reason for Loss from Previous Step
Driving through the remote sensing site	Not Recorded				
Triggered the TILDAS NO remote sensor	1706	100%			1.5 to 2 seconds needed for processing one measurement before another one could start
With larger than minimum TILDAS plume capture (CO_2 signal)	1528	90%	90%	10%	1) Large number of triggers by Hughes remote sensing operator while setting up instrumentation. 2) Not enough plume capture to obtain good signal-to-noise ratio
With valid TILDAS NO data	1473	86%	96.4%	3.6%	Invalid NO data due to interferences or other causes
With valid NO and license plate data	1335	78%	91%	9%	Unreadable license plate or transient failure of plate recording system
With valid NO and DMV data	1268	74%	95%	5%	Errors on license plate reading or DMV database
With valid NO and VIN decoder data	1141	67%	90%	10%	Errors on DMV-supplied VINs or VIN decoder

Table 6-2: Vehicle statistics for the experimental campaign at El Segundo[151]

---

[151] Vehicles with repeated measurements are counted once per measurement.

6.3.2. Distributions of Vehicle Age/Type and Emission Control Technologies

The distribution of passenger cars and light-duty trucks vs. model year for the fleet that we measured are shown in Figure 6-5. Also shown are the VMT distributions in California's emissions factor model, EMFAC (version 7G).[152]

The fleet was dominated by passenger cars, with an increasing light-duty truck fraction for newer model years. The passenger car fleet was slightly older than the EMFAC fleet. The age distribution of the light-duty truck fleet closely matched that in EMFAC.
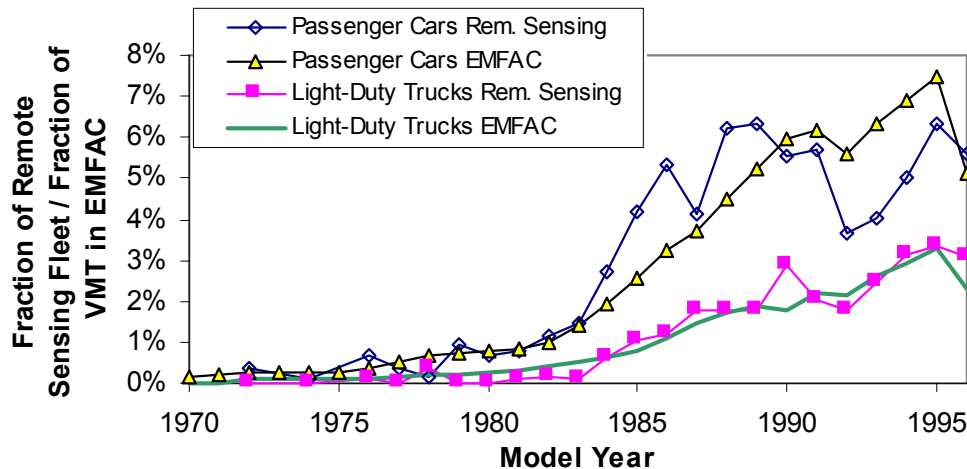
Figure 6-5: Model year distributions of the remote sensing data and of the VMT estimates of EMFAC

The distribution of emission control technologies vs. model year for the vehicles in our remote sensing study[153] is shown in Figure 6-6. There is a clear sequence of technology replacement as new technologies became available and the emission standards were made more stringent.

Closed-loop air-fuel ratio is not shown in the figure because it was tightly associated with catalyst technology. 99.6% of the vehicles with three-way catalysts in the

---

[152] The vehicle population at each model year is also provided by EMFAC. However VMT is the relevant parameter for comparison, because it measures how often vehicles of a given model year are driven, which is the same measurement obtained in remote sensing campaigns.

[153] As obtained from the decoding of the vehicle identification numbers (section 6.2.6).

sample had closed-loop control. Only 20% of the vehicles with oxidation catalyst, and none of the vehicles without catalyst had closed-loop control.
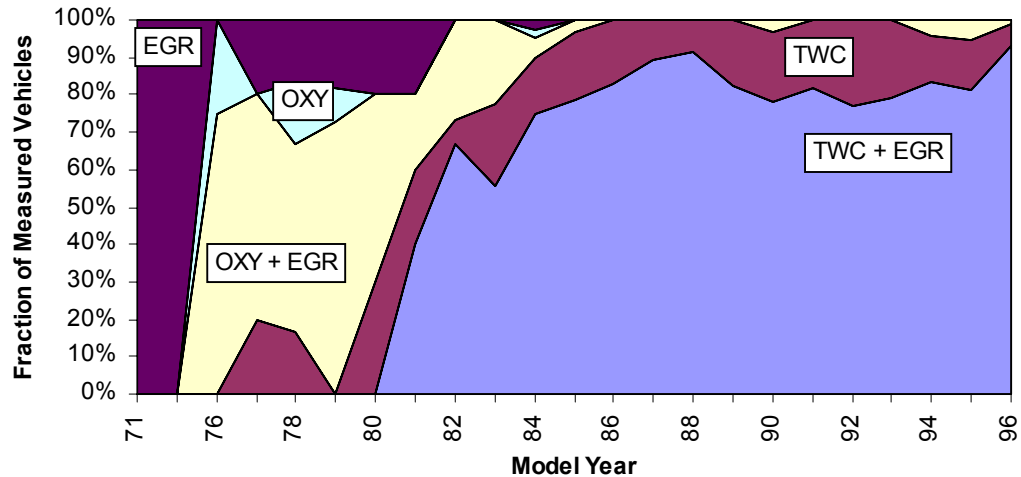
Figure 6-6: Model year distribution of emission control technologies[154]

6.3.3. Speed and Acceleration Distributions

We measured speed and acceleration together with NO emission for 867 vehicles[155] at the Hughes Way site in El Segundo. Figure 6-7 presents the vehicle speed and acceleration distributions. Table 6-3 presents the summary statistics for these distributions. The acceleration data presented here includes the effect of road grade since the forces due to acceleration and grade are indistinguishable in terms of engine load (see section 3.1.1).

Average speed was 31 mph, 50% larger than the average speed on the Federal Test Procedure (19.6mph, see Appendix F), but well within the range of speeds of that cycle. The differences in engine load between our remote sensing site and the FTP and other cycles are analyzed in the next section using the new definition of Specific Power presented in Chapter 3.

---

[154] EGR: exhaust gas recirculation; OXY: oxidation catalyst; TWC: three-way catalyst.

[155] This number is smaller than the numbers presented in section 6.3.1 due to problems with the newly developed hardware and software of the speed and acceleration measurement system. This problem can be easily eliminated from future remote sensing campaigns.
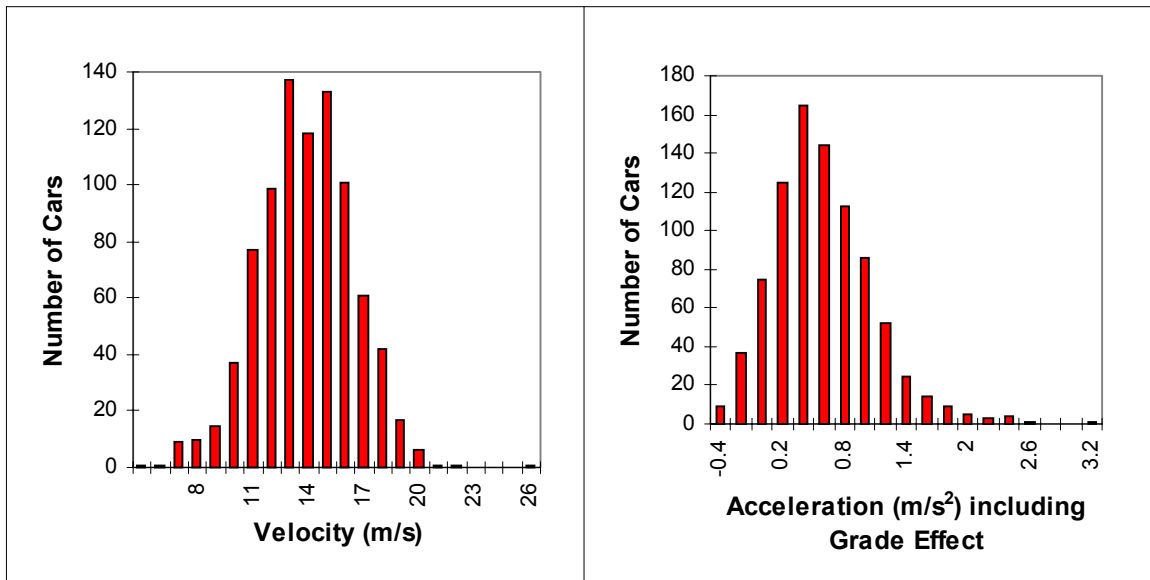
Figure 6-7: Speed and acceleration distributions[156]

	Speed (m/s)	Speed (mph)	Acceleration (m/s^2)	Acceleration (mph/sec)
Mean	14	31	0.59	1.3
Standard Deviation	2.6	6	0.49	1.1
Median	14	31	0.54	1.2
Maximum	26	57	3.21	7.2
Minimum	5.5	12	-0.49	-1.1
Skewness (nondimensional)	0.0	0.0	0.9	0.9

Table 6-3: Summary of statistics of the speed and acceleration distributions

6.3.4. Specific Power Distribution

Specific power has been calculated for every individual vehicle with the new definition presented in section 3.1.[157]

The statistics of the distribution of specific power for these vehicles are given in Table 6-4, and the distribution is shown in Figure 6-8. Almost all of the vehicles were under positive power, due in part to the 4% grade of the measurement site.

[156] To convert m/s to mph (and m/s^2 to mph/s), multiply by 2.24.

[157] The fraction of the specific power which is due to aerodynamic drag is small in this study due to the low average speeds. Values of 0.0135 and $5 \cdot 10^{-4}$ has been used for the rolling resistance coefficient (C_r) and for the aerodynamic drag parameter (C_D*A/m) respectively, for all vehicles.

	Specific Power (kW/Metric Ton)
Number of Vehicles	867
Mean	10.7
Median	9.5
Standard Deviation	7.7
Maximum	66.7
Minimum	-3.8
Skewness (dimensionless)	1.7

Table 6-4: Summary of statistics of the specific power distribution

For comparison purposes, the maximum rated power per unit mass for 27 typical production automobiles and light-duty trucks (model years 92-94) tested on the Supplemental FTP research program was on the range from 45 to 112 kW/Metric Ton (Haskew *et al.*, 1994). The average specific powers in this study are small compared to typical maximum rated powers, indicating that the power demand for most vehicles' engines was on the order of 10-20% of the maximum. However, a few vehicles had very high values, corresponding to relative engine powers in the 50-100% of the maximum range.

Figure 6-8 also shows the distribution of specific powers during the Federal Test Procedure (FTP), which is centered in lower values than what we observed at El Segundo. However, only 7.3% of the remotely sensed vehicles had specific powers larger than the maximum of the FTP (~22 kW/Metric Ton). This is important since commanded enrichment events occur mostly for powers beyond the FTP limits (see section 3.2.4).

Also shown is the distribution of specific powers during the US06 cycle, a cycle designed to supplement the FTP at high powers and account for the high CO emissions that now occur during power enrichment events (U.S. EPA, 1996a). The highest power during this cycle is 53.4 kW/metric Ton, which is smaller than the highest powers that we observed at El Segundo. This fact highlights the possibility that commanded enrichment events may have occurred during our measurements for some vehicles. This would explain some of the high CO measurements observed at high specific powers (see Figure 3-32 and Figure 3-33).
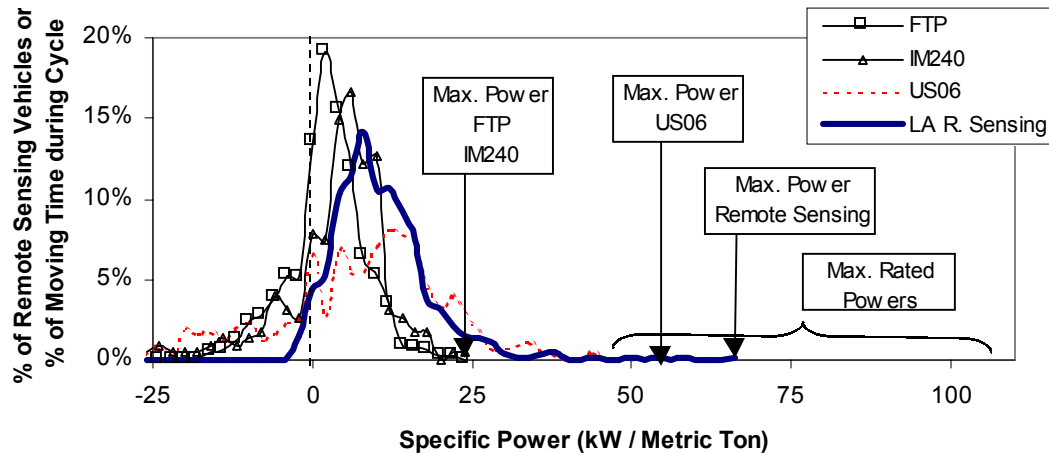
Figure 6-8: Distribution of specific power of the vehicles in this study, compared to the distribution of specific powers during the FTP, IM240, and US06 test cycles

6.3.5. Correlation Between Speed, Acceleration, and Specific Power in this Study

The variation of NO emissions with speed, acceleration, and specific power are discussed in sections 6.4.5, 6.4.6, and 6.4.7 below. Specific power is the most relevant parameter, as demonstrated in Chapter 3. The variation of NO emissions with speed and acceleration are also included here for completeness and to allow the comparison of the result of this study with those of other studies which may not have used our definition of specific power.

Specific power, however, is not independent of either speed or acceleration, since it is an algebraic function of both of them (see section 3.1.1). Their relationship for the vehicles in this study has been explored by means of the scatter plots and linear regressions shown in Figure 6-9 and Figure 6-10. SP of the vehicles measured at this site has a strong linear correlation with acceleration and a somewhat weaker correlation with speed. However, large differences in the value of SP can occur between vehicles with the same acceleration.[158] The correlation between SP and acceleration will be worse at sites with higher speeds, due to the increased relative importance of the aerodynamic resistance, rolling resistance, and grade terms of the SP equation.

---

[158] From Figure 6-10, vehicles with the same acceleration can have differences in acceleration of 10 kW/Metric Ton, or about ½ of the maximum specific power on the FTP driving cycle.
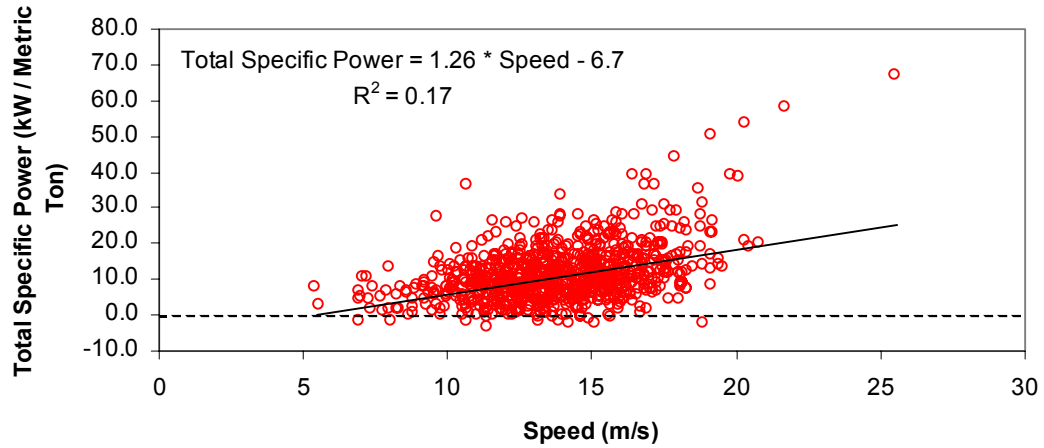
Figure 6-9: Scatter plot and linear regression of vehicle specific power vs. vehicle speed
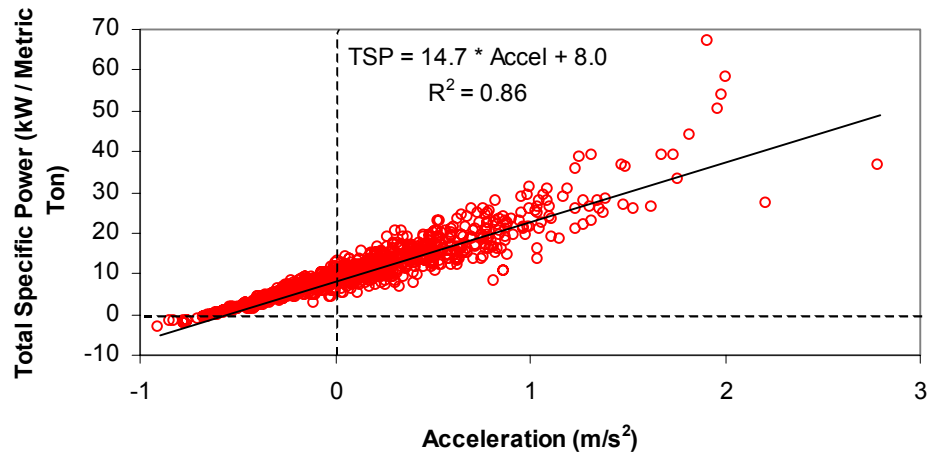
Figure 6-10: Scatter plot and linear regression of vehicle specific power vs. vehicle acceleration

6.4. Results of NO Remote Sensing[159]

6.4.1. NO Emissions Distribution[160]

NO emission measurements from 1528 vehicles were taken with the TILDAS instrument at the Hughes Way site, yielding 1473 valid data points. Only 3.6% of the measurements were discarded as invalid, typically due to suspected interference with the exhaust from a previous vehicle. The statistics of the NO emissions distribution are summarized in Table 6-5.

Parameter	NO Emission (ppm)
Mean	321
Standard Deviation	525
Median	90
Maximum	3753
Skewness (dimensionless)	2.8

Table 6-5: Summary of Statistics of the NO Emissions Distribution

The distribution of the NO emissions is presented in Figure 6-11. It is very skewed with 10.5% of the vehicles, those emitting more than 938 ppm, responsible for 50% of the NO emissions.

Remote sensing studies have typically found automobile CO and hydrocarbon emissions to follow a gamma statistical distribution function (Zhang *et al.*, 1994).[161] The previous NO remote sensing study also concluded that this is true for NO emissions (Zhang *et al.*, 1996a). In order to assess this point, Figure 6-11 also shows a gamma distribution of the same mean and standard deviation as the experimental distribution. The agreement between the two distributions is very good. A gamma distribution signifies that "dirty" vehicles are different from "clean" vehicles, with a few "broken"

---

[159] Note that all of our emission data are reported as parts per million (ppm) of all the exhaust gases (including H_2O), and not as ppm of the dry exhaust. The NO values in ppm of the dry exhaust would be 14.3% larger than the values presented here.

[160] The distribution of the emissions for all vehicles is presented here. The distributions for the individual vehicle / catalyst types are similar in shape with some differences in magnitude which are analyzed in the following sections.

[161] This is strictly true for fleets dominated by catalyst-equipped vehicles. Non-catalyst gasoline vehicles have a much less skewed distribution (Mercer *et al.*, 1997).

vehicles contributing disproportionately to the total emissions.[162] This is in distinction to a normal (or Gaussian) distribution where the emissions of individual vehicles would cluster about the mean and the contribution of dirty vehicles to the total would be smaller. The gamma distribution suggests the feasibility of reducing vehicle emissions by intervening with a selective inspection and maintenance program targeted to the high emitters.
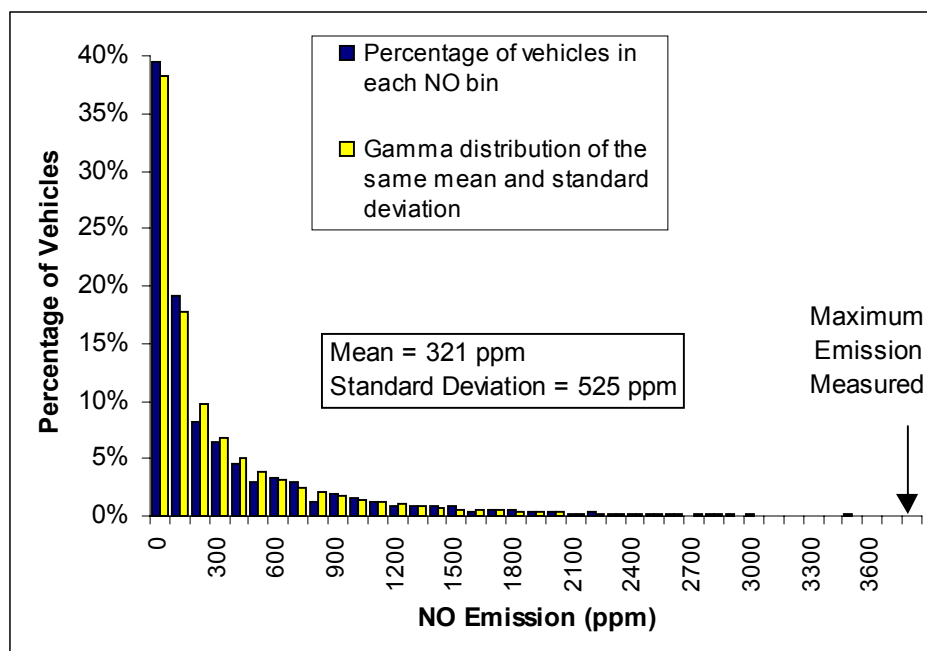
Figure 6-11: Experimental NO emissions distribution and the gamma distribution of the same mean and standard deviation

The high sensitivity of the TILDAS instrument is demonstrated by the distribution of negative concentration readings produced by the instrument. Since negative emissions are physically impossible,[163] their magnitude provides an estimate of the instrument's precision. An instrument with a precision of 300 ppm will produce many negative readings with magnitudes of order 300 ppm. In contrast, the data obtained with the TILDAS instrument show a distribution of negative concentration measurements with a standard deviation of only ~8 ppm.

---

[162] On the other extreme, it could also mean that all of the vehicles are high NO emitters 10% of the time. This possibility is addressed in sections 6.4.2 and 6.4.12.

[163] Ambient NO concentrations are normally below 1ppm (Pun, 1998). That is the maximum negative NO emission that could be real.

Figure 6-12 shows a detailed histogram of the lowest concentration bin in Figure 6-11 spanning the NO concentration range from -50 to 50 ppm. We have modeled our data as the numerical convolution of the measured gamma distribution with a normal distribution with standard deviation 8 ppm. The real distribution is well approximated by this convolved distribution, from which we infer that the precision of the measurements obtained during this study was about 8 ppm of NO in the vehicle exhaust. The expected instrumental precision was 5 ppm (see section 5.6). The slight difference between these two noise estimates may be due at least in part to variations in the NO background due to previous vehicles.[164]
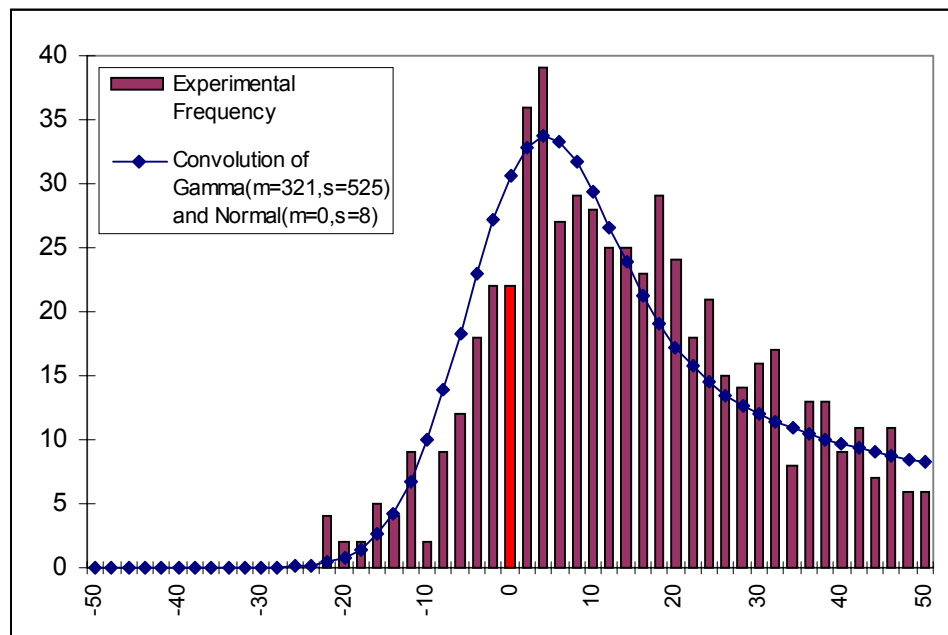
Figure 6-12: Comparison of the frequency of NO emission readings from –50 to +50 ppm; and the convolution of a normal distribution of standard deviation 8 ppm with the experimentally determined gamma distribution shown in Figure 6-11

We observe that the NO emissions of most of the vehicles were low relative to the average NO emissions permitted under existing NO standards. For example, 54% of the vehicles emitted less than 114 ppm. If a vehicle produced an average of 114 ppm over the certification test driving cycle it would satisfy the California ULEV standard at 50,000

---

[164] The negative tail may be composed of a first tail with σ = 5ppm corresponding to the average precision plus a secondary tail due to small interferences from the exhaust of previous vehicles. All of the measurements with large interferences have been already screened out.

miles (assuming a fuel economy of 26 mpg). This result may be due to the fact that most vehicles were measured in a fully warmed-up condition.

Figure 6-13 shows the percentage of the total NO emissions produced by a each decile of the vehicle fleet rank ordered by descending NO emissions. The first decile represents the fraction of the total NO produced by the 10% dirtiest vehicles, the second decile by the next 10% dirtiest vehicles, and so on. Again it is apparent that the distribution of the NO emissions is very skewed with 10.5% of the vehicles, those emitting more than 802 ppm, responsible for 50% of the NO emissions. It is easier to appreciate in this graph the low emissions of most vehicles; e.g. the cleanest 50% of the vehicles are responsible for only 4.2% of the total NO emissions.
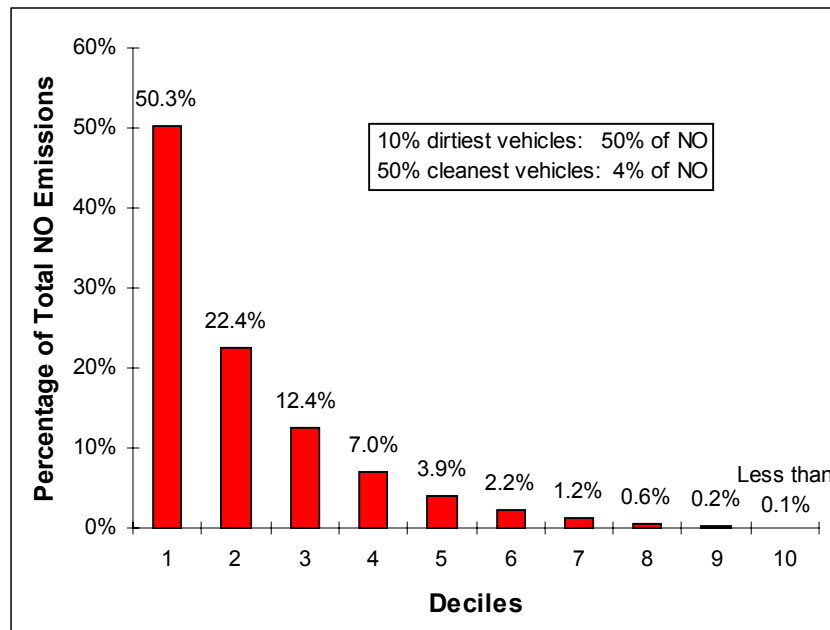
Figure 6-13: Decile plot of NO emissions in El Segundo.

6.4.2. Why is the NO Emission Distribution so Skewed?

In this section the reasons that cause NO emissions to be gamma distributed are discussed. Figure 6-14 shows the comparison of the remote sensing emissions distribution with the distribution of second-by-second engine-out and tailpipe emissions[165] of a modern production vehicle tested in 2 driving cycles.[166] The catalyzed

---

[165] This assumes that second-by-second driving cycle data are analogous to remote sensing data, as discussed in section 3.3.2.

distribution represents the typical emissions levels of a modern properly functioning vehicle equipped with a three way catalyst.[167] The engine-out emission can be thought of as representing a type of high emitter, one for which the catalyst would have completely failed in reducing NO but for which the air-to-fuel ratio control is still working properly.[168]

The engine-out distribution for the second-by-second data of this one vehicle is spread over a large range of values and is not highly skewed. The effect of the catalyst that makes the tailpipe distribution very skewed. The reason for the shape of the remote sensing distribution emerges now clearly: it is a blend of a distribution of 1-second emissions of catalyzed NO emissions with the higher emissions arising from vehicles with partially and totally failed catalysts.
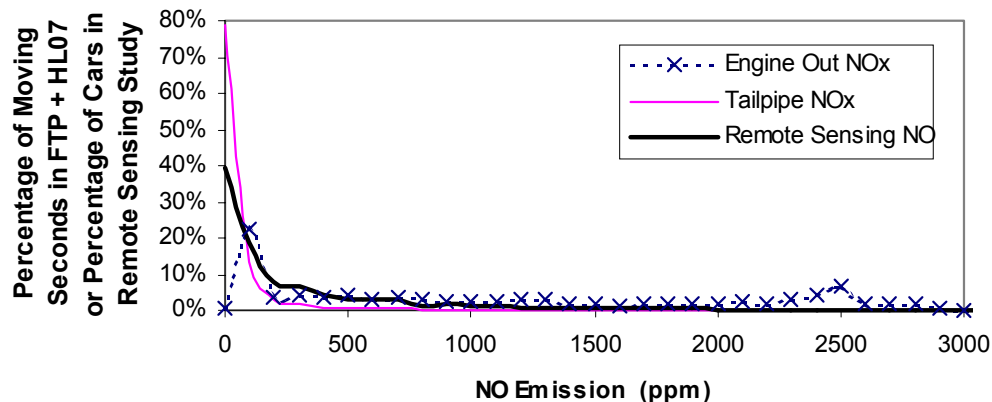
Figure 6-14: Comparison of the distribution of engine out and tailpipe emissions during the FTP and HL07 cycles for a 1994 Jeep Cherokee with the remote sensing distribution measured in California

---

[166] Only data for seconds with a moving vehicle and a hot catalyst have been included in the analysis, since only those conditions are relevant for remote sensing.

[167] These distributions are very similar in shape for other modern production vehicles. The reason is that, while their emissions control systems have some differences of detail, the basic processes of NO formation in stoichiometric premixed combustion and NO reduction on a three-way catalyst are the same for all vehicles.

[168] A vehicle that was systematically running lean would likely produce even higher NO, while one that was always running rich would have lower NO production, due to the dependence of NO production in combustion stoichiometry (Heywood, 1988; Miller and Bowman, 1989).

6.4.3. Comparison to NO$_x$ Emission Factors and Ratios from Other Studies

The emission factor for this study has been estimated at 8.1 ± 0.13 grams of NO per kg of gasoline[169, 170, 171] based on the results presented in section 6.4.1.

This NO emission factor is compared in Figure 6-15 to the NO$_x$ emission factors determined in 10 recent U.S. tunnel studies as reported by Sawyer (Sawyer *et al.*, 1998b). The remote sensing emission factor of this study is within the range of factors reported from the tunnel studies. Interestingly the 3 tunnel studies performed in California produced almost identical emission factors of about 10 grams NO$_x$/kg fuel.

This study produced an emission factor equal to about 80% of the tunnel values.[172] The reasons for this discrepancy are not clear. Different power demand conditions are not likely to explain it since the specific powers measured on the remote sensing study were quite high, partially due to the 4% roadway grade at the site (see Figure 6-8).

A possibility would be better than average maintenance for the commuter fleet. A recent remote sensing study in Texas found that workday commuter fleets were newer and had lower emissions than weekend fleets (Walsh *et al.*, 1997). Our remote sensing fleet was actually slightly older than the average California fleet (see Figure 6-5), but was composed of almost 100% commuter vehicles due to the site location. Our result would then indicate that the commuter fleet is better maintained than the average fleet. Further research on this topic is needed.

---

[169] This emission index has been calculated taking into account the correction due to the effect of different fuel economies for different vehicle types and model years, as described in section 4.7. This results in a 2.5% increase of the emission factor for this study over simply averaging the concentration results of the individual vehicles.

[170] See Appendix A for the conversion procedure from ppm to grams/kg fuel.

[171] Only NO was measured by the remote sensor. The maximum amount of NO$_2$ in gasoline engine exhaust was found to be smaller than 1% under stoichiometric conditions and smaller than 2% under any equivalence ratio (Hilliard and Wheeler, 1979). The NO$_2$ fraction has been neglected in the calculation of this emission index. However the mass of the emission is conventionally computed with the molecular weight of NO$_2$.

[172] The grade of the 1994 tunnel study was +4.2%, while the two 1995 studies were performed in approximately level tunnels. The grade in this remote sensing study was +4%.
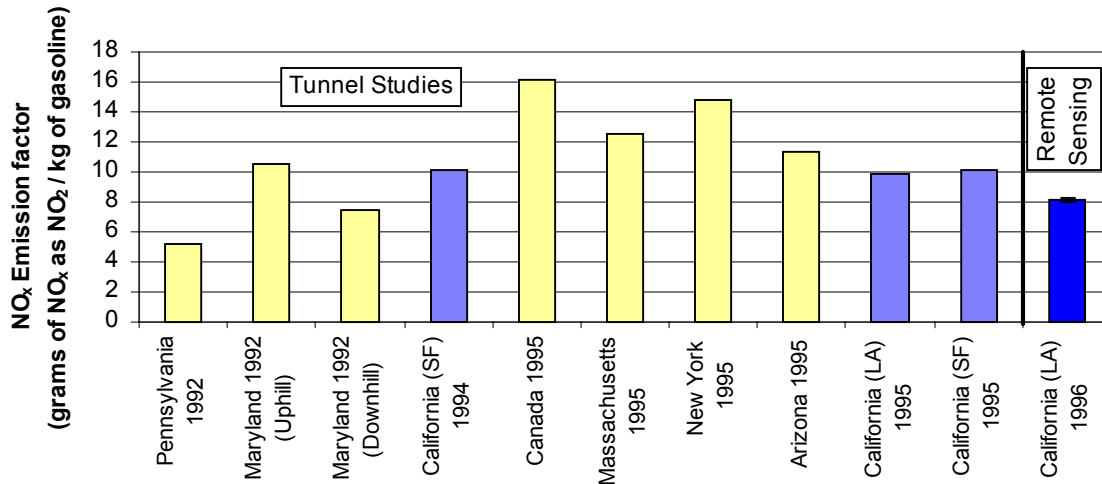
Figure 6-15: Comparison of the NO_x emission factor for light-duty vehicles from this study to those of several tunnel studies

6.4.4. Correlation between Emissions and Vehicle Parameters

A number of vehicle parameters such as speed, acceleration, model year, or catalyst type were also obtained for most NO remote sensing measurement. The following sections analyze the influence of these variables on NO emissions.

The linear correlation coefficient between emissions and all available vehicle variables which could have an influence on emissions were computed using the S-PLUS software (MathSoft, 1997). The complete matrix of correlation coefficients is included in Appendix D.

A summary of the statistically significant linear correlations between the emissions data and the vehicle parameters is presented in Table 6-6. The details of these correlations are explored in the following sections for NO and in Chapter 8 for N_2O. The most important results are :

- NO is positively correlated[173] with specific power and acceleration (see section 6.4.5 for an analysis of the possible causes).

---

[173] The word "correlated" in this section is used to mean that the two parameters have a linear correlation coefficient which is statistically different from zero with a significance level of 1%.

- NO is negatively correlated with the presence of a three-way catalyst and positively with an oxidation catalyst. This can be expected since only three-way catalysts are designed to reduce NO_x emissions.

- HC is negatively correlated with specific power (see Figure 3-35). This can be explained by the increased HC emissions under sudden or prolonged decelerations (see discussion in section 3.2.2).

- CO and N_2O are positively correlated with acceleration but not with specific power. This is an artifact of the calculation procedure: both emissions increase with specific power but in a non-linear fashion (see Figure 3-33 for CO and Figure 8-20 for N_2O) and acceleration can be thought of as a "blurred" specific power (see Figure 6-10) which "diffuses" some of the non-linearities of the physical response.

- NO, CO, and HC are negatively correlated with vehicle model year (i.e. positively correlated with vehicle age (section 6.4.9). This has been previously reported in the literature (Zhang *et al.*, 1993; Zhang *et al.*, 1996a; Stedman *et al.*, 1997a), and is explained by less stringent emission standards and increased deterioration for older vehicles.

	NO	N_2O	CO	HC	Speed	Acc.	SP	MY	Disp	TWC	OXY	EGR	CAR	LDT	USA
NO		↑				↑	↑	↓		↓	↑		↓		↓
N_2O					↓	↑									
CO				↑	↑	↑		↓							
HC					↑		↓	↓							

Table 6-6: Statistically significant correlations ($\alpha=1\%$)[174] between emissions and vehicle parameters[175]

- NO and N_2O are positively correlated due to the formation process of N_2O in the catalyst (see the experimental results in section 8.3.7 and a model of this process in section 8.4.1).

---

[174] As determined by the test on p. 636 of Press et al. (Press *et al.*, 1992), which does not require the assumption of a particular statistical distribution. The level of significance was $\alpha=1\%$. Note that this is the coefficient of *linear* correlation and may not capture non-linear relationships between the variables.

[175] Key to the labels: Acc: acceleration; SP: specific power; MY: model year; Disp: engine displacement; TWC: vehicle equipped with three way catalyst; OXY: oxidation catalyst; EGR: exhaust gas recirculation; CAR: passenger car; LDT: light-duty truck; USA: manufactured in the USA.

- CO and HC are positively correlated. This is due to the catalyst efficiency of both pollutants being highly correlated, since both efficiencies have similar dependence on air-to-fuel ratio and catalyst degradation.[176]

6.4.5. Effect of Specific Power on NO Emissions: Individual Vehicles

The analysis in Chapter 3 demonstrated that vehicle specific power is the best variable for studying the evolution of emissions with changes of engine power demand. The variation of NO emissions measured in our remote sensing study with specific power is analyzed here.

Figure 6-16 presents the scatter plot of NO emissions versus vehicle specific power and Figure 6-22 shows the average NO emissions of each vehicle population decile rank ordered by specific power.[177]
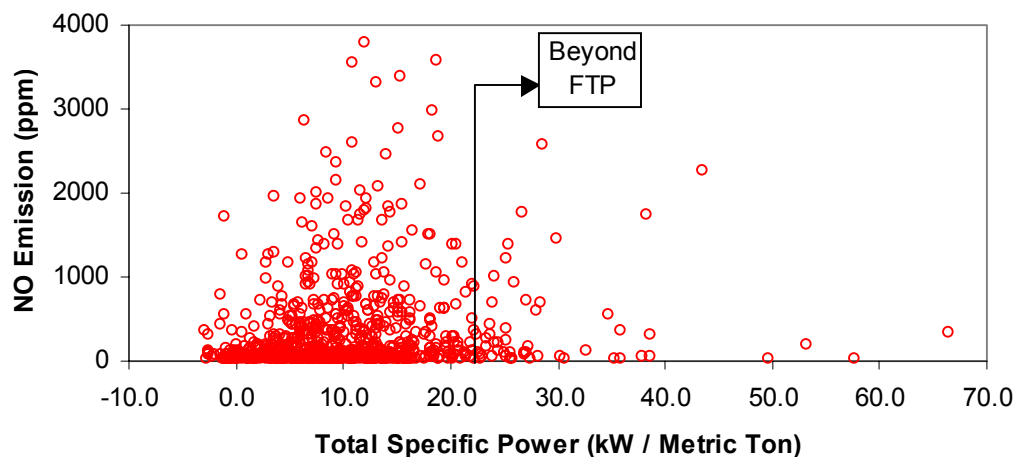
Figure 6-16: Scatter plot of NO emission vs. specific vehicle power

As with other parameters, the correlation between NO emissions and specific power is very small on a vehicle-by-vehicle basis ($R^2 = 0.023$). Although the results in

---

[176] Note that the variation of engine-out CO and HC emissions cannot explain this correlation. Both pollutants have quite constant engine-out emissions under moderate powers (see Figure 3-7, Figure 3-9, and Figure 3-11). During commanded enrichment events engine-out CO increases but HC does not. Engine-out HC increases during high deceleration events but CO does not.

[177] We measured speed and acceleration (which are necessary for calculating specific power, see section 3.1.1) together with NO emission for 867 vehicles.

Figure 6-16 appear highly random, their structure is analyzed here by comparing them to second-by-second emissions of three types of vehicles.[178]

- Figure 6-17 shows the engine-out NO_x emissions of a vehicle without EGR. These data are chosen here to represent the emissions of a kind of high NO emitter, one in which the catalyst has failed completely but which still maintains stoichiometric combustion. For this vehicle emissions increase with specific power for moderate powers. For SPs larger than the FTP maximum (~22 kW/Metric Ton) NO_x may decline during commanded enrichment events.

- Figure 6-18 shows the engine-out emissions of a vehicle with EGR, which represent a similar kind of high NO emitter. The trends are the same as for the vehicle without EGR, but the values are about a factor of 2-3 lower.

- Figure 6-19 shows the tailpipe (catalyzed) emissions of a modern vehicle. These data are chosen to represent a properly functioning vehicle.

- Figure 6-20 shows the tailpipe emissions of a vehicle employing the lean-on-cruise fuel economy improvement strategy.[179] It is shown here for completeness. This strategy consists on using lean mixtures under moderate powers, which yield improved fuel-economy for thermodynamic reasons (Heywood, 1988). The three-way catalyst is totally ineffective for NO due to the presence of excess oxygen, resulting in high NO_x emissions. A properly working vehicle using this strategy could appear to be a high NOx emitter.[180]

---

[178] These emission data come from the tests of the Supplemental FTP Program (Haskew *et al.*, 1994; Liberty *et al.*, 1997).

[179] Ripberger et al. (Ripberger *et al.*, 1998) report that a 1994 Ford escort used this strategy when the speed exceeded 58 mph for over 30 seconds. These authors report claim not to know how widely this strategy has been implemented on the vehicle fleet.

[180] Five Ford Escorts of model years 94-95 were measured during our study and none of them had more than 300 ppm NO in the exhaust, which indicates that they were not using this strategy at the time of the measurement. Our site precluded the kind of high speed operation needed for the engagement of this strategy (see previous footnote). These vehicles could cause erroneous high NO emitter identifications in high speed highway remote sensing.
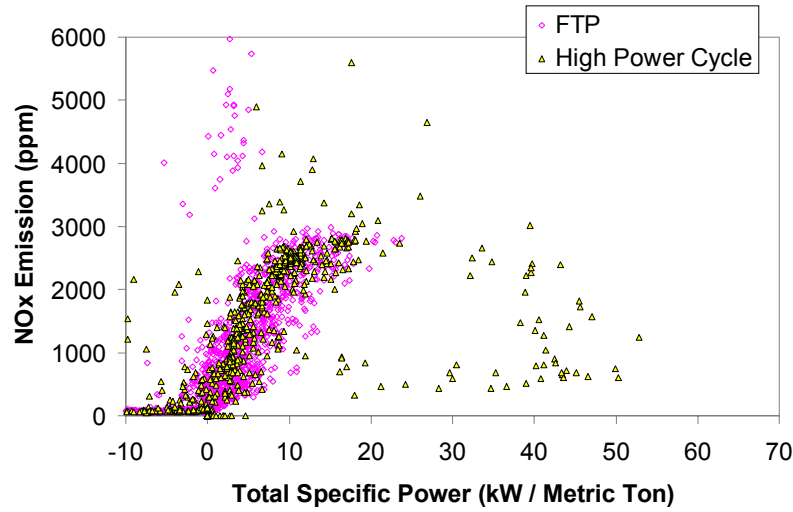
Figure 6-17: Second-by-second <u>engine-out</u> NOx emission for a 1994 vehicle <u>without</u> <u>EGR</u>[181] tested on 2 driving cycles
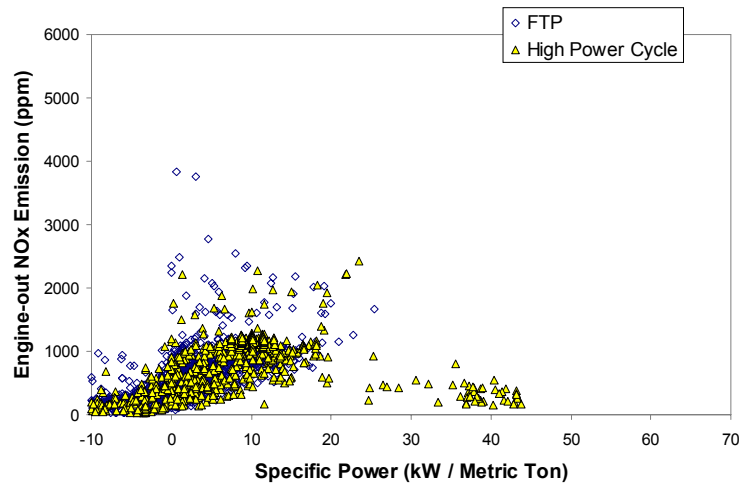
Figure 6-18: Second-by-second <u>engine-out</u> NOx emission for a vehicle <u>with EGR</u> [182] tested on 2 driving cycles

---

[181] A 1994 Jeep Cherokee tested on the FTP and HL07 driving cycles.

[182] A 1994 GM Saturn tested on the FTP and HL07 driving cycles.
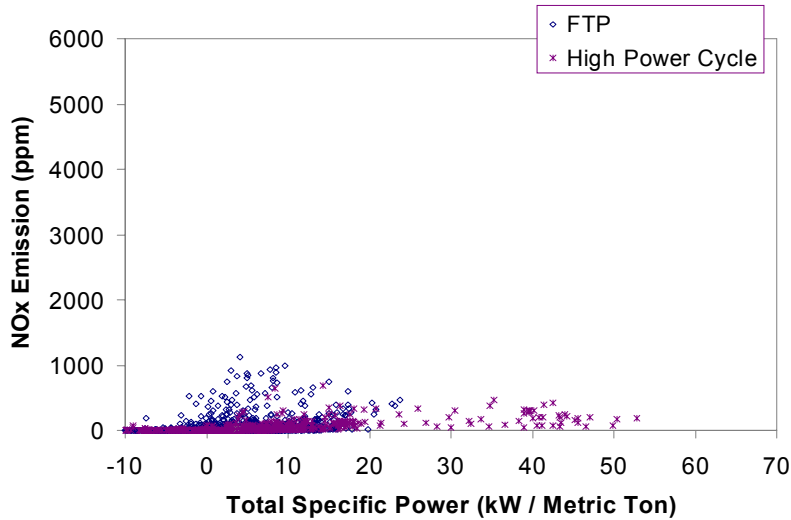
Figure 6-19: Second-by-second <u>tailpipe</u> NOx emission for a 1994 vehicle tested on 2 driving cycles[183]
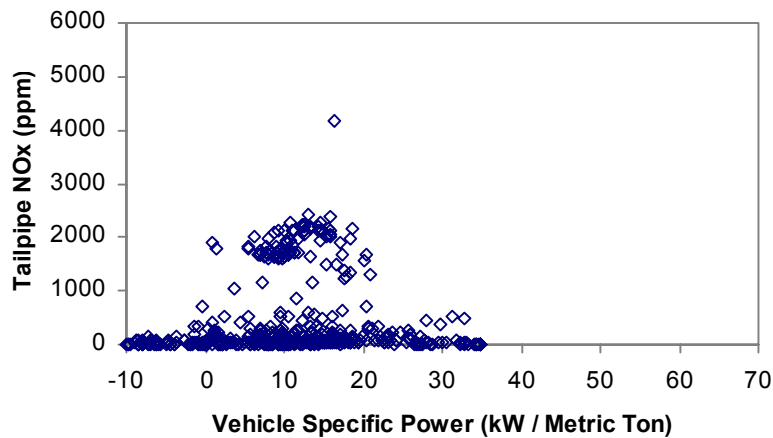
Figure 6-20: Second-by-second <u>tailpipe</u> NOx emission for a 1994 vehicle[184] with the <u>lean-on cruise strategy</u> in a driving cycle

Figure 6-21 shows the regions of most frequent NO$_x$ emissions for the three types of vehicles represented by Figure 6-17, Figure 6-18, and Figure 6-19 on top of the scatter plot of remote sensing NO emissions vs. specific power. As mentioned above, the catalyzed emissions represent typical emissions levels of modern properly functioning vehicles, and the engine-out emissions can be thought of as representing two types of

---

[183] This is the same vehicle of Figure 6-17 which was not equipped with EGR (1994 Jeep Cherokee). The tailpipe emissions of the EGR-equipped vehicle are quite similar.

[184] A 1993 Ford Escort.

high emitters for which the catalyst has failed but the air-fuel ratio is still maintained at stoichiometric. Clearly data on other types of high emitters are needed.

This superposition allows some interpretation of the seemingly random remote sensing data. In particular it highlights that it is very unlikely that the NO emissions beyond 1000 ppm come from properly functioning vehicles. Those high emission levels are far more likely in case of catalyst failure.
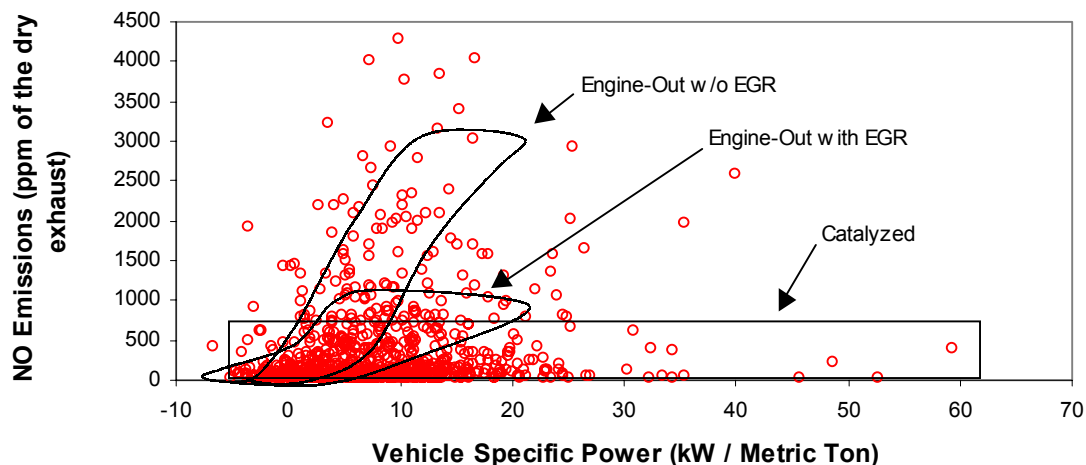
Figure 6-21: NO remote sensing measurements for individual vehicles with superposed regions of most common emission values for 3 types of vehicles

6.4.6. Effect of Specific Power on NO Emissions: Decile-Averaged Emissions

Figure 6-22 shows the average NO emissions of each vehicle population decile rank ordered by specific power. There is a strong correlation between NO emissions and specific power for the lower nine deciles, which is due to the expected increase of NO emissions with engine load (see Figure 3-14 and Figure 3-34). The 10th decile shows the reduction of NO emissions due to commanded enrichment operation of some of the vehicles that were operating at the highest powers.
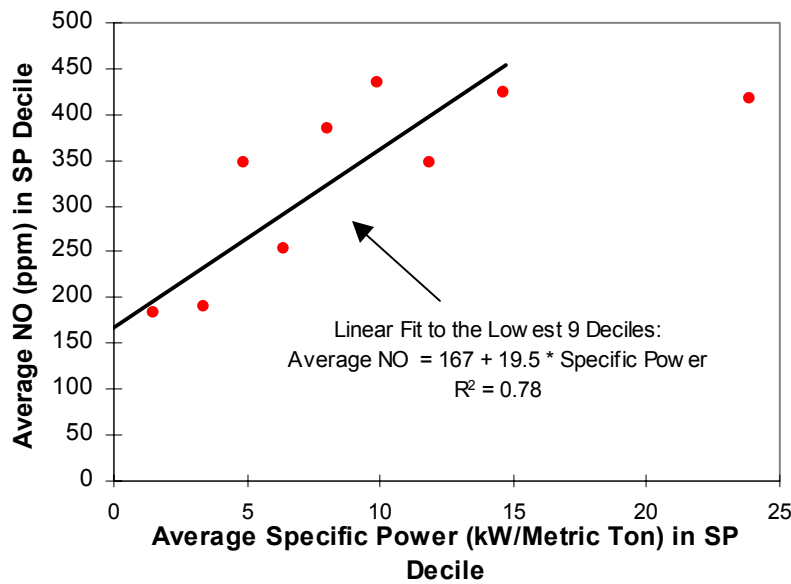
Figure 6-22: Average NO emission vs. average vehicle specific power by population decile

6.4.7. Effect of Speed, and Acceleration on NO Emissions

The effect of speed and acceleration on NO emissions is also presented here for completeness and to allow the comparison with past or future studies for which specific power may not be available. Figure 6-23 is the scatter plot of NO emission vs. vehicle speed. There is no apparent trend in the graphed data, which is corroborated by the very low value of the correlation coefficient.

Figure 6-24 shows the result of averaging the NO emission data for each vehicle speed population decile as described above. Emissions decrease slightly at the higher speeds, but the differences between the deciles are not statistically significant. This result is to be expected since the instantaneous speed of the vehicle does not have any fixed relationship with the engine combustion and emission control catalytic processes that form and destroy NO.[185]

---

[185] Vehicle speed has some correlation with specific power ($R^2 = 0.17$, Figure 6-9), which has significant correlation with NO in decile-averaged form (Figure 6-22). However the relationship of speed and specific power is probably too weak to influence the NO vs. speed curve.
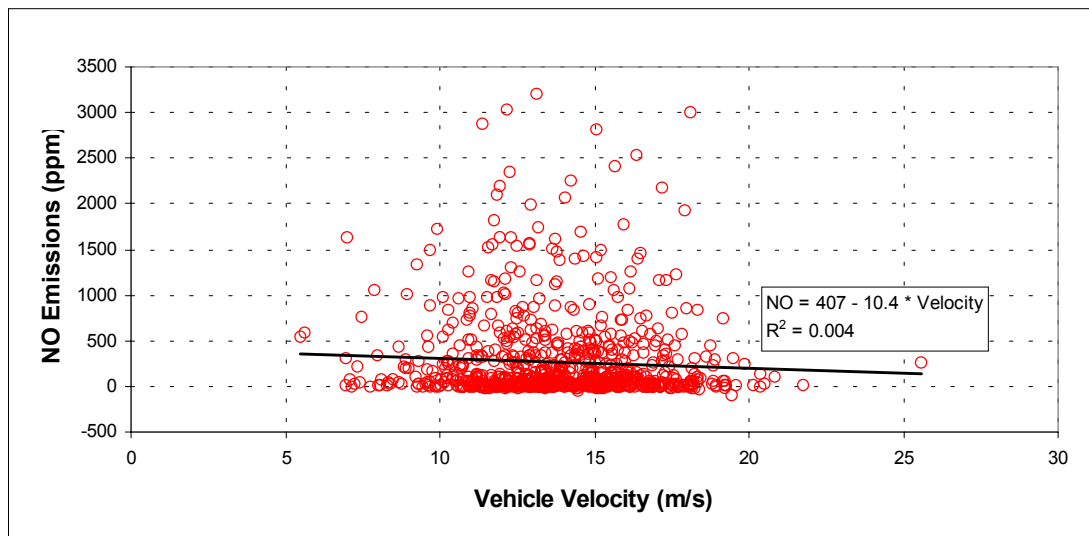
Figure 6-23: Scatter plot and linear regression of NO emission vs. vehicle speed
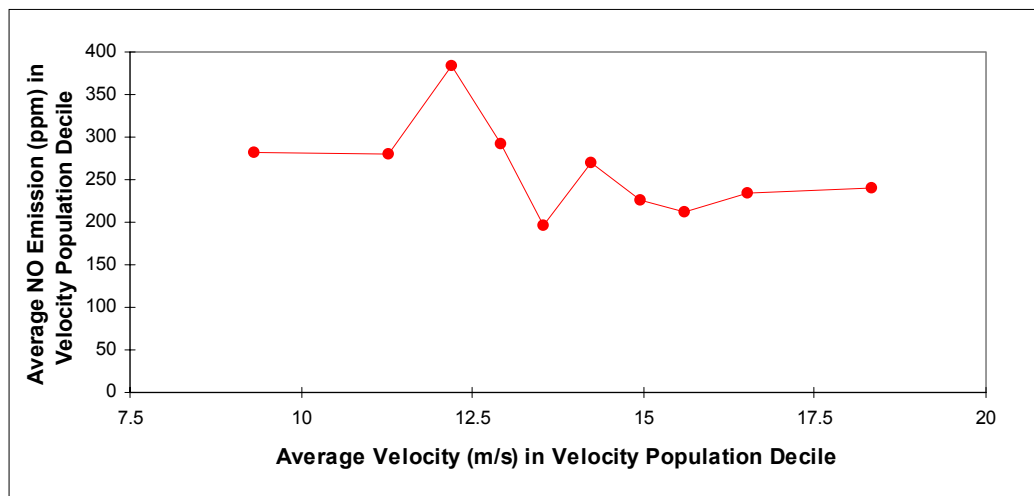
Figure 6-24: Average NO emission vs. average vehicle speed for every speed population decile

Figure 6-25 presents the scatter plot of NO emissions vs. vehicle acceleration. It is hard to see a trend due to the overwhelming majority of cars with low NO emissions, but a larger fraction of the cars with high acceleration tend to have higher emissions.
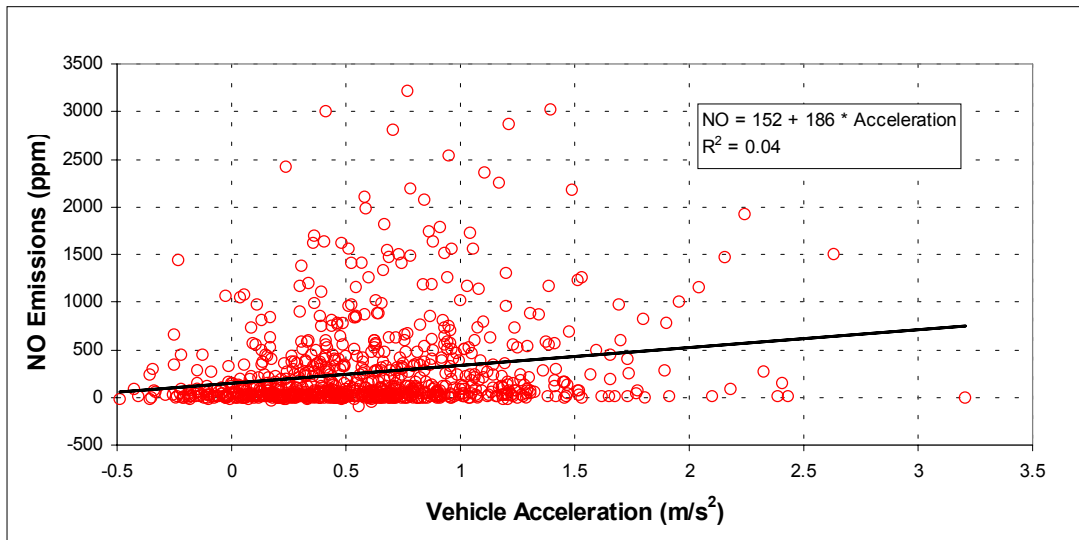
Figure 6-25: Scatter plot and linear regression of NO emission vs. vehicle acceleration.
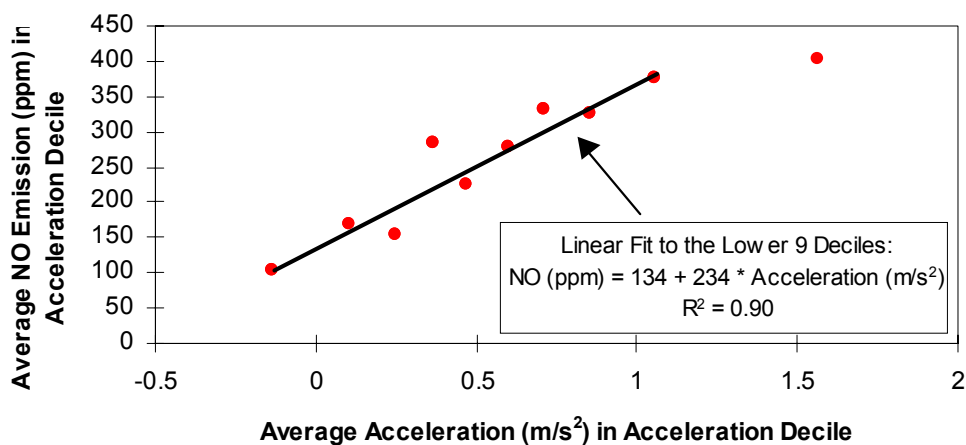
Figure 6-26: Average NO Emission and average vehicle acceleration for every acceleration population decile.

Figure 6-26 shows the result of averaging the NO emission data in the acceleration rank ordered vehicle population decile. A clear correlation between average NO emission and average acceleration appears, with the last decile showing a smaller rate of increase. This result has been recently duplicated with the UV remote sensor of the University of Denver (Popp *et al.*, 1998a). The positive correlation of NO with acceleration as shown by the linear regression line in this figure is caused by the same reasons indicated for specific power (section 6.4.5): the increase of NO concentration

with power which appears for catalyst-equipped vehicles and the effect of commanded enrichment at the largest accelerations.[186]

6.4.8. Correlation between NO Emissions and CO/HC Emissions

The NO, CO, and HC emissions of 822 vehicles[187] were measured simultaneously using the TILDAS instrument to measure NO and the two Hughes SBRC Smog Dog instruments to measure CO and HC.[188]

Figure 6-27 shows a scatter plot of NO versus CO emissions. No relationship between them is apparent on a vehicle-by-vehicle basis. The linear regression correlation coefficient obtained was very small, meaning, among other things, that one can not predict the NO remote sensing emission level of a vehicle from the CO remote sensing emissions of the same vehicle and vice-versa.
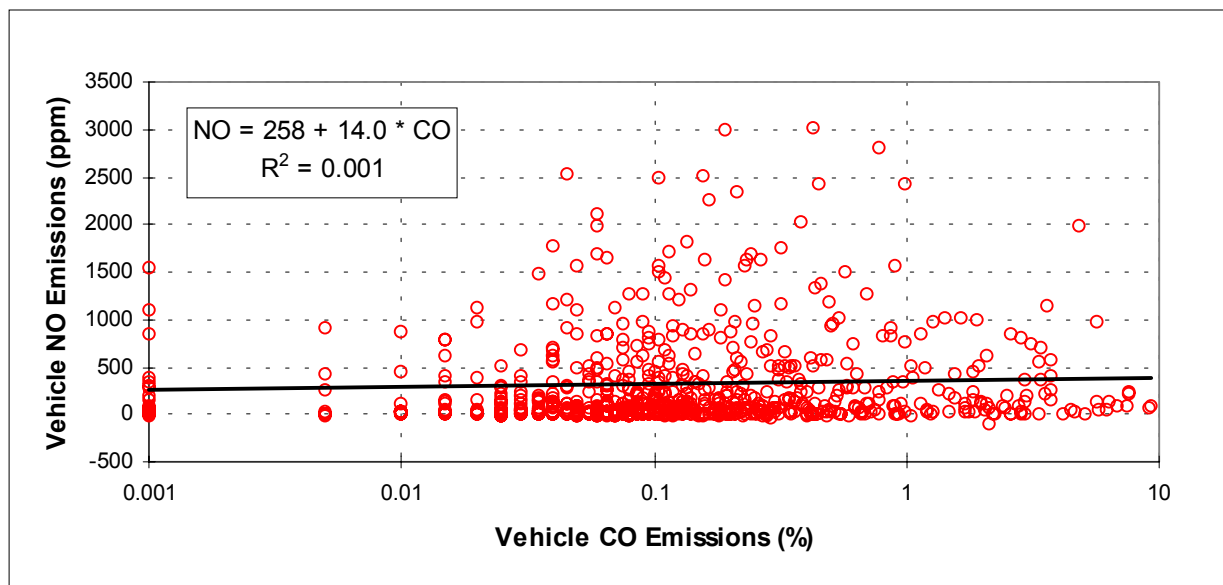
Figure 6-27: Scatter Plot and Linear Regression of NO Emission vs. CO Emission

---

[186] It has been shown in section 3.2.4 that acceleration is not as good a predictor of commanded enrichment as specific power. This may be the reason why Figure 6-26 does not show as clear a departure for the last decile as Figure 6-22.

[187] This number is smaller than the 1473 NO measurements because the Hughes "Smog Dog" instruments were set up only part of the time that the TILDAS instrument was in operation.

[188] When both Hughes "Smog Dog" remote sensing instruments had valid CO and HC measurements, both readings were averaged. Otherwise the one valid measurement was used. The correlation between the results of both instruments measured at the same time for the same vehicle was very good.

In Figure 6-28, the NO and CO binned by rank-ordered CO emission vehicle population deciles are shown. For example, the first point represents the average NO emissions of the 10% of the vehicles with the lowest CO emissions plotted against the average CO emissions of those vehicles. The next point contains the average CO and NO for the next 10% cleaner vehicles for CO, and so on. It is apparent from the figure that for 80% of the vehicles with the lowest CO emissions, there is a weak positive correlation between the binned emissions of both pollutants. This is the opposite of that which was found in the previous study (Zhang *et al.*, 1996a).[189] For the 20% of vehicles with the highest CO emissions, CO and NO appear to be weakly anticorrelated.

We can qualitatively explain this trends in the following way: untreated exhaust from an internal combustion engine running at stoichiometric conditions contains around 0.5% CO (Heywood, 1988; also Figure 3-7 and Figure 3-9). CO would be reduced to about 1/10 of that by a properly functioning catalyst. Thus the last 2 deciles (especially the last one) are made up of vehicles running with rich air-fuel mixtures.[190] On these vehicles we see the well-known inverse relationship between untreated engine NO and CO emissions as a function of combustion stoichiometry (Heywood, 1988).

The 8 lower deciles in Figure 6-28 have CO concentrations lower than 0.5% of the exhaust. We can assume most of them to be running under stoichiometric conditions.[191] This means that these cleaner vehicles have a totally or partially functioning emissions control system which is reducing the engine out CO concentration to lower than 0.5%. For those vehicles we observe a simultaneous increase of both NO and CO. This may be due to the simultaneous increase which appears in tailpipe emissions of properly functioning vehicles for moderate powers (see Figure 3-10 and Figure 3-14) or to catalyst degradation which would affect both pollutants.

---

[189] Actually the same trend of Figure 6-28 is present in the data of the previous study when they are averaged using the same decile approach used here. However Zhang et al. used fixed size bins which would bin most of the first 8 deciles into 1 or 2 bins and spread the last 2 deciles into many bins. This creates the misleading impression that CO and NO are anticorrelated for most of the fleet when in fact that is only true for the higher emitters.

[190] Either by malfunction of by commanded enrichment operation.

[191] CO would be larger than 0.5% if this was the case since the engine-out CO concentration would be larger than 0.5% and the catalyst would be largely ineffective in reducing these emissions due to lack of oxygen. Also, practically all the vehicles in this study had closed-loop air fuel ratio control to maintain stoichiometric conditions.
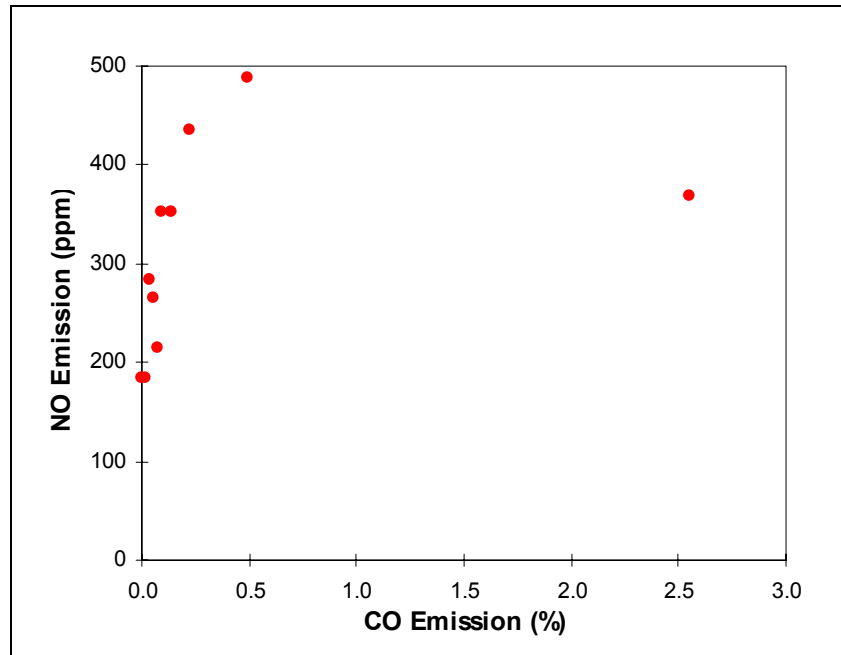
Figure 6-28: Average NO vs. CO emissions for vehicle population deciles
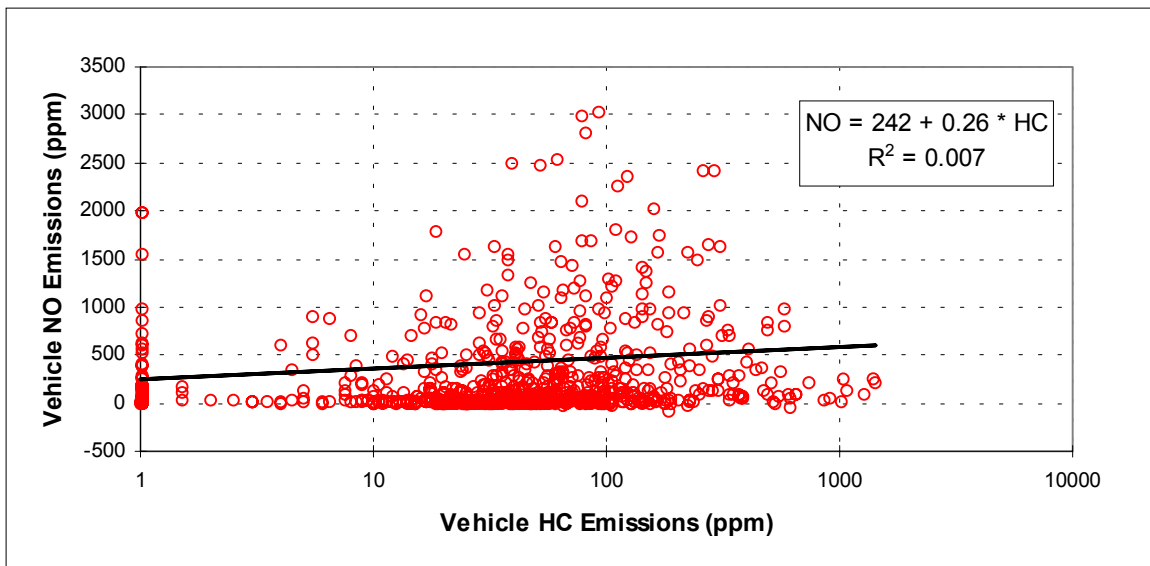
Figure 6-29: Scatter Plot and Regression of NO Emission vs. HC Emission

Figure 6-29 presents the scatter plot of NO vs. HC emissions. Again, there is no apparent correlation on a vehicle by vehicle basis, a result corroborated by the low value of the correlation coefficient.

Figure 6-30 presents the NO vs. HC emissions binned by HC emissions rank ordered vehicle population deciles. The trends are similar to those of the NO vs. CO graph; i.e. increasing NO with increasing HC for the vehicles with lower HC, and decreasing NO with increasing HC for the 20% or so vehicles with the highest HC emissions. These trends can be qualitatively explained by the same effects described above for CO.
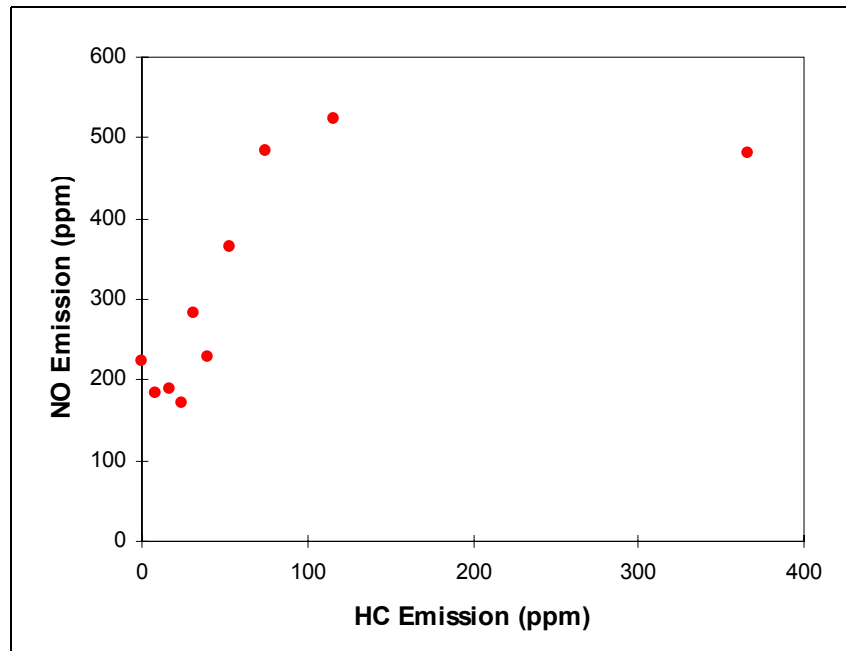
Figure 6-30: Average NO vs. HC emissions for vehicle population deciles

6.4.9. Effect of Model Year on Emissions

Model year (or vehicle age) has been found to have an important effect on average remote sensing emissions (Zhang *et al.*, 1993; Zhang *et al.*, 1996a; Stedman *et al.*, 1997a). This effect is studied here for our TILDAS remote sensing results.

Figure 6-31 shows the scatter plot of NO emissions vs. vehicle age. The correlation between NO emissions and vehicle age is small on a vehicle by vehicle basis ($R^2 = 0.14$). For any single model year there is a very wide variation in emissions values, typically spanning almost three orders of magnitude. High NO emitters are found in every model year, but are more common among older vehicles.

The equation shown on the chart:
$$NO = 33 + 32 * Age$$
$$R^2 = 0.14$$
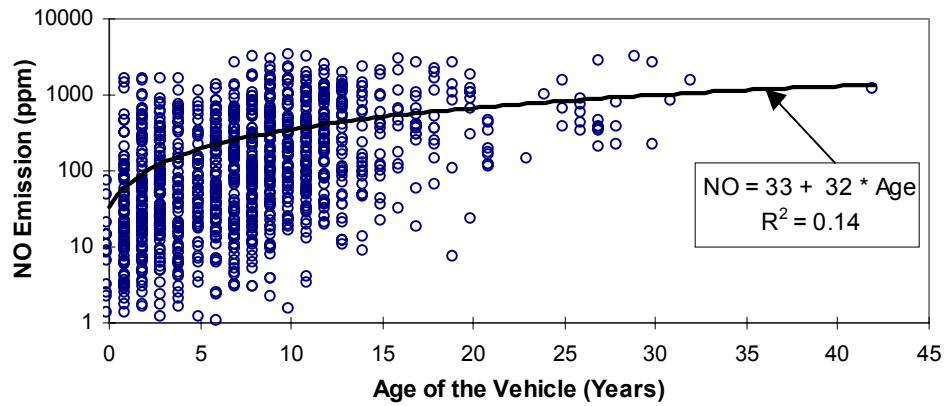
Figure 6-31: NO emission vs. vehicle age for the TILDAS remote sensing data

The average NO emissions for every model year are presented in Figure 6-32. They show an almost monotonic increase in model year average NO emissions with vehicle age as, for both passenger cars and light-duty trucks. Due to the small sample size, data on vehicles built prior to 1983 are not considered reliable for a single model year. However, the aggregated NO emission data for all vehicles prior to 1983 does show these vehicles to be higher NO emitters than subsequent model years. Zhang et al. (Zhang *et al.*, 1996a) reported that average NO ceased to increase with age curve for vehicles more than about 10 years old. In our study the emissions increase steadily for vehicles from 10 to 13 years (1984-1987).
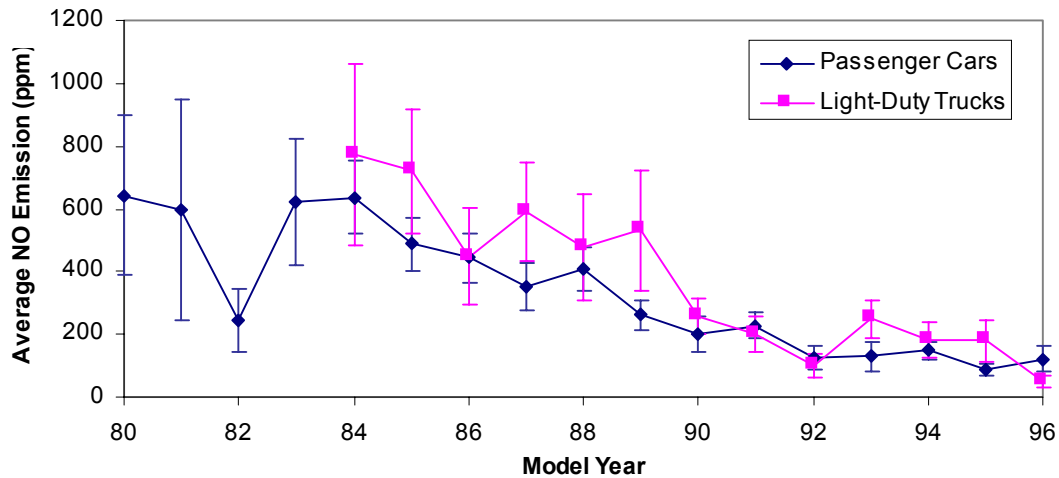
Figure 6-32: Average NO (ppm) emissions versus vehicle model year

Light-duty trucks have higher average emissions in concentration units, owing to their less stringent emissions standards (Sawyer *et al.*, 1998a). Stedman et al. (Stedman *et al.*, 1997a) have also observed this effect in remote sensing data for CO in Colorado. The averages in grams-per-mile units[192] (Figure 6-33) show a larger difference due to the lower fuel economy of light-duty trucks.
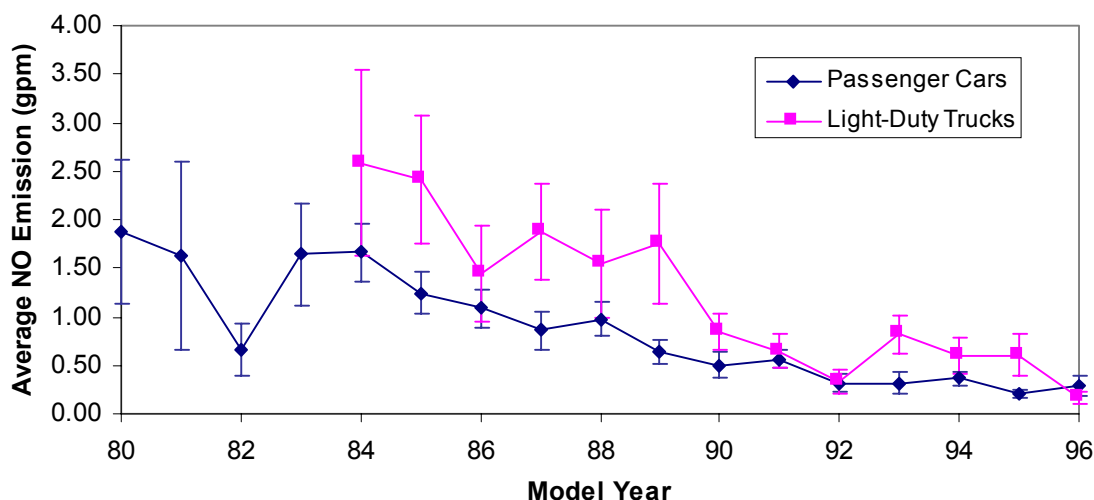
Figure 6-33: Average NO (grams/mile) emissions versus vehicle model year

6.4.10. Comparison with the EMFAC model and Emission Standards

Figure 6-34 compares the average NO emissions of cars vs. their emission standards for every model year[193, 194] and the result of California's emission factor model, EMFAC (version 7G). Figure 6-35 shows the same comparison for light-duty trucks.

In the figures we can appreciate that newer vehicles tend to be at or below their emission standards for NO while older vehicles are generally above them, due to

---

[192] Converted from the concentration units using the average fuel economy for each vehicle type and model year (Heavenrich *et al.*, 1996), using the procedure of Appendix A.

[193] Some emission standards are applicable at 50,000 miles while others are at 100,000 miles. Since the average mileage accumulation in the U.S. is about 11,000 miles per year for passenger cars and 14,000 miles per year for light-duty trucks (U.S. EPA, 1995a), the standards at 50,000 miles were used for passenger cars newer than model year 1993 and light-duty trucks newer than 1994. The emission standards 100,000 miles were used older vehicles.

[194] The emission standards for light-duty trucks are different for each weight class (Sawyer *et al.*, 1998a). A "composite" emission standard for light-duty trucks was calculated as the weighed average of the standards for each weight class. The averaging weights used were the actual fractions of light-duty trucks of each vehicle weight class in the remote sensing sample for the particular model year. This is why the light-duty truck standard line looks jagged on the figure.

degradation of the emission control systems beyond 100,000 miles and their lower durability compared to newer vehicles (Berens *et al.*, 1997).

The output of the EMFAC model consists of emission factors vs. average speed for every model year and vehicle type. The emissions factors represented here are those at 30 mph (the average speed in our data set) and at 55 mph, which is a closer approximation the actual engine power demand at the site.[195]

Comparing with the results at 55 mph, EMFAC predicts well the NO_x emissions of passenger cars from 1991 to 1996. NO_x emissions of older model years are significantly overestimated. A similar result is found for light-duty trucks.
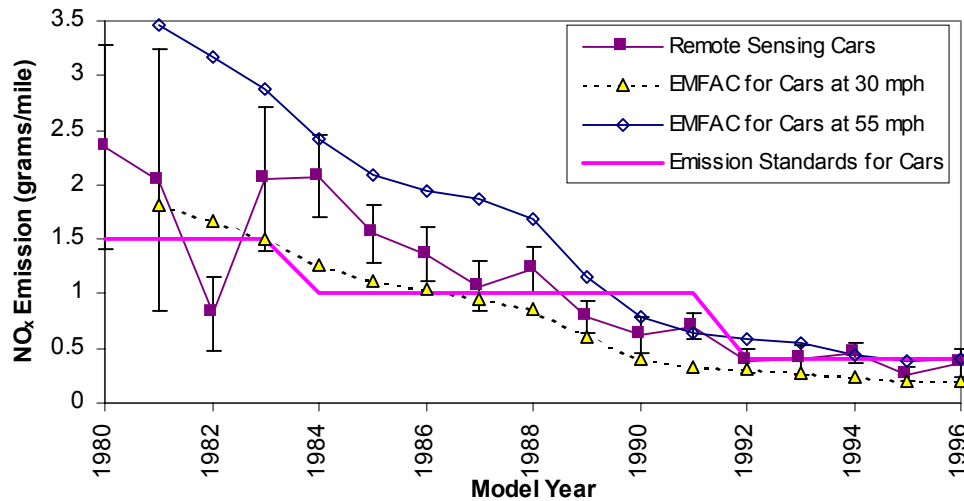
Figure 6-34: Average NO remote sensing emission vs. model year for <u>passenger cars</u> compared to the EMFAC model result and the emission standard of that model year

---

[195] The presence of the 4% grade at the measurement site created higher engine power demand than would be expected for a typical 30 mph urban trip. The emission factors at higher average speed can be chosen to represent higher loads (see Figure 3-41). To find the average speed increase which would result in the same average load increase imposed by the grade, we have used the new definition of vehicle specific power proposed in Chapter 3:

- A 4% grade at 30 mph (average speed at the site) requires an increase of specific power of 5.3 kW/Metric Ton with respect to the case without grade.
- The same increase of 5.3 kW/Metric Ton in specific power is achieved by increasing the average speed from 30 to 55 mph (on a level road). The increase in specific power with increasing speed in this case is due to the rolling resistance and aerodynamic drag terms.
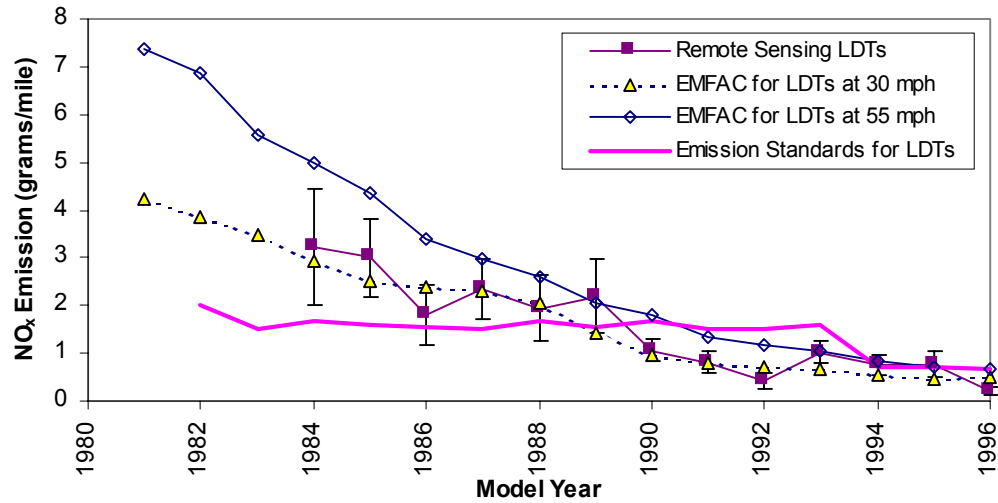
Figure 6-35: Average NO remote sensing emission vs. model year for <u>light-duty trucks</u>, compared to the EMFAC model result and the emission standard of that model year
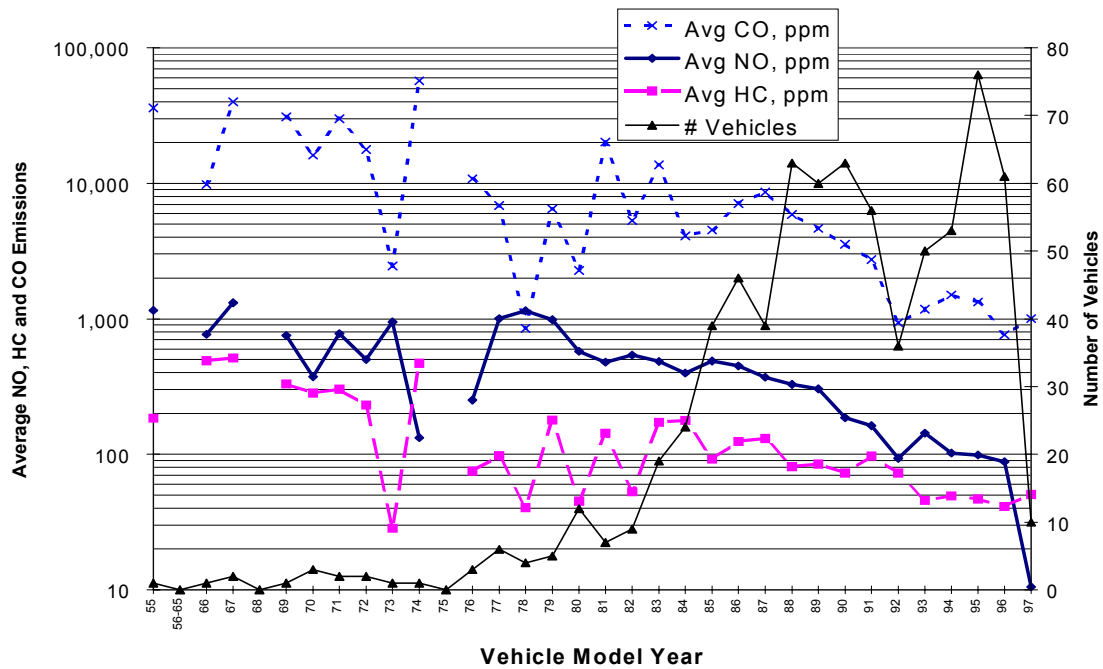
Figure 6-36: Average NO, HC and CO emissions vs. model year

6.4.11. Emission Contribution vs. Model Year

One of the key features of this study was the simultaneous recording of NO, CO and HC emissions for a large and reasonably unbiased population. Figure 6-36 shows the average emission of each pollutant vs. model year. All emission levels increase with vehicle age. This relationship undoubtedly underlies the portion of positive correlation between NO/CO and NO/HC discussed in section 6.4.8.
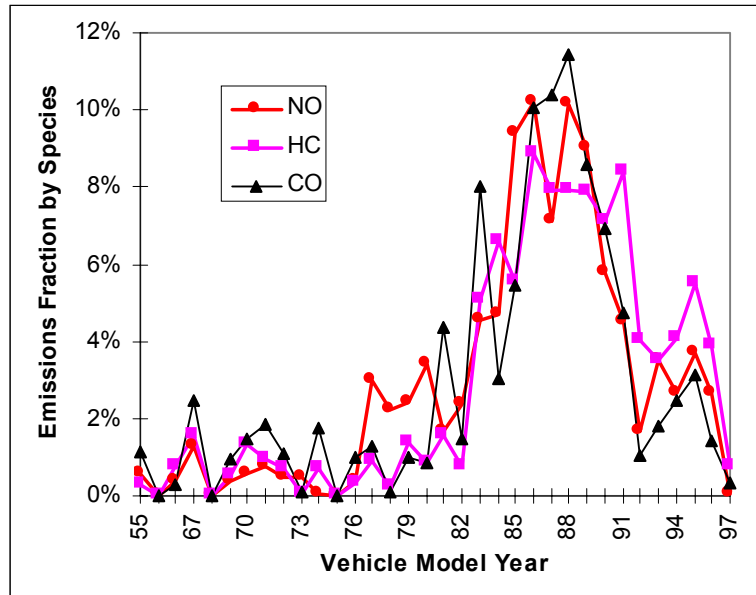
Figure 6-37: Total NO, HC and CO emissions by model year

In Figure 6-37 the total emission contributions, the product of the average model year emission level and the number of vehicles of that model year are shown.[196] The graph shows that for NO, CO, and HC the total contribution of each model year is remarkably similar. Vehicles about 10 years old produce the greatest proportion of the emissions for all three pollutants.

6.4.12. NO Emissions Variability

NO emissions variability for individual vehicles is an important issue since a high variability will make a single remote sensing measurement less meaningful. The data from the present study provide an opportunity to study this issue, as the NO emissions from 117 vehicles were measured more than once. These data are analyzed in Figure

---

[196] A similar analysis for N_2O is shown in section 8.3.5.

6-38 which shows the first two measurements for each vehicle measured more than once plotted versus the average value of the measurements. About half of the vehicles with high NO emissions have high variability while the other half have markedly less variability.[197] Thus some of the high emitters are very consistent while others are more variable ("flippers"), which is not surprising given the strong dependence of NO emissions on specific power (e.g. Figure 6-17). This variability is similar to what has been observed previously for CO and HC emissions (Bishop *et al.*, 1996d).
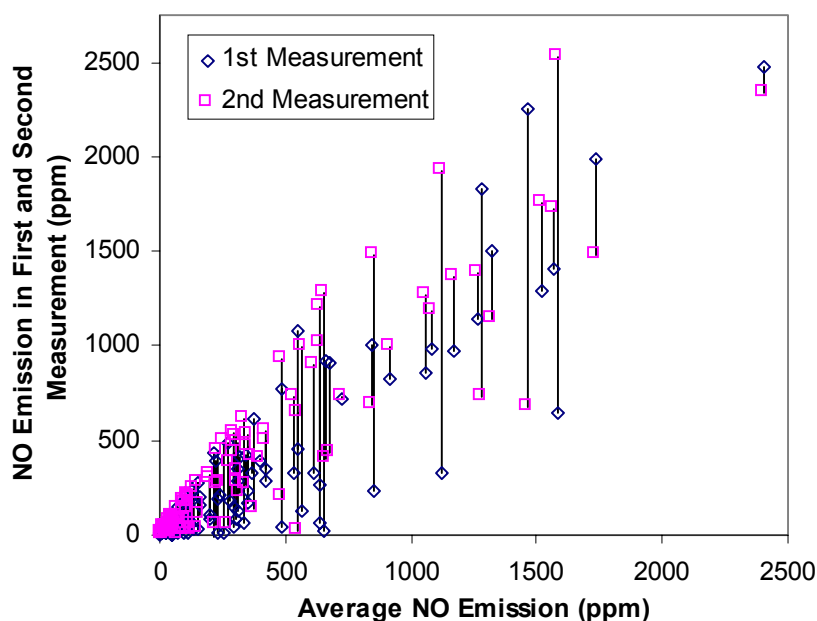
Figure 6-38: NO emissions in the first and second passes vs. the average emissions for vehicles measured more than once

6.4.13. High Emitters vs. Clean Vehicles

The fraction of the total emissions that is emitted by the dirtiest and cleanest cars for each pollutant for the remote sensing data set acquired in this study is analyzed in this section.[198] This information is applicable to the design of remote sensing programs for both high and low-emitter identification.

---

[197] Practically all of the measured NO emissions variability can be attributed to the vehicles themselves and not to the TILDAS instrument, since the variability of most measurements is far larger than the TILDAS measurement precision.

[198] The analysis presented here is limited by the fact that the same emission data used to classify the vehicles are used to represent their emissions. Another limitation is that this analysis is based on remote

These analyses are presented in Figure 6-39 and . Each category in Figure 6-39 represents a different group of vehicles chosen by some property of their emissions. For each category the first column is the percentage of vehicles[199] included, and the next three columns represent the percentage of the total emissions of CO, HC, and NO which are produced by those cars.

The first 3 categories correspond to the 10% dirtiest vehicles for every individual pollutant, which emit 50% or more of that particular contaminant. High CO emitters are responsible also for a significant fraction of the HC emissions, and vice versa. The fraction of the NO emissions captured by those 2 categories is small.[200] High NO emitters, on the other hand, capture half of the NO emissions but only a small fraction of the CO and HC emissions.[201]
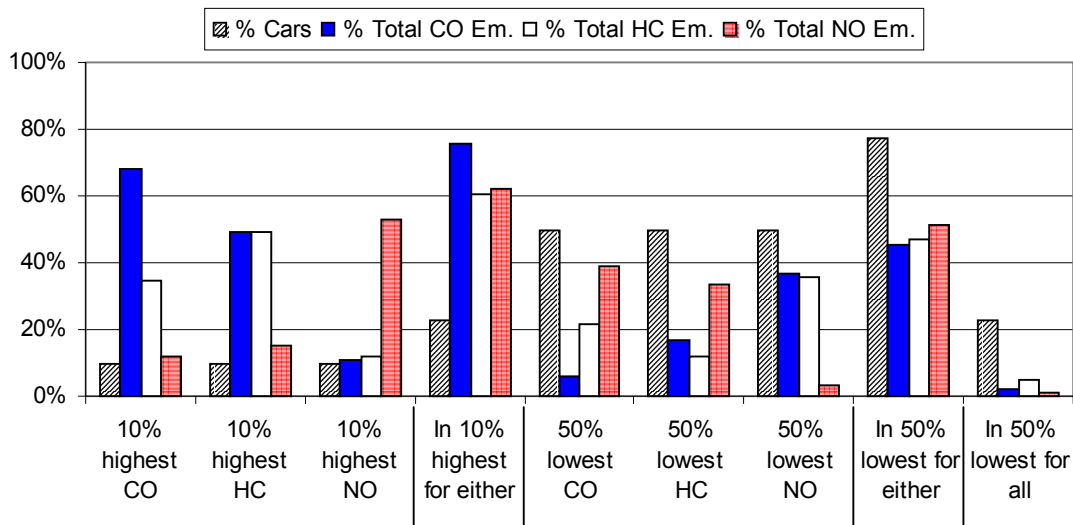
Figure 6-39: Contribution to the total emissions of CO, HC, and NO by different groups of vehicles

---

sensing data, an repeating it with the emissions data for the same vehicles under a range of driving conditions could yield different results.

[199] Out of a sample of 822 for which NO, CO, and HC data are available.

[200] This is expected since high CO and HC emitters are running with rich mixtures which inhibit NO formation in the engine.

[201] This indicates that these vehicles are mostly running lean or stoichiometric. Under these conditions the amounts of CO and HC emitted are much smaller than under rich conditions. If the mixture is lean and the catalyst is working totally or partially, it will reduce the CO and HC very effectively while not acting on the NO.

If we look at the group that are high emitters for either pollutant we would find 30% of the vehicles if the 3 subsets were totally disjoint, 10% if they were identical. We actually find 23% of the vehicles which is due to the fact that the CO and HC high emitters are mostly the same, while the NO high emitters are mostly a disjoint subset of them. This 23% of the vehicles is responsible for more than 60% of the emissions for all pollutants. This is the group that an inspection and maintenance program should focus on.

	% Cars	% Total CO Em.	% Total HC Em.	% Total NO Em.
10% highest CO	10%	68%	35%	12%
10% highest HC	10%	49%	49%	15%
10% highest NO	10%	11%	12%	53%
In 10% highest for either	23%	75%	61%	62%
50% lowest CO	50%	6%	22%	39%
50% lowest HC	50%	17%	12%	33%
50% lowest NO	50%	37%	35%	3%
In 50% lowest for either	77%	46%	47%	52%
In 50% lowest for all	23%	2%	5%	1%
80% lowest CO	80%	19%	50%	73%
80% lowest HC	80%	35%	35%	68%
80% lowest NO	80%	77%	76%	24%
In 80% lowest for all	60%	12%	25%	16%

Table 6-7: Emission contribution of different categories of vehicles

We can also look at the cleaner cars for each pollutant to see whether we could exempt some vehicles in this fleet from an inspection and maintenance program (as in the so-called "clean screen" programs). I have chosen first to look at the 50% cleaner vehicles for each pollutant, which correspond to categories 4th to 7th in Figure 6-39. The results indicate the same trends that those of the high emitting vehicles: low CO emitters and low HC emitters tend to be the same vehicles, while low NO emitters are mostly disjoint from them.

If we look at the vehicles that are low emitters for *all* three pollutants we find 23% of the vehicles that are responsible for only 1-5% of the emissions. This large group could be exempt from an I/M program, which would result in savings of about 14% of

the I/M program cost,[202] since about 60% of the costs of an I/M program are associated with testing (Barrett, 1998; Harrington, 1998).

We can investigate the limits of this approach by analyzing a larger fraction of the clean vehicles. The last four categories in correspond to the vehicles which have the lowest 80% of the emissions for either and all pollutants. The trends for the individual pollutants are similar to those described above. Interestingly, 60% of the vehicles belong to the cleanest 80% for all 3 pollutants. They are responsible for 12-25% of the emissions. This is probably as far as where a clean screen program could go without starting to loose a significant fraction of the achievable emissions reduction. If 60% of the vehicles were exempt from testing the I/M program cost would be reduced by 36%.

Figure 6-40 shows the age distribution of some of the vehicle groupings described above: all the measured vehicles, high emitting vehicles for either pollutant, the vehicles which are in the 50% and 80% cleanest for all pollutants. The very clean cars tend to be newer and the high emitting cars tend to be older. This is also shown by the average age of each group: 8 years for the average fleet, 6 years for the "clean vehicles," and 12 years for the high emitters. In the light of these results it would seem reasonable to exempt the last 3 to 6 model years from having to pass the I/M program as a way to save resources. The same conclusion has been reached in other recent studies using slightly different methodologies than in this section (Kishan *et al.*, 1998; St. Denis, 1998; Wenzel *et al.*, 1998a).
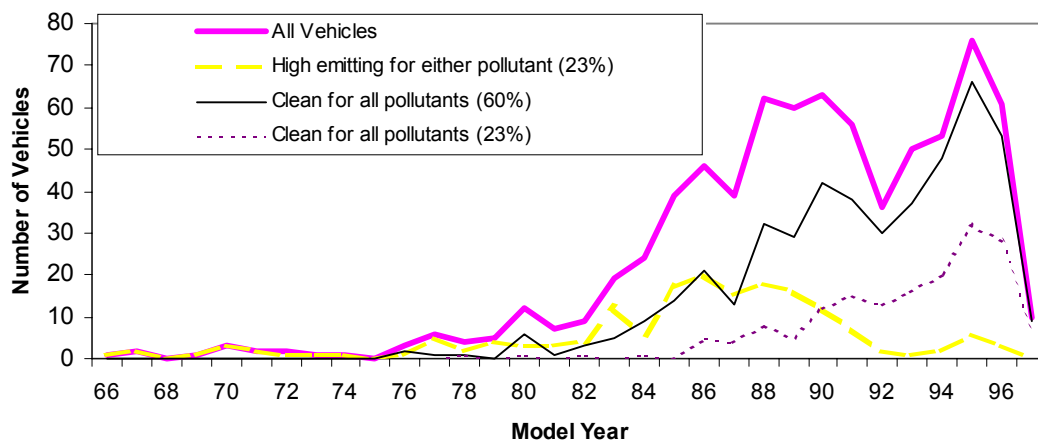
Figure 6-40: Age distribution of several types of vehicles measured by remote sensing

---

[202] Neglecting the costs associated with remote sensing.
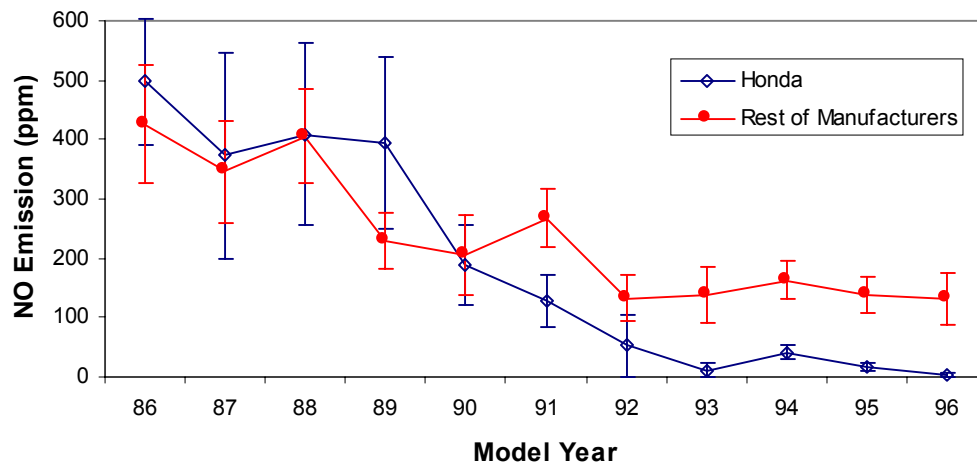
Figure 6-41: NO emissions vs. model year for Honda and the rest of the manufacturers (passenger cars only)

6.4.14. NO Emissions and Vehicle Manufacturers: The Case of Honda 93-96

Wenzel et al. (Wenzel *et al.*, 1996; Wenzel *et al.*, 1997; Wenzel *et al.*, 1998b) have shown that specific vehicle models may have more high CO emitters than the population average. In this section we present evidence that the vehicles of a particular manufacturer and model year range are cleaner on average due to having significantly fewer high emitters than the overall fleet.

Figure 6-41 shows the average NO emissions measured with the TILDAS instrument in California vs. model year, for the passenger cars[203] manufactured by Honda and by the rest of the manufacturers. The Hondas are significantly cleaner than the rest from model year 1993 on, and the differences are statistically significant for model years 94-96 (Table 6-9 and Figure 6-46).

The real difference in grams per mile emission will be actually larger than what is shown in Table 6-9 since the Honda cars have smaller engine displacement[204] in average than the rest of the vehicles as shown in Figure 6-42.

---

[203] Light-duty trucks are excluded since all of the Honda vehicles in this sample were passenger cars and LDTs are subject to less stringent emission standards and do show higher NO exhaust concentrations (Figure 6-32).

[204] Smaller engine displacement is highly correlated with higher fuel economy (Heavenrich *et al.*, 1996), which allows higher emission concentrations to satisfy the same grams/mile emission standards. Thus the differences shown in this section would be even larger in favor of Honda if expressed in grams/mile units.
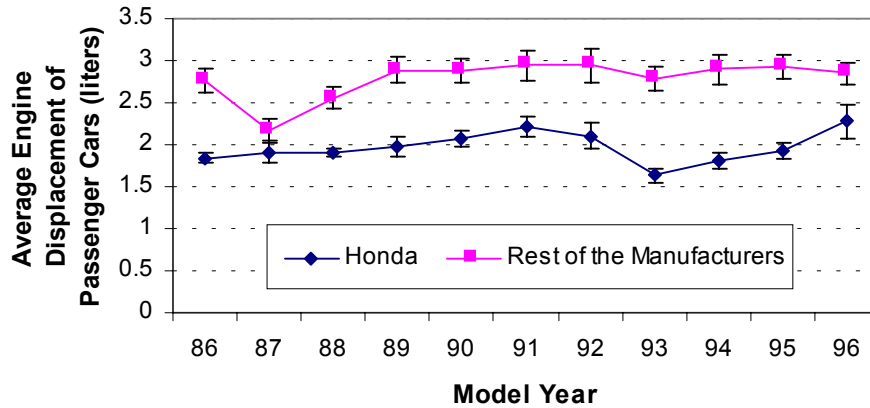
Figure 6-42: Average engine displacement of passenger cars vs. model year for Honda and the rest of the manufacturers

The CO, HC, and N_2O emissions vs. model year for these two groups of vehicles are shown in Figure 6-43, Figure 6-44, and Figure 6-45 respectively. All of them but one show differences in favor of the Honda vehicles, although not all the differences are statistically significant (see Table 6-9 and Figure 6-46).
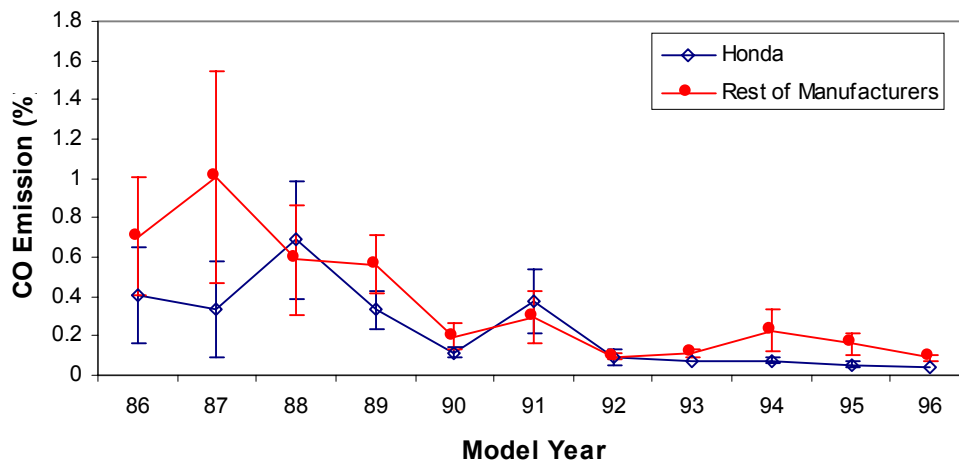
Figure 6-43: CO emissions vs. model year for Honda and the rest of the manufacturers (passenger cars only)
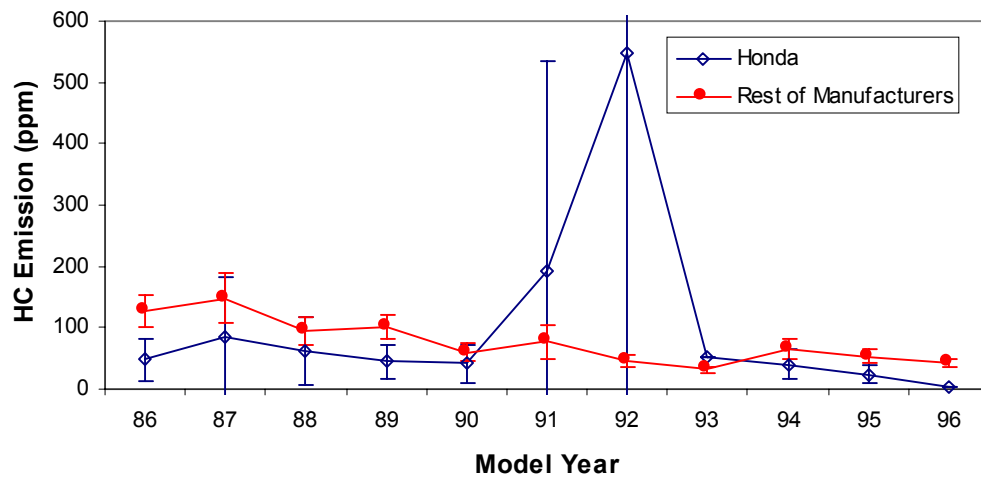
Figure 6-44: HC emissions vs. model year for Honda and the rest of the manufacturers (passenger cars only)
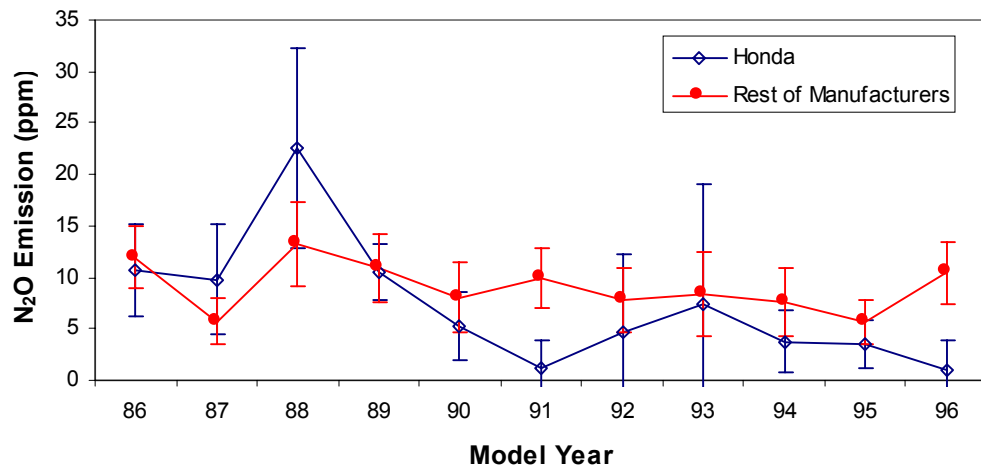
Figure 6-45: N₂O emissions vs. model year for Honda and the rest of the manufacturers (passenger cars only)

As for the reasons of these differences, I. Sakai, Chief Engineer at Honda Research & Development manifested (Sakai, 1998): "We have marketed cleaner vehicles than required by regulation from 1993, which is the TLEV category vehicle. After that we have tried to be beyond regulation." That would indicate that the some or all recent Honda vehicles are cleaner than the average fleet vehicle.
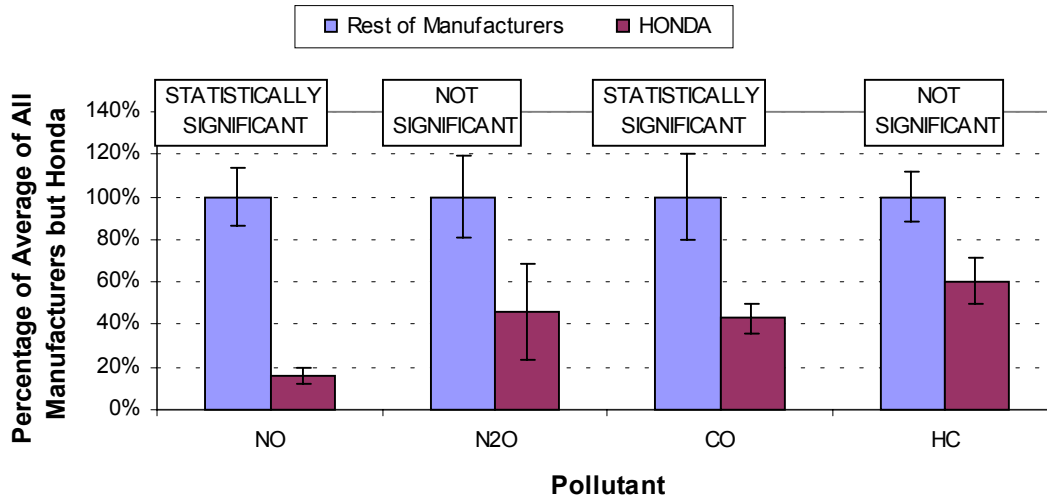
Figure 6-46: Comparison of the average emissions for each pollutant for Honda vs. the rest of the manufacturers (passenger cars only)

MY	# Honda for NO	# Rest for NO	NO Hon./ Rest	SS	# Honda for N2O	# Rest for N2O	N2O H/R	SS for N2O	# Honda for CO & HC	# Rest for CO & HC	CO H/R	SS for CO	HC H/R	SS for HC
93	3	43	8%	No	3	37	87%	No	1	26				
94	10	47	25%	Yes	8	44	49%	No	5	28	33%	No	61%	No
95	12	60	13%	Yes	12	56	63%	No	8	37	33%	Yes	43%	No
96	5	59	2%	Yes	4	51	10%	No	1	35				
All	30	209	16%	Yes	27	188	46%	No	15	126	43%	Yes	60%	No

Table 6-9: Emissions difference and statistical significance (SS) for the different model years and pollutants[205]

This point is analyzed by comparing the distributions of NO emissions for the two groups in Figure 6-47. The reason why the Honda vehicles have lower average emissions seems to be more the lack of high emitters than lower average emission of the normal emitters. This points to a more durable or robust emission control system in the Honda vehicles. Twenty seven percent of the cars from other manufacturers have larger NO emissions than the highest Honda.

---

[205] The statistical significance was determined by the one-sided Wilcoxon rank-sum test. The t-test cannot be used since the distributions cannot be assumed to be normal (MathSoft, 1997).
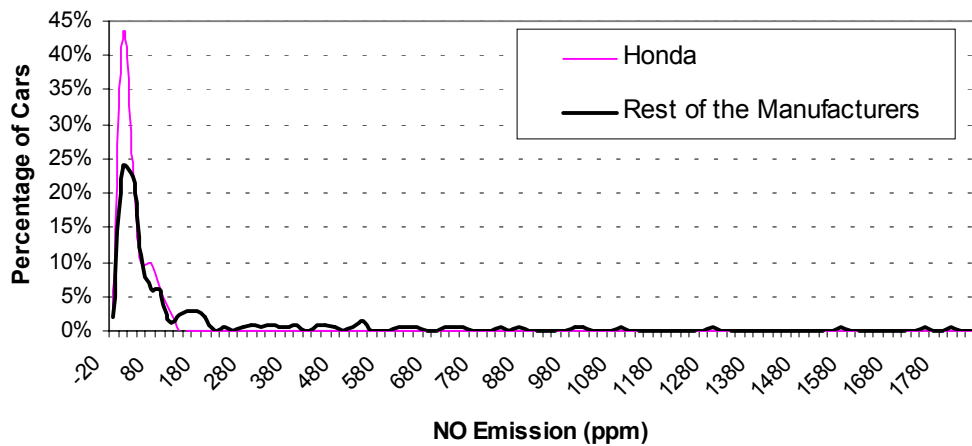
Figure 6-47: Comparison of the distribution of NO emissions between Honda and the rest of the manufacturers for model years 93-96

This analysis also highlights the value of high precision remote sensing, which allows the study of real-world differences such as the one discussed here even for relatively small vehicle samples. Of course larger samples are preferable, but they can be obtained without major problems in future studies.
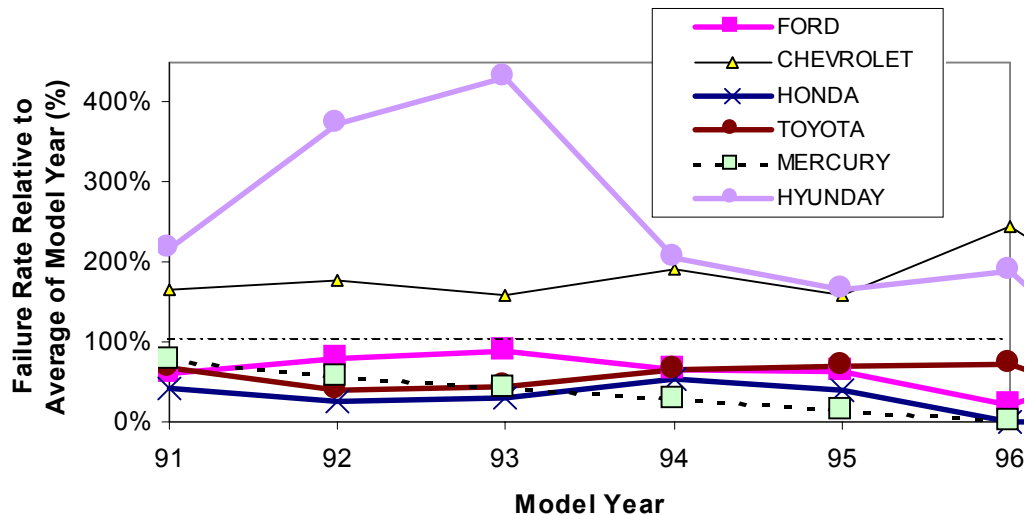
Figure 6-48: Arizona IM240 failure rates of 6 manufacturers relative to the fleet average for a given model year[206]

---

[206] Fleet average failure rates decile from 10.3% for 1991 model year vehicles to 0.79% for 1997.

6.4.15. Analysis of Failure Rates by Make for Arizona IM240 data

The main limitation of the analysis in the previous section is the limited sample size in the TILDAS remote sensing study. In this section we assess if such low high emitter incidence rates appear on a different data set: the data from the Arizona inspection and maintenance program in 1997.[207, 208] The database analyzed included about 170,000 individual IM240 tests. For consistency with the previous section, light-duty trucks have been excluded from this analysis.

The IM240 failure rate vs. model year for 6 makes which showed consistent higher or lower failure rates are shown in Figure 6-48. A vehicle fails the IM240 test if it exceeds an emission cutpoint for at least one pollutant (CO, HC, or NO_x), thus the failure rates can be thought of as a "high emitter frequencies."[209]

Honda appears again among the makes with lower than average failure rates for all model years. Hyunday has consistently higher high emitter incidence, as had been determined previously (Wenzel *et al.*, 1996).

Figure 6-49 shows the relative failure rates (overall and by pollutant) for vehicles of model year 1991.[210] Statistically significant differences[211] appear between the different makes. Again, certain manufacturers have much lower failure rates for all pollutants. Interestingly the luxury makes of Honda (Acura) and Toyota (Lexus) have lower failure rates than the parent makes. A possible explanation is that these manufacturers may fit their luxury vehicles with a more durable control system; in this way their best customers could avoid emission-related problems.

---

[207] This test uses the IM240 6-minute loaded cycle.

[208] These data were supplied by Tom Wenzel, Lawrence Berkeley National Laboratory.

[209] One limitation of these failure rates is that there is no difference between marginal high emitters and those with large excess emissions. Average emission data are not available because Arizona uses "fast passes" and "fast fails" very dirty and very clean vehicles, so a significant fraction of the fleet tested does not complete the full IM240 cycle. Some methods of estimating full IM240 from partial IM240 data exist (Ando *et al.*, 1998; Wenzel, 1998), but their reliability across different makes and model years may be questionable. For these reasons the estimated average IM240 emissions have not been used here.

[210] The total number of vehicles in the sample is 17,851. Only makes with more than 100 vehicles for MY 91 have been included. The makes are ordered by the number of vehicles in the sample, from 2378 cars for Ford to 112 for Volkswagen.

[211] Statistical significance was tested with an statistical test for rates and proportions (Fleiss, 1983; MathSoft, 1997).

Another interesting feature of the IM240 data set is the fact that different makes have significantly different failure rates for the different pollutants. For example, Chrysler, Dodge, and Plymouth vehicles, the three of which are owned by Chrysler Corporation, have significantly higher failure rates for NO_x in 1991. Based on EPA certification data, several Chrysler models of this model year did not use exhaust gas recirculation (EGR) to reduce engine-out NO_x emissions,[212, 213] relying solely on the three-way catalyst for NO_x reduction. Such vehicles will likely fail for NO first when the catalyst starts is deteriorated since their engine-out NO_x emissions are about twice as high as those of vehicles with EGR. Another manufacturer with high failure rates is Chevrolet which is high for CO, indicating a tendency to run rich upon failure.

---

[212] EGR can reduce engine-out NOx emissions levels by about a factor of 2-3 (see Figure 3-26).

[213] The Arizona data set did not include vehicle model, which precluded the verification of whether the failing Chrysler models for NO were predominantly those without EGR.
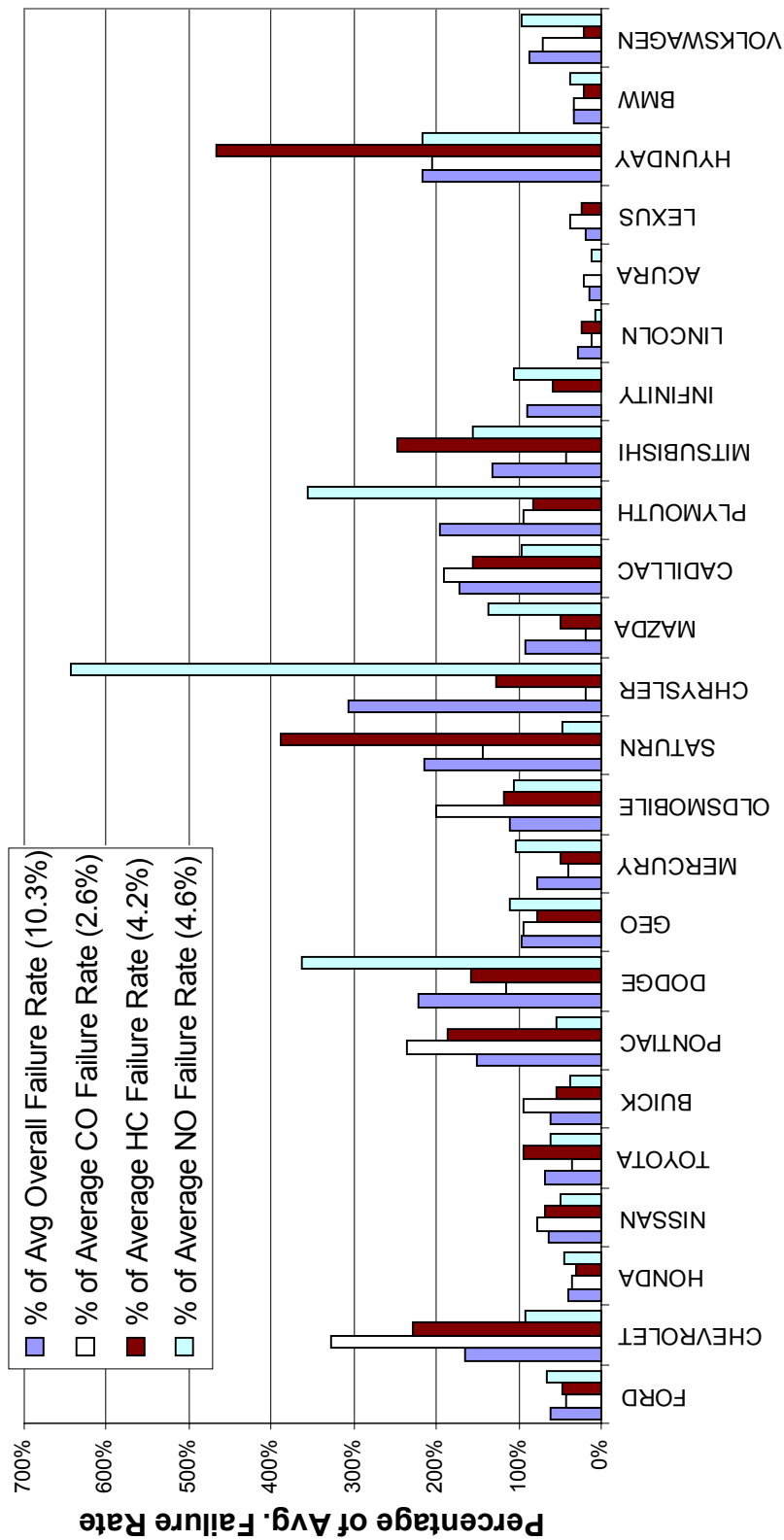
Figure 6-49: Failure rates by manufacturer in Arizona IM240 program for 1991 vehicles[214]

---

[214] Each column is the failure rate relative to the fleet average for that pollutant. The fleet average failure rates for the fleet of MY 91 passenger cars are given in the graph legend. E.g. the overall relative failure rate for Ford is 61%, meaning that the actual failure rate for this make was $10.3\% * 61\% = 6.3\%$. The relative CO failure rate for Ford was 43%, which means that the actual CO failure rate for Ford was $2.6\% * 43\% = 1.1\%$.

6.5. Conclusions of the NO$_x$ Remote Sensing Study

This study yielded a number of significant new findings with respect to the NO emissions of on-road vehicles and the utility of remote sensing emissions measurements:

- The TILDAS instrument consistently and accurately measured the NO emissions of on-road vehicles. The NO emissions of low emitters were measured with precision of approximately 5 ppm.

- The measured vehicle fleet NO emissions closely fit a gamma distribution with the 10 percent of the fleet having the highest emissions contributing about 50 percent of the total fleet emissions.

- The NO emission factor in this study is about 80% of those measured in 3 recent tunnel studies in California. The reason for this lower emission is not clear.

- Newer vehicles have lower average NO emissions than older ones but high NO emitters are found in every vehicle age cohort.

- The light-duty trucks in this study are higher NO emitters than passenger cars. About ½ of the difference is due to their lower fuel economy while the other ½ reflects higher NO exhaust concentrations, possibly due to more lenient emission standards.

- The EMFAC emission model accurately predicts the NO emissions of recent model years in our study and overpredicts those of older vehicles.

- Analysis of the NO data with respect to the other simultaneously recorded data for the subject vehicles shows that on a vehicle-by-vehicle basis NO emissions correlate only weakly with vehicle specific power, speed, acceleration, CO emissions or HC emissions.

- High NO emitting vehicles cannot be identified by remote sensing of CO or HC emissions and vice versa.

- When these same data are aggregated into rank ordered population deciles, positive correlations between decile averaged NO emissions and the decile averaged values of vehicle specific power, CO, and HC for most of the vehicles appear.

- When we compared the remotely sensed NO emissions measurements for 117 vehicles measured more than once, most of them were consistently low emitters. About half of the high NO emitters were found to be consistently high while the other half had significant variability.

- The 10% highest emitters for each of CO, HC, and NO in this study constitute a group of 23% of the vehicles with in excess of 60% of the emissions of each pollutant.

- Vehicles manufactured by Honda showed statistically significant lower NO emissions than the rest of the fleet for model years 93-96. This was mostly due to the lack of high emitters on the Honda fleet. Significant differences in high emitter incidence among makes also appear in Arizona IM240 data.

Chapter 7. Remote Sensing of NO$_x$ Emissions from Heavy-Duty Diesel Trucks

7.1. Introduction

As the NO$_x$ emissions of passenger cars and light-duty trucks have become increasingly controlled, the relative importance of heavy-duty diesel trucks and buses as a NO$_x$ source has increased. At present, heavy-duty diesel vehicles are estimated to contribute about ½ of the on-road NO$_x$ inventory in the U.S. (Sawyer *et al.*, 1998a). However, large uncertainties remain about the magnitude and the distribution of these emissions (Sawyer *et al.*, 1998a). For example a recent study found that California's emission inventory model may underestimate NO$_x$ emissions from heavy-duty diesel trucks by up to a factor of 2.3 (Dreher *et al.*, 1998).

Recent developments highlight the increasing attention being given to these emissions. More stringent U.S. emission standards for heavy-duty diesel engines, which will reduce NO$_x$ emissions by about 50%, were enacted in 1997 (U.S. EPA, 1997a). Also, EPA recently accused 7 major diesel engine manufacturers of disabling the NO$_x$-control strategies under highway cruise conditions in order to improve fuel economy, resulting on large increases on NO$_x$ emissions. This claim was recently settled with a total cost for the manufacturers in excess of $1 billion, including the largest civil penalty even for violation of environmental law ($83 million) (U.S. EPA, 1998b).

The reduction of heavy-duty diesel NO$_x$ emissions remains difficult. Diesel engines use large amounts of excess air under all operating conditions, which results in lean conditions and the associated high NO$_x$ production (Heywood, 1988). Post-combustion NO$_x$ removal is problematic. The three-way catalysts used for NO$_x$ reduction from light-duty vehicles do not reduce NO$_x$ to N$_2$ when the exhaust O$_2$ concentration is high (Kummer, 1980). Lean-NO$_x$ catalysts, incorporating fuel hydrocarbons as the chemical reducing agent, are under very active research (Heimrich, 1996).

The determination of accurate emission factors and inventory contributions for these vehicles has received an increasing amount of attention in recent years, with significant contributions from the EPA group at Research Triangle Park (Harris and King, 1995; Harris, 1996; Harris and Brown, 1996; Harris *et al.*, 1997; Whitfield and Harris, 1998), the group at West Virginia University (Atkinson *et al.*, 1996; Clark and

Lyons, 1996; Clark and Lyons, 1997; Clark *et al.*, 1998), and others (Pierson *et al.*, 1996; Countess and Cohen, 1997; Maldonado, 1997; Rogak *et al.*, 1997; Countess *et al.*, 1998; Graboski *et al.*, 1998; Kirchstetter *et al.*, 1998). The information derived from these research programs can then be used to better design emission control strategies (U.S. EPA, 1995b; NESCAUM, 1997; SCAQMD, 1997).

It has been shown in Chapter 6 and Chapter 8 that highly precise remote sensing of NO and N_2O emissions can provide very detailed information about the distribution and dependence of particular emission species on vehicle and operating parameters, such as vehicle age, control technology, specific power, etc. In this chapter the results of a study in which the TILDAS technique was adapted to heavy-duty truck emission remote sensing are described. The goals of this study were to demonstrate the feasibility of the application of this technique in this context and to clarify some of the outstanding questions.

This chapter is organized as follows: the details of the experiments are summarized in section 7.2. Section 7.3 presents the results of the remote sensing experiments and the analysis of the second-by-second data of the EPA heavy-duty diesel truck. The emission factor estimated from this study is compared to those of other heavy-duty truck studies and to the emissions of light-duty vehicles in section 7.4. Finally, section 7.5 presents the conclusions of this study.

7.2. Experimental

7.2.1. Adaptation of the TILDAS technique for Application to Heavy-Duty Diesel Trucks

The exhaust pipe of most heavy-duty trucks in the U.S. terminates as a vertical stack located immediately behind the tractor cab discharging exhaust gas to the atmosphere at a height of about 11-12 feet (3.3-3.6 meters) above the roadway as shown in Figure 7-1. The exhaust discharge direction is typically vertically up or angled to the rear. Typical exhaust pipe diameter is 12 cm. The trailer height may exceed the exhaust discharge height. The maximum legal height for trailers is 12.5 feet (3.8 m) (MHD, 1997), but some of the trailers observed on the road during our tests were significantly higher than that, up to an estimated 14 feet (4.3 m). An upper limit is given by the design height for interstate overpasses of 16.5 feet (5 m) (MHD, 1997).

Figure 7-1: Two heavy-duty truck tractors showing the location of the exhaust pipes

Some modifications of the optical setup described in section 6.2.1 were necessary in order to adapt the TILDAS technique to the remote sensing of NO$_x$ emissions of heavy-duty diesel trucks. The main reason for this is the higher elevation above the roadway of the exhaust gases that the laser beam needs to intercept.

The modifications of the optical system are illustrated in Figure 7-2. This picture was taken on the parking lot of the main EPA facility in Research Triangle Park, NC. The TILDAS instrument was located inside a parked truck, similarly to the experiments performed in California and described above. In contrast with the automobile setup, the laser beam had to be elevated to a height of about 16 feet (4.9 m) in order to traverse the exhaust gases while avoiding blockage by the truck's trailer.
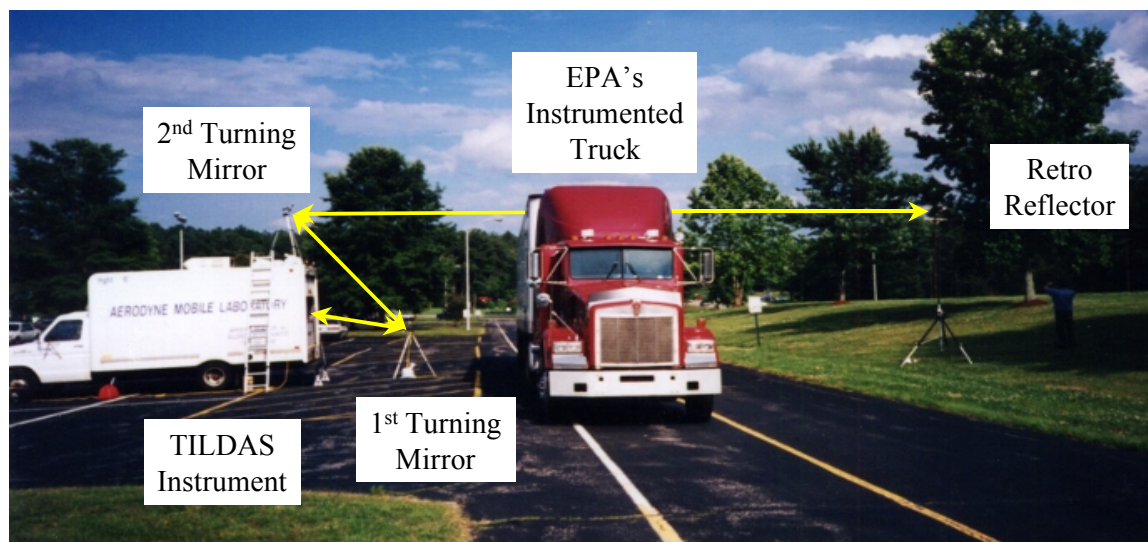
Figure 7-2: Optical layout for the remote sensing of emissions from heavy-duty diesel trucks

To accomplish that objective the laser beam was first sent to a tripod-mounted turning mirror located about 4 feet (1.2 m) above the ground. This mirror directed the beam to a second tripod-mounted mirror which was fixed to the top of the instrument truck. The center of this mirror was located at a height of about 14 feet (4.3 m). From there the laser beam path passed over the road to the retroreflector, which was mounted also at 14 feet on a large tripod and stabilized with the help of 9 guide wires. The laser beam then returned to the optical table following the same path. The total optical pathlength of the laser beam in this configuration was about 165 feet (50m).

The alignment of the system was performed with the help of the visible HeNe laser as described for the automotive experiments. The telescope objective available in the laser optical table was used to position the outgoing beam in the retroreflector.

The triggering of the data acquisition function also needed a modification from the automobile study configuration. In this case, the laser beam is not interrupted by the vehicle and thus the detector signal does not provide an indication for the start of the data acquisition. The solution chosen was to use manual triggering the data acquisition function from the system's computer keyboard when the truck was about to pass under the laser path.[215]

---

[215] A more sophisticated approach could be used in future studies to provide automatic triggering operation. A visible HeNe laser could be sent across the road to a second retro-reflector and its signal monitored by an additional detector. This beam would be set at a height above all automobiles and light-duty trucks but

The statistics of plume capture for heavy-duty trucks in this study have been discussed in section 4.3.7. As a reminder, the CO$_2$ column densities observed varied by about an order of magnitude. The peak CO$_2$ column densities observed were very similar to those of cars and light-duty trucks, but the plumes lasted longer on average for heavy-duty diesel trucks, possibly due to the larger volume of exhaust gases.

7.2.2. The EPA instrumented heavy-duty diesel truck

We carried out a measurement campaign in the Raleigh-Durham area of North Carolina on June 16-19, 1997. The main objective of the campaign was to demonstrate the ability of the TILDAS technique to remotely sense the NO emissions of heavy-duty diesel trucks.

This work was carried out in collaboration with the Jones-Harris research group from the EPA Research Triangle Park Facility. This group has instrumented a heavy-duty trailer with a system to measure and record the gas composition, exhaust opacity, and several operating parameters such as truck speed and acceleration, engine speed and temperature, intake and exhaust temperature, and front-to-rear g force (Harris *et al.*, 1996). The load on the trailer is varied by loading and unloading modular concrete blocks from the back of the trailer. The tractor used during these measurements was a 1990 Kenworth with 60 Series Detroit Diesel Engine, with a displacement of 12.7 liter.

Figure 7-3 and Figure 7-4 (Harris *et al.*, 1995) present an schematic of this EPA instrumented trailer for heavy-duty diesel truck emissions measurement. Figure 7-3 shows the gas analysis system. This system consists of a set of "stationary power-plant" type continuous gas analyzers:

- A paramagnetic analyzer for O$_2$
- A flame ionization detection analyzer (FID) for total hydrocarbons
- NDIR analyzers for CO, CO$_2$, and NO
- A chemiluminescent analyzer for NO and NO$_x$

Figure 7-4 shows the layout of the analyzers, calibration gas bottles, and the load in the trailer .

---

below all heavy-duty trucks, e.g. 3.3 meters (10 ft). The interruption of this beam would send a signal to the TILDAS computer to start the data acquisition cycle.
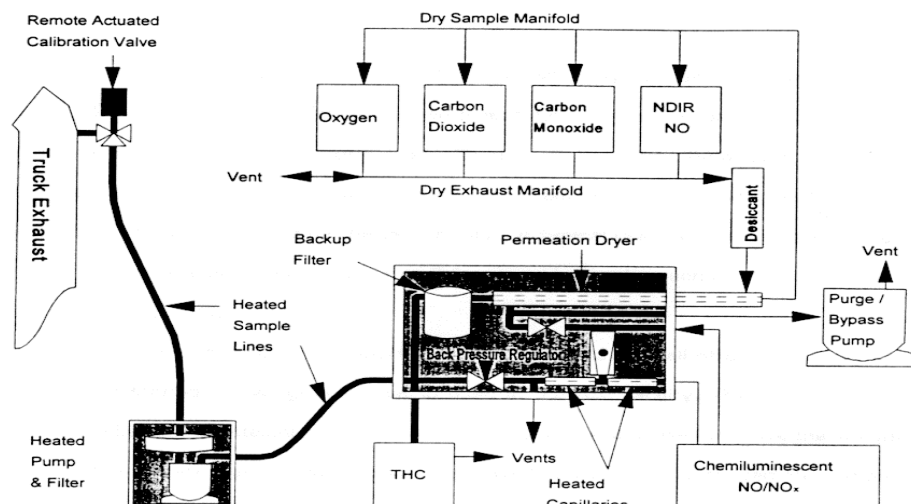
Figure 7-3: Setup of the continuous gas analyzers in the EPA instrumented trailer
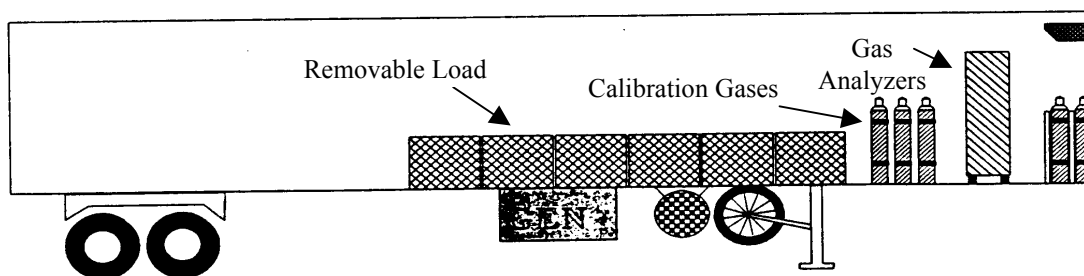
Figure 7-4: Layout of gas analyzers, calibration gas bottles, and load inside the EPA instrumented trailer

7.2.3. Limitations Due to the Size of the Optical Equipment

The quality of the data obtained in this study, while being very good, was not as good as the full potential of the TILDAS technique, specially with the longest pathlength used. This was due to the limited size of the optical elements available which had been selected for a applications with a shorter pathlength.

The main problem was the "spilling" of light from some of the mirrors used. The diameter of the infrared laser beams returning to the optical table after a pathlength of 40 m is on the order of 3-4 cm, which is comparable to the 10 cm diameter of the return mirror. As a heavy-duty truck drives by the TILDAS instrument the beam changes its direction slightly due to the deflection of the road by the truck, ambient and induced wind, and vibrations on the instrument, mirrors and retro-reflector, atmospheric turbulence, and temperature variation in the plume. Given the large diameter of the beam

relative to the return mirror, some of the returning light did not hit the mirror and was lost. This caused loss of some signal intensity, and also caused a large amplification in optical fringes in some of the passes. This problem can be eliminated from future studies by using larger optics for the key elements.

7.3. Experimental Results

7.3.1. Intercomparison of the NO/ CO_2 Ratios from the EPA Truck and the TILDAS Remote Sensor

A series of emissions measurements were performed with the intention of comparing the results from the NO remote sensor and the on-board instrumentation of the EPA truck.

The parameter chosen for the comparison is the NO_x/CO_2 ratio. Expressing the emission index in this way avoids the problem of determining the air-to-fuel ratio in the diesel engine which, unlike gasoline engines, can vary by more than a factor of 2 (Heywood, 1988). This parameter can be converted to grams of NO_x per gallon of diesel fuel in a straightforward way (see Appendix A).
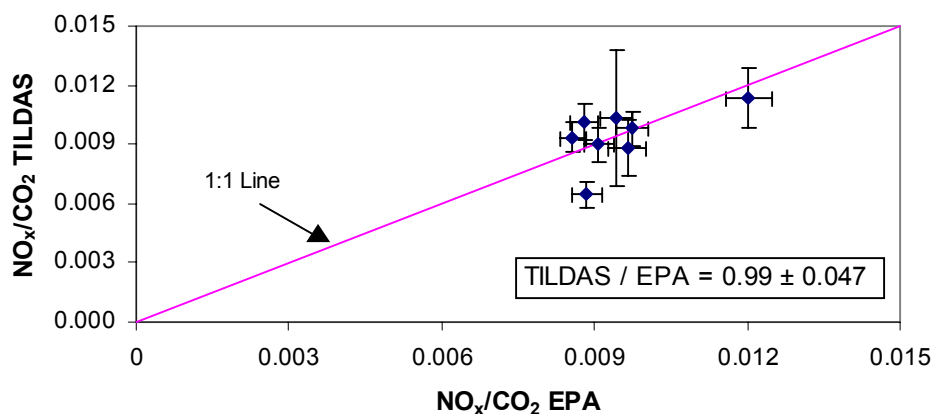
Figure 7-5: Comparison of the EPA and TILDAS NO_x/CO_2 measurement for the measurements taken on June 16, 97

The TILDAS remote sensor measures NO/CO_2 directly. However NO_x/CO_2 was used for the comparison instead of NO/CO_2, since the EPA instrumented truck measured NO_x/CO_2.[216] For this reason the NO/CO_2 ratio produced by the TILDAS instrument needed to be converted to NO_x/CO_2. This was done using the average of the NO_2/NO ratios measured with the TILDAS instrument in June 18, 1997 for the EPA instrumented truck (see section 7.3.4).

---

[216] The instrumented truck is also equipped with an on-board NDIR NO analyzer, but the time response of this instrument was much worse than that of the NO_x analyzer (Brown, 1997) so the later data have been used here.

The comparison of both instruments for the measurements taken on the EPA parking lot on June 16, 1997 can be seen in Figure 7-5. Seven out of 8 measurements are within the 95% confidence interval of the 1:1 line (which represents perfect agreement between both instruments). The reason for the one anomalous measurement is not well understood, but could be due to delays on the EPA truck's analyzers. As described above, the error bar is different for each TILDAS measurement depending on the amount of exhaust gases that intersects the laser path during a given pass.

7.3.2. Measurement of the NO Emissions from Random Trucks on I-40

The magnitude and distribution of real world emissions of heavy-duty diesel trucks are of great interest due to the large contribution of this vehicle type to the mobile source NO$_x$ inventory and the large uncertainties that remain in its quantification (Sawyer *et al.*, 1998a).

For this reason, during the experiment on interstate highway I-40 we measured the NO/CO$_2$ ratios of random heavy-duty diesel trucks. Only the the largest trucks ("heavy-heavy duty" or "18-wheelers") were measured, "medium-heavy duty" and "light-heavy duty" trucks were excluded. Two video frames taken during one such measurement are shown in Figure 7-6. The TILDAS instrument was located inside the Aerodyne Mobile Laboratory parked on the grass beyond the breakdown lane on the far side of the images. The retroreflector was located on the median strip and can be seen near the top of the pictures. The path of the laser beam over the highway is indicated by the clear line.

Figure 7-6: Two video frames taken during an emission measurement on I-40

All of the trucks were driving at undisturbed interstate speeds in low-density traffic. The estimated speeds were on the range 55-70 mph, by comparison with the EPA truck which was driving by every few minutes and provided a visual reference of speed. The grade at the measurement site was +2.1%. No speed, acceleration, vehicle weight, or license plate data were obtained during this experiment.

The measurement was attempted 139 times on this configuration with moderate to strong wind gusts. Seventy-three (or 53%) of those measurements produced valid data. Forty-eight measurements (or 35%) where discarded due to poor signal-to-noise ratio, mostly due to wind-induced vibrations on the optical system that caused a reduction in the signal level. In the remaining 18 measurements (or 13%)[217] the minimum level of CO_2 was not detected because too small a fraction of the exhaust plume crossed the optical path of the laser. This is not too surprising given the wide variability of trailer heights and smoke stack heights and locations, which combined with the strong wind that day caused a large variability in plume dispersion patterns.

	Heavy-Duty Diesel Trucks	Automobiles and Light-Duty Trucks	HDDT / Autos
Average	12.5	2.4	5.2
Standard deviation	4.9	4.0	1.2
Median	12.4	0.7	18
Maximum	27.2	28.6	0.95
Minimum	4.2	0	
Max / Min	6.5	751 [(*)]	0.009
Skewness	0.33	2.80	0.1

All numbers are multiplied by 10^3 except Max/Min and skewness (dimensionless)
*: estimated as (maximum value) / (TILDAS detection limit)

Table 7-1: Summary of statistics for the distributions of NO/CO₂ ratios measured for heavy-duty trucks and automobiles

The distribution of NO/CO_2 emissions for the 73 valid measurements is presented graphically in Figure 7-7, together with the distribution measured for automobiles in El Segundo (section 6.4.1). Some statistics of both distributions are presented in Table 7-1. We can observe that:

---

[217] This is similar to the 10% observed in the passenger car and light-duty truck experiment (section 6.3.1).

- The truck distribution resembles a normal distribution while the automobile distribution is very skewed.
- Most of the automobile readings are clustered at very low NO/CO$_2$ values while no truck measurements are near zero.
- Differences between trucks are small as indicated by a ratio of maximum to minimum emission of 6.5, as compared to about 750 for automobiles.
- The truck distribution has a much larger average value, the difference in the medians is even larger (a result of the automobile distribution's skewness).
- The maximum values of both sets of measurements are very similar.
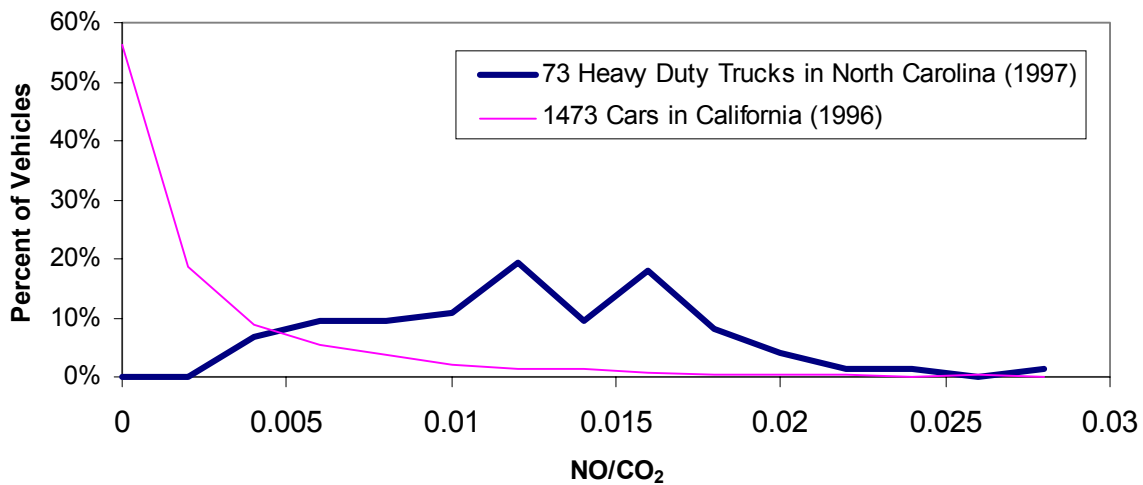
Figure 7-7: Comparison of the distribution of the NO/CO$_2$ ratios in the emissions of automobiles and heavy-duty diesel trucks

	% of Vehicles	% NO Emissions HDD Trucks	% NO Emissions Automobiles and Light-Duty Trucks
Dirtiest	10%	17%	50%
Cleanest	50%	32%	4%

Table 7-2: Percentage of NO emissions of the dirtiest 10% and cleanest 50% of the vehicles for the truck and automobile studies

If we look at the total emissions contribution of a given set of vehicles we see again a very different picture (Table 7-2). While the dirtiest 10% of automobiles contributed 50% of the NO emissions, the dirtiest 10% of the heavy-duty trucks only contributed 17% of the total emissions. Looking from the clean side, while the cleanest

50% of automobiles were responsible for only 4% of the NO emissions, the cleanest 50% of heavy-duty trucks contribute 32% of the total emissions.

These differences are very important since they imply that the concepts of "super-emitters" and "clean vehicles" that are applicable for automobiles emissions are not appropriate for heavy-duty diesel truck NO_x emissions. Emissions variations are much smaller for heavy-duty trucks. This is in agreement with the cycle-averaged results of a chassis dynamometer study in which 152 vehicles were tested (Atkinson *et al.*, 1996), and with an NDIR/UV remote sensing study (Countess *et al.*, 1998) conducted in parallel with this study.

A consequence of this result is that an inspection and maintenance program for HDDTs can not be designed to exclude a large fraction of the fleet[218] or to deal selectively with the high emitters. These results indicate that all or most of the heavy-duty diesel truck fleet needs to be considered in any plan to significantly reduce the NO_x emission of this mobile source component.

7.3.3. Origin of the Shape of the Heavy-Duty Diesel Truck NO_x Emission Distribution

It was shown in section 6.4.2 that the distribution of NO emissions from passenger cars and light-duty trucks may be a blend of the emissions of vehicles with properly functioning three-way catalysts and some high emitters. In the same way, the general shape of the truck NO distribution is a fundamental characteristic related to the diesel engine and the lack of a NO_x reduction catalyst.

To prove this point, Figure 7-8 compares the distribution of the 73 heavy-duty trucks shown above with the distribution of the second-by-second data from the EPA instrumented truck,[219] and the distribution of NO emissions measured with the UV remote sensor in a study carried out in parallel with this one (Countess *et al.*, 1998).

The distribution measured by TILDAS in North Carolina has a larger average value and is less skewed than the other two. However, the 3 distributions are fundamentally similar, span the same range of values, and are very different from the

---

[218] The so-called "clean screening" where likely low-emitting vehicles are exempted from I/M programs based on age, low remote sensing measurements, or low-emitter profiles (Kishan *et al.*, 1998; St. Denis, 1998).

[219] For the measurements taken on interstate highway I-40 on July 17, 97.

automobile distribution shown in Figure 7-7. The truck distributions do not have any readings near zero and are not very skewed.
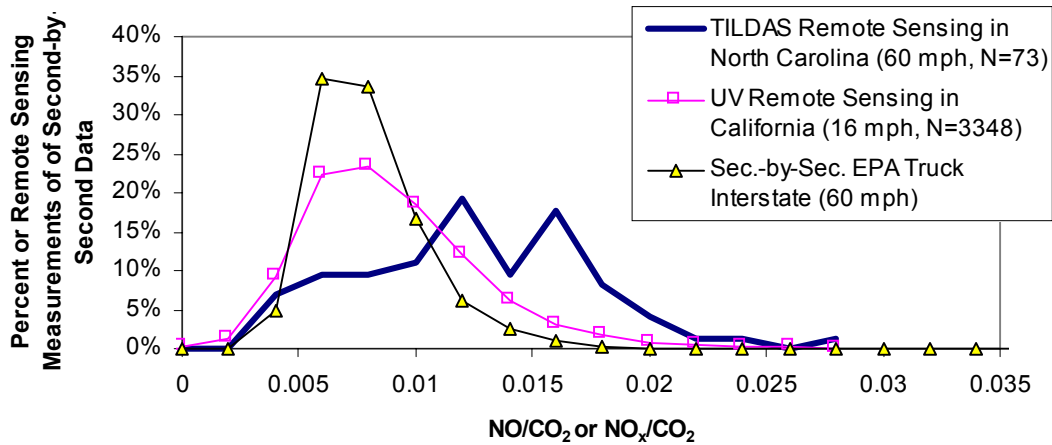
Figure 7-8: Comparison of the distribution of the NO/CO_2 ratios measured in this and another remote sensing study of heavy-duty trucks and the distribution of the second-by-second emissions from the EPA instrumented truck

These differences are traceable to the differences in NO_x production and control between light-duty gasoline vehicles and heavy-duty diesel trucks. A spark-ignition (gasoline) engine can typically generate from 0 to 3,000 ppm NO_x depending on the stoichiometry and load,[220] which are then reduced by the catalyst to values around 100-200 ppm.[221] The shape of the NO remote sensing distribution for this vehicles results from the mixture of two types of vehicles: those with properly functioning control systems, mostly grouped in a clump below 200 ppm NO,[222] and the vehicles with problems in their emission control systems which show up as the long tail of a gamma distribution.

The diesel engine that powers HDDTs is always running lean and always produces a significant amount of NO_x. Since these vehicles are not equipped with a catalyst, this broad engine-out distribution is the same as the tailpipe distribution.

---

[220] See Figure 6-17 and Figure 6-18.

[221] See Figure 3-14 and Figure 6-19.

[222] Though they can occasionally have higher emissions.

7.3.4. Remote Sensing of the NO_2/NO ratio

Although most of the NO_x emitted by heavy-duty diesel trucks is on the form of NO, from 2 to 30% of the NO_x can be present as NO_2 (Hilliard *et al.*, 1979; Heywood, 1988). The higher NO_2 fractions appear at low loads and engine speeds, due to quenching of the NO_2 to NO conversion by the pockets of excess air. Remote sensing of NO_2 emissions could provide a way to quantify this fraction for the real-world diesel fleet under different conditions. This section describes the demonstration of this measurement using the TILDAS instrument.

The TILDAS instrument was adapted to the simultaneous measurement of NO and NO_2. The diode laser used previously for CO_2 measurement was replaced with a different one suitable for NO_2 detection. The NO_2 laser was scanned across a group of 24 transitions at 1605 cm^{-1} (6.2 µm). NO was measured by scanning the stronger of the two groups of transitions used for the NO/CO_2 measurements at a frequency of 1900 cm^{-1} (5.3 µm).

Figure 7-9 shows a spectra obtained with a 10-cm reference cell that contained both NO and NO_2.
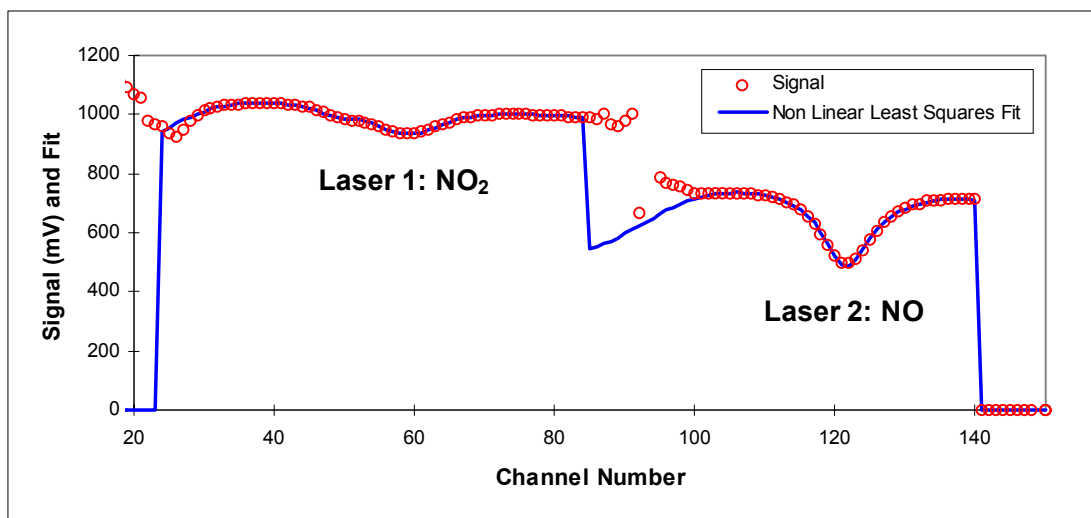
Figure 7-9: Simultaneous spectra of NO_2 and NO from a 10-cm reference cell

Figure 7-10 shows the NO_2 and NO absorption spectra taken during one of the remote sensing measurements of the EPA instrumented truck. The similarity between Figure 7-10 and Figure 7-9 is obvious indicating that a very significant signal can be

obtained when remotely sensing NO$_2$ emissions from heavy-duty diesel trucks, and that no major interferences are present.
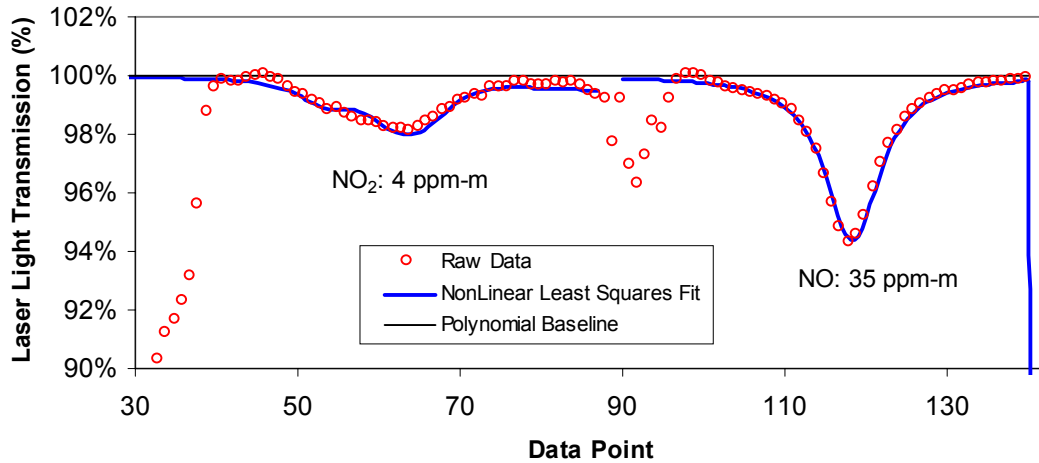
Figure 7-10: Simultaneous NO$_2$ and NO spectra recorded by remote sensing of the EPA instrumented truck
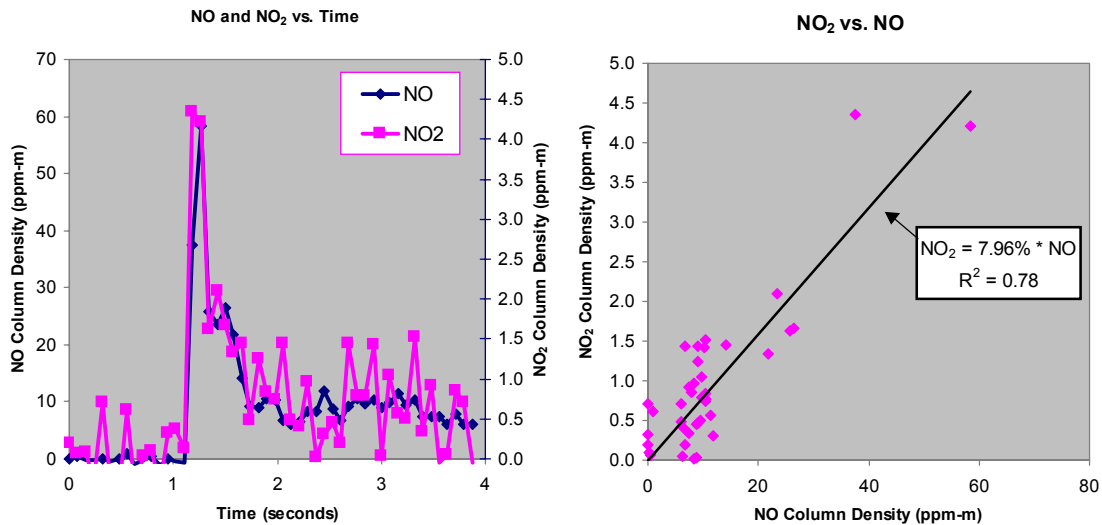
Figure 7-11: Time domain and X-Y plot of a NO/ NO$_2$ remote sensing measurement of the EPA truck

The time-domain and NO$_2$ vs. NO regression plot of a remote sensing measurement of the EPA instrumented truck are presented in Figure 7-11. The close correlation of the two signals is a clear demonstration of the capacity of the TILDAS

instrument to measure NO_2/NO in heavy-duty truck exhaust. This is the first time that NO_2 remote sensing has been accomplished.

Note that in the time domain plot, the signal-to-noise ratio is worse for NO_2 than for NO. This is due to the lower column density of NO_2: since to a first approximation the noise level is similar for both species (of the order of 0.5 ppm-m for this particular measurement) and the signal is about 10 times stronger for NO, the SNR is also about 10 times larger for this species.

Temperature effects such as those described in section 5.6.2 for the NO/CO_2 measurement are minor in the NO/NO_2 measurement since the NO and NO_2 absorption transitions used have very similar temperature dependence.[223] No effect was observed in any of the time domain or regression plots.

The results of the 5 passes for which good signal-to-noise ratio was obtained are shown in Table 7-3.

	NO_2/ NO_x (Volume basis)[224]
Measurement 1	10.9% ± 1.1%
Measurement 2	8.9% ± 0.9%
Measurement 3	5.6% ± 0.5%
Measurement 4	6.2% ± 0.7%
Measurement 5	7.0% ± 0.7%
Average	7.8% ± 2.2%

Table 7-3: Results of the NO_2/NO measurements

---

[223] Exhaust gas temperatures measured on the EPA instrumented truck (1.4 m before the end of the exhaust pipe) reached up to 570 K. This number overestimates the actual gas temperature since mixing is very fast under the cross-wind flow conditions that the exhaust plume encounters. The maximum gas temperatures measured with the procedure of section 5.7 are around 350 K. The ratio of the absorption strengths of the NO_2/NO lines would be only 6% higher at 350 K and 25% higher at 550 K than at 296 K.

[224] The uncertainties reported are the standard error of the mean in absolute units (not as a percentage of the ratio) and are calculated as follows:

- For the individual measurements, the uncertainty reported is the standard error of the NO_2 to NO regression coefficient (see Figure 7-11), with an estimate of the uncertainty due to the HITRAN line parameters added in quadrature (which is equivalent to assuming that both sources of error are independent).
- For the average, the uncertainty reported is the standard error of the mean of the 5 measurements.

The measured NO_2/NO_x ratios range from 5.6% to 10.9% by volume. The average ratio for the 5 measurements was 7.8% ± 2.2%. No comparison can be made with the on-board instrumentation of the EPA truck in this case since the on-board system is not designed or built for NO_2 quantification (Brown, 1997).[225]

These results are within the ranges of those reported in the literature. Hilliard and Wheeler (Hilliard 1979) reported that 2% to 30% (on a volume basis) of the total NO_x emitted from a diesel engine could be in the form of NO_2. They found that this ratio was higher under light load and low engine speed conditions and lower at high load and high engine speeds.

Harris et al. (Harris *et al.*, 1987) measured NO_2 concentration in the range of 0.4 to 33 ppmv of the exhaust with a low-pressure sampling TILDAS system, but did not report NO_2/NO_x ratios. They do report higher NO_2 concentrations at low loads, in agreement with the results of Hilliard and Wheeler.

Clark et al. (Clark *et al.*, 1998) recently reported the results of a study in which diesel engines were operated in steady state conditions on a chassis dynamometer yielded ratios in the 2.2%-18% range. The authors also reported some results from testing diesel buses on an engine dynamometer on the Central Business District cycle. Ratios of up to 4% were measured from current engines under those conditions. The trends with speed and load were consistent with those of Hilliard.

The 5-11% range that we measured with the TILDAS instrument while the EPA instrumented truck was run at about 20 mph under mild accelerations are consistent with these literature studies.

7.3.5. Opacity Measurement

Particulate air pollution has attracted a great deal of interest in recent years due to the recently discovered health effects associated with high environmental concentrations

---

[225] Although the system is equipped with two chemiluminescent NO/NO_x instruments, they are manufactured by different companies and have fundamentally different sample delivery systems. While one of the instrument is used as an NO analyzer (Thermo Electron) and the other one as an NO_x analyzer (Horiba), the response of the two instruments is very different. The NO_x instrument peaks and troughs are much sharper than the NO instrument, possibly because of some flow capillary irregularities in the NO instrument (Brown, 1997). This invalidates the subtraction method of NO_2 quantification. An attempt to numerically convolve the response of the faster instrument with the response function of the slower instrument proved unsuccessful in producing a credible NO_2 vs. time signal.

of PM2.5[226] particles (Wilson and Spengler, 1996). Particulates generated in diesel engines, especially soot, are one of suspected culprits under intensive research (Wilson *et al.*, 1996). For this reason remote sensing of particulate emissions from diesel engines is of great interest.

Stedman et al. (Stedman *et al.*, 1997a) have used the light extinction on the reference channel of their NDIR/UV remote sensing instrument as an indication of particulate mass loading. Countess et al. (Countess *et al.*, 1998), in a study conducted in parallel to this one, have applied the same instrument to heavy-duty truck exhaust opacity.

A similar measurement can be performed with the TILDAS instrument by measuring the extinction of the laser light in the areas of the acquired spectrum were the measured gas is not absorbing light.[227] An independent opacity measurement can be derived at each wavelength at which a laser is operating. For the set of measurements reported here two lasers were used at 4.45 and 5.26 microns.[228] The correlation of the transmitted light level with the measured CO_2 column density (an indication of overlap with the exhaust plume, see section 4.3) is shown in Figure 7-12. A trend of decreased intensity with increased CO_2 appears, which is tentatively attributed to the particle loading. The results of both channels are slightly different, which is to be expected since there is no reason why the radiative properties of the diesel exhaust should be the same at different wavelengths.

This measurement has not been pursued further here because the intensity changes associated with the fringe described in section 7.2.3 obscured the intensity changes in most of the measurements. This problem is easily solvable in future measurements and further attention should be paid to this information.

---

[226] PM2.5 is composed of the particles with a diameter smaller than 2.5 microns.

[227] E.g. channel 140 in Figure 7-9.

[228] The particles with the strongest interaction with a particular laser light are those whose size is similar to the wavelength of the light. Thus these mid-infrared wavelengths would not provide as much information on the amount of PM2.5 particles as shorter wavelength would. A Helium-Neon laser with a wavelength of 0.633 microns could easily be integrated with the TILDAS instrument to simultaneously provide information on particles of that approximate size.
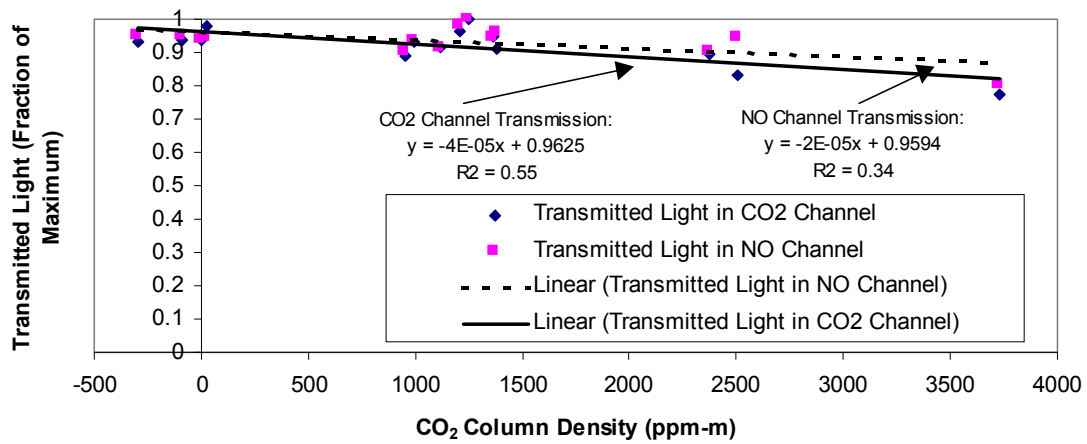
Figure 7-12: Transmitted light vs. CO$_2$ column density (i.e. plume capture) for a measurement on the EPA instrumented truck

7.4. Estimation of the NO$_x$ Emission Factor for Heavy-Duty Diesel Trucks

7.4.1. Estimation of the NO$_x$ Emission Factor Based on the TILDAS Measurements

The on-highway NO and NO$_x$ emission factors[229] for heavy-duty diesel trucks can be estimated from the average of the valid 73 measurements taken on interstate I-40 (section 7.3.2). The conversion procedure from NO/CO$_2$ ratios to grams-per-gallon is detailed in Appendix A. The results are summarized in Table 7-4.

	NO	NO$_x$
Pollutant / CO$_2$ Ratio	0.0125 ± 0.0013	0.0136 ± 0.0015
Emission Factor (grams per gallon of diesel fuel, as NO$_2$)	130 ± 13	141 ± 15

Table 7-4: TILDAS-derived emission factors for NO and NO$_x$ for heavy-duty diesel trucks[230]

7.4.2. Comparison to NO$_x$ Emission Factors from Other Studies

The emission factor derived in the previous section has been compared to the values obtained by other researchers in Table 7-5 and in graphical form in Figure 7-13. The value that we obtained with the TILDAS remote sensor is the highest of those obtained in the U.S.; a slightly larger value was obtained in a Canadian study (Rogak *et al.*, 1997).

The agreement between the emission factors obtained by the different studies can be considered very good, given the different fleets, conditions, times, and techniques of measurement. Their variability is smaller than that for the NO$_x$ emission factors for cars and light-duty trucks shown in Figure 6-15. The explanation for this lower variability probably lies in the fundamental differences between the engines and control systems

---

[229] The quantity determined directly from our measurements is the NO emission factor. To estimate the NO$_x$ emission factor we assumed that the average NO$_2$/NO$_x$ ratio of the fleet was equal to the average of the EPA instrumented truck that we measured by remote sensing (section 7.3.4). Since there could be some variability in the NO$_2$/NO$_x$ ratio for different trucks this assumption introduces some additional uncertainty. TILDAS remote sensing could be used to get a more precise determination of this ratio from a representative sample of heavy-duty diesel trucks.

[230] The uncertainties reported are 95% confidence intervals (1.96 standard errors of the mean).

between both types of vehicles, as described in section 7.3.3: diesel engines produce high levels of NO_x with low variability,[231] while gasoline-powered vehicles can produce more variable levels depending on how well the three-way catalyst is operating.

Place / Reference	Year of Measurement	Method	NO_x Emission Factor (grams of NO_x as NO_2 / gallon of diesel fuel)	
Pennsylvania (Pierson *et al.*, 1996)	1992	Tunnel Study	121	
Maryland (Pierson *et al.*, 1996)	1992	Tunnel Study	Uphill: 115	Downhill: 106
Canada (Rogak *et al.*, 1997)	1995	Tunnel Study	149	
California (Kirchstetter *et al.*, 1998)	1996	Tunnel Study	128 ± 22	
California (Countess *et al.*, 1998)	1997	Remote Sensing	101	
North Carolina (This work)	1997	Remote Sensing	141 ± 15	

Table 7-5: Comparison of the heavy-duty NO_x emission factor obtained in this study and those of other studies
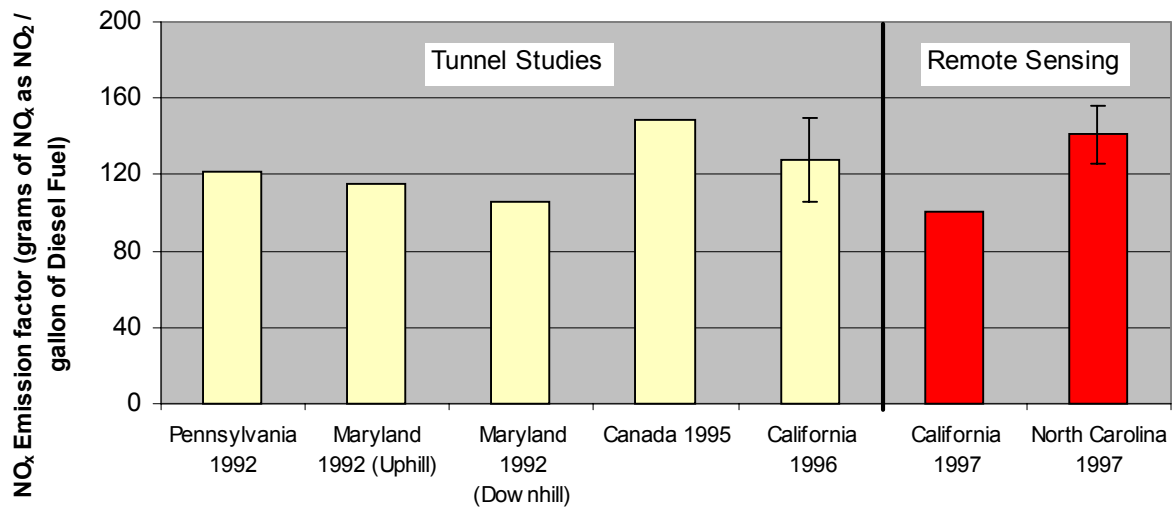
Figure 7-13: Comparison of the heavy-duty NO_x emission factor obtained in this study and those of other studies

---

[231] In terms of NO/CO_2 concentration ratios and grams-per-gallon of fuel. NO_x concentrations and grams-per-mile emissions have higher variability.

7.4.3. Contributions to the NO$_x$ Inventory

Using the emission factors determined by TILDAS remote sensing for automobiles and heavy-duty diesel trucks (sections 6.4.1 and 7.4.1), the fuel consumption for both types of vehicles (Davis, 1997), and the fuel properties (Heywood, 1988), their relative contributions to the NO$_x$ inventory can be estimated. The results are presented in Table 7-6. Since these two vehicle categories account for 94% of the on-road fuel use in the U.S. (Davis, 1997), these contributions are representative of the apportionment of on-road NO$_x$ emissions.

Vehicle Type	U.S. Fuel Mass Use in 1995 (10^6 Metric Tons)	NO$_x$ (grams per kg of fuel, TILDAS)	Total NO$_x$ Emission (10^6 Metric Tons)	**Relative Share of U.S. On-Road NO$_x$**
Light Duty Vehicles & Light Duty Trucks	308.7	8.1	2.71	**42%**
Heavy-Duty Diesel Trucks	76.3	45.9	3.73	**58%**

Table 7-6: Relative contributions of automobiles and heavy-duty trucks to the NO$_x$ inventory based on the TILDAS emission factors

Thus, based on the TILDAS remote sensing measurements, heavy-duty diesel trucks contribute about 3/5 of the on-road NO$_x$ in the US while light duty vehicles and light duty trucks contribute about 2/5. Some uncertainty arises from the different conditions of both studies.[232] This can be compared to the 1998 NARSTO review which estimates an about equal split between the two (Sawyer *et al.*, 1998a).

The latest EPA inventory estimates NO$_x$ emissions from heavy-duty diesel trucks at $1.71 \cdot 10^6$ Metric Tons (U.S. EPA, 1997c). Based on the result of this study, the magnitude of this source is underestimated by a factor of 2.2.

---

[232] Some key differences are: 1) The automobile fleet whose emissions were measured in this study was subject to the more stringent California NO$_x$ standards while the heavy-duty truck fleet was not. 2) The automobile fleet was using low-sulfur gasoline which has been shown to decrease NO$_x$ emissions by 6-11% on Tier 0 and Tier 1 test vehicles (U.S. EPA, 1998d). 3) The automobile fleet was measured under relatively high power requirements. High power increases NO$_x$ emissions for gasoline vehicles (see Figure 3-14). Heavy-duty truck NO$_x$ emissions (in grams-per-gallon) have been shown to be relatively insensitive to vehicle power on a tunnel study (Pierson *et al.*, 1996).

7.5. Conclusions of this study

This study yielded a number of significant new findings with respect to remote sensing of heavy-duty diesel truck (HDDT) emissions and their NO$_x$ emission factors.

- The NO$_x$ emissions of HDDTs can be measured by TILDAS remote sensing under real world conditions with very good accuracy and precision. Very good agreement between the measurements of the EPA instrumented truck and the TILDAS instrument was achieved.

- Based on the results of this study the magnitude of HDDT NO$_x$ emissions is underestimated by a factor of 2.2 in the U.S. The share of HDDTs on mobile source NO$_x$ is larger than that of automobiles and light-duty trucks. The estimated contribution of HDDTs to the NO$_x$ inventory supports the need for lower HDDT emission standards now being implemented (U.S. EPA, 1997a). As much effort needs to be done to reduce HDDT NO$_x$ emissions as has been done for light-duty vehicle NO$_x$, if further meaningful improvements in mobile source NO$_x$-related air quality problems are to be achieved.

- The HDDT NO$_x$ emission factors are remarkably constant across several tunnel and remote sensing studies. Thus the inventory contribution of HDDT NO$_x$ can be reliably estimated from these emission factors.

- The concept of "super-emitter" is not applicable to HDDTs for NO$_x$, since the differences between the lowest and the highest emitters are just a factor of 6.5, compared to a factor of 750 for automobiles. Some consequences of this fact are:

  - The potential of significant reductions on emissions through targeting an inspection and maintenance program on the high emitters (or savings by clean-screening low emitters) is small for HDDTs.

  - Conversely, approaches that deal with the whole fleet such as emission standards and reformulated diesel fuel have the largest potential.

- The successful remote sensing of heavy-duty truck NO$_x$ opens the possibility of exploring many interesting questions of the kind posed for automobile emissions on Chapter 6 and previous studies. For example:

− The fleet average emission factor for HDDTs can be determined under real-world conditions under a variety of circumstances such as geographical location, altitude, ambient temperature, roadway grade, etc. These could be combined with the vehicle activity or fuel sales data to produce a more accurate NO_x emission inventory.

− The variation of HDDTs emissions vs. power can be studied. The concept of specific power, defined in Chapter 3, is also applicable to HDDTs. However, due to the very large variations in vehicle weight for these vehicles, HDDT remote sensing studies should also obtain this information.[233]

− The variation of emissions with vehicle age, manufacturer, engine family, state or country of vehicle registration, vehicle operating company, etc., can be studied. This information can be used in the design of more effective emission control strategies.

− By monitoring for a period of several years, the rates of deterioration as well as the effects of emission reduction programs (such as diesel fuel reformulation, low-NO_x diesel engines, inspection and maintenance, etc.) can be determined. This information can be invaluable for the design of the next generation of emission control strategies.

---

[233] This can be achieved by installing the remote sensing equipment at the exit of a weight station (Countess *et al.*, 1998) or near a weight-in-motion system (U.S. DOT, 1997b).

Chapter 8. Remote Sensing of N_2O Emissions from Automobiles and Light-Duty Trucks

8.1. Introduction

N_2O emissions from motor vehicles are important due to their contribution to the increase of the greenhouse effect and to stratospheric ozone depletion (Bouwman *et al.*, 1995).

Concentrations of atmospheric N_2O have been increasing at a rate of about 0.25% per year, which has been attributed to human activities, although the relative contributions from the different anthropogenic sources are still very uncertain (IPCC, 1995). Even though the rate of increase of the N_2O concentration in the atmosphere is three orders of magnitude lower than that of CO_2, the global warming potential of N_2O is about 320 times larger than that of CO_2 (IPCC, 1995), so the contributions of both gases to the increase of the greenhouse effect are of the same order of magnitude. It has been estimated that to stabilize N_2O concentrations at today's levels would require reducing current rates of anthropogenic emission by more than 50% (IPCC, 1996a).

N_2O is also involved in stratospheric ozone depletion. Since it is very inert in the troposphere, N_2O is slowly transported into the stratosphere where it is photolyzed and yields NO_x, which converts ozone into molecular oxygen. Approximately half of the ozone removal in the stratosphere has been attributed to reactions of nitrogen oxides (Bowman, 1992).

Small amounts of N_2O are formed in spark-ignition engines. Larger amounts of N_2O may be formed in automotive catalysts during NO reduction at relatively low temperatures. Catalyst aging shifts the N_2O production to higher catalyst temperatures, which occur more often during typical driving. This causes an increase in N_2O emissions.

Large uncertainties in the size of this N_2O source remain. The 1998 EPA Draft Greenhouse Gas Inventory (U.S. EPA, 1998c) estimated that this source could account for about 4% of the U.S. net greenhouse emissions. This was reported in the front page of the New York Times (Wald, 1998) and caused significant controversy. The U.S. EPA Office of Mobile Sources reacted by performing some additional N_2O measurements and concluded that the source is much smaller than the 1998 draft inventory suggested, although still highly uncertain (Michaels, 1998).

This chapter presents the results of an N_2O remote sensing campaign and a new exhaustive compilation of the literature studies, in order to address some of the outstanding questions about N_2O emissions. The usefulness of remote sensing for estimation of N_2O emissions factors of on-road motor vehicles is evaluated first (section 8.2). The analysis of the results of the remote sensing study performed in 1996 in California are presented later (sections 8.3 and 8.4). Section 8.5 presents the N_2O emission factors determined in this study and a comparison to those in the literature. The implications of the results and the analysis in this chapter are summarized in section 8.6.

8.2. Evaluation of Remote Sensing for the Measurement of On-Road N_2O Emissions

8.2.1. Cold start vs. Total N_2O Emissions

It has been shown in previous studies that the exhaust N_2O concentration of vehicles equipped with catalysts can be very variable during a dynamometer driving cycle (Barton and Simpson, 1994; Laurikko and Aakko, 1995). This is due to the temperature-dependence of N_2O formation in the catalyst. The main cycle used for measuring light-duty vehicle emissions is the U.S. Federal Test Procedure (FTP) cycle.[234] In this cycle the catalyst starts at ambient temperature and is heated by the exhaust gases. New catalysts[235] produce N_2O at lower temperatures which are reached early in the cycle. Aged catalysts generate N_2O at much higher temperatures, thus later during the FTP (Prigent *et al.*, 1991).

In this section the adequacy of remote sensing to measure N_2O emissions for individual vehicles is evaluated by using literature and unpublished data. If N_2O emissions from individual vehicles are mostly produced during cold starts, and the cold start level is poorly correlated with the hot stabilized emission level of the vehicle, remote sensing measurements of warmed-up vehicles may provide little information. If, on the contrary, there is a relationship between the warmed-up N_2O emission level and the overall emission level of the vehicle, remote sensing could provide important information about this pollutant.

The N_2O exhaust concentration vs. time on the FTP is shown in Figure 8-1 for 3 vehicles from the study of Barton et al.[236] (Barton *et al.*, 1994). The lowest N_2O emitter (Oldsmobile Cutlass) reaches the maximum concentration earlier than the intermediate emitter (Dodge Dakota) which in turn reaches it earlier than the highest emitter tested in this study (Chevrolet Astrovan). The emissions of all vehicles stay at a rather constant level during the hot stabilized phase of the FTP ("Bag 2").

---

[234] This cycle is composed of three phases or "bags." Bags 1, 2, and 3 are referred to as the cold start phase, hot stabilized phase, and hot start phase respectively.

[235] "New" meaning that they have not undergone significant mileage accumulation. Aging seems to be a continuous process, and there is not a clear mileage transition point between new and "aged" catalysts (Prigent *et al.*, 1991). Prigent *et al.* (1991) report significant aging after 15,000 miles.

[236] This data set includes the only published data of real-time concentrations on bag 2 of the FTP.
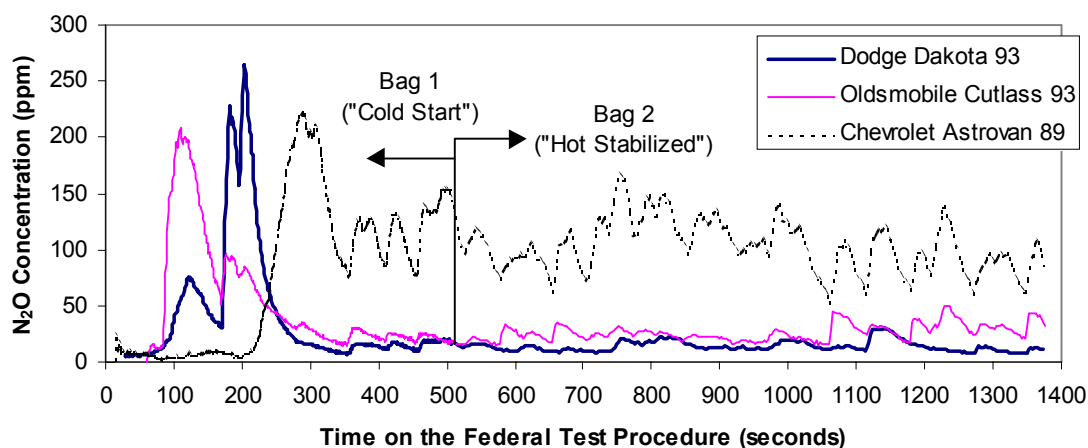
Figure 8-1: N_2O exhaust concentration vs. time during the FTP for 3 vehicles (from the data of Barton and Simpson (Barton et al., 1994)[237, 238]

A remote sensing study, performed in a urban location where vehicles are fully warmed-up and driving is similar to that on the FTP, will obtain a concentration measurement similar to those on the FTP Bag 2. As the cold-start N_2O emissions may be significantly higher than the hot stabilized emissions, it is important to be able to relate the hot stabilized emissions (which would be measured by remote sensing) with the average FTP emission level of the vehicle.

This point is explored in Figure 8-2 and Figure 8-3. In those figures the FTP composite[239] N_2O emission is plotted vs. the FTP hot stabilized (bag 2) emission for 5 literature studies, first in a log-log scale and then in a linear scale. There is a clear correlation between both levels, which can be modeled very well with a simple power law relationship (R^2=0.96).

The combination of these 2 results indicates that measuring the hot stabilized N_2O emissions with remote sensing can provide an indication of the FTP-composite level of N_2O emissions for a particular vehicle and also provide emission factors for types of vehicles.

---

[237] These are unpublished data supplied by the author.

[238] The response time of the sampling and analysis system is estimated at less than 3 seconds for these data (Barton, 1998).

[239] The FTP-composite is calculated as a weighed average of the results of the three phases or "bags." The formula can be approximated by FTP_composite = 0.206 * Bag1 + 0.521 * Bag2 + 0.273 * Bag3 (Pollack *et al.*, 1991). Thus the hot stabilized phase is weighed roughly ½ of the total.
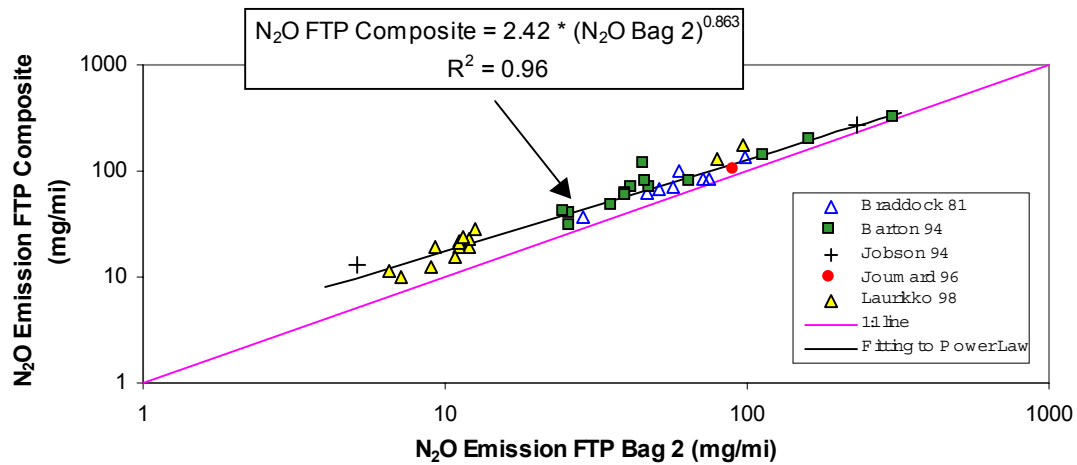
Figure 8-2: FTP-composite vs. FTP-bag 2 (hot stabilized) N_2O Emission for 5 literature studies (log-scale)
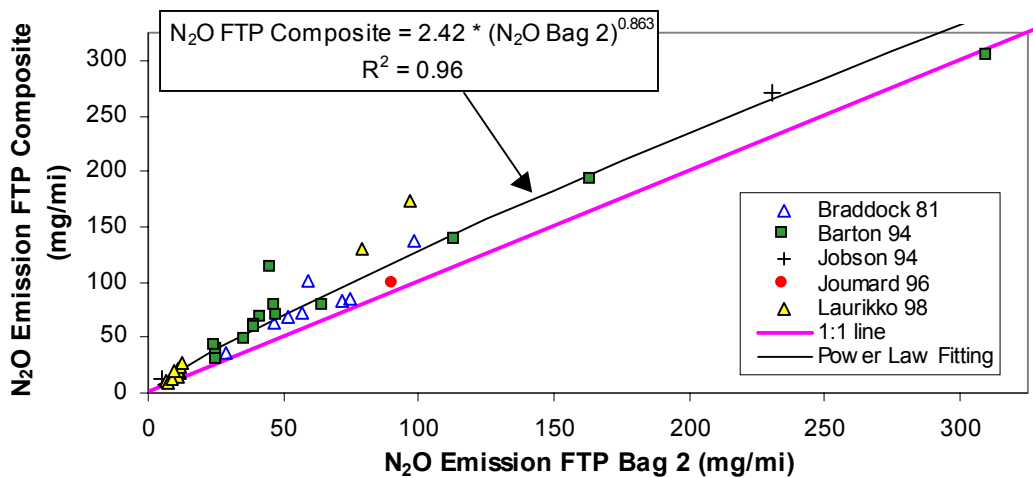
Figure 8-3: FTP-composite vs. FTP-bag 2 (hot stabilized) N_2O Emission for 5 literature studies (linear scale)

8.2.2. Variations on N_2O Emissions for Different Driving Conditions

It is well known that not all driving conditions are well-represented by the FTP driving cycle (U.S. EPA, 1993a). To better control the excess emissions of the regulated pollutants in some of these off-FTP driving modes, new vehicles starting in the year 2000 will be tested on the US06 and the SC03 cycles. These cycles simulate the effects aggressive driving and air conditioning loads respectively (U.S. EPA, 1996a). Other test cycles are used to account for non-FTP driving in the EPA mobile source emissions model, MOBILE (Carlson *et al.*, 1997).

Since N_2O emissions may be different for some of these off-FTP driving conditions it is important to study the relationship between the N_2O emissions on the FTP cycle and those on other cycles. The available data in the literature allow the FTP N_2O emissions to be compared with those on the Highway Fuel Economy Test Cycle (HFET or HWFET),[240] and the IM240 cycle.[241]

The relationship between the FTP and the HWFET N_2O emissions for four literature studies is shown in Figure 8-4. There is a trend of increasing HWFET emissions with increasing FTP emissions. The HWFET emissions are about 40% of those on the FTP. The most likely cause of this difference is the lack of a cold start and the higher catalyst temperatures reached in this highway cycle, that result in lower N_2O formation on the catalyst (Rabl *et al.*, 1997; Odaka *et al.*, 1998).

Though more data are clearly needed to better determine the relationship between FTP and HWFET N_2O emissions, the relationship between both levels could be used in a number of ways, e.g.:

- Given an FTP N_2O emission index (obtained by remote sensing or otherwise), the regression equation can be used to determine an on-highway index to better account for the lower N_2O emissions under these conditions.

- If N_2O remote sensing is performed under on-highway conditions, the regression equation allows the estimation of the FTP emission index.[242]

---

[240] This test cycle is used by EPA to estimate fuel economy under highway conditions.

[241] This test was designed by EPA for enhanced inspection and maintenance programs.

[242] These corrections are uncertain to the extent that the FTP and the HWFET cycles do not represent accurately all urban and highway driving respectively.
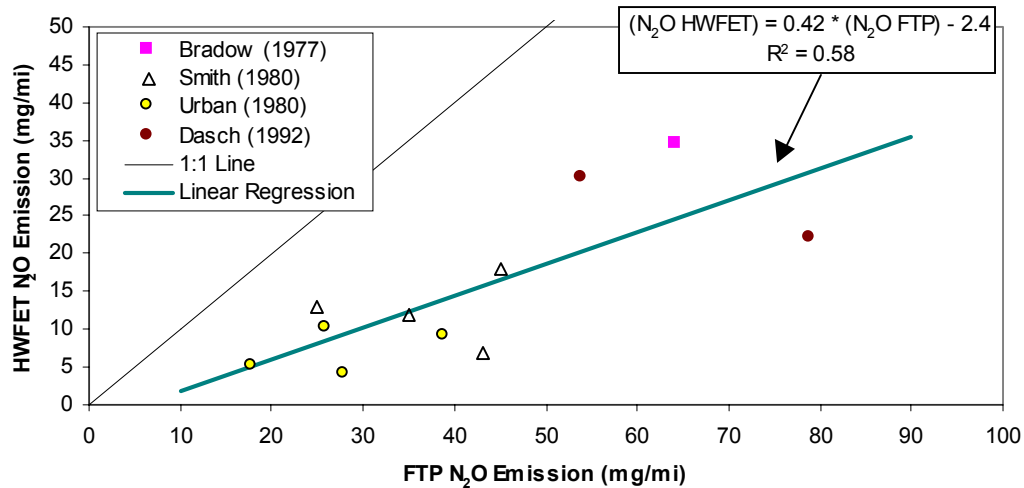
Figure 8-4: HWFET cycle N_2O emission vs. FTP composite emission for 4 literature studies

Figure 8-5 shows the relationship between the FTP and IM240 N_2O emissions for the only study that measured both rates for the same set of vehicles (Barton *et al.*, 1994).[243] A very linear relationship between the N_2O emission rates on both cycles exists, excluding the highest point. More data are needed at high N_2O levels.

The correlation for the 13 vehicles with lower emissions is as good or better than those found for the regulated pollutants (CO, HC, and NO_x) in a recent study which included 569 vehicles (DeFries and Williamson, 1997). IM240 emission rates are smaller than those on the FTP due to the lack of a cold or a hot start. Although additional data are needed (especially at high emission rates), this relationship allows the estimation of FTP N_2O emission factors from IM240 emission factors. A very interesting application of this result would be to perform N_2O testing together with inspection and maintenance programs using the IM240 test. Since large,[244] relatively unbiased vehicle samples must participate in these programs, such a measurement would provide a large N_2O emissions database. This would allow a precise estimation of N_2O emission factors, emission distributions, and correlations with vehicle factors. This information would allow a more precise estimation of this N_2O source and also the study of which vehicle characteristics may be correlated with high N_2O emissions.

---

[243] The IM240 cycle in this study was performed 15 minutes after the end of the FTP, and after a 5-minute 60 km/h steady state warm-up period (Barton, 1998).

[244] For example the Arizona database described in section 0 includes IM240 tests on over 170,000 vehicles.

The chart's embedded text reads:

Y-axis: N_2O Emission on IM240 (mg/mi)

X-axis: N_2O Emission on FTP Composite (mg/mi)

Text box:
Linear Fit to the points with FTP < 200
(N_2O IM240) = 0.71 * (N_2O FTP) + 1.1
$R^2 = 0.88$
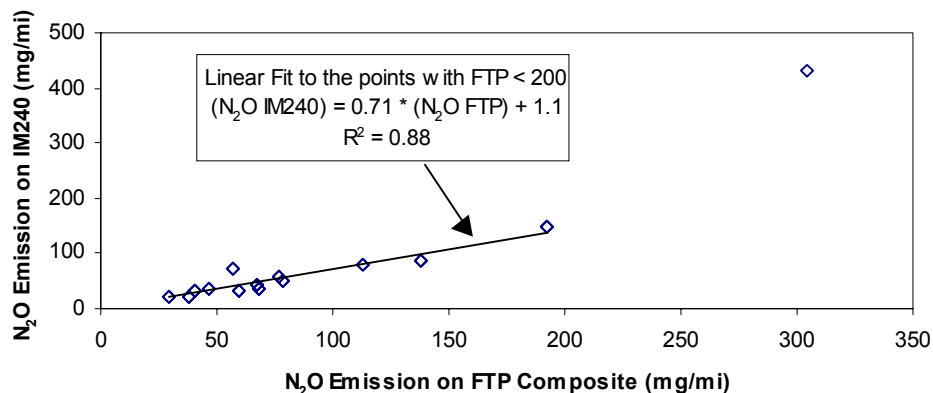
Figure 8-5: IM240 vs. FTP-composite N_2O emissions for the study of Barton et al. (Barton et al., 1994)

The conclusion of this subsection is that the tendency to produce N_2O is a characteristic of every individual vehicle. Different driving conditions produce different absolute emission rates but the proportionality between different vehicles is maintained. Thus measurement of N_2O emission rates under a particular driving condition may be used to predict N_2O emissions under a different condition.

8.3. N_2O Remote Sensing Results

8.3.1. Remote Sensing of N_2O Emissions with TILDAS

The N_2O emissions of automobiles and light-duty trucks were measured during our experimental campaign in California in Nov. 1996 using the TILDAS technique. The details of the experiments are presented in section 6.2. This technique had been used previously to monitor N_2O levels on directly sampled automotive exhaust (Jobson *et al.*, 1994) and on directly sampled aircraft gas turbine exhaust (Wiesen *et al.*, 1996).

As explained in section 5.3, we were able to obtain N_2O column densities with the same laser used for determination of CO_2 column densities by choosing a spectral region with strong, non-overlapping N_2O and CO_2 transitions. The combined laser scan, time trace and N_2O to CO_2 regression are shown in Figure 5-4, Figure 5-5, and Figure 5-6 respectively. A small systematic negative bias[245] due to a beamsplitter fringe was detected and corrected for, as detailed on Appendix E. We obtained a total of 1361 valid N_2O emissions measurements in this way. The analysis of these results is presented in the following sections.

8.3.2. N_2O Emissions Distribution[246]

The statistics of the distribution of the N_2O emissions are presented in Table 8-1. The mean N_2O emission value of the data set is 12.6 ± 3.95 ppm.[247]

A histogram of the distribution of the N_2O emissions is presented in Figure 8-6. The remote sensing N_2O distribution is very skewed, with most of the readings at low emission values and a long tail. The maximum reading is 245 ppm, which is well within the range of concentrations reported in the literature, for example Prigent at al. (Prigent *et al.*, 1994) report a

---

[245] All of the analysis presented below has been performed after adding a constant value of +6.7 ppm to every individual data point, as estimated in Appendix E. The estimated uncertainty of the correction has not been added to the data in this section since only the relative uncertainties are important here. It has been added to the comparison of the emissions factors derived in this study with those of the literature (section 8.5.2) since in this case we are comparing results of this study (which are subject to the uncertainty of the bias) with those of other studies (which are not).

[246] The distribution of the emissions for all vehicles is presented here. The distributions for the individual vehicle / catalyst types are similar in shape with some differences in magnitude which are analyzed in the following sections.

[247] The uncertainty of the mean was calculated by adding in quadrature the standard error of the mean of ± 0.65 ppm and the estimate of the uncertainty on the magnitude of the systematic negative bias described in Appendix E (± 3.9 ppm).

maximum exhaust concentration of 560 ppm N_2O. The maximum warmed-up N_2O concentration in Figure 8-1 is 170 ppm, which is also of the order of this result.[248]

Note that negative emissions below about –0.3 ppm[249] are physically impossible. The negative emissions in the distribution correspond to noisy measurements of small emission rates, an should be kept because rejecting them would bias the average measurement.

Parameter	Value
N	1361
Mean	12.6 ppm
Median	8.0 ppm
Standard Deviation	23.5 ppm
Maximum	245 ppm
Skewness	3.3

Table 8-1: Summary of Statistics of the N_2O Emissions Distribution[250]
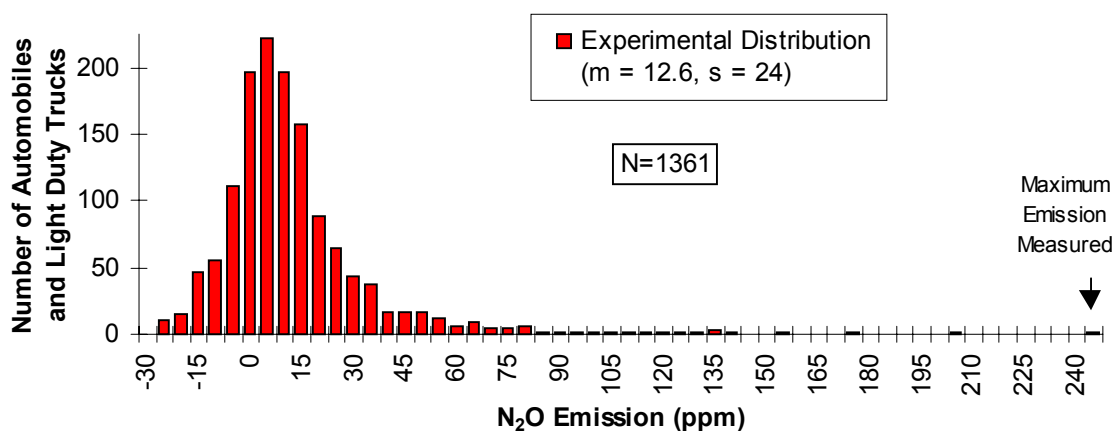
Figure 8-6: Histogram of N_2O emissions for the 1386 measurements taken at El Segundo

---

[248] It is also possible that a few of the vehicles measured on this study had been operating only about 2-3 minutes (see section 6.2.2), which would most likely result on high N_2O concentrations at the time of remote sensing (see Figure 8-1). The number of vehicles in this situation is estimated to be very small, since the large majority of the vehicles measured were those of commuters coming from other cities.

[249] Which would correspond to the destruction of the ambient N_2O level.

[250] Note that our emissions data are reported as parts-per-million (ppm) of all the exhaust gas (including H_2O), and not as ppm of the dry exhaust. The N_2O values in ppm of the dry exhaust would be 14.3% larger than the values presented here. A detailed description of the conversion between different emission units is presented in Appendix A.

It has been shown in section 6.4.1 that the NO remote sensing distribution was well approximated by the convolution of a gamma distribution (signal) with a normal distribution (measurement noise). Since N$_2$O is produced during NO reduction in the catalyst and its distribution is also very skewed, it seems plausible that N$_2$O could also have a gamma distribution. This would be obscured in the experimental distribution by the smearing resulting from the detection noise at these low N$_2$O concentrations, and would result in a distribution such as the one in Figure 8-6.

In order to test this point, Figure 8-7 shows a numerical convolution of a normal distribution (our estimated noise distribution) and a gamma distribution. The comparison between both distributions is very good indicating that this convolution is a good model of the measured emissions distribution.

The value chosen for the standard deviation of the normal distribution was 8 ppm, as providing the best fit to the experimental distribution. As for the case of NO, this value is larger than the estimated sensitivity of 5 ppm, due to the variety of signal levels obtained with the fleet that we measured (section 4.3.4).
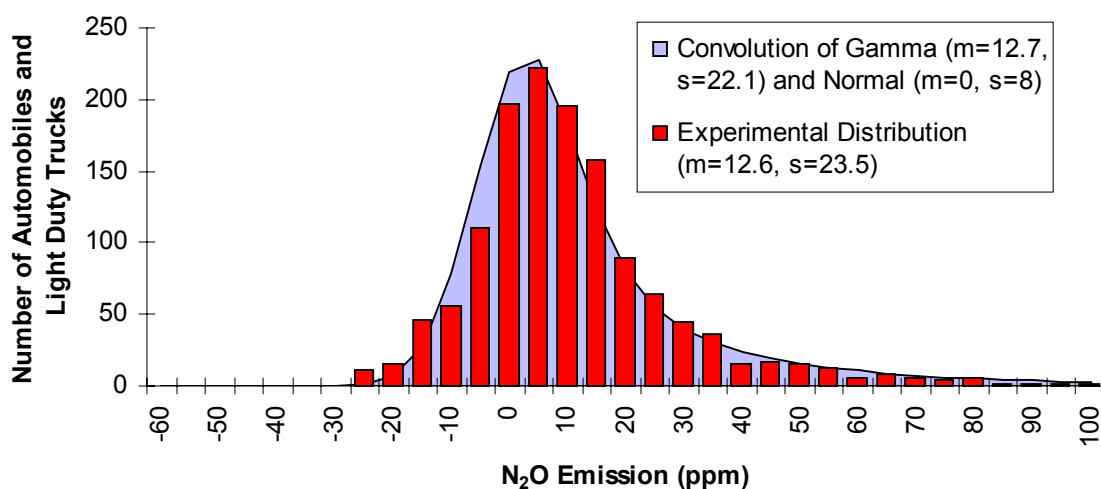
Figure 8-7: Convolution of gamma and normal distributions vs. experimental N$_2$O distribution

As mentioned above, the true emissions distribution cannot have negative N$_2$O emissions.[251] Thus the gamma distribution may be better approximation to the true distribution

---

[251] As mentioned above, it could theoretically have negative emissions up to –0.3 ppm, corresponding to the destruction of the ambient N$_2$O level. This level is very small compared to the negative tail of the measured distribution.

than the raw experimental distribution. Figure 8-8 shows the hypothesized gamma distribution, together with the experimental distribution. This gamma distribution is very skewed, with 45% of the vehicles emitting less than 2.5 ppm and a very slowly decaying tail. This could be of great practical importance for determining N_2O emission factors for light-duty vehicles, since the presence or absence of N_2O super-emitters will heavily influence the emission factor of a small sample of vehicles, as has been found to happen for CO, HC, and NO emissions (Zhang *et al.*, 1994; Zhang *et al.*, 1996a; Jiménez *et al.*, 1997). This has indeed been the case for some literature studies as described in sections 8.4.3 and 8.4.4.
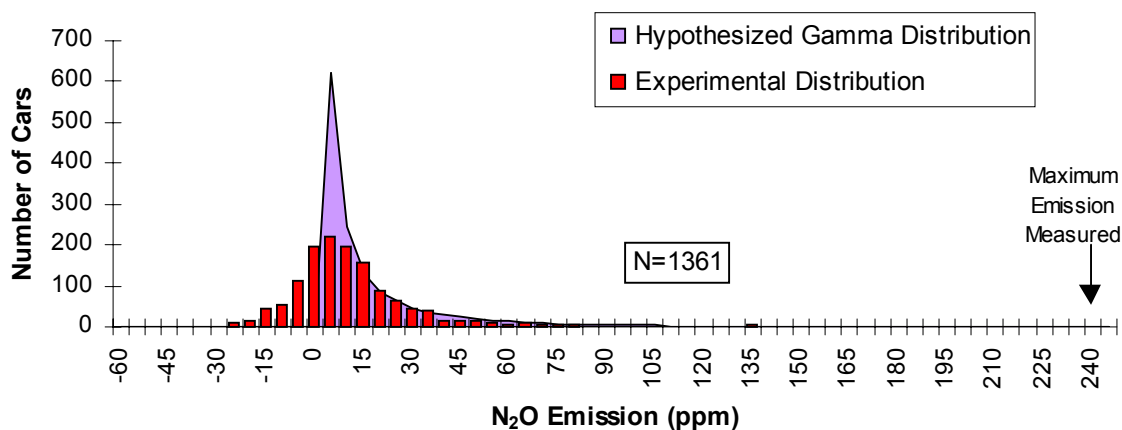
Figure 8-8: Theoretical gamma distribution of N_2O emission and experimental distribution

Figure 8-9 shows the emissions contribution of each decile to the total fleet emissions for the experimental and the assumed gamma distribution. In excess of 50% of the N_2O emissions are produced by the 10% highest emitters, as found previously for CO, HC, and NO_x (Zhang *et al.*, 1994; Zhang *et al.*, 1996a; Jiménez *et al.*, 1997) but not for N_2O.
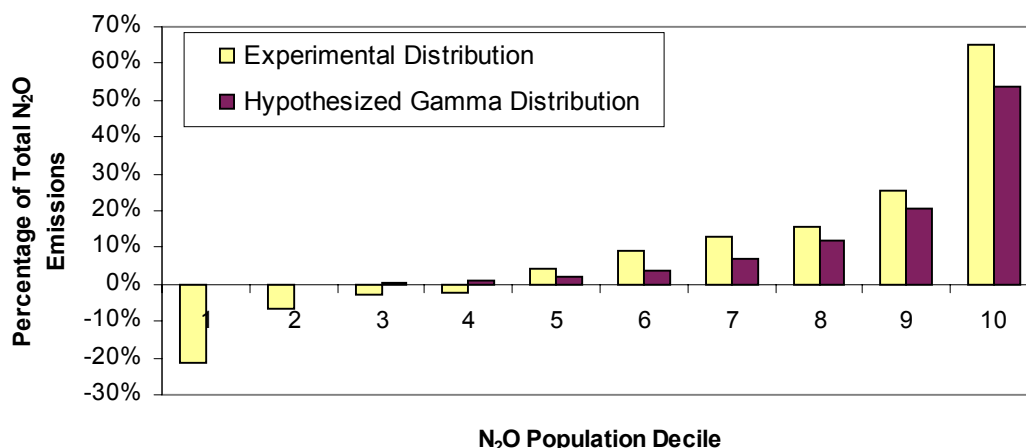
Figure 8-9: Decile plot of the experimental N$_2$O distribution and of the hypothesized gamma distribution

8.3.3. Effect of Vehicle Type and Emission Control Technology on N$_2$O Emissions

Using the data decoded from the vehicle identification numbers (VINs) we were able to determine whether a vehicle was subject to passenger car or light-duty truck emission standards, and also which vehicles were equipped with three-way catalysts, oxidation catalysts or no catalysts (see section 6.2.6). Since three-way catalysts were introduced massively in California around 1980, most of the vehicles that we measured were equipped with them (93.5% of the 1080 vehicles with both valid N$_2$O and VIN data). Some (5.4%) had oxidation catalyst and a few (1.1%) had no catalyst at all.

A further distinction has been made in this chapter between new and aged three-way catalysts. This is based on the results from several catalyst bench studies and engine dynamometer tests that have found much larger N$_2$O emissions from aged vs. new catalysts (Prigent *et al.*, 1991; Ballantyne *et al.*, 1994; Jobson *et al.*, 1994; Prigent *et al.*, 1994; Laurikko *et al.*, 1995; Odaka *et al.*, 1998). Catalyst aging seems to be a continuous process, causing significant differences in N$_2$O production from new catalysts after 1 hour of accelerated engine bench aging and continuing after 200 hours at engine powers of 25-54 hp (Prigent *et al.*, 1991). Since no clear mileage transition point for real vehicles was determined in the previous studies (Prigent *et al.*, 1991; Ballantyne *et al.*, 1994; Michaels, 1998), in this study vehicles of model year 1996 were considered to have new catalysts while older vehicles were considered to have aged catalysts.

The recent study by Michaels (Michaels, 1998) makes a further distinction in the TWC-equipped vehicles between those subject to "Tier 0," "Tier 1," and "LEV" emissions regulations,[252] showing significant differences in N_2O emissions between them. For this reason this distinction has also been adopted in this study.[253]

The average N_2O emission for each vehicle type / technology group in the remote sensing data is shown in Figure 8-10. The results indicate that:

- All vehicle-catalyst combinations produce higher N_2O emissions than the non-catalyst vehicles. We do not have an independent measurement of the absolute N_2O emission level of vehicles without catalysts, since they have been used to correct the absolute levels of the study. Instead the average level of 12 literature studies has been adopted (Appendix E).

- Light-duty trucks produce significantly more N_2O than passenger cars with all catalyst types except new three-way catalysts.

- The evidence on catalyst aging is mixed.[254],[255] A significant difference appears between the "new catalyst" and the "Tier 1" LDTs implying early catalyst aging. However, this difference is not present for PCs. Both conclusions are very uncertain due to the small number of "new TWC" vehicles in this study. Model year and/or age effects are important, and are analyzed in section 8.3.4.

- "Tier 1" PCs have lower emissions than "Tier 0" as found in a chassis dynamometer study (Michaels, 1998). LDTs do not show a clear difference between "Tier 0" and "Tier 1" vehicles.[256]

---

[252] The terms "Tier 0" and "Tier 1" refer to Federal emission regulations. Nevertheless the technologies used to satisfy Tier 1 emission standards are similar to those introduced a few years before to satisfy California standards. The breakup of our vehicles in each technology type has been done using the model year distributions of Michaels (Michaels, 1998).

[253] It is not possible to know whether a remotely-sensed vehicle is subject to "Tier 0" and "Tier 1" emission standards based on the information provided by the California Department of Motor Vehicles or the VIN decoder. The emission factors in the table have been determined using the model year distributions of both types of vehicles for California (Michaels, 1998).

[254] Only first-year aging is analyzed here. Continuous aging is explored in section 8.3.4.

[255] Only vehicles of model year 1996 were included on the new TWC category since N_2O emissions increases due to catalyst aging are significant at 15,000 miles (Prigent *et al.*, 1991), which is comparable to the 11,000 average yearly mileage of U.S. passenger cars (U.S. EPA, 1995a).

[256] If the "New Catalyst LDT" group, which is subject mostly to "Tier 1"-equivalent standards is averaged with the "Tier 1 LDT" group, a difference appears though it's still much smaller than between both groups for passenger cars. This averaging may or may not be justified in light of the mixed evidence on catalyst aging in this and other studies.

- No significant differences are observed between oxidation catalysts and three-way catalyst in terms of N$_2$O production. This is not too surprising since oxidation catalysts are a combination of Pt and Pd, while three-way catalysts contain Pt and Rh (Heck and Farrauto, 1994), and the three metals are active for N$_2$O formation (Cant *et al.*, 1998).
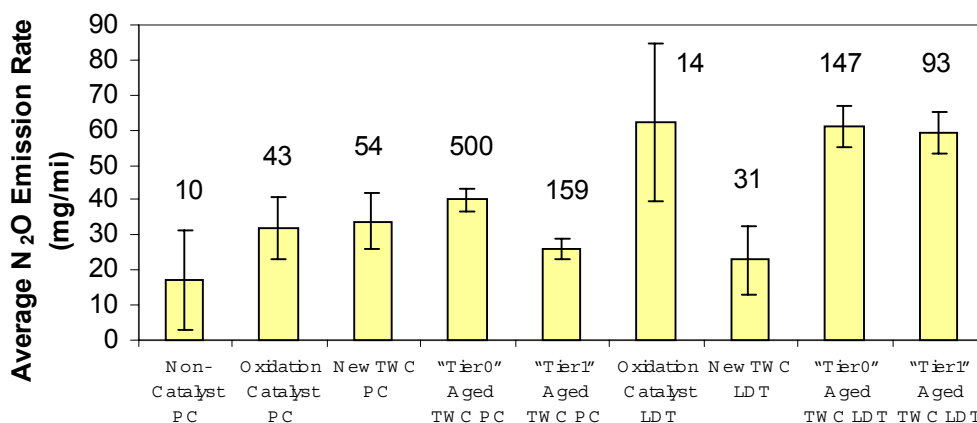
Figure 8-10: Average N$_2$O emission rate for each vehicle type / control technology group for the remote sensing data (labels are the number of vehicles for each type)[257, 258]

A comparison of these results with those proposed by IPCC and EPA and the average of the literature is presented in section 8.5.2.

8.3.4. Effect of Vehicle Model Year for TWC-equipped vehicles

Model year (or vehicle age) was found to be the parameter with the strongest correlation with NO remote sensing data (see section 6.4.9). The effect of model year on N$_2$O emissions is presented here.

The correlation between N$_2$O and model year is very small on a vehicle by vehicle basis ($R^2 = 0.003$). The average N$_2$O emissions measured by remote sensing for vehicles grouped by model year is shown in Figure 8-11 in concentration units (ppm), which are directly proportional to grams of N$_2$O per gallon of fuel.[259] The vehicles have been divided into passenger cars and

---

[257] The error bars are standard errors of the mean for each vehicle type / technology group.

[258] Total number of vehicles is smaller than the 1361 vehicles sampled because license plates were not captured for 10% of the vehicles, the California Department of Motor Vehicles could not provide registration information for about 10% of the license plates captured, and the VIN decoder could not decode about 10% of the VINs from the DMV.

[259] For the conversion procedure see Appendix A.

light-duty trucks since both groups have been shown to have significantly different emissions levels (section 8.3.3).
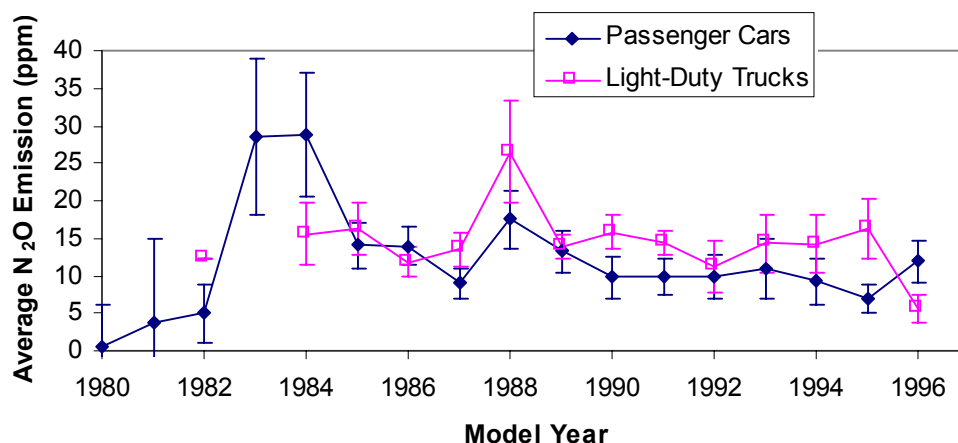
Figure 8-11: Average N$_2$O emissions (ppm) vs. vehicle model year for vehicles subject to passenger car and light-duty truck standards (remote sensing data)^{260}

N$_2$O exhaust concentrations are about constant for TWC-equipped PCs after 1990, and increase for older vehicles after 1983. Vehicles of model year 1988 have significantly higher emissions, the reason for which is not clear. Emissions from LDTs remain about constant within the experimental uncertainty. This uneven aging effect for cars is not consistent with the continuous catalyst aging reported in the literature (Prigent *et al.*, 1991), and may be caused by changes in catalyst technology and composition. It is not clear either why this effect does not appear for LDTs.

Cars of model years 1980-1982 show much lower N$_2$O emissions than those of later years. This could be due to widespread failure of those catalyst systems (if the catalyst is not reducing any NO it will not make any N$_2$O), or to lower N$_2$O emission properties owing to a different emission control system design or catalyst composition. A look at the individual and average CO and NO emissions of the cars of MY 80-82 indicates that they are not significantly different from those in later years, but it is not possible to draw any firm conclusion about which of the above possibilities may be true given the small sample size for these model years.

---

[260] The error bars represent the standard error of the mean for every model year.
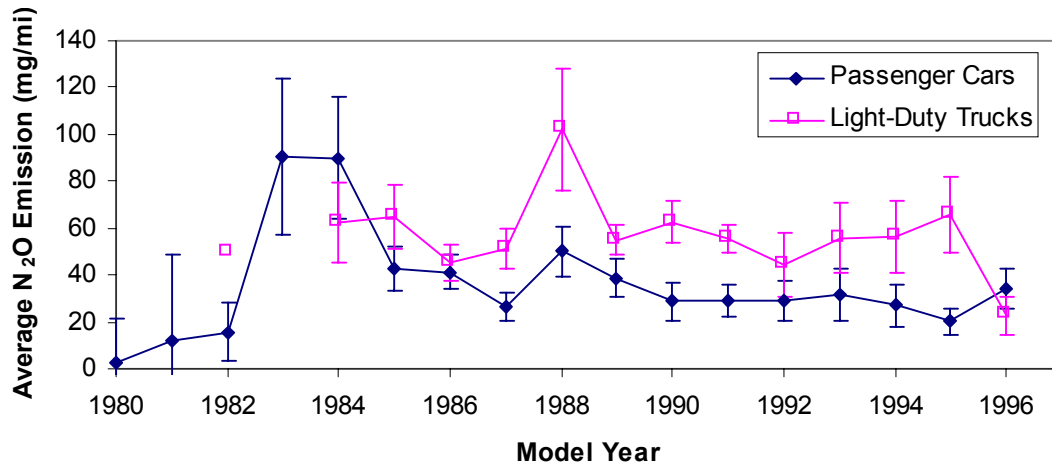
Figure 8-12: Average N$_2$O emissions (mg/mi) vs. vehicle model year for vehicles subject to passenger car and light-duty truck standards (remote sensing data)

Figure 8-12 shows the same results in emission rate units, mg/mi. The difference between PCs and LDTs is significantly larger than in grams-per-gallon units for most model years. This result indicates that about half of the difference in the N$_2$O emission rates between both types of vehicles is due to the difference in fuel economies, and that light-duty trucks also tend to generate more N$_2$O per unit fuel consumed.[261]

8.3.5. Fraction of Total Emissions Contributed by Every Model Year (TWC only)

The fraction of the total N$_2$O emissions for every model year has been calculated by adding the emissions of each vehicle observed at every model year and dividing by the sum of the total emissions. The results of this procedure are shown in Figure 8-13.

All model years from 1984 on contribute very similar fractions of about 7% of the total N$_2$O. This results from the slight increase in emissions compensating the decrease in the vehicle population. Passenger cars are the dominant contributor for older model years and light-duty trucks become equal or larger from 1990 on, due to the increase in the number of trucks as a fraction of the fleet.

---

[261] The possible reasons for the higher N$_2$O emission per unit fuel for LDTs are unclear. Some possibilities include increased catalyst aging due to more aggressive driving, slightly lower average catalyst temperatures due to differences in exhaust system design and mass flows, or differences in catalyst loading and/or composition with respect to passenger cars.
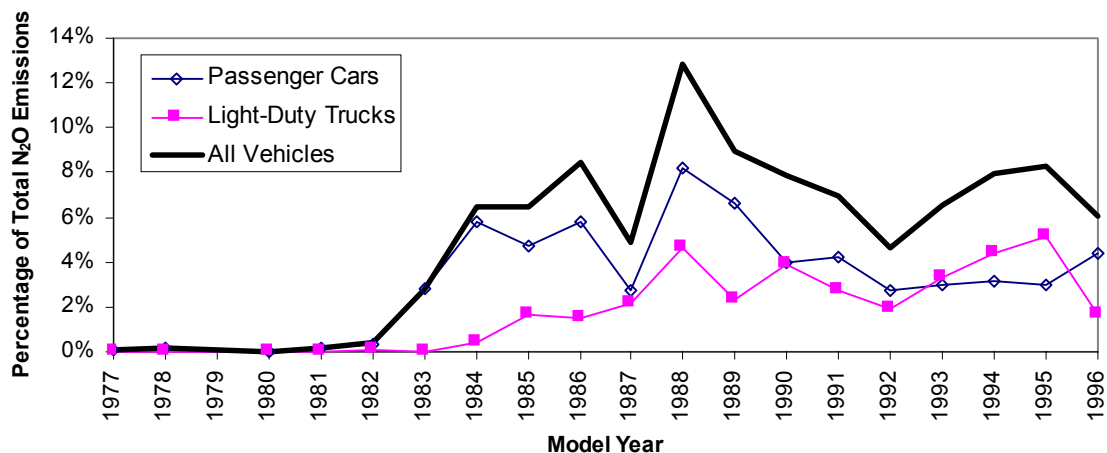
Figure 8-13: Total contribution of every model year to the fleet N$_2$O emissions

A comparison of the contributions of every model year to total N$_2$O to those for NO is shown in Figure 8-14.[262] N$_2$O contributions are more constant that those of NO, due to the smaller increase of average N$_2$O with model year compared with that of NO (Figure 6-24 vs. Figure 8-12).
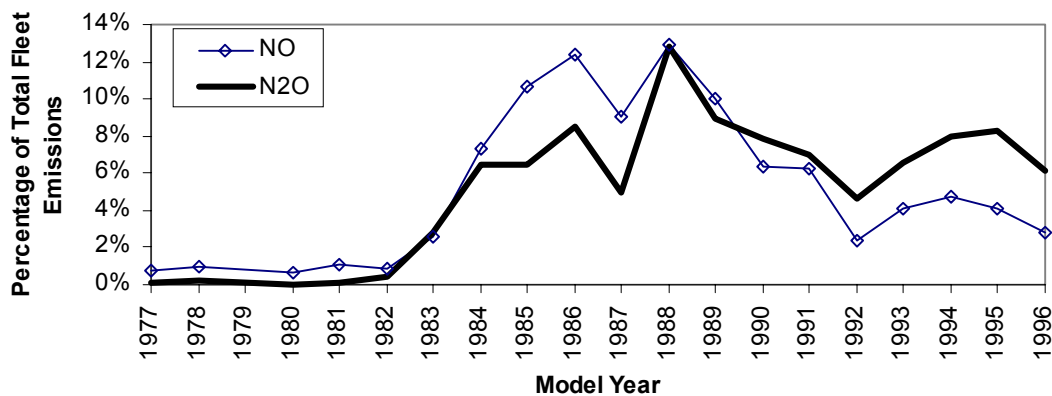
Figure 8-14: Comparison of the model year contribution to total emissions for NO and N$_2$O

---

[262] It was shown in Figure 6-37 that CO and HC model year contributions are very similar to those for NO.

8.3.6. Characteristics of the N$_2$O High Emitters

The distribution of N$_2$O emissions has been shown to be very skewed (section 8.3.1). An important question is whether there is any vehicle characteristic that can be used to predict whether a vehicle will be a high N$_2$O emitter. This is explored in this section.[263]

For the purposes of this section a high N$_2$O emitter has been defined as a TWC-equipped vehicle in the 10% highest emission bin. This has been done separately for cars and light-duty trucks. Two questions are discussed here:

1) Can high N$_2$O emitters be predicted by measuring NO, CO or HC?

It is shown in sections 8.3.7 and 8.3.11 that some relationships between the decile averaged NO, CO, and HC emissions and the N$_2$O emission exist. However, individual N$_2$O high emitters cannot be predicted by measuring the regulated pollutants (see Figure 8-16, Figure 8-25, and Figure 8-27).

2) What is the age distribution of the high N$_2$O emitters?

Figure 8-15 shows the fraction of high emitters at each model year[264] vs. model year for cars and trucks. If all model years had the same fraction of high emitters all of the points will be on the 10% line. These graphs show similar trend to that of the average emissions vs. model year, which is reasonable since high emitters contribute most of the N$_2$O emissions.

Older model years are enriched in high emitters for passenger cars, especially 1983 and 1984. Model years after 1991 seem to have slightly less high emitters than the average. 1996 vehicles seem to depart from this trend, but this could be an artifact of the small sample size in this study. Light-duty trucks show a similar trend.

---

[263] It has been found that that specific vehicle models can have more CO higher emitters than the average fleet (Wenzel *et al.*, 1996; Wenzel *et al.*, 1997; Wenzel *et al.*, 1998b). The possibility that specific manufacturers or vehicle models had more high N$_2$O emitters than the average was explored with this remote sensing data set. Unfortunately the differences found are not statistically significant due to small sample sizes.

[264] Defined as the number of high emitters divided by the number of vehicles for that model year.
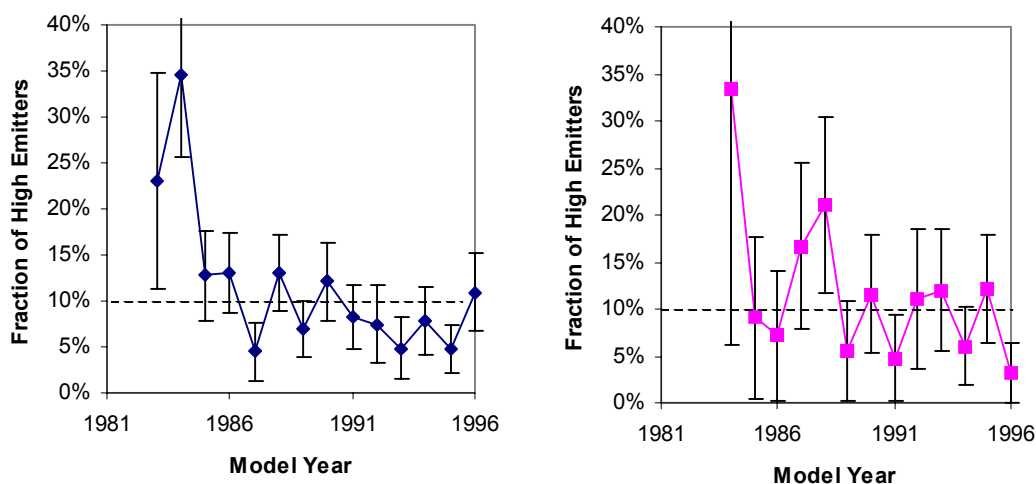
Figure 8-15: Fraction of high N_2O emitters for every model year for TWC-equipped passenger cars (left) and light-duty trucks (right)

8.3.7. Correlation of NO and N_2O Emissions

Since N_2O is mostly produced from NO reduction on the catalyst it is interesting to study the relationship between the emissions of both pollutants. Figure 8-16 shows the scatter plot of N_2O vs. NO emissions. The correlation between the two pollutants is poor on a vehicle to vehicle basis but is statistically significant (see Appendix D). There is a tendency to have a larger proportion of the high-N_2O emitters for larger values of NO.
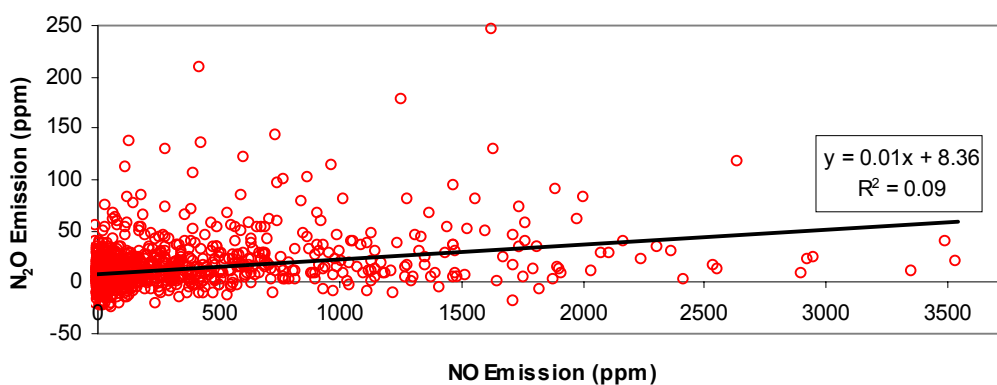
Figure 8-16: Scatter Plot of NO Emission vs. N_2O Emission

It has been found previously that even though scatter plots showing the emissions of individual vehicles vs. a given parameter show significant scatter, representing the same data in a

decile-averaged form is able to capture the underlying trends (see e.g. sections 6.4.5 and 6.4.5). To clarify the trends contained in the N_2O vs. NO scatter plot, Figure 8-17 shows the average N_2O versus the average NO for the 5% of the vehicles with the lowest NO, then the next 5% and so on. There is a consistent trend of increasing N_2O with increasing NO, with somewhat lower values for the last 2 bins (which correspond to the 10% highest NO emitters).

The average N_2O/NO ratio of the data set is 3.6%. It is heavily influenced by the 10% highest NO emitters (the 2 rightmost points in the graph) which produce 50% of the NO and have an N_2O/NO ratio of only 1.45%. An interpretation of these results with a simple model of N_2O production in a catalyst is presented in section 8.4.1 below.
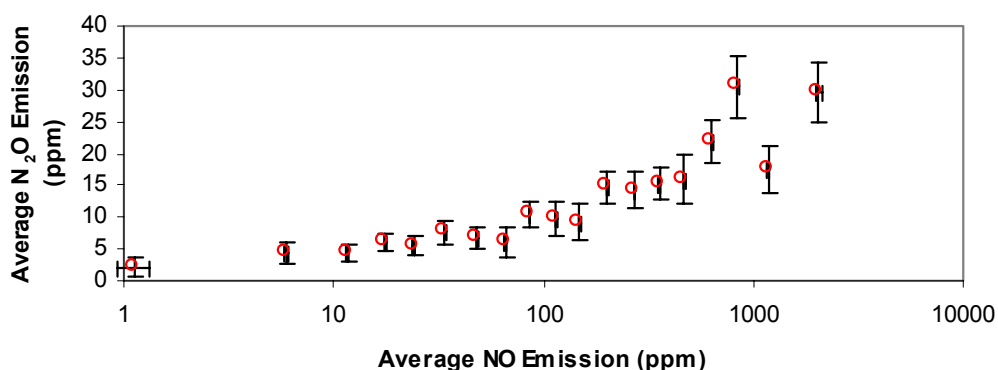
Figure 8-17: Average N_2O Emission for Vehicles of Different NO levels.

8.3.8. N₂O to NO Ratio vs. Model Year

Given the relationship between N_2O and NO emissions described in the previous section, it is interesting to study whether model year influences it. The ratio of average N_2O to average NO vs. model year for TWC-equipped vehicles is shown in Figure 8-18. This ratio decreases with vehicle age. This can be explained by the variation of the individual emissions with age: as vehicles get older the fraction of them who have a seriously degraded or failed catalyst increases. This causes a 10-fold increase on NO emissions for those vehicles, from catalyzed levels to engine out levels, which drives the average NO emissions up (Figure 6-32). Since the N_2O exhaust concentration does not change very much with model year (Figure 8-11), the N_2O/NO ratio is lower for older than for newer vehicles.
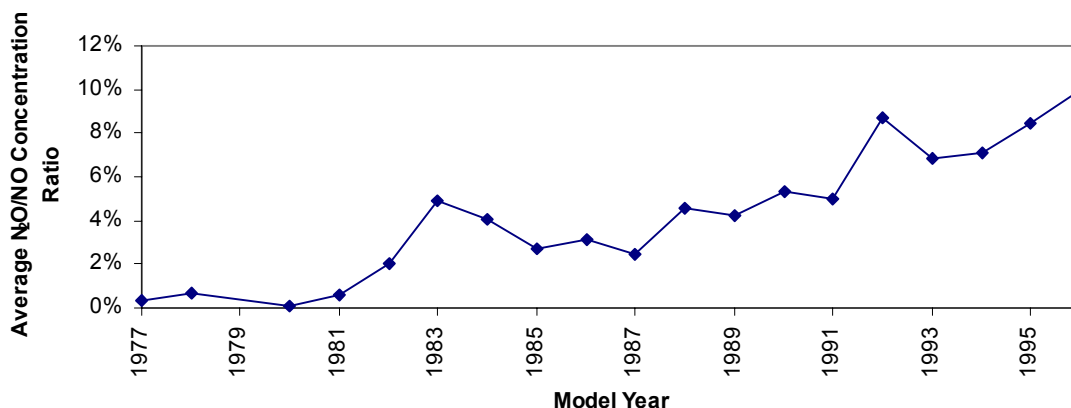
Figure 8-18: Ratio of average N$_2$O to average NO emission vs. model year (TWC-equipped vehicles only)

8.3.9. Effect of Vehicle Specific Power on N$_2$O Emissions

It has been shown in Chapter 3 of this thesis that CO, HC, and NO$_x$ emissions have a strong dependence on Specific Power (SP). For this reason the dependence of N$_2$O emissions on this parameter is studied in this section. Figure 8-19 presents the scatter plot of N$_2$O vs. Specific Power.[265] The correlation between N$_2$O and Specific Power is poor on a vehicle-by-vehicle basis.

When vehicles are binned in SP deciles a trend of increasing N$_2$O emissions with increasing specific power emerges, except for the last decile at the highest powers (Figure 8-20). This can be explained by the trend of NO formation with SP and the N$_2$O formation mechanism:

- As SP increases the engine-out NO$_x$ emission increases and thus more NO$_x$ is reduced in the catalyst. Since the N$_2$O formation is proportional to the amount of NO$_x$ reduced, higher powers yield higher N$_2$O emissions. The relative increase is not as large as that for NO (Figure 6-22).

- At the highest specific powers some of the vehicles may be in commanded enrichment operation (see the discussion about Figure 3-32). These vehicles produce lower engine-out NO$_x$, which means less NO$_x$ reduction in the catalyst and thus lower N$_2$O.

---

[265] We measured speed and acceleration (which are necessary for the calculation of Specific Power) simultaneously with N$_2$O emission for 814 vehicles.
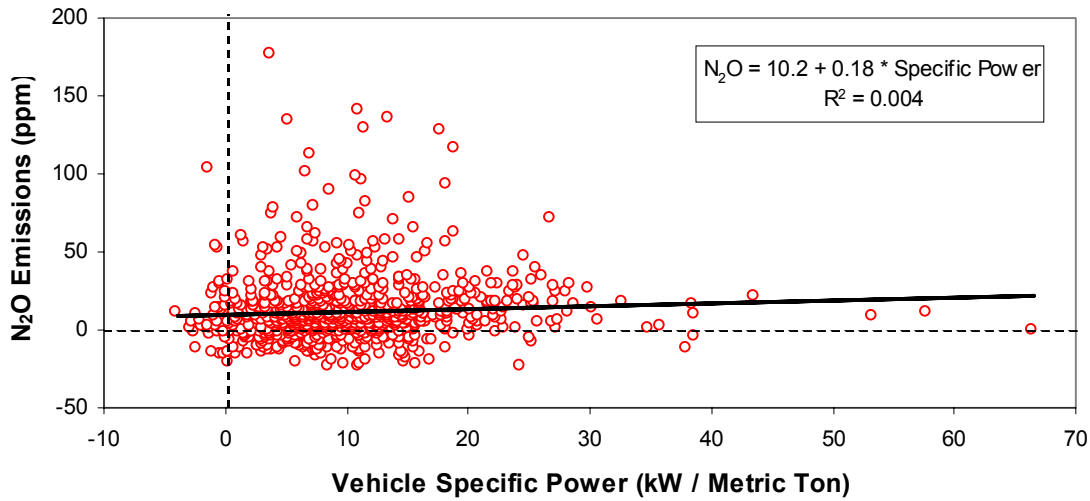
Figure 8-19: Scatter Plot and Linear Regression of N$_2$O Emission vs. Vehicle Specific Power
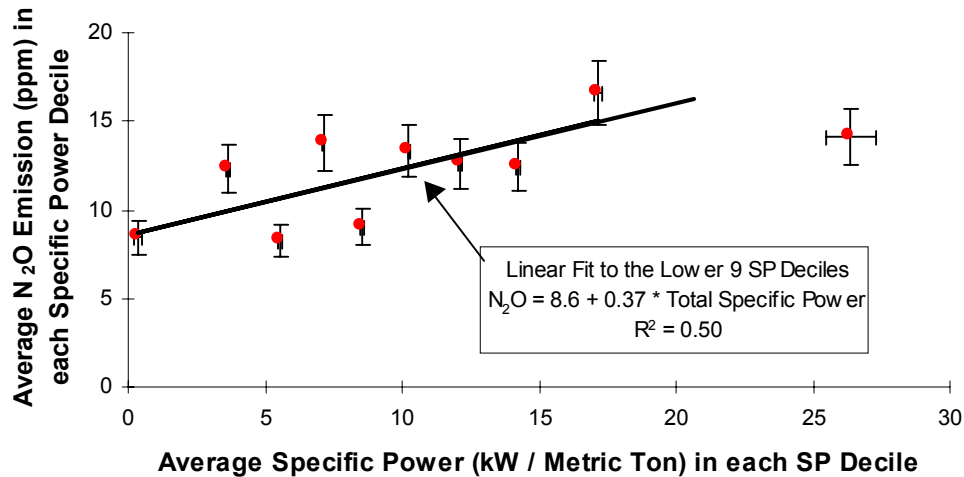
Figure 8-20: Average N$_2$O emission vs. average specific power for each specific power population decile.

8.3.10. Effect of Speed and Acceleration on N$_2$O Emissions

The effect of speed and acceleration on N$_2$O emissions is also presented here for completeness and to allow the comparison with future studies for which vehicle specific power may not be available.

A scatter plot of N$_2$O emission vs. vehicle speed is shown in Figure 8-21. Again the correlation between the two parameters on a vehicle-by-vehicle basis is small but is statistically

significant[266] (see Appendix D). The same data grouped by rank ordered speed population decile are shown in Figure 8-22. There is a trend of decreasing N_2O with increasing speed.[267] This same trend has been observed in constant-speed chassis dynamometer tests (Wehinger and Meyer-Pitroff, 1994) and in a tunnel study (Sjödin *et al.*, 1997b).
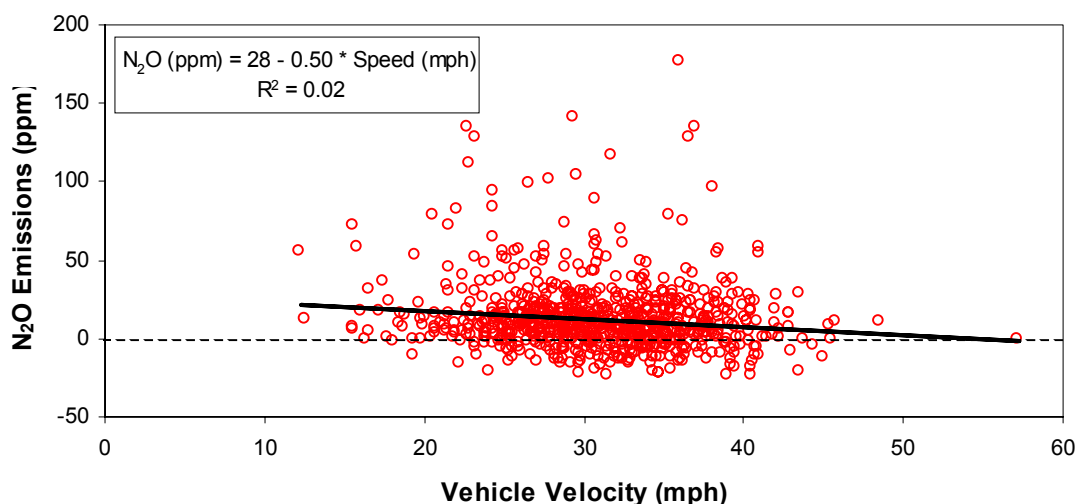
Figure 8-21: Scatter Plot and Linear Regression of N_2O Emission vs. Vehicle Speed

A possible explanation for this trend is the fact that catalyst temperature increases with average speed, because the average power demand is larger which leads to larger exhaust temperatures and flow rates. Increased catalyst temperature would in turn lead to lower N_2O emissions. However, changes in catalyst temperature due to this mechanism occur on a time scale of tens of seconds and are of limited magnitude unless the speed differences are sustained over a long period of time.[268] This mechanism is the likely cause of the trends on the tunnel and dynamometer studies. It could also explain the trend in this remote sensing study if the average speed during the last 10-20 seconds before the remote sensing site was correlated with instantaneous speed at the remote sensing site, which is plausible.

Another plausible explanation for this trend would be an increase of the size of the negative bias for higher speeds. Vibration-induced fringes are the cause of this bias for the particular experimental configuration in this study (see Appendix E). Since the amplitude of vehicle-induced vibrations increases with vehicle speed, this mechanism could also generate the

---

[266] As determined by the test on p.636 of Press et al. (Press *et al.*, 1992). The level of significance was $\alpha=1\%$.

[267] Note that the regression equation is almost the same as that in the scatter plot (Figure 8-21).

[268] Based on SFTP second-by-second data (Liberty *et al.*, 1997).

trend in Figure 8-22. Unfortunately there is no way to distinguish which of the two effects may be responsible for the observed trend.
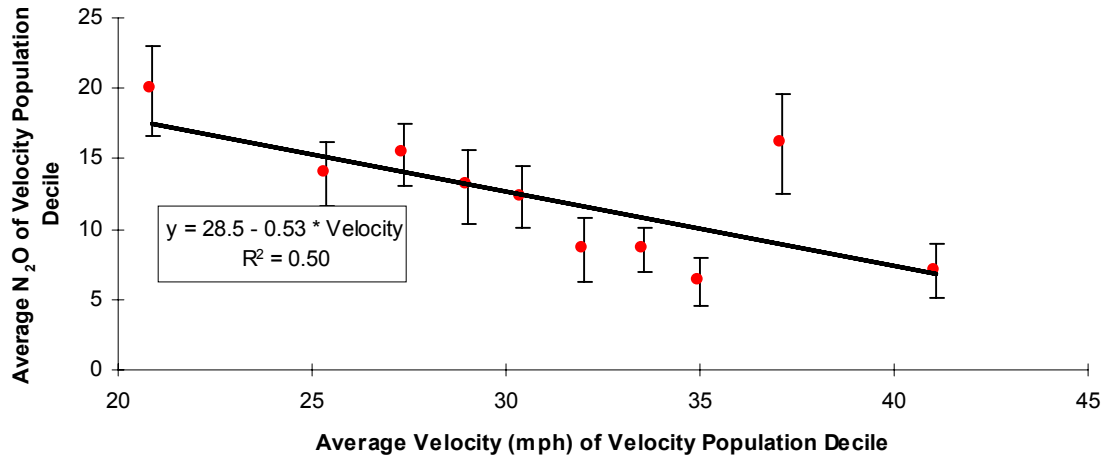
Figure 8-22: Average N$_2$O emission and average vehicle speed for every speed population decile[269]

The scatter and decile binned plots of N$_2$O emissions vs. vehicle acceleration are presented in Figure 8-23 and Figure 8-24. The general characteristics and trends of the graphs are very similar to those of N$_2$O vs. vehicle specific power, which is to be expected since both parameters are highly correlated (Figure 6-10).
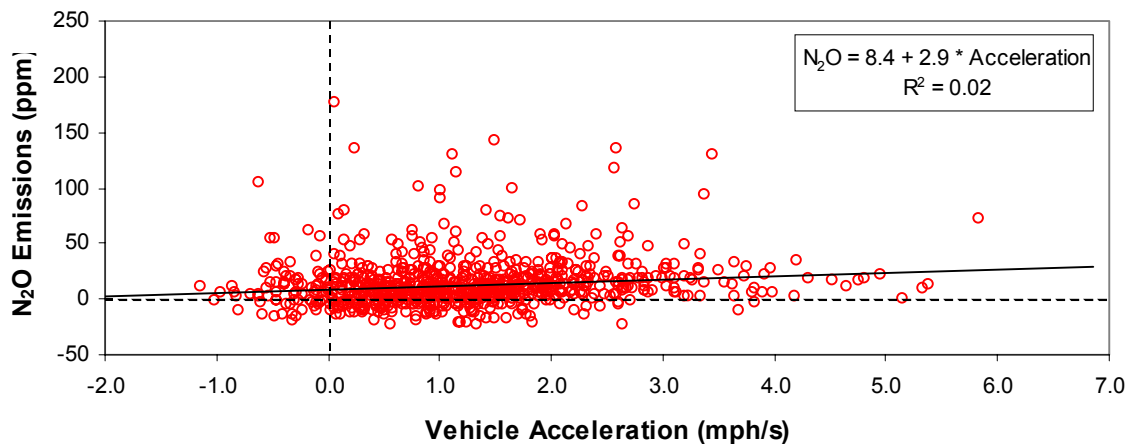
Figure 8-23: Scatter plot and linear regression of N$_2$O emission vs. vehicle acceleration

---

[269] Note that the regression equations are once again very similar in the scatter and decile-averaged plot.
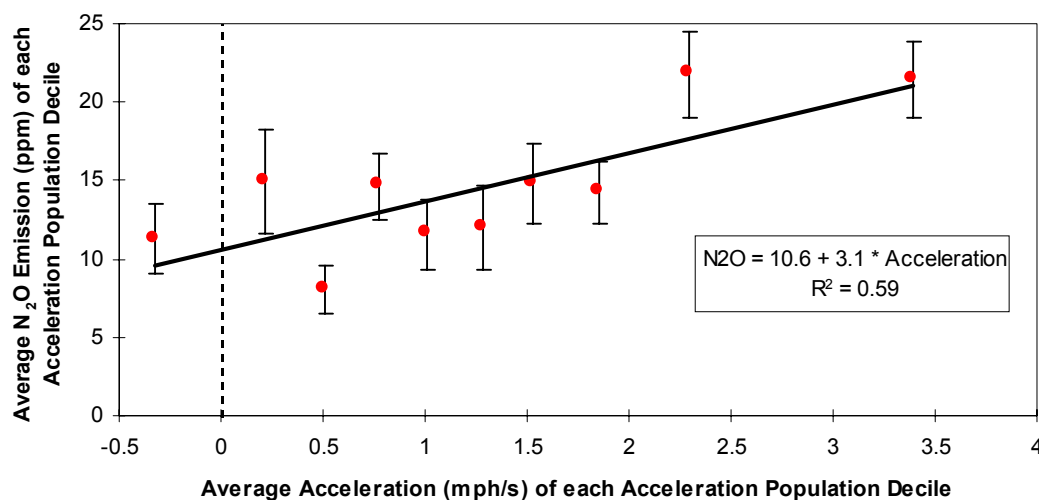
Figure 8-24: Average N₂O emission vs. average acceleration for every acceleration population decile[270]

An important difference is that acceleration is less suitable than specific power for predicting the onset of commanded enrichment in modern vehicles, as explained in section 3.2 (Figure 3-21). This is probably why the point with highest acceleration on the decile plot does not show the lower N_2O emissions that are expected with commanded enrichment because of decreased engine-out NO emissions, which do appear at the highest specific powers (Figure 8-20).

8.3.11. Correlation of N₂O with CO and Hydrocarbon Emissions

NO emissions showed some correlation with CO and HC emissions (see section 6.4.5). In this section the relationship of N_2O emissions with CO and HC is explored.[271]

Figure 8-25 to Figure 8-28 present the scatter and binned population decile plots of N_2O emission vs. CO and HC emission. No clear trend is apparent in either of the scatter plots, and the correlation coefficients on a vehicle-by-vehicle basis are very small. Again binning the data with the decile approach succeeds in highlighting the structure of the relationship (Figure 8-26

---

[270] Note that the regression equations are very similar in the scatter and decile-averaged plot.

[271] We measured N_2O simultaneously with CO and HC emission for 780 vehicles.

and Figure 8-28). Both plots show a trend of increasing N$_2$O with increasing CO and HC for the lower 8 or 9 deciles and a decline for the last 1 or 2.
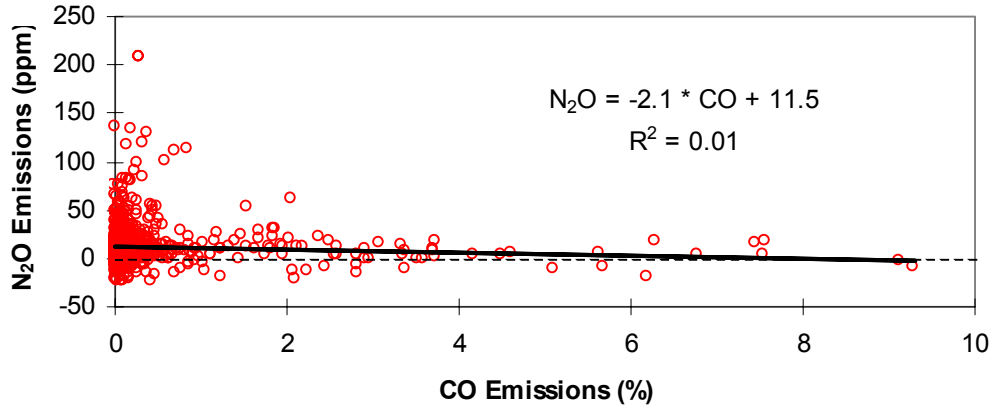
Figure 8-25: Scatter plot of N$_2$O emission vs. CO emission.
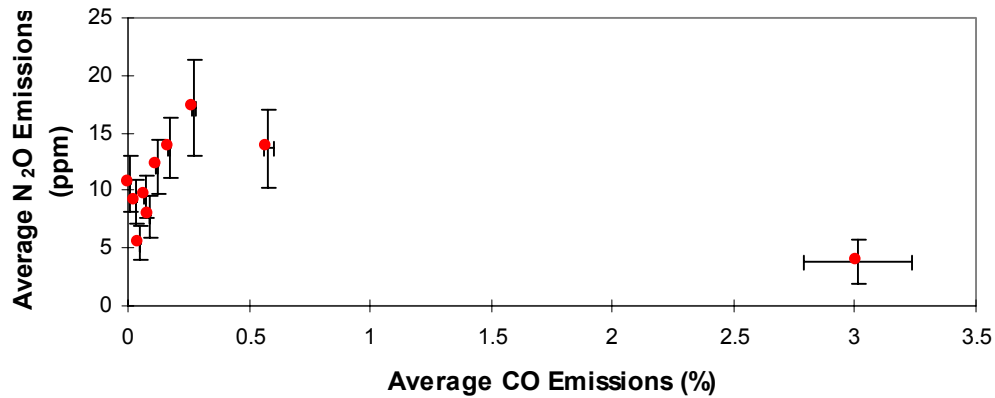
Figure 8-26: Average N$_2$O emission vs. average CO emission for each CO population decile

A mechanistic explanation for this relationship is that NO emission also follows the same trend with CO and HC (Figure 6-28 and Figure 6-30) and since N$_2$O and NO are positively correlated (Figure 8-17), the N$_2$O vs. CO and HC trends mimic those of NO. The reason why NO follows these trends was discussed in section 6.4.5.
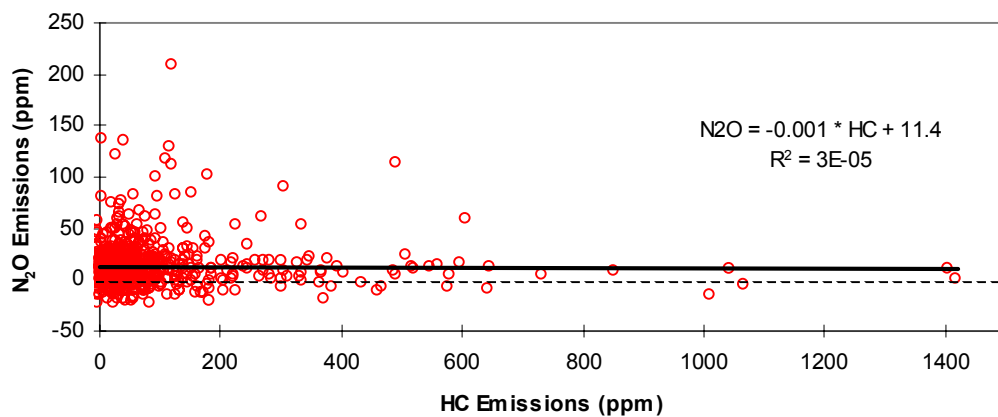
Figure 8-27: Scatter Plot of N$_2$O Emission vs. HC Emission
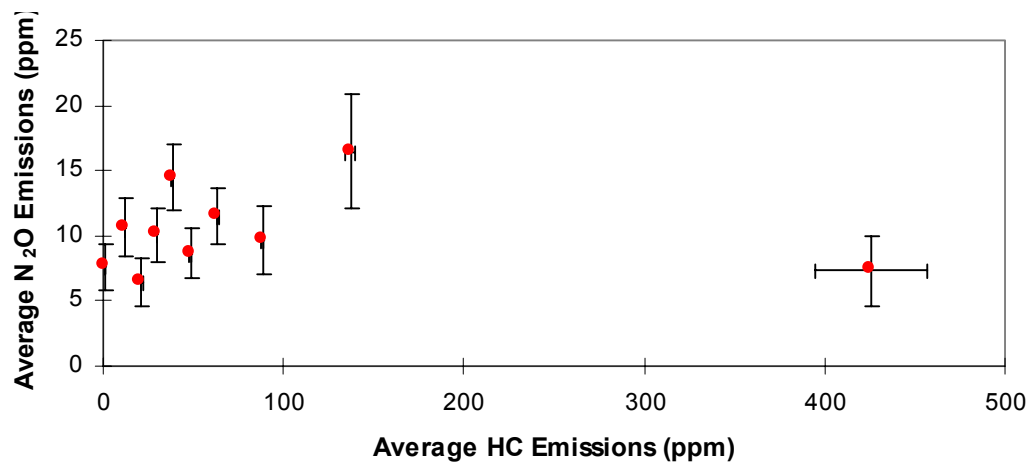
Figure 8-28: Plot of average N$_2$O emission vs. average HC emission for each HC population decile

8.3.12. N$_2$O Emission Variability

The significant variability of remote sensing measurements has received attention in recent years (Bishop *et al.*, 1996d; Stephens *et al.*, 1996a), and continues to be a major argument against the use of remote sensing in inspection and maintenance programs (Lorang, 1998). The variability of N$_2$O emissions is studied here through remote sensing emission data on 102 vehicles that were measured more than once at different times.

The comparison of the first vs. the second measurement is shown in Figure 8-29. Most of the vehicles had low N$_2$O emissions on both occasions. Of those with 1 high measurement, about 1/3 were not very variable while the other 2/3 were quite variable. This is similar that was found for NO emissions (Figure 6-38) and also can be partially explained by changes on engine load between the 2 measurements.
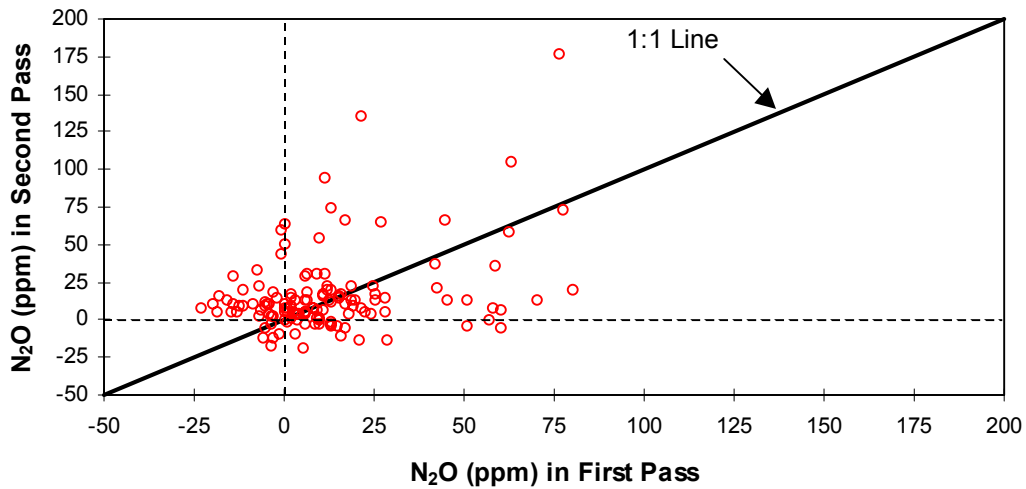
Figure 8-29: N$_2$O emission on second pass versus N$_2$O emission on first pass for vehicles measured more than once

8.4. Further Analysis and Comparison to the Literature Studies

In this section some of the experimental results are interpreted and compared to a new compilation of literature studies.

8.4.1. Interpretation of the N_2O vs. NO Results

The relationship between the remote sensing measurements of NO and N_2O emissions exhibits some interesting features as described in section 8.3.7. This section proposes a simple catalyst model to explain the observed trends.

A simple model for the change of N_2O emissions with NO emissions has been constructed based on the results of Gifhorn, Rabl *et al*. (Gifhorn, 1997; Rabl *et al.*, 1997). In a catalyst bench study these authors found that within a limited range of pre-catalyst NO concentrations, N_2O emission increased linearly with pre-catalyst NO and also with the amount of NO reduced in the catalyst.

Since N_2O is an intermediate produced during the decomposition of NO in the catalyst it seems plausible that the amount of N_2O will be proportional to the amount of NO reduced in the catalyst. This is consistent with the results of Rabl *et al.* A simple model based on this idea is shown in Figure 8-30. In this model the engine-out NO is decomposed with an efficiency η_{NO}, and N_2O is generated from this conversion with an N_2O selectivity η_{N2O}.

$$\eta_{NO} = \frac{\text{NO Reduced}}{\text{NO Combustion}} \qquad \eta_{N2O} = \frac{N_2O \text{ Formed}}{\text{NO Reduced}}$$
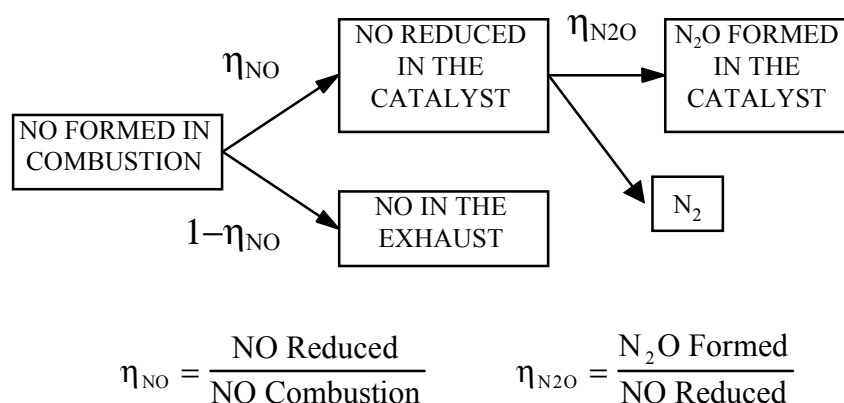
Figure 8-30: Mass-balance model of the formation of N_2O in three-way catalyst

This simple model has been executed by applying a constant N_2O selectivity (η_{N2O}) of 0.6%[272] to the second-by-second NO conversion data[273] of a 1994 Jeep Cherokee[274] tested on 8 driving cycles during the SFTP program (Liberty *et al.*, 1997).

The comparison of the models to the experimental N_2O/NO ratios is shown in Figure 8-31. The model predicts that the N_2O to NO ratio will increase at low tailpipe NO concentrations due to increased NO destruction in the catalyst. This is the same trend found in the experimental data.
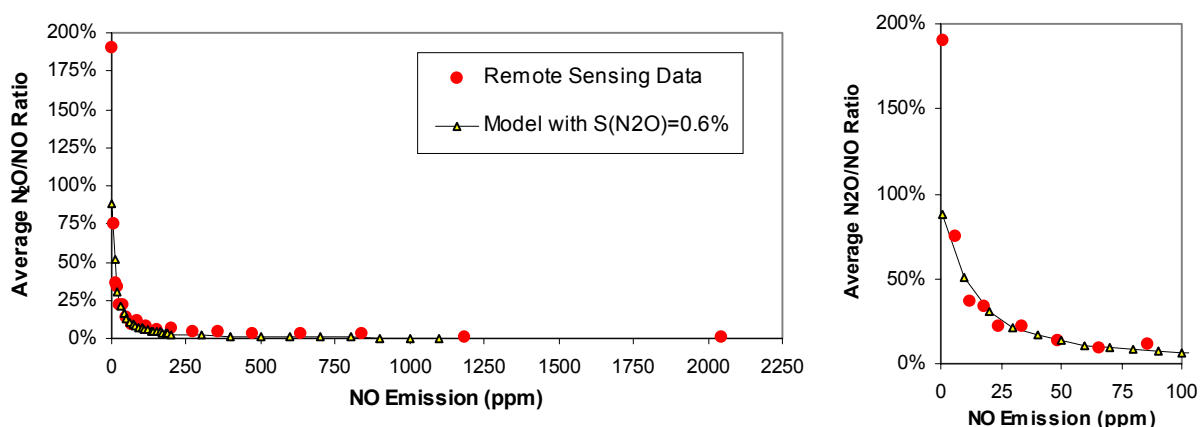
Figure 8-31: (Left): Experimental N₂O/NO ratio vs. NO in the exhaust compared to the model results; (Right): detail of the same graph for low NO

Some additional insights can be gained by examining the N_2O vs. NO trends shown in Figure 8-32. The model predicts the N_2O for NO levels below 100 ppm when the selectivity (η_{N2O}) is set at 0.6% while a larger selectivity is needed at larger NO emissions levels.

We can interpret this trend based on the N_2O formation process: although vehicles with properly working new catalysts can occasionally have high NO emissions, it is more likely that the higher NO emissions in our study correspond to vehicles with partially degraded catalysts. These catalysts have been found to produce more N_2O by several studies (Prigent *et al.*, 1991; Jobson *et al.*, 1994), which requires a larger N_2O selectivity.[275]

---

[272] Adjusted to provide good agreement with the experimental data.

[273] Only points of the second-by-second data with a warmed-up catalysts and with speeds larger than 10 mph have been included, since only those conditions are relevant to remote sensing.

[274] This vehicle was not equipped with an exhaust gas recirculation (EGR) system to reduce engine-out NOx emissions. Vehicles with EGR produce about ½ of the engine-out NO as vehicles without EGR (Figure 3-26). Thus the selectivity used here should be scaled by about a factor of 2 for vehicles with EGR.

[275] NO emissions also increase with specific power (Figure 3-14 and Figure 6-22), but this tendency is already incorporated into the model by the second-by-second data.
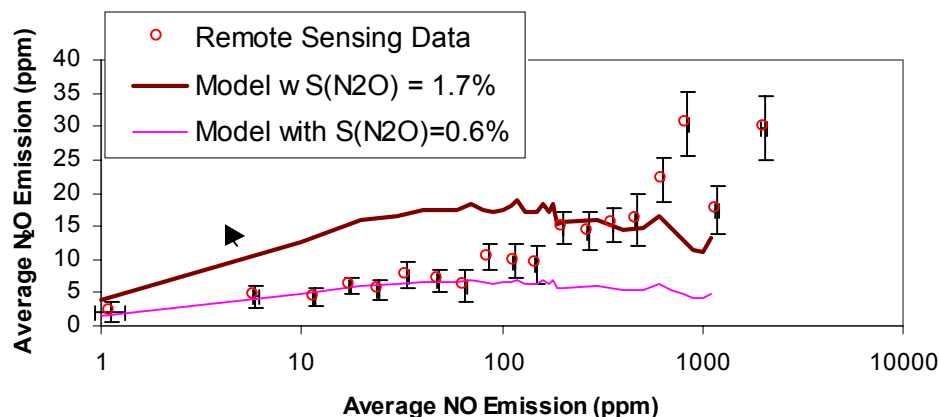
Figure 8-32: Experimental N_2O vs. NO trend compared to the model results

8.4.2. Compilation of Literature Studies

An extensive effort was made to collect all available literature studies in which N_2O emission rates from automobiles and light-duty trucks had been measured. Twenty-four such studies could be obtained. A summary of their results for the different vehicle/catalyst combinations are shown in Table 8-2. Most of these studies involved dynamometer testing of a few vehicles on one or several driving cycles. Three were tunnel studies, all of them performed in Europe.

The next sections analyze the literature results and compare them to the results of this study.

The study of Ballantyne et al. (Ballantyne *et al.*, 1994) has been excluded because ambient N_2O levels were not subtracted from the measurements, resulting in emission rates which are estimated to be too high by a factor of 2 (Barton *et al.*, 1994).[276]

---

[276] Michaels (Michaels, 1998) also suggests that the high sulfur gasoline levels used in Ballantyne's study may have contributed to the unrepresentatively high N_2O emissions in that study.

Study	Test Conditions	Number of Vehicles [5]	Sulfur level in gasoline (ppm)	N2O Meas. Tech.	Notes	Passenger Cars															Light-Duty Trucks					
						No Catalyst			Oxidation Catalyst			New TWC			Aged TWC			Low Emission Vehicles			New TWCs			Aged TWCs		
						M	SE	SK	M	SE	SK	M	SE	SK	M	SE	SK	M	SE	SK	M	SE	SK	M	SE	SK
Pierotti 76 (USA)	Grab sample	1 N		GC	(16)	<0																				
Bradow 77 (USA)	FTP	1 NT	300		(9)							64														
Urban 79 (USA)	FTP	1 N + 4 Ox	290	GC		5			38	12	-0.2															
Urban 80 (USA)	FTP	4 NT	290	GC								17	3	0.4												
Smith 80 (USA)	FTP	4 NT + 4 AT	290	GC	(9)(18)							29	4	-1.8	44	6	0.8									
Braddock 81 (USA)	FTP	4 NT	250	GC	(6)(9)							79	10	1.4												
Smith 82 (USA)	FTP	7 Ox + 3 AT	290	GC	(7)				55	12	2.3				117	16	1.6									
De Soete 89 (France)	ECE & EUDC	1 with 8 TWCs + 1 Ox.		GC	(3)	21			148			95			278											
Dasch 90 (USA)	FTP	1 N, 7 T, 1 LT		GC	(1)(9)	4.8									49	11	0							89		
Knapp, 90 (USA)	FTP			FTIR	(9)(18)	4									38											
Warner-Selph, 90 (USA)	FTP	1N + 1 Ox + 3 AT				16			10			42			153	64										
Berges 93 (Germany & Sweden)	Tunnel Study			GC	(19)										170											
Prigent 94 (France)	ECE	3 with 15 TWCs		GC	(8)	12	0.5	1.7				32	7	-1.7	86	16	2.6									
Ballantyne 94 (Canada)	FTP	3 NT + 8AT + 3 LT	700	FTIR	(2)(9)	0						74	30	-0.1	126	18	0.9				237	28				
Jobson 94 (Sweden)	FTP	1 with 2 TWCs & w/o		TILDAS		72						13			271											
Wehinger 94 (Germany)	Constant speed	1 with 3 TWCs & w/o		GC	(10)	6	0.3																			
Barton 94 (Canada)	FTP	2 NT + 9 AT + 2 LNT + 1 LAT	500	FTIR								53	15		79	18					95	18		304		
Sjodin 95 (Sweden)	Tunnel Study			GC	(12)										40											
Koike 96 (Japan)	ECE	1 N + 2 Ox + 1 AT		NDIR		13			68	25					232											
Joumard 96 (France)	FTP	10 N + 10 T		GC	(9)(13)	48									98											
Sjodin 97 (Sweden)	Tunnel Study			FTIR	(12)										32											
Laurikko 98 (Finland)	FTP	7 AT		FTIR											34	16	2.5									
Michaels 98 (USA)	FTP	13 AT + 6 LAT + 4 LEV	285 / 24	FTIR	(11)(17)										72	13	1.0	28	2.5					130	13	0.8
IPCC estimates 96 (USA)						32			121						274			64						378		
IPCC estimates 96 (Europe)						8			8						80											
This Study (California)	Remote Sensing	10 N + 58 Ox. + 63 NT + 698 AT + 35 LNT + 266 LAT	30	TILDAS	(14)(15)	16.6	14	0.3	41	9	0.9	34	8	1.8	37	3	2.9				23	10	1.8	60	6	3.9

Table 8-2: Average Results of N2O Automobile Emission Measurements (mg / mi)

Notes for Table 8-2

Key: M: mean; SE: Standard Error of the Mean; SK: Skewness

(1): No distinction was made between new and aged catalysts in Dasch' study, and the mileage of the tested vehicles was not provided. Dasch averaged his results with those of previous studies, but only the measurements performed during his study have been included here.

(2): The N_2O detection limit is not reported. I estimate it at about 360 ppb based on the reported results. The ambient N_2O level was not subtracted from the measurements. For this reason this study has not been included in the average of the literature.

(3): Only the data for which the subtraction of the ambient N_2O concentration from the bag samples was performed systematically have been included (table XXIX of this report, line 2).

(5): N: non-catalyst; Ox: Oxidation Catalyst; T: three-way catalyst; NT: New Three-Way Catalyst; AT: Aged Three-Way Catalyst; L: Low Emission Vehicle; LT: light-duty truck with three-way catalyst

(6): The vehicles were new with conditioning "by on road mileage accumulation." The conditioning mileage is not reported. These vehicles have been included in the "new three-way catalyst" category

(7): This study tested the vehicles "as received" and after a tune-up. Only the "as received" data are used here since they are more representative of real-world emissions

(8): Catalysts aged 50, 100, and 150 hours have been combined into the "aged catalyst" group in this table.

(9): These studies included data on driving cycles other than the FTP, which are not presented in this table. Some of these results have been presented in section 8.2.

(10): Results are reported in ppm. The conversion to mg/mi assumed a fuel economy of 10L/100km (Berges 1993). All three catalysts with 16,000-95,000 miles have been grouped under "aged catalysts" here

(11): Averages of all data for both air conditioning modes. Results with standard sulfur content presented here for all vehicles except Low Emission Vehicles; low-S fuel results presented for the later

(12): These results correspond to a mixed vehicle fleet of about 45% TWC passenger cars, 45% non-catalyst cars, and 10% heavy-duty vehicles

(13): No mileage reported for the TWC vehicles; all have been included in the "aged catalyst" category

(14): No independent measurement for the non-catalyst vehicles since this value was used to correct the average systematic bias of the data set (Appendix E).

(15): Total number of vehicles is smaller than the 1361 vehicles sampled because license plates were not captured for 10% of the vehicles, the California Department of Motor Vehicles could not provide registration information for about 10% of the license plates captured, and the VIN decoder could not decode about 10% of the VINs from the DMV.

(16): The results of this study are reported in more detail in Dasch (1992) than in the original paper.

(17): This study makes a further distinction between the three way catalyst-equipped vehicles subject to "Tier 0" and "Tier 1" US emission standards. This distinction has been used in the calculation of emission factors in section 8.5.1 but is not presented on this table.

(18): This publication did not provide data for all the FTP tests included on their averages. The author was contacted and was not able to provide those data either.

(19): This study tested 4 vehicles new and after three 5,000-miles accumulation periods. The results of the new vehicles have been included on the "new" catalyst category and those at the end of the 3rd accumulation period on the "aged" catalyst category. The results of the intermediate accumulation periods have not been used here.

(20): This study estimated the emission rate from the N_2O/CO_2 ratio by extrapolating the emission to global conditions by using global gasoline consumption, and then dividing by a global estimate of vehicle-miles traveled. This procedure may have introduced significant errors in the result.
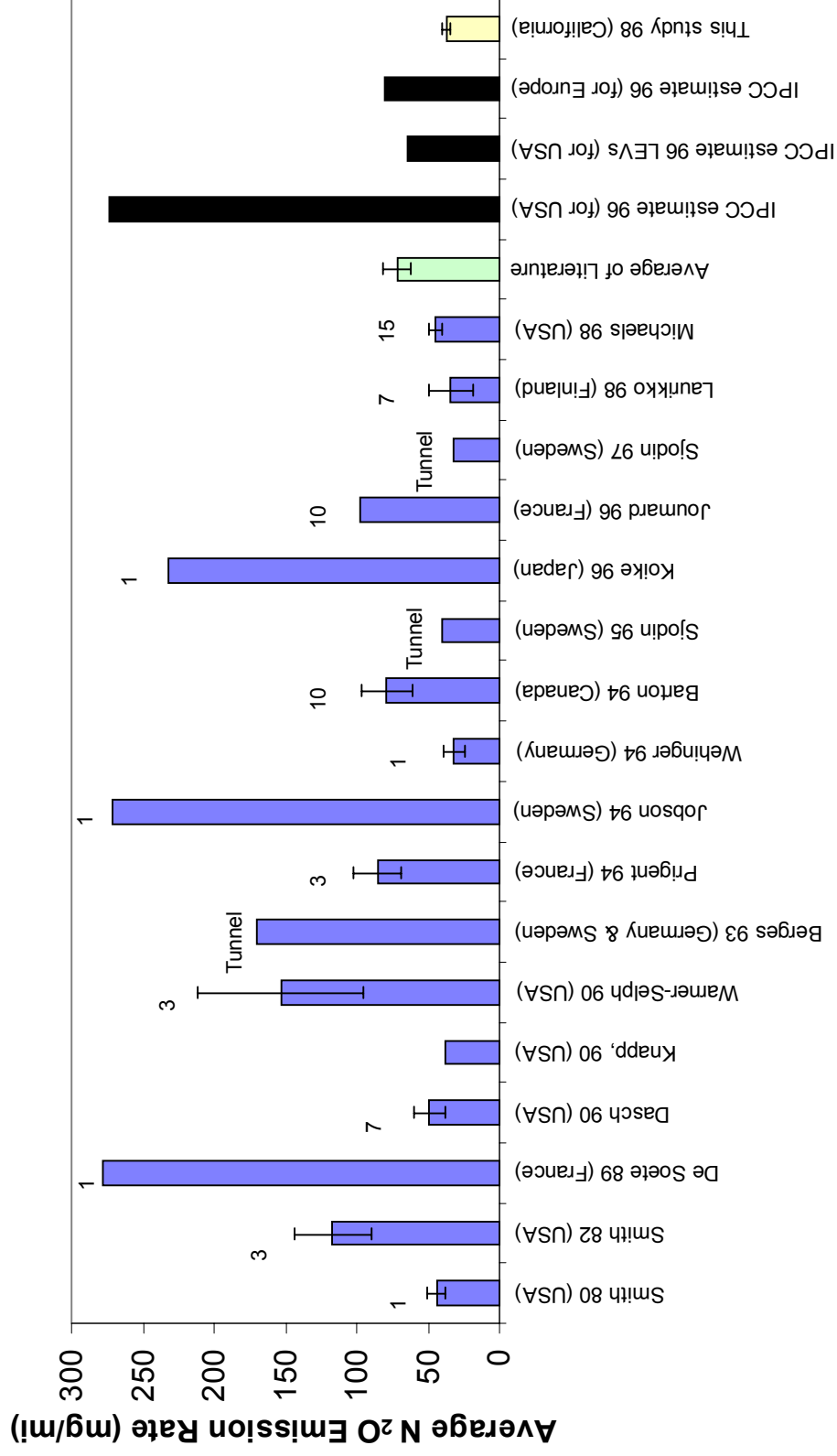
Figure 8-33: Comparison of the N_2O emission rates for passenger cars equipped with aged three-way catalysts[277]

[277] The numbers above the columns are the number of cars tested on each study.

8.4.3. Comparison of the Literature Studies

A comparison of the emission rates for three-way catalyst equipped passenger cars in the literature is shown in Figure 8-33. The range of emission rates reported in the different studies span an order of magnitude, without a clear trend with time, location of the study, or analysis technique.[278]

This large variability can be explained, however by the skewness of the N_2O emissions distribution, this is, the fact that the N2O distribution is composed of a few super-emitters and a large majority of low-emitters (section 8.3.2). Given that most of the studies only tested a few vehicles, the presence or absence of high emitters in the sample can result in high or low emission rates. In particular, *the three studies with the highest emission rates only involved 1 vehicle*.

The study by De Soete (De Soete, 1989), was basically adopted as the 1996 IPCC emission factor for the U.S. (IPCC, 1996b; Michaels, 1998), which explains why this factor was so high: it is based on the measurements on a single vehicle and several non-production catalysts with high emitting characteristics. All of the studies in which larger samples were used yielded significantly lower results.

Just the opposite happened in the study of Dasch at General Motors Research Labs (Dasch, 1992). This researcher tested several vehicles with (possibly) new catalysts[279] (thus lower N_2O emitters). Dasch also rejected two high emitters as outliers with an statistical criterion which was not appropriate for highly skewed distributions.

This issue is further explored in the next section by analyzing the emissions distribution of the literature studies.

8.4.4. Further Evidence of the Skewness of the N_2O Distribution

The remote sensing study reported here has found evidence of the skewness of the N_2O emission distribution. In order to further verify this point, the distribution of N_2O

---

[278] A large positive bias in the measurement of N_2O from combustion sources was found for studies using gas chromatography due to a sampling artifact (Muzio *et al.*, 1989). However this problem was found to be insignificant when the SO_2 concentration in the combustion gases was lower than 500 ppm (Muzio *et al.*, 1989), which is about two orders of magnitude larger than in diluted gasoline-powered vehicle exhaust.

[279] The mileage of the vehicles tested in not reported in Dasch' study.

emission rates for the FTP tests for several of the literature studies has been evaluated. Only passenger cars equipped with aged three-way catalysts have been selected, because cars equipped with new three-way catalysts and light-duty trucks have significantly different N_2O emissions rates. These literature studies are listed in Table 8-3.

Study	Number of Vehicles	Driving Cycle	Average N₂O Emission (mg/mi)	Skewness
Smith 1980	4	FTP	44	0.8
Smith 1982	3	FTP	117	1.6
Warner-Selph 1990	2	FTP	153	
Barton 1994	9	FTP	79	1.6
Jobson 1995	1	FTP	271	
Koike 1996	1	FTP	232	
Laurikko 1998	7	FTP	34	2.5
Michaels 1998	13	FTP	45	2.1
ALL STUDIES	40	FTP	72	1.8

Table 8-3: Literature studies used for the N_2O emissions distribution of passenger cars with aged three-way catalysts[280]

All of the studies for which the sample skewness can be calculated yield positive values for this parameter. Given the very small samples tested in all studies, the presence or absence of high emitters results in large differences on the average emission rates. Some differences may also be due to differences in engine / catalyst technology between the tested vehicles.

Parameter	Value (mg/mi)
Number of Vehicles	40
Average	72
Median	47
Maximum	271
Minimum	10
Standard Deviation	64
Skewness (non-dimensional)	1.8

Table 8-4: Statistics of the N_2O FTP literature tests of passenger cars with aged three-way catalysts

---

[280] The study of Ballantyne et al. (Ballantyne *et al.*, 1994) has been excluded because ambient N₂O levels were not subtracted from the measurements, resulting in emission rates which are estimated to be too high by a factor of 2 (Barton *et al.*, 1994).

A histogram of the results of the 40 vehicles is shown in Figure 8-34, while the main statistics are presented in Table 8-4. The distribution of N_2O emissions is positively skewed.

The distribution of literature results is compared to a gamma distribution in Figure 8-34. The general trends of both distributions are the same, while there are some discrepancies in detail.
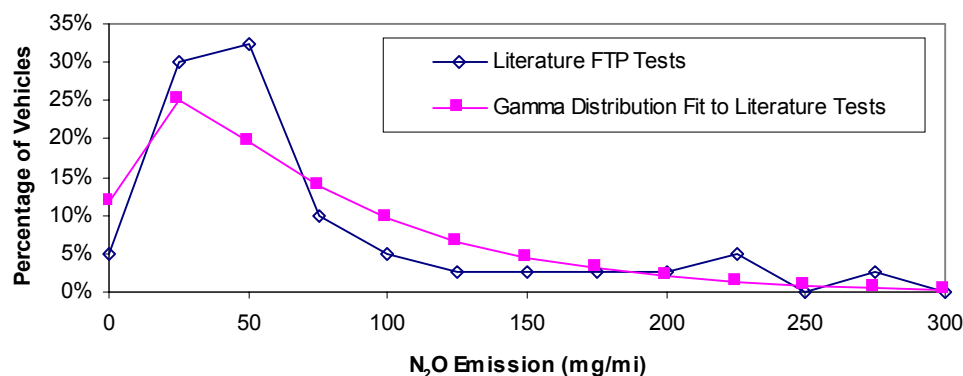
Figure 8-34: Distribution of the N_2O emission rates reported in the literature and comparison to a gamma distribution (aged-TWC cars only)

The comparison of the literature and the experimental N_2O distributions is shown in Figure 8-35.[281] The contribution of the highest and lowest emitters to the total emissions of the literature N_2O distribution and the TILDAS N_2O and NO distributions are presented in Table 8-5. It can be seen that, while being skewed, the N_2O distribution from the literature is less skewed than the experimental N_2O and NO distributions. The 10% highest emitters in the literature are responsible for only 30% of the emissions as compared to 53% for the N_2O remote sensing distribution.

Zhang et al. (Zhang *et al.*, 1994) compare a remote sensing and an FTP distribution for CO and find the same qualitative shape difference shown in Figure 8-35.[282] This indicates that the explanation of the different shape of remote sensing and FTP-composite results may be that the distribution of second-by-second emissions is

---

[281] The experimental data have been corrected to FTP conditions and normal sulfur fuel by the procedure described in section 8.5.1.

[282] These authors tentatively attribute the shape difference to "an insufficient number of testing vehicles [on the FTP data set] and/or unrepresentative testing vehicle recruitment."

qualitatively different from the distribution of cycle-averaged results for a fleet of vehicles.
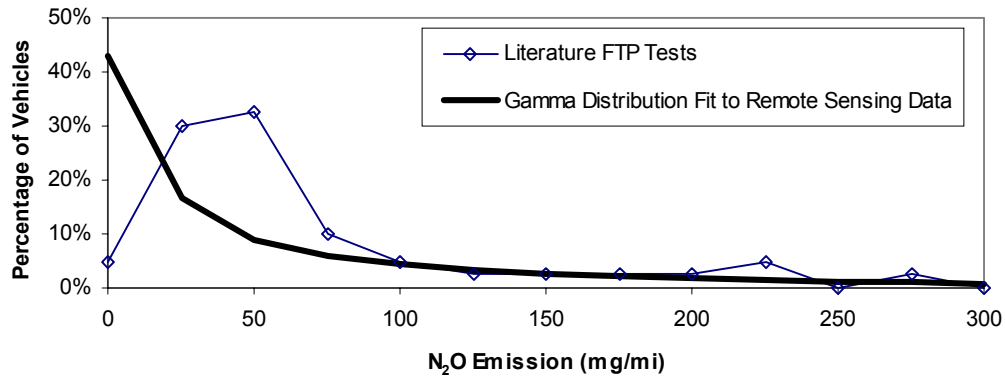
Figure 8-35: Distribution of the N$_2$O emission rates reported in the literature compared to the remote sensing distribution (aged-TWC cars only)[283]

Parameter	N$_2$O Literature	N$_2$O TILDAS	NO TILDAS
Emissions of the 10% Highest Emitters	32%	53%	50%
Fraction of the Cars for 50% of the Emissions	20%	9%	10%

Table 8-5: Comparison of the high emitter statistics for the literature N$_2$O and the TILDAS N$_2$O and NO distributions.

---

[283] The gamma distribution fit is used instead of the raw data to avoid the negative tail in the experimental N2O distribution caused by measurement noise. This is the same procedure illustrated in section 8.3.2.

8.5. N_2O Emission Factors

8.5.1. N_2O Emission Factor Estimation from TILDAS Remote Sensing Data

The estimation of real-world N_2O emission factors from passenger cars and light-duty trucks is of great interest due to the large uncertainties that remain about their value (Michaels, 1998). We have shown that remote sensing can produce emission factors for NO_x for light-duty vehicles and heavy-duty diesel trucks which are close to those determined in several tunnel studies (see Figure 6-15 and Figure 7-13). Also we have shown in section 8.2 that remote sensing is well suited for estimating emission factors for N_2O emissions. This section details the calculation procedure and the results based on the N_2O remote sensing data collected in California.

The emission factors for this study were determined separately for each catalyst vehicle type and technology. The remote sensing emission factor for each technology group has been estimated in the following way:

- The average N_2O emission (ppm) of every model year passenger cars and light-duty trucks has been calculated separately from the experimental data.

- The average N_2O emission rate (mg/mi) has been calculated using the fuel economy of each vehicle type and model year.

- The emission factor for passenger cars, light-duty trucks, and all vehicles has been computed as the average of the emission rates of every model year and vehicle type, weighed by the number of vehicles in each year and type.

This procedure results in an estimate of the N_2O emission factors that each type of vehicle was actually emitting at our remote sensing site. In order to make the remote sensing results comparable with the literature results and IPCC / EPA estimates which have mostly used the FTP cycle and high sulfur gasoline, some factors need to be corrected for:

- First we have to account for the fact that although we measured warm-running emissions at our remote sensing site, the vehicles were not exactly on average at the same conditions as during the FTP Bag 2. Vehicle emissions have been shown to be closely related to vehicle specific power in Chapter 3. Average specific power in our study was larger than the average specific power in Bag 2 of the FTP. The emission

factors have been corrected for this effect by using the regression line in Figure 8-20. This results in an average correction of –11% of the catalyst emission factors.

- The second effect is the fact that in this remote sensing study only warm-running vehicle emissions were measured. These are slightly lower than FTP emissions as shown in section 8.2. For this purpose the regression equation in Figure 8-2 has been used. This results on a 28% average increase. The combination of the first and second corrections yields an FTP composite estimate which is 14% larger on average than the remote sensing emission factors.
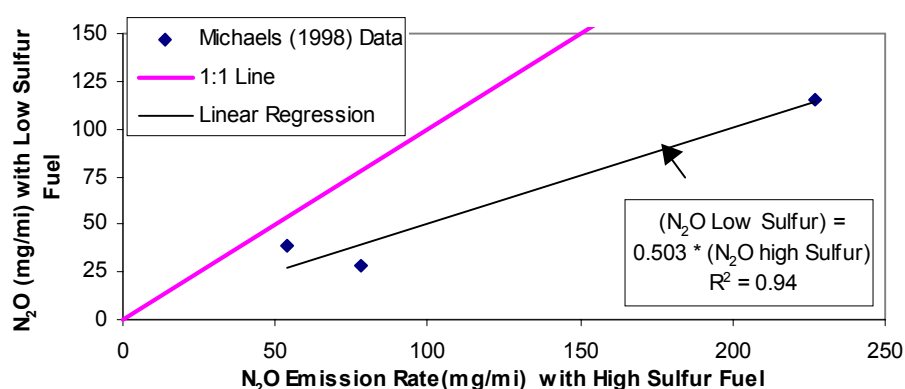
Figure 8-36:Effect of sulfur content of the fuel on N$_2$O emissions from TWC-vehicles

- Next, the equivalent FTP-Bag 2 emissions obtained in this way have been corrected for the fact that California gasoline only contained 30 ppm of sulfur at the time of the testing, while all other studies have been conducted with levels of 250 ppm sulfur or larger. The only data that can be used for a correction of this effect are those of (Michaels, 1998) and are shown in Figure 8-36.[284] Only 3 data points exist for "Tier 1" and low-emission vehicles. No data are available for "Tier 0" or oxidation catalyst vehicles, and the impact for these vehicles could be smaller than for those tested by Michaels.[285] This correction results in a factor of 2 larger emission factors. Because of these facts the sulfur-corrected emission factors are very uncertain and should be

---

[284] Michaels data show lower N$_2$O emissions with low-sulfur fuel for 2 Tier 1 vehicles and the average of 4 low-emissions vehicles.

[285] The evidence for Tier 0 vehicles is unclear. NO$_x$ reductions due to sulfur reductions are very similar to those for Tier 1 vehicles. Because the sulfur effects on N$_2$O and NO$_x$ emissions seem to be closely tied this would indicate that similar sulfur effects on N$_2$O emissions should be expected.

On the other hand two studies seem to indicate no effect of sulfur on N$_2$O emissions, although the effect of sulfur is not separable from the effect of ambient temperature for one study (Braddock, 1981) and the effect of other fuel properties for the other study (Smith and Black, 1980).

taken as tentative, while the factors without the sulfur correction can be taken as lower limits.

- ▪ Previous inventories account for all U.S. vehicle-miles-traveled (VMT) with N_2O emission factors derived on the FTP. This ignores the fact that a significant part of the VMT is accumulated on highways, where N_2O emissions tend to be lower due to higher catalyst temperatures. Highway emission factors have been estimated here by applying the regression equation of the HWFET to the FTP driving cycle emissions (Figure 8-4)[286] to the emission factors determined in this study.

8.5.2. Comparison to the Literature and IPCC / EPA N_2O Emission Factors

The results of this study are compared to the latest IPCC and EPA estimates (IPCC, 1996b; U.S. EPA, 1997b; Michaels, 1998) and to the averages of the literature values in Table 8-6. The averages of the literature values have been calculated from the results from 23 literature studies in which N_2O emission rates of on-road vehicles were measured are reported in Table 8-2. Most of the studies involved a testing one or few vehicles in a chassis dynamometer, and 3 were tunnel studies.

---

[286] Differences in Specific Power distributions between the two cycles may not be as important as for other pollutants, since N_2O emissions are not highly sensitive to Specific Power (Figure 8-20).

	IPCC 96 for USA	IPPC 96 for Europe	Michaels 98	Average of Literature	This Remote Sensing Study[287]	This Study corrected for FTP conditions[288]	This Study corrected for gasoline sulfur and FTP conditions	This Study corrected for Highway (HWFET) Conditions[289]	This Study corrected for gasoline sulfur and Highway Conditions[290]
Non-Catalyst PC	32	8	17	17	17	17	17	17	17
Oxidation Catalyst PC	121	8	52	56	32	34	69	12	27
New TWC PC	274	80	46	44	34	40	80	14	31
"Tier 0" Aged TWC PC	274	80	82	72	40	45	90	17	35
"Tier 1" Aged TWC PC	274		46	46	26	30	59	10	22
Non-Catalyst LDT			19	22[291]					
Oxidation Catalyst LDT	156		67	117[292]	62	76	151	30	61
New TWC LDT	365		64	64	23	28	55	9	21
"Tier 0" Aged TWC LDT	365		136	151	61	71	141	27	57
"Tier 1" Aged TWC LDT	380		64	64	59	65	128	25	51

Table 8-6: Summary of the emission factors from previous studies and this study for each vehicle and catalyst type

---

[287] It is not possible to know whether a remotely-sensed vehicle is subject to "Tier 0" and "Tier 1" emission standards based on the information provided by the California Department of Motor Vehicles or the VIN decoder. The emission factors in the table have been determined using the model year distributions of both types for California (Michaels, 1998).

[288] The same correction procedure has been applied to all catalyst types even though only data for TWC exist. This is based on the assumption that the fundamental physical and chemical processes which justify each correction are the same for all catalysts. No correction was applied to non-catalyst vehicles since the available information on the dependence on N$_2$O emissions with power is very limited (De Soete, 1989) and the FTP and sulfur corrections deal with physical processes that only happen in catalysts.

[289] This column has been calculated by taking the values corrected to FTP conditions and using the regression equation from Figure 8-4.

[290] This column has been calculated by taking the values corrected by gasoline sulfur and FTP conditions and using the regression equation from Figure 8-4.

[291] No data for vehicles of this type in the literature. The estimate in the table has been obtained by multiplying the emission rate for passenger cars by the ratio of average fuel economies (Heavenrich *et al.*, 1996).

[292] No data for vehicles of this type in the literature. The estimate in the table has been obtained by multiplying the emission rate for passenger cars by the ratio of the emission rates for LDTs and PCs for "Tier 0" TWC vehicles.

These comparisons are also shown in Figure 8-37 and Figure 8-38. The main conclusions of the comparison between the average literature values and the results of this study (Figure 8-38) are:[293]

- The results of this remote sensing study are lower than the average of the literature values for all the vehicle/catalyst combinations. Once corrected to FTP conditions and normal sulfur gasoline, the results of this study are slightly higher for all the passenger car types. These differences are not highly significant, given the uncertainties in this study[294] and in the correction for the gasoline sulfur content.

- For light-duty trucks the uncorrected results are about ½ of the literature values for new catalysts and "Tier 0" TWC vehicles, and about the same for "Tier 1" TWC vehicles.

- The light-duty truck results corrected to FTP conditions and normal gasoline sulfur levels are very close to the average of the literature for new catalysts and "Tier 0" TWC vehicles.

- The corrected remote sensing result is twice as large for "Tier 1" TWC LDTs than for the literature.[295] This is important since this vehicle type accounted for 10% of the vehicle-miles traveled (VMT) in the U.S. in 1996 (U.S. EPA, 1998i) and will be increasing as all new light-duty trucks are subject to this or stricter standards.

- LDTs equipped with oxidation catalysts have the largest emission rate of the remote sensing study.[296] This result is highly uncertain due to the small number of vehicles in this category (14). No N_2O measurements on vehicles of this type have been reported in the literature, so a comparison is not possible. Again a larger vehicle sample would be needed to get a more precise estimate. This point is not too important because this vehicle type accumulated only 5% of the VMT (U.S. DOT, 1997a), and this share

---

[293] Non-catalyst emission factors are discussed in Appendix E.

[294] Due to the uncertainty in the correction of the negative bias (Appendix E).

[295] This difference would be about slightly less if the "new catalyst" LDTs (which are subject to Tier 1 or stricter standards) [295] and "Tier 1" TWC vehicle categories were combined. This may or may not be fair, since the lower emissions of the "new catalyst" category could be due to lack of catalyst aging. A larger sample than the one in this study would be needed to ascertain this point.

[296] This emission rate is similar to that of the LDTs equipped with aged TWCs. The emission rate of passenger cars equipped with oxidation catalyst is also similar to the levels from TWC-equipped cars, which indicates that this result is plausible.

will be declining with time as oxidation catalysts are no longer used by themselves in automotive applications (Michaels 1998).

▪ Estimated highway emission rates are only 42% of the FTP emission rates. This fact has an important impact on the estimates of the total U.S. N_2O mobile source emissions.

The conclusions of the comparison between the IPCC 96 / EPA 98 estimates, the average literature values, and the results of this study (Figure 8-38) are:

▪ The average literature values for catalyst vehicles are within ±15% of the newest EPA emission factors proposed by Michaels (Michaels, 1998).[297] The raw remote sensing results are generally lower than EPA's new factors and the sulfur-corrected numbers are higher.

▪ The IPCC 96 / Draft EPA 98 N_2O emission factors (IPCC, 1996b; U.S. EPA, 1998c) that originated from the report of Weaver and Chan (Weaver and Chan, 1996) are a factor of 3-5 higher than the average literature values and the corrected results of this study, and about a factor of 7 higher than the uncorrected remote sensing results. The main reason for this discrepancy (as pointed out by Michaels (Michaels, 1998)) is that the emission factors of Weaver and Chan are based mostly on the results of De Soete (De Soete, 1989),[298] which are much higher than the average literature results. De Soete tested only 1 vehicle with several three-way catalysts. The vehicle-catalysts combinations tested had high emissions, but not higher than the higher emitters tested by other researchers. The key point is that the N_2O emissions distribution is very skewed (see sections 8.3.2, 8.4.4, and 8.4.3) and De Soete happened to test a set of mostly high emitting vehicle-catalyst combinations.

▪ The European emission factors in the IPCC 96 guidelines (IPCC, 1996b) for aged-TWC passenger cars are very close to the average of the literature and the results of this study.

---

[297] The "Tier 1" emission factors are the same as those of Michaels since his study is the only one that has measured N_2O emission rates from this type of vehicles.

[298] Actually Weaver and Chan took their numbers from a table on Ballantyne et al. (Ballantyne *et al.*, 1994), which cited De Soete's data (Michaels, 1998). Ballantyne's own data were too high by a factor of 2 because ambient N_2O levels had not been substracted (Barton *et al.*, 1994) from the analysis and maybe the high sulfur in the test gasoline (Michaels, 1998). This fact probably made the very high emission factors from De Soete appear "within the range" of plausible values.

- The European emission factor for oxidation catalysts is a factor of 5-10 too low. This discrepancy may not be important since oxidation catalysts are not very common in Europe.
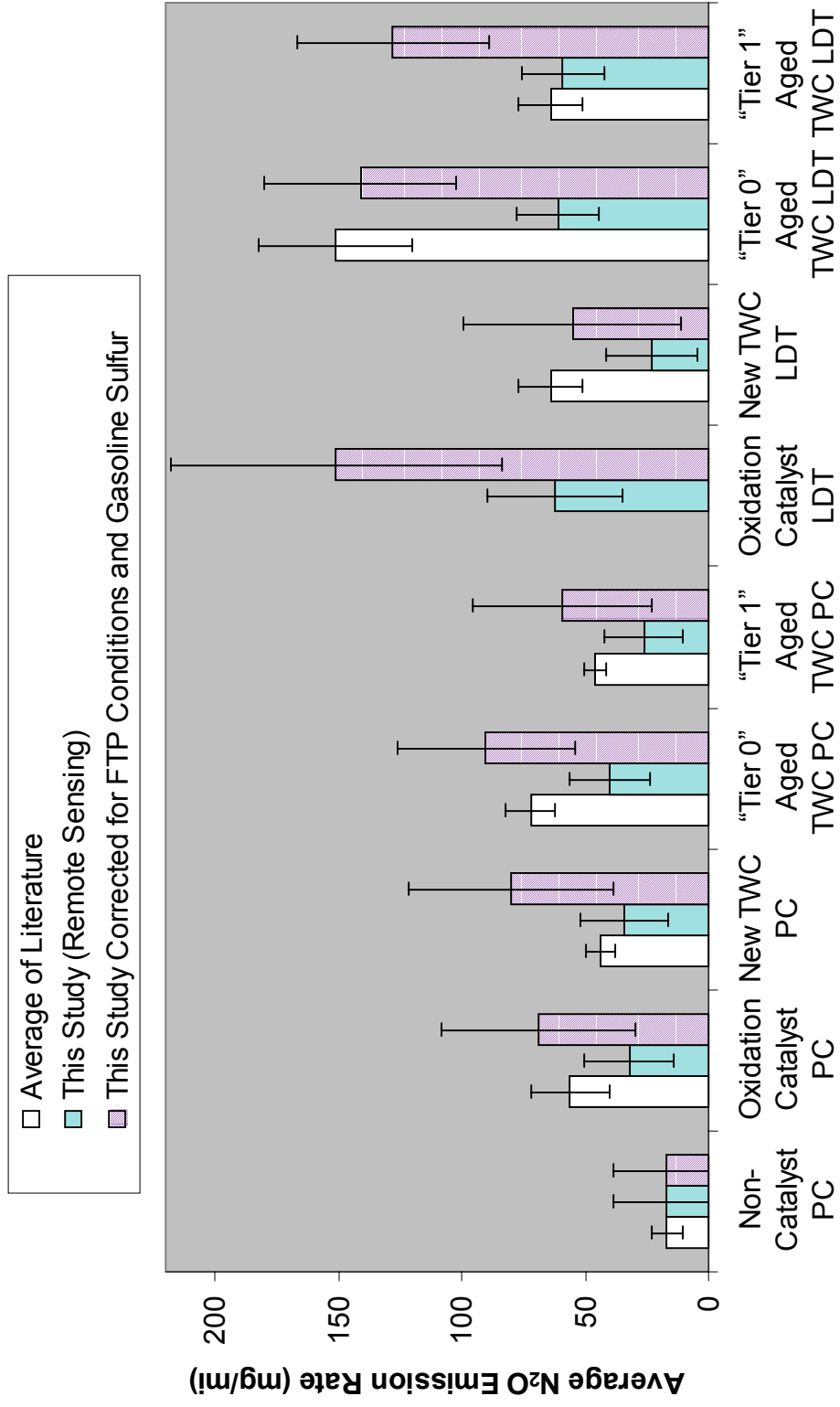
Figure 8-37: : Comparison of N$_2$O emission levels for all vehicle and catalyst types (II)
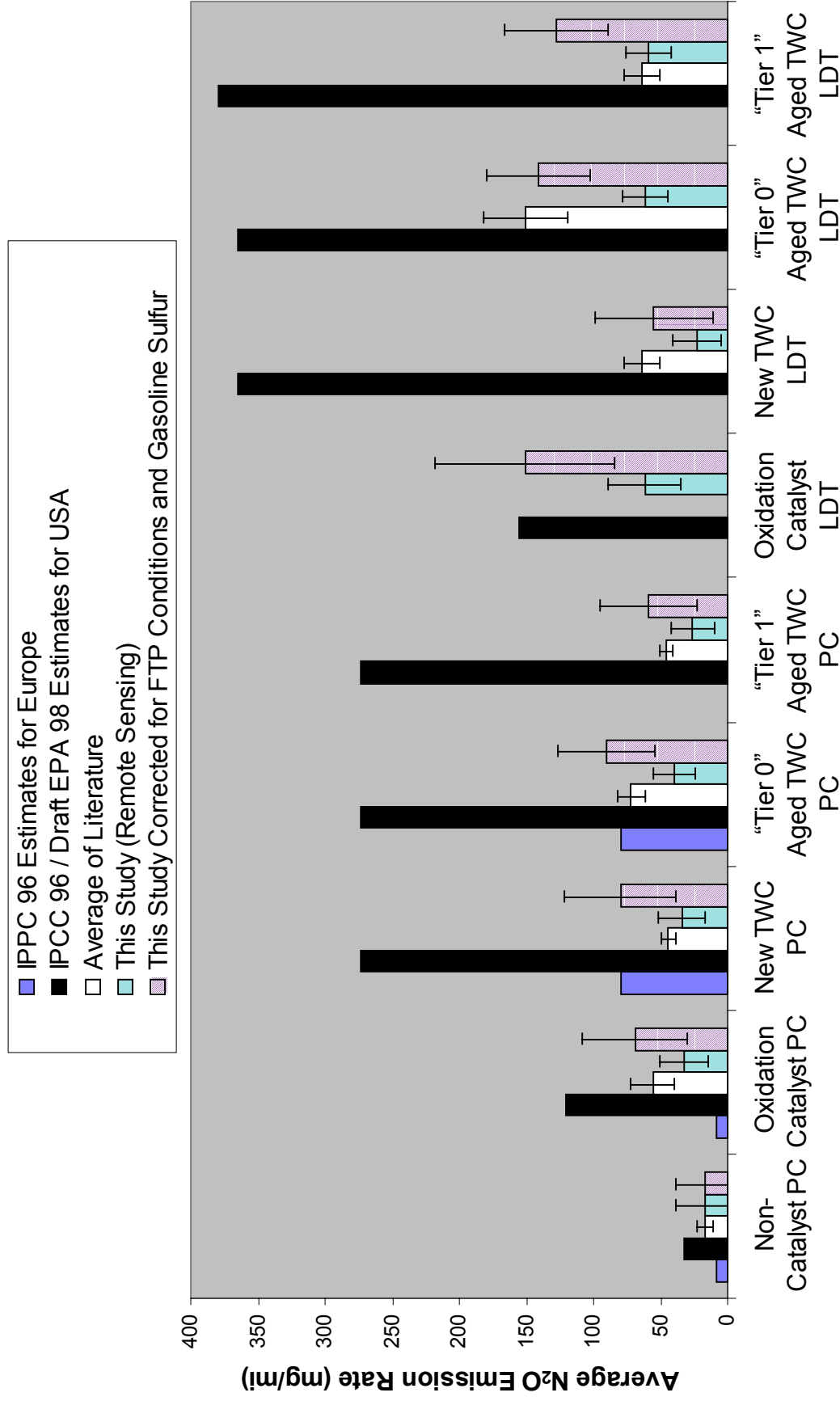
Figure 8-38: : *Comparison of N₂O emission factors all vehicle and catalyst types*

8.5.3. Mobile Source Contribution to the U.S. Greenhouse Gas Inventory

The 1997 and 1998 EPA estimates (U.S. EPA, 1997b; U.S. EPA, 1998c) of the contribution of mobile sources to 1996 U.S. greenhouse gas emissions, together with four new estimates, are shown in Figure 8-39. The new estimates have been calculated using the literature and remote sensing emission factors derived in this study and the newest EPA emission factors (Michaels, 1998). These estimates have been calculated using the emission factors in Table 8-6 (in mg/mi) and multiplying them by the vehicle-miles traveled for each vehicle / catalyst technology combination.[299]

The VMT traveled on highways[300] have been multiplied by the estimated highway emission rates, while the FTP emission rates have been used for the rest of the VMT. The N$_2$O emission estimates would be 14% higher if the lower highway emission factors were not taken into account.

The comparison of the estimates is shown in. The total contribution based on the remote sensing results is estimated at 0.46% of the 1996 U.S. greenhouse emissions[301] if no sulfur effect was present, and 0.92% if the sulfur effect is as large for the whole fleet as estimated in section 8.5.1. This in reasonable agreement with the estimated contribution of about 0.79% using the average of the literature tests and the newest EPA emission factors.[302] These estimates indicate that this source is non-negligible, but is a

---

[299] The VMT for each vehicle / catalyst combination have been calculated from the vehicle population and average yearly mileage to be used in the next EPA emission model, MOBILE6 (U.S. EPA, 1998i). The breakup of catalyst technology vs. model year for the U.S. and California has been obtained from Michaels (Michaels, 1998). California VMT has been weighed by the lower N$_2$O emission factors observed in this study.

[300] The fraction of VMT traveled on highways and other roads has been estimated from Table VM-1 of *U.S. DOT 1996 Highway Statistics* (U.S. DOT, 1997a). Only the "interstate urban" and the "interstate rural" VMT categories in this table have been considered highway miles for the purposes of N$_2$O production. These two categories account for 22% of the 1996 VMT for passenger cars and light-duty trucks. The other VMT categories in the table ("other arterial rural," "other rural," and "other urban"), which account for 78% of the total VMT, have been considered to yield N$_2$O emissions at the same rates at the FTP. Significant uncertainties remain in what is the proper emission rate for each driving condition. Remote sensing could be used to determine these emission rates by choosing several sites deemed representative of each type of driving.

[301] 1% of the 1996 net U.S. greenhouse gas emissions equals 15.8 MMTCE, 187,000 Tons of N$_2$O (as N$_2$O) or 119,000 Tons of N$_2$O (as N).

[302] These two sets of emission factors yield the same results by the compensation of 13% higher EPA estimates for "Tier 0" passenger cars with the lower factors for "Tier 0" and oxidation catalyst-equipped light-duty trucks.

factor of 4 to 7 lower than the 1998 EPA estimate that caused public concern (Wald, 1998).
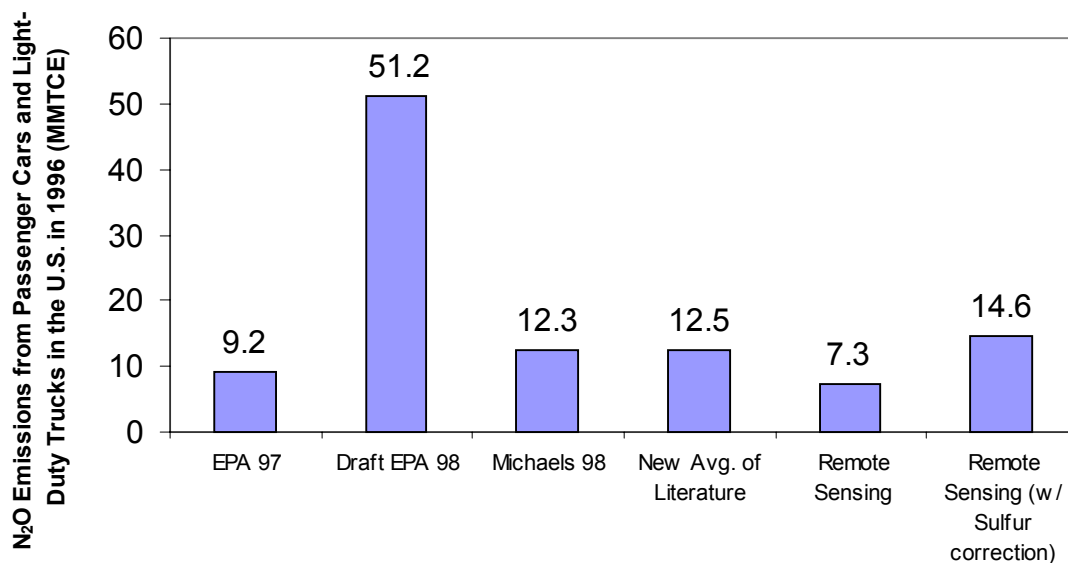
Figure 8-39: Comparison of the mobile source contribution to U.S. greenhouse gas emissions for different sets of emission factors
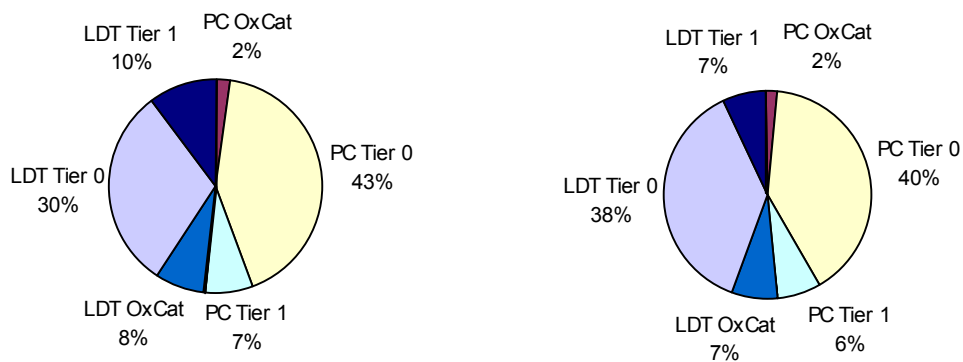
Figure 8-40: Comparison of the contribution of the different vehicle / technology types to mobile source N_2O in the U.S. using the remote sensing estimates (left) and the average of the literature (right)[303]

The fraction of the total emissions calculated with the remote sensing emission factors due to each vehicle / technology combination is shown in Figure 8-40. Passenger

---

[303] Key to the labels: PC: passenger car; LDT: light-duty truck; NonCat: no catalyst; OxCat: with oxidation catalyst.

cars and light-duty trucks contribute equal amounts to the inventory. "Tier 0" TWC vehicles dominate the contribution of both vehicle types due to their larger share of VMT.

For light-duty trucks "Tier 1" TWC contribute a larger fraction relative to "Tier 0," due to the larger relative sales of light-duty trucks in recent years. The contribution of LDTs with oxidation catalysts is significant,[304] although it is uncertain since few measurements on vehicles of this type were obtained by remote sensing and none have been reported in the literature.

8.5.4. Net Impact of Automotive Catalysts on the N_2O Budget

It is interesting to examine what would be the N_2O budget if automotive catalysts were not in use. This is directly applicable to countries were catalyst-equipped vehicles are being or will be introduced.
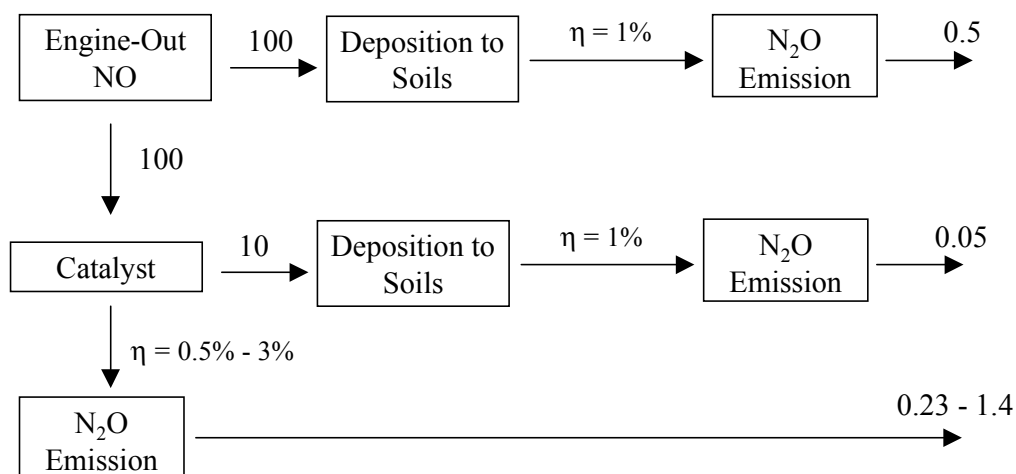
Figure 8-41: Schematic budget of N_2O emissions with and without automotive catalysts[305]

If catalysts were not in use the direct mobile source of N_2O will not be present[306] but N_2O production from soils due to deposition of NO and its products would be enhanced. The production of N_2O from nitrogen deposition is estimated to have an

---

[304] Though it will decline with time as vehicle of this type are scrapped or driven less.

[305] The efficiencies shown are in terms of nitrogen atoms. Thus a conversion of 100 moles of NO with an efficiency of 1% yields 0.5 moles of N_2O.

[306] N_2O formed on the engine of non-catalyst cars is neglected in this calculation, since it would be also emitted in principle from catalyst cars.

efficiency of about 1% (Bouwman *et al.*, 1995), though this estimate is highly uncertain. The use of automotive catalysts increases direct N_2O emissions. From the results in section 8.4.1 we can estimate an N_2O selectivity in the catalyst of 0.5%-3%. Comparing both situations in Figure 8-41 we find that a significant part of the increased N_2O formation in the catalyst may be offset by decreased N_2O formation in soils, thus lowering the overall impact of introducing three-way catalysts.

8.6. **Discussion**

8.6.1. Conclusions of the Experimental Results and the Analysis of the Literature

The main conclusions of this study with respect to N_2O emissions from catalyst-equipped vehicles are:

- The N_2O emissions of vehicles on several driving cycles are correlated, which indicates that the tendency to emit more or less N_2O is a characteristic of each vehicle. Based on the limited data available, remote sensing is a useful technique for measuring the N_2O emission levels of catalyst-equipped vehicles.

- The TILDAS technique is able to remotely measure N_2O emissions with an average fleet detection limit of ~8 ppm of the exhaust.

- Measuring N_2O emissions in inspection and maintenance programs using IM240 could provide very detailed information about N_2O emissions which can be used to better estimate the strength of this source and to investigate the causes of high N_2O emissions.

- Both the remote sensing and the literature distributions of N_2O emissions from catalyst vehicles are highly skewed. This is the main reason for the conflicting N_2O emission factors for mobile sources.

- High N_2O emitters are not the necessarily the same as NO, CO or HC emitters. All model years have a significant high emitter fraction.

- N_2O Emission rates were found to be more constant with vehicle age than those for NO, CO or HC. The contribution of each model year from 1983 to 1996 to total emissions is similar at about 7%.

- Light-duty trucks were found to have higher emissions than passenger cars. About 1/2 of this difference can be explained by the fuel economy difference and the other 1/2 is due to increased N_2O generation for light-duty trucks per unit mass of fuel.

- N_2O emissions show some correlation with NO emissions. The results of this study are consistent with N_2O formation being proportional to the amount of NO reduced in

the catalyst. The constant of proportionality is larger for higher NO emitters, which can be explained by catalyst aging.

- N_2O emissions increase with vehicle specific power, but not as much as NO emissions.

- N_2O emissions from remote sensing are about a factor of 7 lower than the 1996 IPCC estimates and a factor of 1.6 lower than the average of the literature values and the newest EPA estimates. This difference is tentatively attributed to the lower-sulfur content of California's gasoline, although insufficient data exist to confirm this point.

- The contribution of gasoline on-road motor vehicles to U.S. greenhouse gas emissions is estimated at 0.46%-0.92% based on the literature and on this study. This is a factor of 4 to 7 lower than the 1998 Draft EPA estimate and brackets the newest EPA estimate.

- Sulfur reduction in gasoline may be an effective way to reduce N_2O emissions from catalyst-equipped vehicles. Further research on this topic is needed.

8.6.2. N_2O High Emitters

High N_2O emitters are different from CO, HC, or NO_x high emitters. Remote sensing could be used to detect vehicles with excess N_2O emissions. Little is known about the vehicle characteristics that lead to high N_2O emissions, besides catalyst aging. Catalyst replacement would probably reduce N_2O emissions from high emitters but at a significant cost. Further study of high emitter characteristics and repair strategies is needed before the feasibility of this approach to reduce N_2O emissions can be evaluated.

Repair strategies that would result in simultaneous reductions of other regulated or unregulated pollutants would be easiest to implement in the U.S., because they will provide an incentive to the states to implement them. Actions that are geared exclusively towards the N_2O emissions will be more difficult to implement.

The determination of vehicle or catalyst characteristics that result on high N_2O emissions may allow the avoidance of such characteristics on future vehicles. Remote sensing or IM240 data with very large vehicle samples[307] could provide the real-world data needed for such a study.

---

[307] It is estimated that at least 20,000 vehicles would be necessary to start to see stable statistics.

8.6.3. Lowering Sulfur Gasoline for Reducing N$_2$O Emissions

Based on the very limited data acquired recently by EPA (Michaels, 1998) and the comparison between remote sensing and literature results, decreasing fuel sulfur may be a viable strategy to reduce N$_2$O emissions.

Fuel sulfur reduction programs are already in place in the U.S., Europe, and Japan as a way to increase catalyst efficiency for CO, HC, and especially NO$_x$ (U.S. EPA, 1998d; Walsh, 1998b). California and Japan have already adopted a 30 ppm sulfur limit and Europe has adopted a reduction in steps, reaching 150 ppm in 2000 and 50 ppm in 2005 (Walsh, 1998b). Canada recently announced a phased program to reach 30 ppm in 2005 (Environment Canada, 1998). Further reductions are being debated, with a coalition of automobile manufacturers supporting a worldwide target of 30 ppm sulfur and the oil industry resisting such efforts (ES&T, 1998). EPA recently concluded that a program limiting sulfur content of gasoline is necessary for the reduction of the regulated pollutants and has yet to decide on the form and limits of such a program (U.S. EPA, 1998d).

Gasoline sulfur reduction may be an important method way to reduce N$_2$O mobile source emissions. If a low-sulfur gasoline program was implemented nationwide, a reduction of about ½ of the N$_2$O emissions from catalyst-equipped vehicles could be achieved, based the very limited data currently available.[308] This could mean a reduction of the order of 0.5 % of the U.S. greenhouse gas emissions.[309] This is a very sizeable reduction that will significantly help for the implementation of the Kyoto protocol.

The total estimated cost would be about US$5.4 billion,[310] or $868 per ton of carbon equivalent (TCE) if all the cost is attributed to the N$_2$O reduction. This is relatively expensive in comparison with the $100 to $200 per TCE of the most expensive solutions estimated to be needed for compliance with the Kyoto protocol in the U.S. (Ellerman and Decaux, 1998). Consequently, a sulfur reduction program may be too expensive if the only objective was to reduce N$_2$O emissions. N$_2$O reduction, however, is

---

[308] The reduction will come immediately if the sensitivity of N$_2$O to fuel sulfur of "Tier 0" and oxidation catalyst vehicles is the same than for the "Tier 1" and LEVs tested by Michaels (Michaels, 1998). If N2O from "Tier 0" vehicles is in fact insensitive to sulfur reductions the N$_2$O reduction will come as "Tier 0" vehicles are replaced by "Tier 1" and low-emission vehicles by fleet turnover.

[309] In terms of global warming potential (MMTCE).

[310] Assuming a cost of 5 cents per gallon of gasoline for sulfur removal (Cackette, 1998; U.S. EPA, 1998d) and a gasoline consumption by light-duty vehicles and light-duty trucks of 308.7·10^6 kg (Davis, 1997).

an additional benefit that should be considered when analyzing gasoline sulfur reduction programs for CO, HC, and NO$_x$ reduction purposes. Currently EPA is considering whether to implement national, year-round sulfur limits, or local, seasonal limits (U.S. EPA, 1998d). A permanent, national program will provide the most N$_2$O benefit.

Chapter 9. Directions for Future Research

The findings reported in this thesis suggested many new interesting research questions about vehicle emissions. This chapter summarizes some of the key future research directions and some possible approaches for addressing them based on what was learnt during this project.

9.1. Further Analysis of the Possibilities of Vehicle Specific Power

The analyses presented in Chapter 3 demonstrate the usefulness of the new definition of vehicle specific power for remote sensing and emission studies. Having a single, readily measurable parameter that captures most of the dependence of vehicle emissions on driving conditions opens up several important applications.

A New Structure for Emissions Models

Current inventory emission models such as MOBILE and EMFAC are based on emission factors expressed in grams of pollutant per mile (gpm) traveled and estimates of the vehicle-miles traveled. Speed correction factors are used to account for the effect of driving conditions on emissions.

In this thesis it has been shown that the dependence of fuel consumption and emissions in driving conditions is better captured by specific power (SP), and that second-by-second emissions of light-duty vehicles are one to two orders of magnitude more constant when expressed in grams of pollutant per gallon of fuel (gpg). These are compelling reasons to base emissions models on SP and gpg.

Evaluation of Inspection and Maintenance Programs

A possible application of remote sensing is the evaluation of I/M programs (Zhang *et al.*, 1996b; Sjödin *et al.*, 1997a; Stedman *et al.*, 1998; U.S. EPA, 1998e). EPA recently stated that it would approve this use "if RSD-measured fleet average emissions can be correlated back to the IM240" (U.S. EPA, 1998e). Establishing the dependence of

emissions on SP and weighing them by the SP distribution in the IM240 test could be used for this purpose (see section 3.3.6 for a detailed description of this approach).

Reevaluation of High Emitter Detection in Remote Sensing

This study showed that SP can be used to screen out most of the occurrence of commanded enrichment and enleanment operation, eliminating those sources of false high emitter detection. This reopens the possibility of using remote sensing for this important application, which should be evaluated taking into account economic considerations.

Acquisition and Analysis of Second-by-Second Data from High Emitters

This thesis has shown that powerful insights can be gained from the analysis of second-by-second operational and emissions data of vehicles operated in chassis dynamometers. A data set of this kind with as many types of high emitters as possible would allow the study of numerous questions, including the dependence of their emissions on SP for these vehicles and the evaluation of the probability of detection with remote sensing.

9.2. Improved Quantification of Emissions from Mobile Sources

Large uncertainties remain in the estimates of the mobile source emissions inventory. A number of research programs that could reduce these uncertainties are:

Detailed Study of the Emissions of Heavy-Duty Diesel Trucks

The successful remote sensing of heavy-duty diesel truck (HDDT) NO_x opens the possibility of exploring many interesting questions of the kind posed for automobile emissions in Chapter 6 and Chapter 8. In particular, the variation of HDDTs emissions vs. power can be studied. The concept of specific power, defined in Chapter 3, is also applicable to HDDTs. However, due to the very large variations in vehicle weight for these vehicles, HDDT remote sensing studies should also obtain this information.[311]

Long-Term Monitoring of Heavy-Duty Truck Emissions by Remote Sensing

By remotely sensing the emissions of heavy-duty trucks for a period of several years, the rates of deterioration as well as the effects of emission reduction programs such as diesel fuel reformulation, low-NO_x diesel engines, or inspection and maintenance programs can be determined. This information could then be used for the design of more effective emission control strategies.

Measurement of heavy-duty truck emissions by low-pressure sampling

Low-pressure sampling could be an alternative to remote sensing for the measurement of emissions from heavy-duty diesel trucks. A probe could be located at the bottom of a highway bridge and a sample continuously drawn into a low pressure multipass cell of a TILDAS instrument. This approach would yield sensitivities about 1,000 times larger than the remote sensing approach (Nelson *et al.*, 1996) and would permit the quantification of many more species besides NO and NO_2.

Measurement of Emissions from Off-Road Mobile Sources

"Off-road mobile sources" refers to ships, trains, airplanes, and farm and construction equipment. As on-road mobile source emissions have become increasingly controlled, the estimates of the share of the less controlled off-road mobile sources in

---

[311] From weight stations or weight-in-motion systems.

total emissions has been increasing. These sources are not as well quantified as those of on-road mobile sources.

An NDIR-UV remote sensor has been recently applied to the measurement of aircraft emissions (Popp *et al.*, 1998b), but the measurement was constrained by the pathlength limitations of the technique. This same remote sensor will be used to measure train locomotive emissions in the near future (Popp, 1998).

The TILDAS technology is ideally suited for remote sensing measurements of off-road mobile sources such as airplanes and ships due to its larger range and excellent sensitivity. Some potential applications would be the measurement of the emissions from airplanes across airport runways and of ships in large harbors.

9.3. N$_2$O Emissions from Mobile Sources

Better Quantification of N$_2$O Emissions from Mobile Sources

N$_2$O emissions from catalyst-equipped vehicles were estimated to account for 0.5% to 0.9% of U.S. greenhouse emissions based on the results of this study. However, very large uncertainties remain, and additional research its needed in this topic. A number of approaches could provide better information about the magnitude of N$_2$O emissions:

- Cold start emissions could be quantified with remote sensing by measuring the emissions from cars which have been parked for significant time at several distances from the parking lot. Two possibilities would be an airport and a stadium. This experiment would provide a profile of average N$_2$O vs. distance (or time) in cold start that may allow a more precise estimation of cold start emission factors.

- Remote sensing and/or IM240 can provide good estimates of real world emission factors. Both systems would provide large, unbiased samples. They would also allow the study of which vehicle/catalyst characteristics are correlated with high N$_2$O emission.

- Repeating the same test (e.g. remote sensing or IM240 tests) under the same conditions each year or few years would provide a robust estimate of the evolution of these emissions. A program like this one for CO, HC, and NO is now in its second year with remote sensing.

- Ambient N$_2$O/CO$_2$ in a urban area where other N$_2$O and CO$_2$ sources are well-characterized can be used to obtain a driving-mode integrated N$_2$O/CO$_2$ emission factor. Such an approach has been used for estimating CH$_4$ emissions (Shorter *et al.*, 1996).

- N$_2$O emissions are highest during starts. Some emissions models such as EMFAC account for cold and hot start excess emissions separately. Integrating that approach with cold start emission estimates for the U.S. would probably improve the inventory estimate.

- ▪ The current N_2O estimates are based on grams-per-mile and vehicles-mile traveled. Estimates based on grams-per-gallon and fuel should be used as an alternative check on the inventory.

Reduction of N_2O Emissions Through the Reduction of Gasoline Sulfur

The above estimate indicates that N_2O emissions from catalyst-equipped vehicles are not negligible with regard to the limitations that may be needed to comply with the 1997 Kyoto protocol, and that the possibilities for its reduction should be investigated.

It was recently observed that lower gasoline sulfur content results in reduced N_2O emissions (Michaels, 1998). Sulfur levels are being reduced worldwide (Walsh, 1998b). EPA has yet not decided whether to implement sulfur limits in some areas and seasonally, or nationally and permanently (U.S. EPA, 1998d). This issue is highly controversial, with the oil companies advocating the less stringent programs and the automobile manufacturers the most stringent (ES&T, 1998).

This effect needs to be better quantified better in order to evaluate the potential reductions that could be achieved by lower gasoline sulfur. Current data are limited to two Tier 1 vehicles and three low emission vehicles (Michaels, 1998). No data on Tier 0 vehicles, which comprise most of the fleet, exist. Dynamometer cycle testing of a larger sample (including Tier 0 vehicles) with both high and low sulfur gasoline could provide the data needed. Alternatively carrying out remote sensing measurements (or measurements during IM240 testing) before and after the gasoline sulfur level is changed on a given area would provide robust real-world estimates of the effect of sulfur on N_2O. Studies of this kind have provided insights on the effect of reformulated gasoline on CO, HC, and NO_x emissions (Bishop and Stedman, 1990).

Investigation of the Causes of High N_2O Emissions

This study has shown that the N_2O emissions distribution is highly skewed, and that the concept of "super-emitter" is applicable to N_2O. For example the ratio of the maximum N_2O emission from a car to the average level of all cars was 47, compared to only 12 for NO.

A N_2O remote sensing campaign with a large number of vehicles or the integration of N_2O emission measurements in IM240 programs would allow the study of whether specific manufacturers or vehicle models tend to have much higher N_2O

emissions than the rest. A similar analysis for regulated pollutants using remote sensing and IM240 data has been able to pinpoint specific models with emission control system problems (Wenzel *et al.*, 1996; Wenzel *et al.*, 1997).

It would also be of great interest to identify and borrow the few highest emitters and study what vehicle characteristics may be causing such high N_2O emission. This information may then be used for achieving lower N_2O emissions from new vehicles, and also for repairing high N_2O emitters, if repairs were determined to be a cost-effective alternative or if they could be done simultaneously with repairs for other pollutants.

9.4. Quantification of Ammonia Emissions from Three-Way Catalyst Equipped Vehicles

Ammonia (NH_3) is very important for fine particulate matter and acid deposition. While NH_3 is present in the exhaust of internal combustion engines, both gasoline and diesel, three-way catalysts increase NH_3 emissions from gasoline vehicles. Conflicting emission factors are reported in the literature for three-way catalyst equipped vehicles. Emission rates up to 268 mg/mi have been reported when cars were forced to run with rich air-fuel mixtures (Cadle and Mulawa, 1980). Moeckli *et al.* (Moeckli *et al.*, 1996) report a range from 5 to 24 mg/mi based on a tunnel study in Switzerland. Two recent studies have reported significant amounts of NH_3 in the vehicle exhaust. Baum (Baum, 1997) measured concentrations of up to 628 ppm in the exhaust of TWC-equipped cars, and reported that NH_3 was larger when the engine was running under lean conditions, in contradiction to Cadle and Mulawa's findings. Fraser and Cass (Fraser and Cass, 1998) reported an average emission rate of 116 mg/mi for three-way catalyst cars, based on a tunnel study in the Los Angeles area.

Some catalyst studies suggest that the chemistries of N_2O and NH_3 in the catalyst are tightly linked (Cant *et al.*, 1998; Odaka *et al.*, 1998), and that NH_3 is formed in the catalyst from NO at relatively low temperatures (Cant *et al.*, 1998), lower than those of maximum N_2O production. If this is indeed the main process producing NH_3 from TWC-equipped cars, NH_3 emissions from light-duty vehicles will be largest for vehicles under cold-start conditions.

<u>Quantification and Understanding of NH_3 Emissions from Motor Vehicles</u>

Many questions remain about the magnitude and the mechanism of formation of NH_3 emissions from TWC-equipped vehicles: What is the NH_3 emission factor for each type of vehicles? What is the nature of the NH_3 emissions distributions? Are there NH_3 high emitters? What are the NH_3 emissions in cold start vs. hot stabilized conditions? What is the correlation of NH_3 emissions with vehicle characteristics (passenger cars vs. light-duty trucks, emission control technology, model year, manufacturer, etc.)? With vehicle operating conditions (speed, acceleration, specific power)? With other emissions (CO, HC, NO, N_2O)? This information would help understand the importance of the problem, the processes by which NH_3 is emitted from vehicles, and give clues as to ways or reducing NH_3 emissions from current and future vehicles.

The same approaches outlined in the previous section for N_2O can also be used for NH_3. Dynamometer testing, especially with collection of second-by-second data, and/or TILDAS remote sensing[312] could provide answers to some of these questions by quantifying and characterizing NH_3 emissions in the same way described in Chapters 6 and 8 of this thesis for NO and N_2O, respectively.

Synergy with Research of N_2O Emissions from TWC vehicles

Both NH_3 and N_2O are mostly incomplete byproducts of NO reduction in three-way-catalysts. Both species should be measured simultaneously (by remote sensing or during dynamometer testing) in order to shed light on the catalyst processes which may result in elevated emissions.

---

[312] We estimate that the TILDAS technique can perform NH_3 remote sensing with good sensitivity. Ammonia has many individual strong infrared absorption features in the 875-1125 cm^{-1} region, with little interference from background air species or other species in car exhaust. A preliminary test performed at Aerodyne Research in May 1998 indicated that the measurement is possible with the existing instrument and that the sensitivity could be of the same order of that achieved for NO, depending on the laser diode used.

9.5. Further Development of the TILDAS Remote Sensor

<u>Design of an Commercial TILDAS-only Remote Sensor</u>

The TILDAS instrument used in this thesis is a one-of-a-kind laboratory type instrument. It has shown impressive remote sensing capabilities and has produced results suggesting that such measuring capability has great value. Simplifying the operation and reducing the cost of the instrument are necessary tasks. Such a system would need to be equipped with at least four diode lasers, to be able to measure CO, an HC surrogate, NO, and CO_2 simultaneously.

<u>Comparison of TILDAS to other remote sensing technologies</u>

The performance of the TILDAS remote sensor should be compared to that of the other existing remote sensing technologies. Puffs from gas cylinders mounted on moving cars, and remote sensing of emissions from low-emitting and high emitting vehicles should be used for this purpose.

<u>Design of a TILDAS Addendum to NDIR/UV Instruments</u>

Another possibility is to design a TILDAS module that can be incorporated into existing NDIR/UV instruments to provide measurements that those instruments cannot acquire, such as N_2O, NH_3, C_2H_2, C_2H_4, CH_4 or CH_2O. Such a design would reduce the cost and the operational requirements of the TILDAS instrument.

Chapter 10. Conclusions

Air pollutant emissions from motor vehicles are a large contributor to many important environmental problems, including local and regional air quality and the increased greenhouse effect. The first regulations controlling emissions from motor vehicles were established 33 years ago (1965) in California and since then have spread to most countries and become increasingly stringent. The emission reductions achieved through the successive control strategies, however, have been smaller than anticipated. That fact, combined with the continuous increase in the use of motor vehicles, means that on-road motor vehicles are, and will continue to be in the foreseeable future, a major source of air pollutants around the world and that further control is needed.

Despite their importance, real-world motor vehicle emissions are still unsatisfactorily quantified and understood, owing to the many factors that influence the emissions of each individual vehicle, and to the difficulty of characterizing hundreds of millions of them. This thesis presents several significant contributions that address these basic problems in the following ways:

- First, a new, directly measurable parameter (specific power) was defined and shown to capture most of the dependence of light-duty vehicle emissions on driving conditions. The use of this parameter could simplify emission studies and establish a common language between the different emission research and modeling approaches.

- Second, a new, TILDAS-based remote sensor was developed and tested which can provide high quality real-world emission measurements on large vehicle samples, including the emissions of the cleanest vehicles. Very high precision and long pathlenth were demonstrated.

- Third, this new remote sensor was used to answer some of the outstanding questions about mobile source emissions by conducting 2 experimental field campaigns where the emissions of about 1,500 random cars and light-duty trucks, a instrumented heavy-duty diesel truck, and 73 random heavy-duty diesel trucks were measured. These experiments provided the first high precision remote sensing data of NO_x emissions from passenger cars, light-duty trucks, and heavy-duty diesel trucks, plus

the first remote sensing ever of N_2O and NO_2 emissions. An in-depth analysis of these data was carried out.

The detailed conclusions of this work are summarized below:

A new parameter for emission studies

Vehicle specific power (SP) is defined as the mechanical power used for the vehicle's motion. This parameter has a number of important advantages for remote sensing and emission studies for three reasons:

- SP is a better predictor of emissions that any other roadside measurable parameter. In particular SP is a very good predictor of commanded enrichment situations.

- SP can be calculated with good approximation from measurements of vehicle speed and acceleration.

- Dynamometer driving cycles used for emission certification of new vehicles directly specify the value of SP (and not the total power or fraction of available power) at each second in the cycle. Evidence is presented that automobile designers make use of this fact.

These properties make SP an very useful parameter for emission studies. The applications of this parameter include:

- Specific power can be used to make meaningful comparisons between the results of different dynamometer driving cycles, experimental emission studies, remote sensing studies, and emission models. This would be a great improvement over the status quo in which the differences in power demand obscure the comparisons.

- Specific Power is highly valuable for the interpretation of remote sensing measurements. It allows more precise identification of high emitters by screening out remote sensing measurements under conditions that lead to transient high emissions in properly functioning vehicles, since these emissions may not be repairable through an inspection and maintenance program. Low-emitter identification can be improved as well.

- Emissions models can benefit from using Specific Power as the main parameter to represent load since this parameter has a strong relationship with emissions and is directly measurable in the real world. Inventory models such as MOBILE and EMFAC would be improved by using SP correction factors to replace the speed correction factors that they now use to account for differences in driving conditions.

An in-depth analysis of remote sensing measurements

Remote sensing of on-road vehicle emissions was pioneered by Don Stedman and Gary Bishop of the University of Denver in 1987. Together with several other groups and companies, they have made remote sensing measurements on millions of vehicles. However, some basic aspects of the measurements have not been studied or documented until now. Several important topics have been addressed here:

- The signal levels observed in remote sensing measurements ("plume capture") are highly variable due to changes in the amount of exhaust gases emitted with power, and especially due to differences in plume dispersion. Experimentally plume capture decreases with vehicle speed and increases with power demand at a constant speed.

- Plume capture in the heavy-duty diesel truck measurements was about twice as large than on the automobile measurements, which can be explained by 4 times more CO_2 flow and twice as strong dispersion.

- The noise in the remote sensing measurements depends both on plume capture and on the level of the pollutant measured. High plume captures and low pollutant concentrations yield the best precision while low plume captures and high pollutant concentrations result in lower absolute precision. These effects should be taken into account when using remote sensing measurements for the detection of low and/or high emitters.

- The location of interest for the speed and acceleration measurements taken in conjunction with remote sensing measurements is where the exhaust which is leaving the tailpipe was generated in the engine. This distance has been estimated to vary between 0.1 and 25 meters for one vehicle. Smaller distances correspond to low speed and high specific power, and large distances to high speed and low specific power. The consequence is that a

fixed location speed and acceleration measurement may not be sufficient for the determination of the appropriate specific power. It is suggested that an array of low-cost diodes is used to determine the speed and specific power profile of each vehicle as it approaches the remote sensor.

- Second-by-second driving cycle emissions for a modern car are one to two orders of magnitude less variable when expressed in units of grams of pollutant per unit of fuel consumed than in grams per unit distance traveled. It is suggested that gpg emission factors should be used in emission inventories and models for this reason.

The development and demonstration of a laser-based remote sensor

Current remote sensors are limited in sensitivity and range. The use of tunable diode laser spectroscopy (known as TDL spectroscopy, TLDAS or TILDAS) in remote sensing can help overcome those limitations.

In this study a TILDAS instrument has been modified for use as a remote sensor of vehicle emissions. It operates two diode lasers in two different frequency regions. The average sensitivity of the instrument is estimated at 5 ppm fo the exhaust for NO and 4 ppm for N_2O under real-world conditions. This sensitivity has been demonstrated by measuring the emissions of an Ultra Low Emission Vehicle (ULEV). The TILDAS measurements compared very well with the simultaneous measurements of the on-board system of an instrumented heavy duty truck.

The main advantages of the TILDAS technique for its application to remote sensing of vehicle emissions are:

- The high sensitivity of the technique, which allows the measurement of the emissions from even the cleanest vehicles.

- The unique ability of this technique to remotely sense minor species of interest in automotive exhaust such as NO_2, NH_3, N_2O, formaldehyde, and other small hydrocarbons.

- The absence of interferences from other gases or particulates in the vehicle exhaust or in ambient air, or from infrared emission from the vehicle or the exhaust, due to the its very high spectral resolution and fast time response.

- The higher information content of the technique with respect to NDIR or NDUV make it more robust against anoumalous effects such as interferences from the exhaust of previous vehicles, vibrations, etc.

- The absolute nature of this technique, which makes repeated calibrations unnecessary. Other techniques require frequent field calibration to resist inherent drifts.

- The longer path length achievable with this technique with only minor degradation of sensitivity, due to the coherent nature of laser radiation. Measurements of NO/CO_2 ratios over a total pathlength of 88 meters (289 ft) have been demonstrated. This is more than 7 times longer than those reported for NDIR-based instruments.

- This fact eliminates the need for constricting the traffic, alleviates safety concerns, and provides much more freedom in choosing remote sensing sites. The authors of the Texas Remote Sensing Feasibility study (Walsh *et al.*, 1997) conclude that finding adequate sites was very difficult in some urban areas.

- The Texas study also found that for repeated measurements in the same location, the first reading was higher 60% of the time, which they attribute to changes on driving behavior after noticing the presence of the remote sensor. The longer paths achievable with TILDAS would allow the instrument to be hidden from motorists, eliminating this potential source of measurement bias.

Exhaust gases may have elevated temperatures as they leave the tailpipe, and quickly cool down as they mix with ambient air. These elevated temperatures may be detectable by the TILDAS instrument, depending on the absorption lines being used. Little effect was observed in the automobile measurements, while significant effects appeared in the heavy-duty diesel truck NO/CO_2 measurements. A numerical optimization scheme was successfully developed to allow the estimation of the gas temperatures from the remote sensing spectra.

<u>The first high precision remote sensing measurements of NO emissions from a large real-world fleet</u>

Remote sensing of on-road NO emissions has lagged with respect to CO and HC emissions due to instrumentation problems. This study reported the first remote sensing measurements of NO emissions with a high precision instrument from a large fleet of cars and light-duty trucks. This study yielded a number of significant new findings with respect to the NO emissions of on-road vehicles and the utility of remote sensing emissions measurements:

- The TILDAS instrument consistently and accurately measured the NO emissions of on-road vehicles. The NO emissions of low emitters were measured with an average precision of about 5 ppm.

- The measured vehicle fleet NO emissions closely fit a gamma distribution with the 10 percent of the fleet having the highest emissions contributing about 50 percent of the total fleet emissions.

- The NO emission factor in this study is about 80% of those measured in 3 recent tunnel studies in California. The reason for this lower emission is not clear.

- Newer vehicles have lower average NO emissions than older ones but high NO emitters are found in every vehicle age cohort.

- The light-duty trucks in this study are higher NO emitters than passenger cars. About ½ of the difference is due to their lower fuel economy while the other ½ reflects higher NO exhaust concentrations, possibly due to more lenient emission standards.

- The EMFAC emission model accurately predicts the NO emissions of recent model years in our study and overestimates those of older vehicles.

- Analysis of the NO data with respect to the other simultaneously recorded data for the subject vehicles shows that on a vehicle-by-vehicle basis NO emissions correlate only weakly with vehicle specific power, speed, acceleration, CO emissions or HC emissions. High NO emitting vehicles cannot be identified by remote sensing of CO or HC emissions and vice versa. When these same data are aggregated into rank ordered population deciles, positive correlations between decile averaged NO

emissions and the decile averaged values of vehicle specific power, CO, and HC for most of the vehicles appear.

▪ When we compared the remotely sensed NO emissions measurements for 117 vehicles measured more than once, most of them were consistently low emitters. About half of the high NO emitters were found to be consistently high while the other half had significant variability.

▪ The 10% highest emitters for each of CO, HC, and NO in this study constitute a group of 23% of the vehicles responsible for more than of 60% of the emissions of each pollutant.

▪ Vehicles manufactured by Honda showed statistically significant lower NO emissions than the rest of the fleet for model years 93-96. This was mostly due to the lack of high emitters in the Honda fleet. Significant differences in high emitter incidence among makes also appear in a large database of inspection and maintenance data from Arizona. An important implication is that emissions could be significantly reduced by providing the manufacturers with incentives for the design of emission control systems with lower failure rates.

Remote sensing of NO and NO_2 emissions from heavy-duty diesel trucks

Heavy-duty trucks are a large contributor to the on-road NO_x inventory. In this study the TILDAS instrument was used to remotely sense the NO and NO_2 emissions of heavy-duty diesel trucks (HDDTs). These experiments yielded a number of significant new findings with respect to remote sensing of heavy-duty diesel truck (HDDT) emissions and their NO_x emission factors:

▪ The NO_x emissions of HDDTs can be measured by TILDAS remote sensing under real world conditions with very good accuracy and precision. Very good agreement between the measurements of the EPA instrumented truck and the TILDAS instrument was achieved.

▪ Based on the results of this study the magnitude of HDDT NO_x emissions is underestimated by a factor of 2.2 in the U.S. The share of HDDTs on mobile source NO_x is larger than that of automobiles and light-duty trucks, with an estimated share of 58% of the on-road NO_x inventory. These results imply that as much effort needs to be done to reduce HDDT NO_x emissions as has been done for light-duty vehicle

NO_x, if further meaningful improvements in mobile source NO_x-related air quality problems are to be achieved.

- The HDDT NO_x emission factors are remarkably constant across several tunnel and remote sensing studies. Thus the inventory contribution of HDDT NO_x may be reliably estimated from these emission factors.

- The HDDT NO_x emission distribution, unlike the distribution for light-duty vehicles, is not highly skewed. The nature of the distributions of NO_x emissions from light-duty gasoline and heavy-duty diesel vehicles is shown to be directly related to the nature of the engine and emission control system.

- The concept of "super-emitter" is not applicable to HDDTs for NO_x, since the differences between the lowest and the highest emitters are just a factor of 6.5, compared to a factor of 750 for automobiles. A consequence of this fact is that the potential of significant reductions on emissions through targeting an inspection and maintenance program on the high emitters (or savings by clean-screening low emitters) is small for HDDTs. Conversely, approaches that deal with the whole fleet such as emission standards and reformulated diesel fuel have the largest potential.

The first remote sensing measurements of N_2O emissions from passenger cars and light-duty trucks

The catalytic converter used to reduce the emissions of CO, HC, and NO_x in cars and light-duty trucks increases the emissions of nitrous oxide (N_2O), which is an important greenhouse gas and also causes stratospheric ozone depletion. The total amount of N_2O emitted to the atmosphere due to this source is highly uncertain. This study reports the first on-road remote sensing measurements of N_2O and a thorough compilation of the literature studies that measured N_2O emissions from vehicles. A number of significant new findings include:

- The N_2O emissions of different vehicles on several driving cycles are highly correlated, which indicates that the tendency to emit more or less N_2O is a characteristic of each vehicle. Measuring N_2O emissions in inspection and maintenance programs using IM240 could provide very detailed information about N_2O emissions.

- Based on the limited data available, remote sensing is appropriate for measuring N_2O emissions from catalyst-equipped vehicles. The TILDAS technique is able to remotely sense the N_2O emissions of low-emitters with a fleet average sensitivity of about 8 ppm of the exhaust.

- Both the remote sensing and the literature distributions of N_2O emissions from catalyst vehicles are highly skewed, and the concept of "high emitter" is applicable to N_2O emissions. The presence or absence of high emitters in the small vehicle samples tested in most previous studies is the main reason for the conflicting N_2O emission factors for mobile sources.

- High N_2O emitters not the necessarily the same as NO, CO or HC emitters. All model years have a significant high emitter fraction.

- N_2O Emission rates were found to be more constant with vehicle age than those for NO, CO or HC. The contribution of each model year from 1983 to 1996 to total emissions is similar at about 7%.

- Light-duty trucks were found to have higher emissions than passenger cars. About ½ of this difference can be explained by the fuel economy difference and the other ½ is due to increased N_2O generation for light-duty trucks.

- N_2O emissions show some correlation with NO emissions. The results of this study are consistent with N_2O formation being proportional to the amount of NO reduced in the catalyst. The constant of proportionality is larger for higher NO emitters, which can be explained by catalyst aging.

- N_2O emissions increase with vehicle specific power, but not as much as NO emissions.

- N_2O emissions from remote sensing are about a factor of 7 lower than the 1996 IPCC estimates and a factor of 1.6 lower than the average of the literature values and the newest EPA estimates. The former estimate is too high due to a poor use of the literature sources. The difference with the later estimates is tentatively attributed to the lower-sulfur content of California's gasoline, though insufficient data exist to confirm this point.

- When a correction for the sulfur content of gasoline is used, the corrected remote sensing and literature average N_2O emission factors are about a factor of 3-5 lower than the IPCC 96 estimates and slightly higher than the latest EPA estimates.

- The contribution of passenger cars and light-duty trucks to net 1996 U.S. greenhouse gas emissions is estimated at 0.46 %-0.92% based on the literature and on this study. This is a factor of 4 to 7 lower than the 1998 Draft EPA estimate and very similar to the newest EPA estimate.

- Sulfur reduction in gasoline may be an effective way to reduce N_2O emissions from catalyst-equipped vehicles.

Chapter 11. Appendix

Appendix A. Units Used for Emission Factors

Four units which are commonly used to express motor vehicle emission factors are. This section presents their definition and the conversions between them.

1. **the mixing ratio** of a given species on the exhaust gases, expressed as percent or parts-per-million (ppm). This is the same as the molar fraction or volume fraction of that species. Two variations exists, the so called "wet basis" and "dry basis."

    - On the "wet basis," (used in this thesis) the mixing ratio is calculated as the molar fraction of the given species with respect to all the molecules in the exhaust, <u>including</u> water.

    - On the "dry basis," the mixing ratio is calculated as the molar fraction of the species with respect to the exhaust <u>excluding</u> all water. This is done for historical reasons because most sampling gas analyzers (such as NDIR analyzers for CO_2 and CO, or chemiluminescent analyzers for NO_x) need to operate with a dry feed gas, to avoid internal condensation.

    To convert between the two unit systems one only has to know the mixing ratio of water in the exhaust. For stoichiometric combustion of gasoline this mixing ratio is 12.5%, and the conversion between dry and wet basis is:

    $$[\text{Dry Pollutant Concentration}] = \frac{[\text{Wet Pollutant Concentration}]}{1 - [H_2O]} =$$

    $$= 1.143 * [\text{Wet Concentration}]$$

2. The **species/CO$_2$ ratio**. This is advantageous for example when dealing with diesel engines, which have variable amounts of excess air which cannot be determined by remote sensing. It is also the primary variable determined from remote sensors by ratioing the measured column densities of each species. In order to be comparable with other emission indices, the CO_2 used in this ratio should be based on complete combustion of the fuel. The following equation is used to correct for any incomplete combustion products:

$$\frac{[\text{Species}]}{[CO_2 \text{ in Complete Combustion}]} = \frac{[\text{Species}]}{[CO_2] + [CO] + N_{HC} * [HC]}$$

where [x] is either the mixing ratio or the column density of the given species and N_{HC} is the average number of carbons on exhaust hydrocarbons. For FID analyzers $N_{HC} = 1$ since they work as carbon atom counters, for NDIR remote sensors $N_{HC} = 3$ is generally used, since they are calibrated with propane (C_3H_8) (Guenther *et al.*, 1995).

3. The **grams of pollutant per unit of fuel consumed**, e.g. grams per kg of fuel (g/kg) or grams per gallon of fuel (gpg). These can be calculated from the species/CO_2 ratio and the fuel composition and density in the following manner:

$$\frac{\text{Grams of Pollutant}}{\text{Unit Fuel Consumed}} =$$

$$(\text{Molecular Weight Pollutant}) \cdot \frac{\text{Species Mixing Ratio}}{CO_2 \text{ Mixing Ratio (Complete Combustion)}} * \frac{\text{Moles of C}}{\text{Unit Fuel}}$$

The moles of carbon per unit of a particular fuel can be calculated its elemental composition and density. For typical gasoline and diesel fuels (Heywood, 1988):

	Gasoline	Oxygenated Gasoline	Diesel
H/C Molar	1.87	1.87	1.80
O/C Molar	0	0.022	0
Density (kg/l)	0.75	0.75	0.82
Moles of C per kg of fuel	72.1	70.3	72.5
Moles of C per liter of fuel	54.1	52.8	59.4
Moles of C per gallon of fuel	205	200	225

Table A-1: Moles of carbon per unit fuel for the most common transportation fuels

4. The **grams of pollutant per unit distance traveled**. Grams-per-mile (gpm) are customarily used in the U.S. while grams-per-km (g/km) are used in most other countries. Emissions regulations for light-duty vehicles in the U.S., Europe, and Japan are written in these units (Walsh, 1998a).

The conversion between emission per unit distance and emissions per unit fuel can be done if the fuel economy is known:

$$\text{Emission / Distance} = \frac{\text{Emission / Fuel}}{\text{Fuel/Distance}}$$

Or with the usual U.S. units:

$$\text{grams of pollutant / Mile Traveled} = \frac{\text{grams of pollutant / Gallons consumed}}{\text{Miles Traveled/Gallons consumed}}$$

$$\Rightarrow \quad \text{gpm} = \frac{\text{gpg}}{\text{mpg}}$$

Appendix B. Scatter Plots of Second-by-Second Emissions vs. Specific Power for a Vehicle and 4 Driving Cycles

The variation of emissions with specific power has been investigated in Chapter 3. To serve as a reference of the trends and the scatter that can be expected when plotting emissions vs. specific power for the same vehicle, the following set of plots show the second-by-second NO_x, CO and HC emissions (engine-out first, then tailpipe) of a 1994 Jeep Cherokee tested twice on each of 4 driving cycles.

Note that the FTP cycle (used for emissions certification) includes a narrower power band compared to the other cycles. Because of this fact commanded enrichment situations (indicated by high CO emissions at high power) do not appear during the FTP cycle. The same is true for the high engine-out HC emissions associated with strong or prolonged decelerations.

Figure B-1 (below): Second-by-second engine-out NOx, CO, and HC emissions vs. vehicle specific power for a 1994 Jeep Cherokee tested twice in each of 4 driving cycles
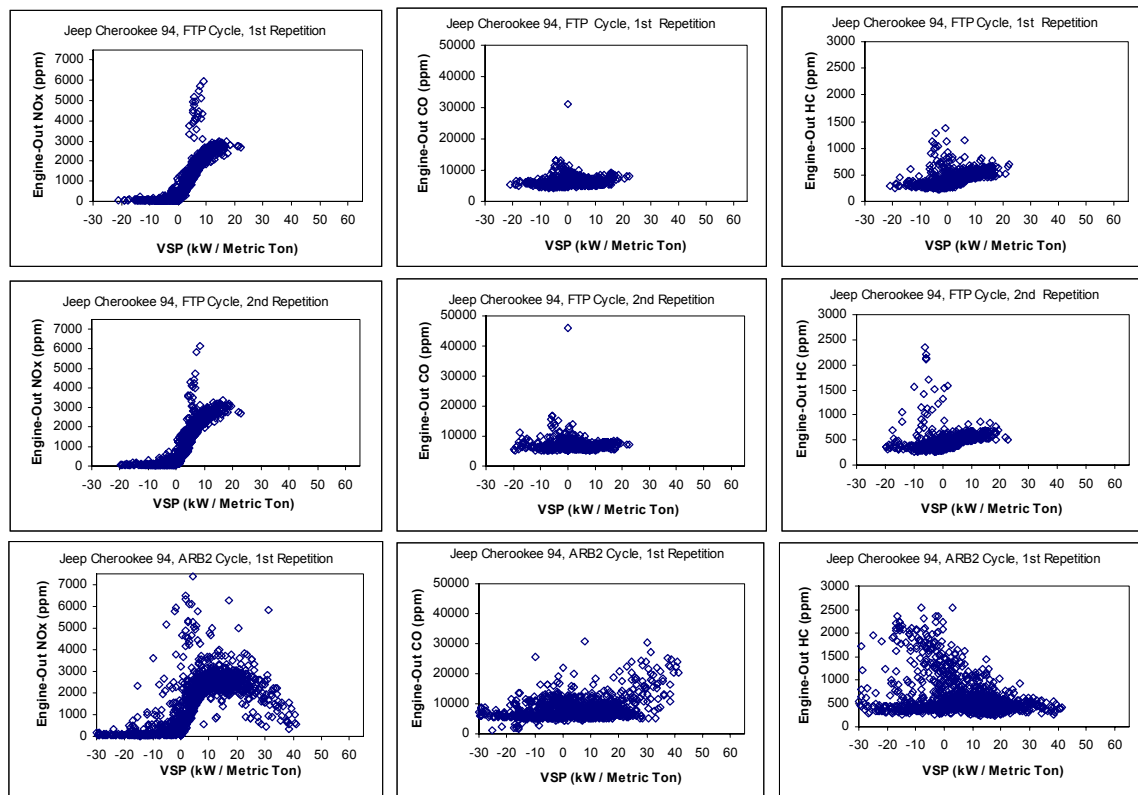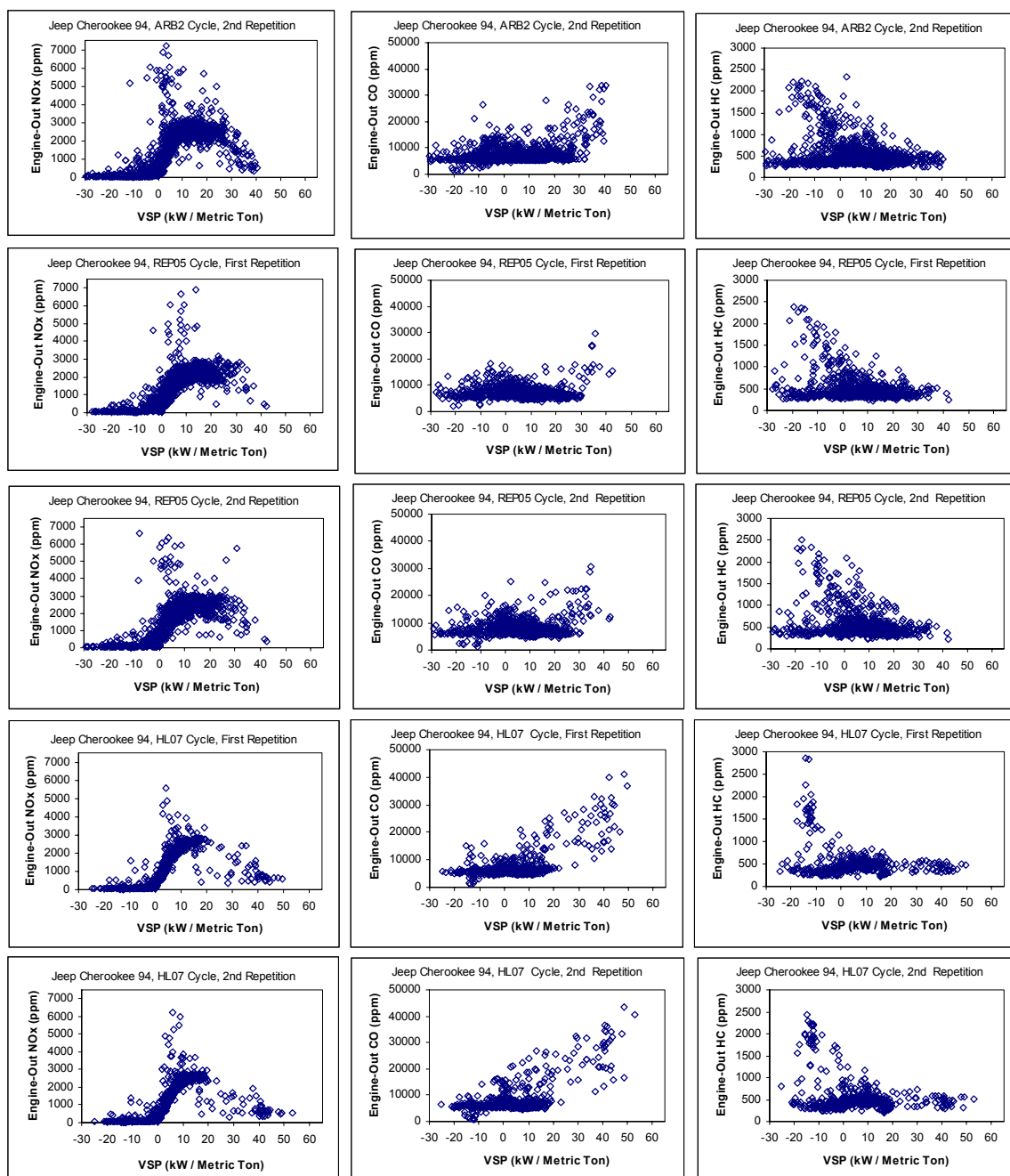
Figure B-2(below): Second-by-second tailpipe NOx, CO, and HC emissions vs. vehicle specific power for a 1994 Jeep Cherokee tested twice in each of 4 driving cycles

Jeep Cherookee 94, HL07 Cycle, First Repetition

Jeep Cherookee 94, HL07 Cycle, First Repetition

Jeep Cherookee 94, HL07 Cycle, First Repetition

Jeep Cherookee 94, HL07 Cycle, 2nd Repetition

Jeep Cherookee 94, HL07 Cycle, 2nd Repetition

Jeep Cherookee 94, HL07 Cycle, 2nd Repetition
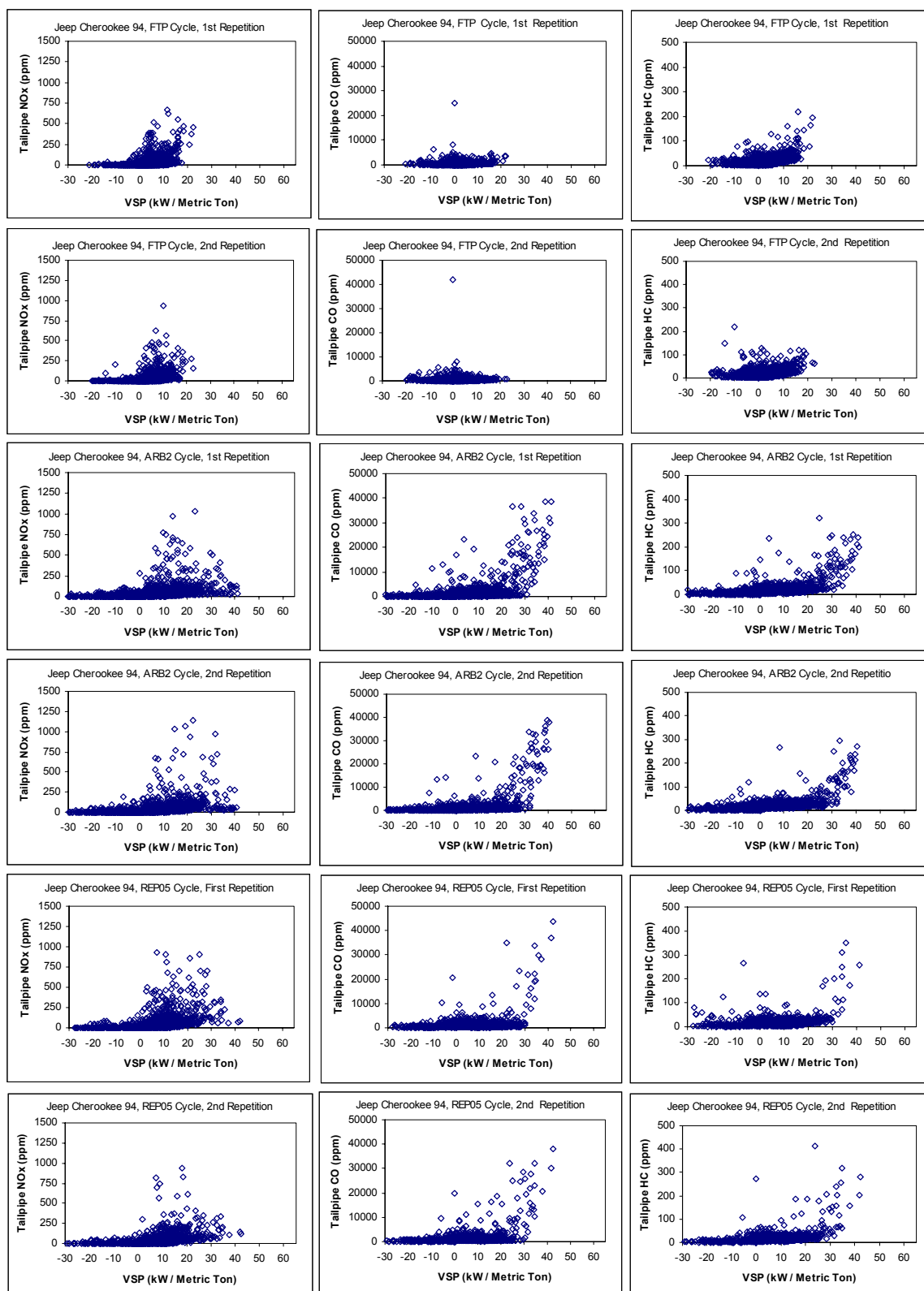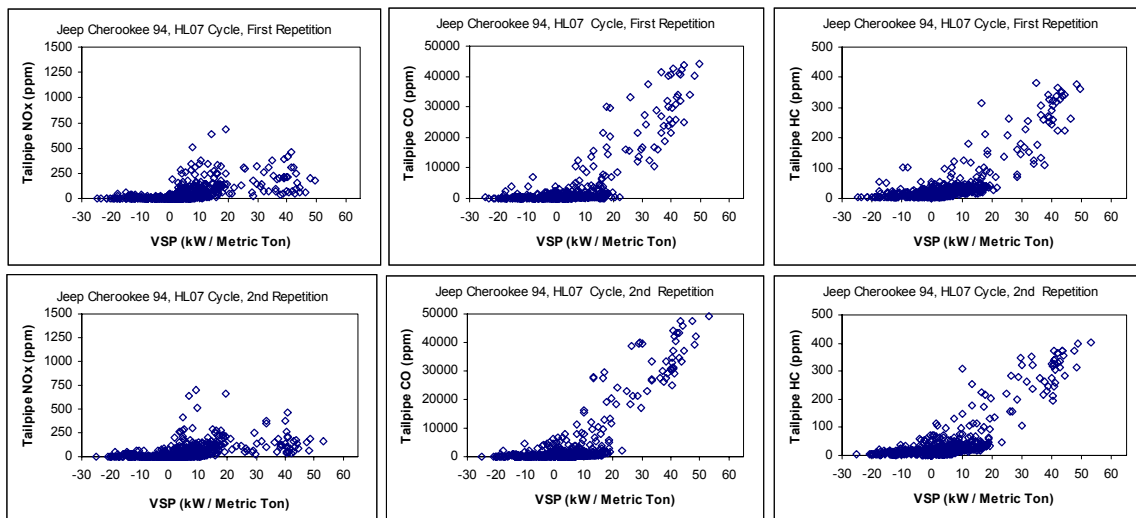
Appendix C. Determination of Improved Air Broadening Coefficients for some NO Absorption Lines

During this study it was observed that the spectral fits to the NO absorption lines had significant errors when the broadening coefficients (BCs) supplied in HITRAN 96 were used. This was due to two factors:

▪ A mistake in the compilation of HITRAN 96, by which the air BCs of the fundamental NO band were set to 0.05 cm^{-1} in this HITRAN version for all transitions.

▪ The BCs in HITRAN 92 and in the references of HITRAN 96 for NO were obtained from measurements of broadening of NO in nitrogen. The oxygen contribution to broadening was not included, even though it had been estimated to be significantly different than for nitrogen by two modeling studies (Tewjani *et al.*, 1976; Houdeau *et al.*, 1983).

Highly accurate values of the BCs were required in this study, especially for temperature estimation (section 5.7). New values were estimated from the BCs for NO in nitrogen determined by Spencer *et al.* (Spencer *et al.*, 1994) and the BCs for NO in oxygen recently measured by Chackerian (Chackerian, 1998) by using the expression (Rothman *et al.*, 1998):

$$b_{air} = 0.79 * b_{N2} + 0.21 * b_{O2}$$

where b_i is the BC of a given NO transition due to gas i. The improved values of b_{air} for the NO lines used in this study are summarized in Table C-1.

Transitions	Frequency (cm^{-1})	Air Broadening Coefficient (cm^{-1})
$^2\Pi_{1/2}$ R(6.5)e	1900.0706	0.0571
$^2\Pi_{1/2}$ R(6.5)f	1900.0816	0.0575
$^2\Pi_{3/2}$ R(6.5)e	1900.5171	0.0593
$^2\Pi_{3/2}$ R(6.5)f	1900.5179	0.0593
$^2\Pi_{1/2}$ R(7.5)e	1903.1228	0.0571
$^2\Pi_{1/2}$ R(7.5)f	1903.1336	0.0574
$^2\Pi_{3/2}$ R(7.5)e	1903.6434	0.0586
$^2\Pi_{3/2}$ R(7.5)f	1900.6444	0.0586

Table C-1: Improved air broadening coefficients for the NO transitions used in this study

Appendix D. Correlation Between Emissions and Vehicle Parameters

The correlation between remote sensing emissions and vehicle parameters are analyzed in Chapter 6 and Chapter 8. The complete matrix of linear correlation coefficients between emission and vehicle variables for the data acquired in California is presented in Table D-1 below for reference.

	NO	N2O	N2O/NO	Dec. NO	Speed	ACC	MY	Disp.	CO	HC	SP	TWC	OXY	EGR	CAR	LDT	GM	FOR	HON	TOY	CHR	MAZ	NISS	USA	JAP	CAN	GER
NO	1.000	0.299	0.007	0.727	-0.072	0.248	-0.340	-0.048	0.032	0.066	0.185	-0.156	0.121	-0.031	-0.012	-0.002	-0.070	0.002	0.009	-0.006	0.007	-0.018	0.015	-0.092	0.071	-0.008	0.038
N2O		1.000	0.021	0.319	-0.133	0.128	-0.052	0.029	-0.052	0.011	0.054	0.033	-0.021	0.009	-0.050	0.037	0.012	0.031	-0.039	-0.032	-0.025	-0.033	0.064	0.009	-0.002	0.015	-0.010
N2O/NO			1.000	0.028	0.072	0.042	-0.056	-0.028	0.009	0.011	0.051	-0.006	0.006	-0.038	0.026	-0.029	-0.082	0.012	0.031	0.014	0.013	0.002	0.029	-0.053	0.033	0.010	0.039
Decile NO				1.000	-0.058	0.255	-0.425	-0.027	0.102	0.134	0.198	-0.184	0.155	0.010	-0.010	-0.004	-0.059	0.000	0.023	0.001	0.020	-0.009	-0.004	-0.117	0.107	0.006	0.015
Speed					1.000	0.114	0.021	-0.016	-0.108	-0.153	0.412	-0.027	0.012	-0.020	0.062	-0.064	-0.057	0.029	0.114	-0.030	0.022	0.002	-0.059	-0.053	0.023	0.032	0.017
ACC						1.000	-0.049	-0.083	0.117	-0.097	0.930	0.000	-0.030	0.034	0.088	-0.090	-0.068	0.006	-0.012	0.066	0.030	0.072	0.046	-0.034	0.103	-0.031	-0.066
MY							1.000	0.137	-0.246	-0.203	-0.038	0.439	-0.345	0.042	-0.162	0.164	0.220	0.073	-0.071	-0.027	-0.025	-0.044	-0.095	0.245	-0.261	0.146	-0.117
Disp.								1.000	-0.064	-0.053	-0.071	-0.041	0.059	0.143	-0.426	0.389	0.512	0.181	-0.318	-0.247	0.028	-0.162	-0.144	0.412	-0.484	0.205	-0.090
CO									1.000	0.490	0.081	-0.009	-0.010	0.085	0.014	-0.009	0.027	-0.052	-0.042	-0.013	-0.033	0.000	0.061	-0.038	0.046	-0.011	-0.055
HC										1.000	-0.120	-0.073	0.065	0.026	-0.017	0.017	0.026	0.007	0.002	-0.036	-0.065	-0.020	0.047	-0.004	0.018	-0.038	-0.038
SP											1.000	-0.012	-0.020	0.039	0.104	-0.106	-0.077	0.015	0.019	0.060	0.031	0.072	0.020	-0.048	0.101	-0.010	-0.059
TWC												1.000	-0.905	-0.058	-0.040	0.044	0.050	0.028	-0.025	0.012	-0.059	0.030	-0.067	0.089	-0.066	-0.036	-0.005
OXY													1.000	0.043	0.013	-0.018	-0.027	-0.014	0.046	0.007	0.075	-0.023	-0.035	-0.057	0.037	0.053	-0.037
EGR														1.000	-0.080	0.072	0.218	-0.076	-0.097	0.168	0.042	-0.127	0.121	0.111	0.117	0.050	-0.445
CAR															1.000	-0.979	-0.238	-0.049	0.238	0.033	-0.123	0.080	0.083	-0.271	0.244	-0.036	0.114
LDT																1.000	0.218	0.057	-0.233	-0.025	0.119	-0.077	-0.078	0.258	-0.233	0.035	-0.110
GM																	1.000							0.506	-0.505	0.155	-0.179
FOR																		1.000						0.250	-0.237	-0.024	-0.055
HON																			1.000					-0.235	0.348	-0.029	-0.089
TOY																				1.000				-0.323	0.473	-0.119	-0.097
CHR																					1.000			0.051	-0.107	0.160	-0.054
MAZ																						1.000		-0.137	0.219	-0.056	-0.045
NISS																							1.000	-0.151	0.254	-0.082	-0.067
USA																								1.000			
JAP																									1.000		
CAN																										1.000	
GER																											1.000

Table D-1: Linear correlation coefficients between emission and vehicle variables. Grayed boxes indicates that the correlation is significant with α=1%.

DEC NO: NO decile; Acc: Acceleration; MY: model year; Disp.: engine displacement; SP: Specific power; TWC: three-way catalyst; OXY: oxidation catalyst; EGR: exhaust gas recycle; CAR: vehicle subject to passenger car standards; LDT: vehicle subject to light-duty truck standards; GM: manufactured by General Motors; FOR: Ford; HON: Honda; Toy: Toyota; CHR: Chrysler; MAZ: Mazda; NISS: Nissan; USA: manufactured in the USA; JAP: Japan; CAN: Canada; GER: Germany.

Appendix E. Correction of the N_2O Automobile Measurement

This section presents a correction of the emissions data acquired at El Segundo in order to compensate for a small negative bias that was detected in the data set. This problem was caused by a beamsplitter fringe and can be eliminated in future studies.

E.1. Effect of Fringes on the N_2O Emission Measurement

Deflections of the laser beam while a measurement was being performed resulted in the appearance of a small fringe in some of the acquired spectra. This problem did not affect the NO or CO_2 measurements, and it is an easily correctable problem for future studies.[313] Nevertheless, the presence of this fringe resulted in small distortions of the polynomial baseline of the CO_2/N_2O channel (Figure 5-4) which affected the returned column density for N_2O, adding a small negative bias. No effect was observed for CO_2 since its absorption was always much larger and the baseline was well-defined above the main CO_2 peak.

An example of this problem is shown in Figure. The fringe manifests itself in the large curvature of the simulated baseline intensity. The modeled small negative absorption for the N_2O peak is shown on the right side.
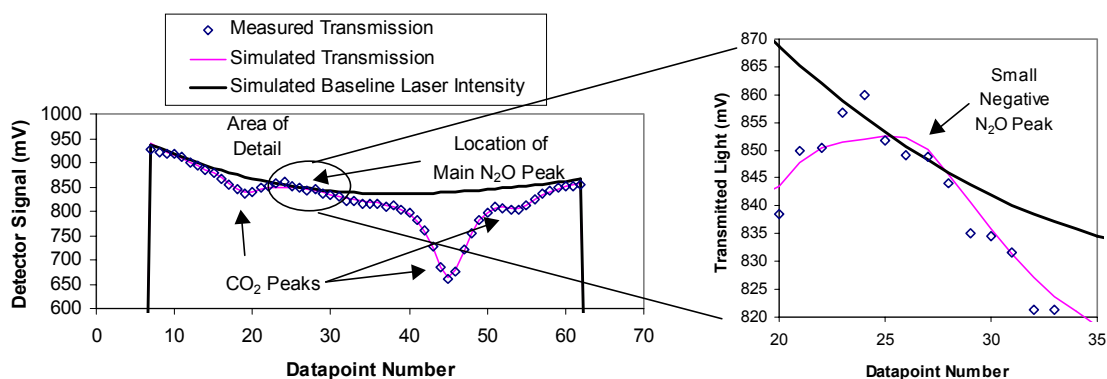
Figure E-1:CO_2-N_2O channel spectra from a car's exhaust plume showing the baseline curvature and the small negative N_2O peak produced by the non-linear least squares fitting

---

[313] This problem can be eliminated by using a different beamsplitter (of the pellicle or wedge types). It can also be suppressed by using a higher order polynomial (3rd or 4th order as opposed to 2nd order which was used here) to represent the laser baseline intensity. Unfortunately only a few spectra were recorded for each vehicle during this study, because saving all of the spectra slowed the measurement considerably due to an unexpected hard disk speed problem. Thus a reanalysis of the whole data set to eliminate this problem is not possible in this case.

The size of the fringe varied widely from measurement to measurement, based on a visual inspection of the recorded spectra. The bias is estimated to have been variable in magnitude, but predominantly negative, based on available spectra. Its effect has been to add a negative shift and increase the noise in the N_2O measurements.

E.2. Estimation of a Lower Bound of the Bias Size

A lower bound for the average magnitude of the bias can be estimated by studying the N_2O vs. NO emissions. The average N_2O for groups of 1% of the total number vehicles rank-ordered by NO emissions is shown in Figure for low NO concentrations. Catalyst studies suggest that vehicles with lower NO emissions would have lower N_2O emissions (Gifhorn, 1997; Rabl *et al.*, 1997), which is indeed the trend in the graph for our experimental results. The negative emissions of the last few bins are not possible physically, however. The maximum negative emission that could be real would be –0.3 ppm, corresponding to the destruction of the N_2O present in ambient air.

Two linear fits to the lower 10 and 30 bins give intercepts of about –4.3 ppm at 0 NO emissions, providing a rough estimate of a lower bound of the negative N_2O bias. The result of the linear fit to the individual measurements (as opposed to the binned measurements) is the same.[314] This intercept is a lower bound of the negative bias because there is no firm evidence that vehicles with zero NO emissions will have zero N_2O emissions.
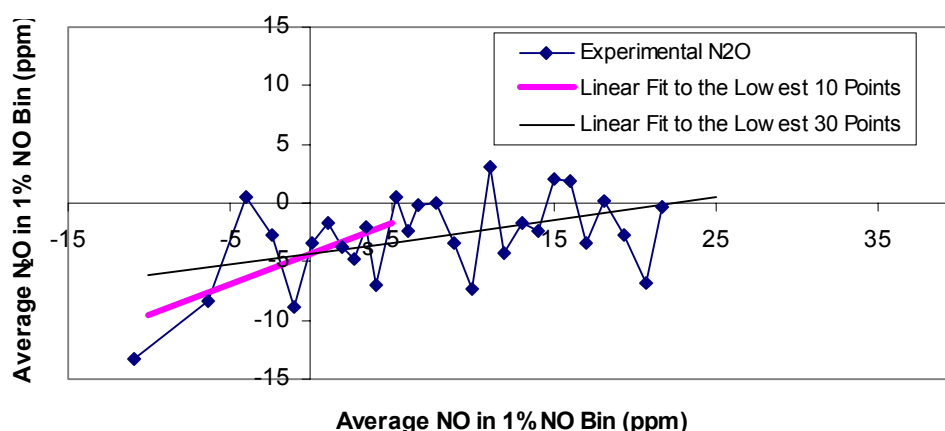
Figure E-2: Average N_2O vs. Average NO for the lowest 28 bins of 1% of the cars ranked by NO

---

[314] That graph is not shown here since the scatter in the data obscures the trend.

E.3. Average Correction of the Bias in the N_2O Data Set

In order to find an average correction for the whole data set, a reference point must be established. The only possibility that was estimated to be feasible was to use the N_2O emissions of vehicles without catalysts, which are generally lower than those of vehicles with catalysts, according to the literature (De Soete, 1989; Warner-Selph and Harvey, 1990; Dasch, 1992; Prigent *et al.*, 1994; IPCC, 1996b; Koike and Odaka, 1996).

The results of all the published studies that could be found are presented in Table 8-2 and in graphical form in Figure. Most of the studies report emissions in the range from 0 to 20 mg/mi except two European studies which measured much higher emission rates. Both authors were contacted and corroborated the correctness of their figures.
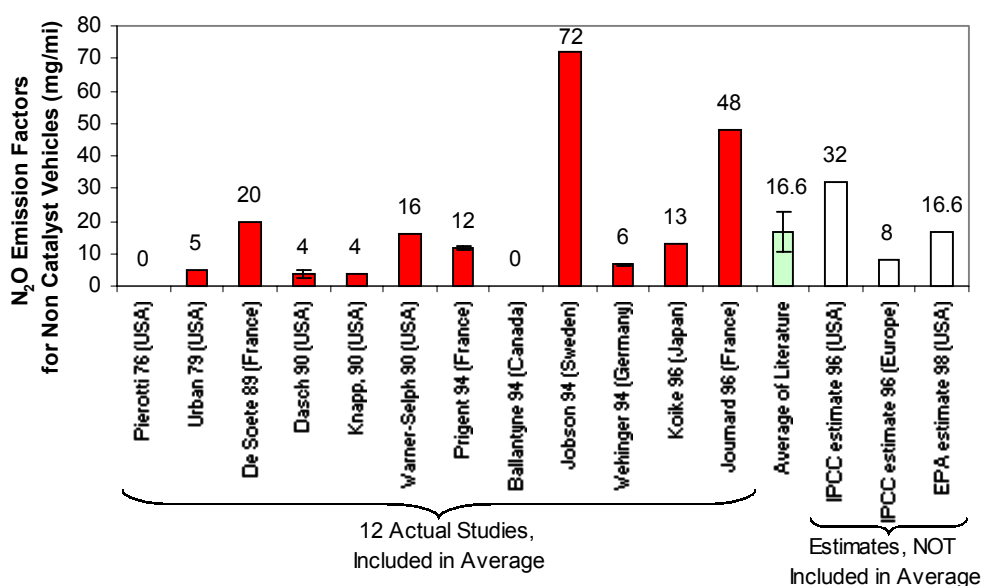
Figure E-3: N_2O emissions reported in the literature for non-catalyst vehicles and IPCC estimates

The average emission factor of all the literature studies is 16.6 ± 6.3 mg/mi.[315] This is about twice the IPCC European estimate of 8 mg/mi. The IPCC estimate for the USA is 32 mg/mi N_2O, but these estimates are believed to be flawed due to a very poor use of the literature values (Michaels, 1998). A recent EPA study also estimated 16.6 mg/mi for non-catalyst cars based on the literature (Michaels, 1998). The exact numerical

---

[315] The uncertainty reported is the standard error of the mean.

coincidence is fortuitous though, as only 3 studies were included in that average while 12 studies were included here.

The average emission rate for the 10 non-catalyst cars in our study, as calculated from the raw N_2O data and the average fuel economies of each model year vehicles[316] is -9.9 ± 14.3 mg/mi.[317] This result in itself does not indicate the presence of a bias, since it the 95% confidence intervals of the remote sensing and the literature result overlap. The additional evidence from the visual inspection of the spectra, and from the N_2O vs. NO trend at low NO concentrations, however, indicate that an average bias is indeed present.

The size of the bias was estimated to be the difference between the literature (16.6 $\pm$ 6.3 mg/mi) and the measured (-9.9 ± 14.3 mg/mi) N_2O emission rates for non catalyst cars, giving a result of -26.6 ± 15.7 mg/mi.[318] This process is illustrated in Figure. Converting this result to parts-per-million of the exhaust (see Appendix A) gives an estimate of the bias of -6.7 ± 3.9 ppm of the wet exhaust. This result is consistent with the estimate of the lower bound of the bias derived above from the N_2O vs. NO changes at low NO concentrations in section E.2 (-4.3 ppm). Consequently, a value of $+6.7$ ppm N_2O was added to all of our measurements presented below.
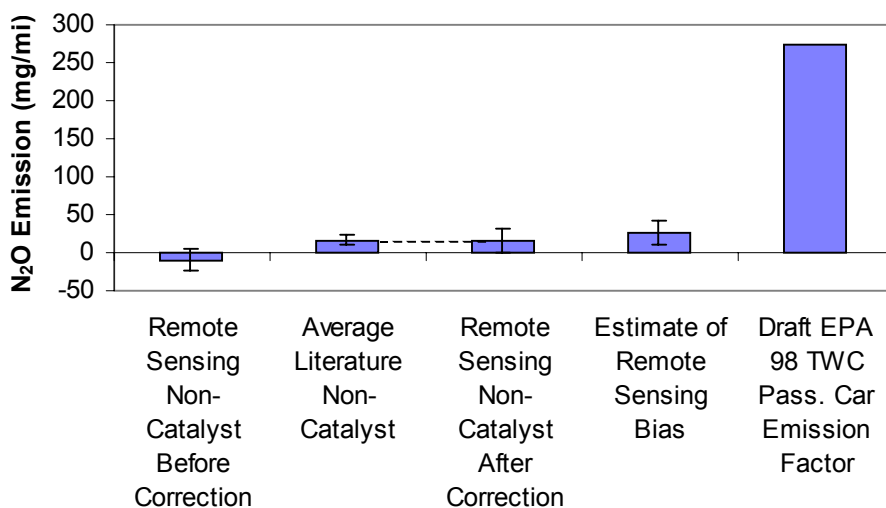
Figure E-4: N_2O Emission for non-catalyst cars and estimate of the average bias on the N_2O measurements

---

[316] See Appendix A for the conversion procedure.

[317] The uncertainty reported is the standard error of the mean.

[318] The uncertainties have been added in quadrature since they are assumed to be independent of each other.

An independent check on the bias correction procedure was provided by the N_2O measurements on the prototype ultra-low emissions vehicle (ULEV) described in section 5.4.2, which are not included in the previous analysis. The average of the 16 N_2O readings corresponding to NO values within ±10 ppm yielded an average of 2.2 ± 1.12 ppm N_2O (after bias correction). This is very similar to the average level of the vehicles in our data set which had similarly low NO emissions (2.4 ppm).

The correction deduced here is significant[319], and some uncertainty remains on the absolute values of our N_2O remote sensing results. It was implemented due the unique nature of this data set, and after realizing that all the trends of N_2O emissions described in the following sections (with emission control technology, vehicle age, type of vehicle, speed, acceleration, and NO emissions) were very similar to those described in the literature. It is impossible that all those trends will be matched by chance, and this indicates that while there was a systematic negative bias in this particular measurement, the measured values do bear a relationship with the N_2O emission level of the vehicle.

---

[319] Even though the correction is significant when compared with the average value of the data set, it is small compared to the range of emission values that were observed and to the some of the emission factors proposed for vehicles with three-way catalysts, as shown in Figure.

Appendix F. Characteristics of the Urban and Highway Test Cycles

The speed vs. time traces of the FTP and HFET test cycles are presented below for comparison.

Time duration (seconds)	1,372
Distance (miles)	7.5
Avg. speed (mph)	19.5
Maxiumum speed (mph)	56.7
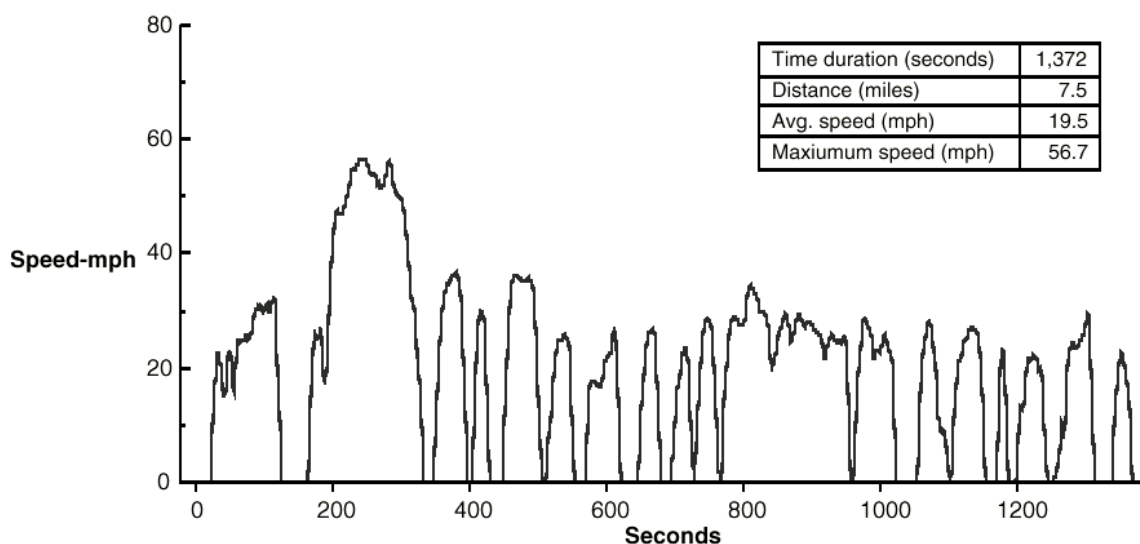
Figure F-1: Speed vs. time profile and main statistics of the FTP (urban) driving cycle[320]

Time duration (seconds)	765
Distance (miles)	10.2
Avg. speed (mph)	48.2
Maxiumum speed (mph)	59.9
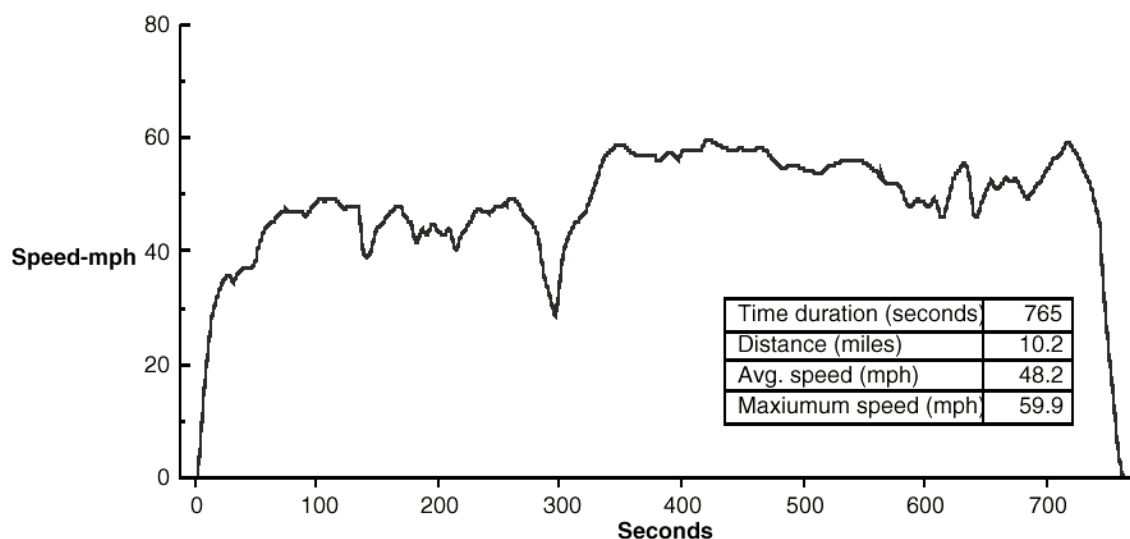
Figure F-2: Speed vs. time profile and main statistics of the HFET (highway)   driving cycle

---

[320] Only bags 1 and 2 of the cycle are shown. The cycle also includes a repetition of the first 505 seconds after a 10 minute break (with the engine off), the so called bag 3.

Ahmed, S. R. and W. Baumert (1979). The Structure of Wake Flow Behind Road Vehicles. Aerodynamics of Transportation. New York, NY, ASME.

Allen, M. G. (1998). "Diode Laser Absorption Sensors for Gas-Dynamic and Combustion Flows." *Measurement Science and Technology* **9**: 545-562.

Allen, M. G. and W. J. Kessler (1996). "Simultaneous Water Vapor Concentration and Temperature Measurements Using 1.31-μm Diode Lasers." *AIAA Journal* **34**(3): 483-488.

An, F., Ross, M. (1996). "A Simple Physical Model for High Power Enrichment Emissions." *Journal of the Air and Waste Management Association* **46**: 216-223.

An, F. and G. Scora (1997). "Characterization and Modeling of Vehicular Unburned Hydrocarbon Emissions." Seventh CRC On-Road Vehicle Emissions Workshop, San Diego, California.

Ando, A. W., W. Harrington and V. McConell (1998). "Estimating Full IM240 Emissions from Partial Tests Results: Evidence from Arizona." Resources for the Future, Discussion Paper 98-24, Washington, DC.

Arroyo, M. P. and R. K. Hanson (1993). "Absorption Measurements of Water-Vapor Concentration, Temperature, and Line-Shape Parameters Using a Tunable InGaAsP Diode Laser." *Applied Optics* **32**(30): 6104-6116.

Arroyo, M. P., S. Langlois and R. K. Hanson (1994). "Diode-Laser Absorption Technique for Simultaneous Measurements of Multiple Gasdynamic Parameters in High-Speed Flows Containing Water Vapor." *Applied Optics* **33**(15): 3296-3307.

Atkinson, C. C.M., N.N., T. W. Long and E. L. Hanzevack (1998). "Neural Network-Based Vehicle Emissions Modeling for Inventory Applications-An Update on Virtual Sensing." Eighth CRC On-Road Vehicle Emissions Workshop, San Diego, California.

Atkinson, C. M., N. N. Clark and D. W. Lyons (1996). "An Estimation of the Comparative Contribution of Heavy-Duty Diesel Buses and Trucks to Mobile Source Emissions." Sixth CRC On-Road Vehicle Emissions Workshop, San Diego, California.

Baer, D. S., R. K. Hanson, M. E. Newfield and N. K. J. M. Gopaul (1994). "Multiplexed Diode-Laser Sensor System for Simultaneous H2O, O2, and Temperature Measurements." *Optical Letters* **19**(22): 1900-1902.

Baer, D. S., V. Nagali, F. E.R. and R. K. Hanson (1996). "Scanned- and Fixed-Wavelength Absorption Diagnostics for Combustion Measurements Using Multiplexed Diode Lasers." *AIAA Journal* **34**(3): 489-493.

Baker, R., J. McFarland, S. Kishan, R. Klausmeier, D. Grubbe and F. Cox (1997). "Use of Remote Sensing Devices to Identify Clean Vehicles for Exemption from I/M Testing." Seventh CRC On-Road Vehicle Emissions Workshop, San Diego, California.

Ballantyne, V. F., P. Howes and L. Stephanson (1994). "Nitrous Oxide Emissions from Light Duty Vehicles." *Society of Automotive Engineers Paper 940304*.

Barnard, R. H. (1996). Road Vehicle Aerodynamic Design: An Introduction. Addison Wesley Longman Ltd., Harlow, England.

Barrett, R. (1998). "Colorado's I/M Program." 1998 Summer Symposium of the EPA Center on Airborne Organics, Dedham, MA.

Barth, M. and J. Norbeck (1997). "NCHRP Project 25-11: The Development of a Comprehensive Modal Emissions Model." Seventh CRC On-Road Vehicle Emissions Workshop, San Diego, California.

Barth, M., J. Norbeck and M. Ross (1998). "Recent Progress on NCHRP Project 25-11: The Development of a Comprehensive Modal Emissions Model." Eighth CRC On-Road Vehicle Emissions Workshop, San Diego, California.

Barton, P. (1998). Environment Canada. Personal Communication.

Barton, P. and J. Simpson (1994). "The Effects of Aged Catalysts and Cold Ambient Temperatures on Nitrous Oxide Emissions. (Unpublished)." Technology Development Directorate, Environment Canada, MSED #94-21, Ottawa, Canada.

Batchelor, G. (1973). Introduction to Fluid Dynamics. Cambridge University Press, .

Bauer, H. (1996). Bosch Automotive Handbook, 4th Ed. Robert Bentley Publishers, Cambridge, Massachusetts.

Baum, M. M. (1997). "Characterizing and Analyzing Components of Vehicle Exhaust Emissions by UV Spectroscopy." World Car Conference, Riverside, CA.

Beardsley, M. (1998). Emission Inventory Group, U.S. EPA. Personal Communication.

Beaton, S. P., G. A. Bishop and D. H. Stedman (1992). "Emission characteristics of Mexico City vehicles." *Journal of the Air & Waste Management Association* **42**: 1424-9.

Beaton, S. P., G. A. Bishop, Y. Zhang, L. L. Ashbaugh, D. R. Lawson and D. H. Stedman (1995). "On-Road Vehicle Emissions: Regulations, Costs, and Benefits." *Science* **268**: 991.

Beer, J. M. and N. A. Chigier (1972). Combustion Aerodynamics. Applied Science Publishers Ltd., London.

Berens, D., H. H. Haskew and R. Orteca (1997). "FTP Emissions from 1991-93 MY in Use Vehicles." Seventh CRC On-Road Vehicle Emissions Workshop, San Diego, California.

Berges, M. G., R. M. Hofmann, D. Scharfe and P. J. Crutzen (1993). "Nitrous Oxide Emissions from Motor Vehicles in Tunnels and Their Global Extrapolation." *Journal of Geophysical Research* **98**(D10): 18527-18531.

Bishop, G. A., B. R. Hutton and D. H. Stedman (1996a). "Design and Operation of a Public Information System for Voluntary Emissions Reduction Using RSD Technology and Its Operational Test." Sixth CRC Workshop on Vehicle Emissions, San Diego, California.

Bishop, G. A., S. E. McLaren and D. H. Stedman, Pierson, W.R.,Zweidinger, R.B., Ray, W.D. (1996b). "Method Comparisons of Vehicle Emissions Measurements in the Fort McHenry and Tuscarora Mountain Tunnels." *Atmospheric Environment* **30 no12**: 2307-16.

Bishop, G. A., J. R. Starkey and A. Ihlenfeldt (1989). "IR long-path photometry: a remote sensing tool for automobile emissions." *Analytical Chemistry* **61**: 671A.

Bishop, G. A. and D. H. Stedman (1990). "On-road carbon monoxide emission measurement comparisons for the 1988-1989 Colorado oxy-fuels program." *Environmental Science & Technology* **24**: 843-7.

Bishop, G. A. and D. H. Stedman (1996c). "Measuring the Emissions of Passing Cars." *Accounts of Chemical Research* **29**(10): 489.

Bishop, G. A., D. H. Stedman and L. Ashbaugh (1996d). "Motor Vehicle Emissions Variability." *J. Air Waste Manage. Assoc.* **46**: 667-675.

Bishop, G. A., D. H. Stedman and J. de la Garza Castro (1997). "On-road remote sensing of vehicle emissions in Mexico." *Environmental Science & Technology* **31**: 3505-.

Bishop, G. A., D. H. Stedman and T. Jessop (1992). "Infrared emission and remote sensing." *Journal of the Air & Waste Management Association* **42**: 695-7.

Bishop, G. A., D. H. Stedman and J. E. Peterson (1993). "A cost-effectiveness study of carbon monoxide emissions reduction utilizing remote sensing." *Air & Waste* **43**: 978-88.

Bishop, G. A., Y. Zhang and S. E. McLaren, Guenther, P.L., Beaton, S.P., Peterson, J.E., Stedman, D.H., Pierson, W.R., Knapp, K.T., Zweidinger, R.B., Duncan, J.W., McArver, A.Q., Groblicki, P.J., Day, J.F. (1994). "Enhancements of Remote Sensing for Vehicle Emissions in Tunnels." *Journal of the Air and Waste Management Association* **44**(2): 169-175.

References

Bouwman, A. F., K. W. Van der Hoek and J. G. J. Olivier (1995). "Uncertainties in the Global Source Distribution of Nitrous Oxide." *Journal of Geophysical Research* **100**(D2): 2785-2800.

Bowman, C. T. (1992). "Control of Combustion-Generated Nitrogen Oxide Emissions: Technology Driven by Regulation." 24th Symposium (International) on Combustion, The Combustion Institute, Pittsburgh.

Braddock, J. N. (1981). "Impact of Low Ambient Temperature on 3-Way Catalyst Car Emissions." *Society of Automotive Engineers Paper 810280*.

Brown, J. E. (1997). Acurex, Inc. Personal Communication.

Cackette, T. (1998). "The Cost of Emission Controls. Motor Vehicles and Fuels: Two Case Studies." 1998 Summer Symposium of the EPA Center on Airborne Organics, Dedham, Massachusetts.

Cadle, S. H., R. A. Gorse and T. C. Belian (1997). "Real-world vehicle emissions: a summary of the Sixth Coordinating Research Council On-Road Vehicle Emissions Workshop. (San Diego, Calif., Mar. 18-20, 1996)." *Journal of the Air & Waste Management Association (1995)* **47**: 426-38.

Cadle, S. H., R. A. Gorse and T. C. Belian (1998). "Real-world vehicle emissions: a summary of the Seventh Coordinating Research Council On-Road Vehicle Emissions Workshop. (San Diego, Calif., Apr. 9-11, 1997)." *Journal of the Air & Waste Management Association (1995)* **48**: 174-85.

Cadle, S. H. and P. A. Mulawa (1980). "Low Molecular Weight Aliphatic Amines in Exhaust from Catalyst-Equipped Cars." *Environmental Science and Technology* **14**(6): 718-723.

Cadle, S. H. and R. D. Stephens (1994). "Remote sensing of vehicle exhaust emissions." *Environmental Science & Technology* **28**: 258A-.

Calvert, J. G., J. B. Heywood, R. F. Sawyer and J. H. Seinfeld (1993). "Achieving Acceptable Air Quality: Some Reflections on Controlling Vehicle Emissions." *Science* **261**: 37-45.

Cant, N. W., D. E. Angove and D. C. Chambers (1998). "Nitrous Oxide Formation During the Reaction of Simulated Exhaust Streams over Rhodium, Platinum, and Palladium Catalysts." *Applied Catalysis B: Environmental* **17**: 63-73.

CARB (1996a). "California exhaust Emission Standards and Test Procedures for 1988 and Subsequent Model Passenger Cars, Light-Duty Trucks, and Medium-Duty Vehicles." Mobile Source Division, California Air Resources Board, Sacramento, California.

CARB (1996b). "Low-Emission Vehicle and Zero-Emission Vehicle Program Review." Mobile Source Division, California Air Resources Board, Sacramento, California.

CARB (1997a). "Draft Preliminary Staff Report: Proposed Amendments to California's Low-Emission Vehicle Regulations "LEV II"." Mobile Source Division, California Air Resources Board, El Monte, California.

CARB (1997b). "Proposed Amendments to Exhaust, Evaporative, and ORVR Emission Standards." LEV II Workshop, El Monte, California, Mobile Source Division, California Air Resources Board.

CARB (1998a). "EMFACX Workshop Reports." Mobile Source Division, California Air Resources Board, Sacramento, California.

CARB (1998b). "News Release: Air Board Continues California's World Leadership in Auto Emission Standards." California Air Resources Board, Sacramento, California.

CARB (1998c). "Proposed California Exhaust Emission Standards and Test Procedures for 2001 and Subsequent Model Passenger Cars, Light-Duty Trucks, and Medium Duty Vehicles." California Air Resources Board, El Monte, California.

Carduner, K. R., A. D. Colvin and R. Y. Leong, Schueltze, D., Mackay, G.I., Karecki, D.R., Schiff, H.I. (1992). "Application of Tunable Diode Laser Spectroscopy to the Real-Time Analysis of Engine Oil Economy." *Environmental Science and Technology* **26**(5): 930-934.

Carlson, T. R. and T. C. Austin (1997). "Development of Speed Correction Cycles." Sierra Research, Inc., SR97-04-01, Sacramento, California.

Cass, G. (1998). California Institute of Technology. Personal Communication.

Chackerian, C. (1998). NASA Ames Research Center. Personal Communication.

Chang, A. Y., M. D. Dirosa, D. F. Davidson and R. K. Hanson (1991). "Rapid Tuning CW Laser Technique for Measurements of Gas Velocity, Temperature, Pressure, Density, and Mass Flux Using NO." *Applied Optics* **30**(21): 3011-3022.

Chen, G., T. J. Prochnau and D. L. Hofeldt (1996). "Feasibility of Remote Sensing of Particulate Emissions from Heady-Duty Vehicles." *Society of Automotive Engineering Paper 960250*.

Cicero-Fernandez, P. and J. R. Long (1995). "Grades and Other Loads Effects on On-Road Emissions: An On-Board Analyzer Study." Fifth CRC On-Road Vehicle Emissions Workshop, San Diego, California.

Cicero-Fernandez, P. and J. R. Long (1996). "Assessment of Commuting Under Grade Loads and Ramp Metering: Preliminary On-Road Emissions Findings." World Car Conference '96, University of California at Riverside.

Clark, N. N. and D. W. Lyons (1996). "Driving Routes (or Icon Tests) for Heavy-Duty Truck Emissions Measurement." Sixth CRC On-Road Vehicle Emissions Workshop, San Diego, California.

Clark, N. N. and D. W. Lyons (1997). "Emissions from CNG and Diesel Refuse Haulers Using Six Engine Types in New York City." Seventh CRC On-Road Vehicle Emissions Workshop, San Diego, California.

Clark, N. N., R. D. Nine and J. J. Daley, Atkinson, C.M., Peerenboom, W.H., Suski, V.A. (1998). "Heavy-Duty Truck Emissions: Vehicle Activity, Driving Routes, and NO_2/NO Ratios." Eighth CRC On-Road Vehicle Emissions Workshop, San Diego, California.

Clifford, M. J., R. Clarke and S. B. Riffat. (1997). "Local Aspects of Vehicular Air Pollution." *Atmospheric Environment* **31**(2): 271-276.

Cohen, J. P. and A. M. Noda (1995). "Auto/Oil Air Quality Improvement Research Program: Description of Phase II Working Data Set." Systems Applications International, SYSAPP-95/048, San Rafael, California.

Countess, R. and L. Cohen (1997). "Evaluation of Utilizing Remote Sensing to Monitor Tailpipe Emissions from Heavy-Duty Vehicles." Seventh CRC On-Road Vehicle Emissions Workshop, San Diego, California.

Countess, R., L. Cohen and S. J. Countess, Bishop, G.A., Stedman, D.H. (1998). "Remote Sensing of Heavy-Duty Diesel Truck Exhaust." Eighth CRC On-Road Vehicle Emissions Workshop, San Diego, California.

Dasch, J. M. (1992). "Nitrous oxide emissions from vehicles." *Journal of the Air & Waste Management Association* **42**(1): 63-67.

Davis, S. C. (1997). "Transportation Energy Data Book: Edition 17." Oak Ridge National Laboratory, ORNL-6919, .

de Nevers, N. (1995). Air Pollution Control Engineering. McGraw-Hill, Inc., New York.

De Soete, G. (1989). "Updated Evaluation of Nitrous Oxide Emissions from Industrial Fossil Fuel Combustion. Draft final report for the European Atomic Energy Community." Institut Francais du Petrole, IFP 37-559, Rueil-Malmaison, France.

DeFries, T. (1997). Radian International LLC. Personal Communication.

DeFries, T. H. and H. J. Williamson (1997). "Methodology for Estimating California Fleet FTP Emissions." Radian International, RCN 800916.01, Austin, Texas.

DiDomenico, J., J. Johnson and J. Webster, Rendahl, C.S. (1997). "Preliminary Results from Cold Start Sensor Testing." Seventh CRC On-Road Vehicle Emissions Workshop, San Diego, California.

Dreher, D. B. and R. A. Harley (1998). "A Fuel-Based Inventory for Heavy-Duty Diesel Truck Emissions." *Journal of the Air and Waste Management Association* **48**: 352-358.

References

Eckbreth, A. C. (1981). "Recent Advances in Laser Diagnostics for Temperature and Species Concentration in Combustion." Eighteenth Symposium (International) on Combustion, The Combustion Institute.

Ellerman, A. D. and A. Decaux (1998). "Analysis of Post-Kyoto CO_2 Emissions Trading Using Marginal Abatement Curves." MIT Joint Program on the Science and Policy of Global Change, 40, .

Emmelman, H. J. and W. H. Hucho (1998). Performance of Cars and Light Trucks. Aerodynamics of Road Vehicles, 4th Ed. W. H. Hucho. Warrendale, Pennsylvania, Society of Automotive Engineers, Inc.

Environment Canada (1998). "News Release: Low Sulfur Gasoline Will Improve Health of Canadians." , Ottawa, Canada.

ES&T (1998). "Automakers Call for Low-Sulfur Fuel Sales." *Environmental Science and Technology* **32**(15): 352A.

Eskridge, R. E., Petersen, W.B., Rao, S.T. (1991). "Turbulent Diffusion Behind Vehicles: Effect of Traffic Speed on Pollutant Concentrations." *Journal of the Air and Waste Management Association* **41**: 312-317.

Flagan, R. C. and J. H. Seinfeld (1988). Fundamentals of Air Pollution Engineering. Prentice-Hall, Englewood Cliffs, N.J.

Fleiss, J. L. (1983). Statistical Methods for Rates and Proportions. John Wiley & Sons, Inc., New York, NY.

Fraser, M. P. and G. R. Cass (1998). "Detection of Excess Ammonia Emissions from In-Use Vehicles and the Implications for Fine Particle Control." *Environmental Science and Technology* **32**: 1053-57.

Fujita, E. M., B. E. Croes and C. L. Bennett (1992). "Comparison of emission inventory and ambient concentration ratios of CO, NMOG, and NOx in California's South Coast Air Basin." *Journal of the Air & Waste Management Association* **42**: 264-76.

Fujita, E. M., Z. Lu and L. H. Sheetz, Sagebiel, J.C., Zielinska, B. (1996). "Determination of Mobile Source Emission Source Fraction using Ambient Field Measurements." Sixth CRC On-Road Vehicle Emissions Workshop, San Diego, CA.

Fujita, E. M., J. G. Watson and J. C. Chow, Lu, Z. (1994). "Validation of the Chemical Mass Balance Receptor Model Applied to Hydrocarbon Source Apportionment in the Southern California Air Quality Study." *Environmental Science and Technology* **28**: 1633-1649.

Gammariello, R. and J. Long (1996). "Development of Unified Correction Cycles." Sixth CRC On-Road Vehicle Emissions Workshop, San Diego, California.

Gautam, M., D. Gupta and S. Popuri, Lyons, D.W. (1997). "Speciation and Reactivities of Diesel Exhaust Emissions." Seventh CRC On-Road Vehicle Emissions Workshop, San Diego, California.

Gertler, A., J. Sagebiel and W. Dippel (1997). "Results of the High Exhaust Emitters Project: Site Characterization, Selection, Feasibility Study." Seventh CRC On-Road Vehicle Emissions Workshop, San Diego, California.

Gertler, A. W., J. C. Sagebiel and W. A. Dippel, Gillies, J.A., Gofa, F., O'Connor, C.M. (1998). "Comparison of the 1995 and 1996 Emissions at the Los Angeles Sepulveda Tunnel Including the Impact of California Phase 2 RFG." Eighth CRC On-Road Vehicle Emissions Workshop, San Diego, CA.

Gifhorn, A. (1997). "Einfluss der Abgas-zusammensetzug auf die N_2O-Konvertierung an einem Dreiwegekatalysator mit Pd/Rh-Beschichtung." *Fortschritt-Berichte VDI* **12**(337).

Gifhorn, A., H.-P. Rabl and R. Meyer-Pitroff (1997). "The Production of N_2O over Three-Way Catalysts." World Car Conference '97, Riverside, California.

Glover, E. L. and W. B. Clemens (1991). "Identifying Excess Emitters with Remote Sensing Devices: A Preliminary Analysis." *Society of Automotive Engineers Paper 911672*.

Good, D. (1998). US EPA Office of Mobile Sources. Personal Communication.

Graboski, M. S., J. Yanowitz and R. L. McCormick (1998). "In-Use Emissions from Heavy-Duty Vehicles Operating in the Colorado Northern Front Range Area." Eighth CRC On-Road Vehicle Emissions Workshop, San Diego, California.

Guensler, R., W. Bachman and S. Washington, Rodgers, M.O., Meyer, M.D. (1997). "Motor Vehicle Activity and Emissions Algorithms in the Georgia Tech GIS-Based Modal Emissions Model." Seventh CRC On-Road Vehicle Emissions Workshop, San Diego, California.

Guenther, P. L., D. H. Stedman and G. A. Bishop, Hannigan, J.W., Bean, J.H., Quine, R.W. (1991). "Remote Sensing of Automobile Exhaust." University of Denver, Department of Chemistry, Denver, Colorado.

Guenther, P. L., D. H. Stedman and G. A. Bishop (1995). "A hydrocarbon detector for the remote sensing of vehicle exhaust emissions." *Review of Scientific Instruments* **66**: 3024-9.

Halberstadt, M. L. (1990). "Mobile Source Emission Factors and Models." *Journal of the Air and Waste Management Association* **40**: 1615.

Hamilton, B. (1998). "FAQ: Automotive Gasoline." *http://www.jmas.co.jp/faqs/autos/gasoline-faq*.

Harnisch, J. (1998). MIT Joint Program on the Science and Policy of Global Change. Personal Communication.

Harrington, W. (1998). "The Economics of the Arizona Enhanced I/M Program." 1998 Summer Symposium of the EPA Center on Airborne Organics, Dedham, MA.

Harris, D. B. (1996). "State of the Art in VOC/NOx Measurements." 1996 Summer Symposium of the EPA Center on Airborne Organics, Boston, MA.

Harris, D. B. and J. E. Brown (1996). "On-Road Emissions Measurements for Emission Factor Development." Sixth CRC On-Road Vehicle Emissions Workshop, San Diego, CA.

Harris, D. B., F. King and J. E. Brown, Nine, R.D., Clark, N.N., Kopasko, J.P. (1997). "Comparison of On-Road and Chassis Dynamometer Emissions Results." Seventh CRC On-Road Vehicle Emissions Workshop, San Diego, California.

Harris, D. B. and F. G. King (1995). "Development of On-Road Emission Factors for Heavy-Duty Diesel Vehicles Using a Continuous Sampling System." AWMA-EPA Conference: The Emission Inventory, Program and Progress, Research Triangle Park, NC.

Harris, D. C. (1987). Quantitative Chemical Analysis. W.H. Freeman and Company, New York, NY.

Harris, G. W., G. I. Mackay and T. Iguchi, Schiff, H.I., Schuetzle, D. (1987). "Measurement of NO_2 and HNO_3 in Diesel Exhaust Gas by Tunable Diode Laser Absorption Spectroscopy." *Environmental Science and Technology* **21**(3): 299-304.

Harris, J. N., A. G. Rusell and J. B. Milford (1988). "Air Quality Implications of Methanol Fuel Utilization." *Society of Automotive Engineers Paper 881198*.

Haskew, H. (1998). General Motors PowerTrain Group. Personal Communication.

Haskew, H., K. Cullen and T. F. Liberty, Langhorst, W.K. (1994). "The Execution of a Cooperative Government-Industry Exhaust Emission Test Program (SAE Paper # 94C016)." 1994 Convergence International Congress on Transportation Electronics, Dearborn, Michigan.

Hayhurst, A. N. and A. D. Lawrence (1992). "Emissions of Nitrous Oxide from Combustion Systems." *Progress in Energy and Combustion Science* **18**: 529-552.

Heavenrich, R. M. and K. H. Hellman (1996). "Light-Duty Automotive Technology and Fuel Economy Trends Through 1996." U.S. Environmental Protection Agency, EPA/AA/TDSG/96-01, Ann Arbor, Michigan.

Heck, R. (1998). Engelhard Corporation. Personal Communication.

References

Heck, R. M. and R. J. Farrauto (1994). Catalytic Air Pollution Control: Commercial Technology. Van Nostrand Reinhold, New York, New York.

Heimrich, M. J. (1996). "Diesel NOx Catalytic Converter Development: A Review." *Journal of Engineering for Gas Turbines and Power* **118**: 668-672.

Herzberg, G. (1945). Infrared and Raman Spectra of Polyatomic Molecules. D. Van Nostrand Company, Inc., New York, NY.

Herzberg, G. (1950). Molecular Spectra and Molecular Structure: I. Spectra of Diatomic Molecules. D. Van Nostrand Company, Inc., New York, NY.

HES (1992). "Feasibility Study for the Use of Remote Sensors to Detect High Emitting Vehicles." Hughes Environmental Systems, Inc.,, Manhattan Beach, California.

Heywood, J. B. (1988). Internal Combustion Engine Fundamentals. McGraw-Hill, New York.

Hilliard, J. C. and R. W. Wheeler (1979). "Nitrogen Dioxide in Engine Exhaust." *Society of Automotive Engineers Paper 790691* **SAE Transactions Vol. 88**.

Hinkley, E. D. and P. L. Kelley (1971). "Detection of Air Pollutants with Tunable Diode Lasers." *Science* **171**: 635-639.

Houdeau, J. P., C. Boulet and J. Bonamy, Khayar, A., Guelachvili (1983). "Air-Broadened NO Linewidths in a Temperature Range of Atmospheric Interest." *Journal of Chemical Physics* **79**: 1634-1640.

Hucho, W.-H. (1987). Wind Tunnels for Automobile Aerodynamics. Aerodynamics of Road Vehicles. W.-H. Hucho. London, England, Butterworth & Co.

Hucho, W. H. (1998). Aerodynamics of Road Vehicles, 4th Ed. Society of Automotive Engineers, Inc, Warrendale, Pennsylvania.

Hucho, W.-H. S., Gino (1993). "Aerodynamics of Road Vehicles." *Annual Review of Fluid Mechanics* **25**: 485-536.

IPCC (1995). Climate Change 1994: Radiative Forcing of Climate Change and an Evaluation of the IPCC IS92 Emission Scenarios. Cambridge University Press, New York, NY.

IPCC (1996a). Climate Change 1995: Impacts, Adaptations, and Mitigation of Climate Change. Cambridge University Press, New York, NY.

IPCC (1996b). Revised 1996 IPCC Guidelines for National Greenhouse Gas Inventories: Reference Manual. International Energy Agency: http://www.iea.org/ipcc.htm, New York, NY.

Ipps, D. T. and D. Popejoy (1998). "An Updated Verification of the On-Road Vehicle Emission Inventory for the Los Angeles Basin Using Ambient Air Quality Data." Eighth CRC On-Road Vehicle Emissions Workshop, San Diego, California.

Jack, M. D., T. P. Bahan and M. N. Gray, Hanson, J.L., Heidt, T.L., Huerta, F.A., Nelson, D.R., Paneral, A.J., Peterson, J., Sullivan, M., Polchin, G.C., Rubin, L.H., Tacelli, C.B., Trautfield, W.C., Wageneck, R.O., Walter, G.A., Wills, J.D., Alves, J.F., Berger, B.A., Brown, J., Shelton, J.A., (1995). "Remote and On-Board Instrumentation for Automotive Emissions Monitoring." *Society of Automotive Engineers Paper 951943*.

Jacquinet-Husson, N. E., J. Arié, A. Ballard and L. R. B. Barbe, B.Bonnet, C.Camy-Peyret, J.P.Champion, A.Chédin, A.Chursin, C.Clerbaux, G.Duxbury, J.M.Flaud, N.Fourrié, A.Fayt, G.Graner, R.Gamache, A.Goldman, Vl.Golovko, G.Guelachvili, M.Hartmann, J.C.Hilico, G.Lefèvre, S.N.Mikhaïlenko, O.V.Naumenko, V.Nemtchinov, D.A (1998). "The 1997 Spectroscopic GEISA Databank." *Journal of Quantitative Spectroscopy and Radiative Transfer*: Accepted for Publication.

Jesion, G., C. A. Gierzack and G. V. Puskorius, Feldkamp, L.A., Butler, J.W. (1998). "Estimation of Modal Feedgas Vehicle Emissions Using Dynamic Neural Networks." Eighth CRC On-Road Vehicle Emissions Workshop, San Diego, California.

Jiménez, J. L., D. D. Nelson and M. S. Zahniser, McManus, J.B., Kolb, C. E., Koplow, M. D., and Schmidt, S.E. (1997). "Remote Sensing Measurements of On-Road Vehicle Nitric Oxide Emissions and of an Important Greenhouse Gas: Nitrous Oxide." Seventh CRC On-Road Vehicle Emissions Workshop, San Diego, CA.

Jiménez, J. L., D. D. Nelson and M. S. Zahniser, Koplow, M.D., Schmidt, S.E (1998). "Characterization of On-Road Vehicle NO Emissions by a TILDAS Remote Sensing Instrument." *Accepted for Publication, Journal of the Air and Waste Management Association*.

Jobson, E., G. Smedler and P. Maimberg, Bernier, H., Hjortsberg, O. (1994). "Nitrous Oxide Formation Over Three-Way Catalyst." *Society of Automotive Engineers Paper 940926*.

Johns, J. W. C. (1987). "Absolute Intensity and Pressure Broadening Measurements of CO_2 in the 4.3 μm-Region." *Journal of Molecular Spectroscopy* **125**: 442-464.

Johns, J. W. C. (1989). "Absolute Intensities in CO_2: The 4.3- and 2.7-μm Regions Revisited." *Journal of Molecular Spectroscopy* **134**: 433-439.

Johnson, A. A. and T. E. Tezduyar (1996). "Parallel Computation of Incompressible Flows with Complex Geometries." Supercomputer Institute, University of Minnesota, UMSI 96/4, Minneapolis, Minnesota.

Joumard, R., R. Vidon and L. Paturel, De Soete, G. (1996). "Changes in Pollutant Emissions from Passenger Cars Under Cold Start Conditions." *Society of Automotive Engineers Paper 961133*.

Kirchstetter, T. W., A. H. Miguel, R. A. Harley and S. V. Hering, Kendall, G.R. (1998). "On--Road Comparison of Exhaust Emissions from Gasoline and Diesel Engines." Eighth CRC On-Road Vehicle Emissions Workshop, San Diego, California.

Kirchstetter, T. W., B. C. Singer and R. A. Harley (1996). "Impact of oxygenated gasoline use on California light-duty vehicle emissions." *Environmental Science & Technology* **30**: 661-70.

Kirschenmann, C. J., D. R. Nelson, J. Peterson and N. Sorbo (1996). "Influence of Real-World Vehicle Operating Modes on Remote Sensing Measurements." Sixth CRC On-Road Vehicle Emissions Workshop, San Diego, California.

Kishan, S., M. Weatherby and C. Palacios (1998). "Clean Screening Methodologies." 14th Annual Mobile Sources/Clean Air Conference 98, Breckenridge, Colorado.

Knapp, K. (1990). "Continuous FTIR Measurements of Mobile Source Emissions." European Workshop on the Emissions of N2O, Lisbon, Portugal.

Knepper, J. C., V. R. Burns and W. R. Leppard, Koehl, W.J., Gorse, R.A., Rapp, L.A., Benson, J.D., Hochhauser, A.M., Reuter, R.M. (1993). "Fuel Effects in Auto/Oil High Emitting Vehicles." *Society of Automotive Engineers Paper 930137*.

Kobayashi, T. and K. Kitoh (1992). "A Review of CFD Methods and Their Application to Automobile Aerodynamics." *Society of Automotive Engineers Paper 920338*.

Koike, N. and M. Odaka (1996). "Methane and Nitrous Oxide (N_2O) Emission Characteristics from Automobiles." *Society of Automotive Engineers Paper 960061*.

Kolb, C. E., J. C. Wormhoudt and M. S. Zahniser (1995). Recent Advances in Spectroscopic Instrumentation for Measuring Stable Gases in the Natural Environment. Biogenic Trace Gases: Measuring Emissions from Soil and Water. H. Matson. P.A., R.C.

Koltsakis, G. C. and A. M. Stamatelos (1997). "Catalytic Automotive Exhaust Aftertreatment." *Progress in Energy and Combustion Science* **23**: 1-39.

Koplow, M. (1998). EMDOT Corporation. Personal Communication.

Koupal, J. (1998). "Air Conditioning Effects in MOBILE6." U.S. EPA, M6.ACE.001, Ann Arbor, Michigan.

References

Koupal, J. and J. German (1995). "Simulation of Vehicle Emissions Using the Modal Emission Model VEMISS." Fifth CRC On-Road Vehicle Emissions Workshop, San Diego, California.

Ku, R. T., E. D. Hinkley and J. O. Sample (1975). "Long-Path Monitoring of Atmospheric Carbon Monoxide with a Tunable Diode Laser System." *Applied Optics* **14**: 854.

Kummer, J. T. (1980). "Catalysts for Automotive Pollution Control." *Progress in Energy and Combustion Science* **6**: 177-199.

Kurima, J., M. Miyamot, N. Kasagi and M. Hirata (1994). "Effect of periodic disturbance on behavior of ring vortices in axisymmetric jet." *Transactions of the JSME* **60**(574): 2007-2013.

Laurikko, J. (1998). "On Exhaust Emissions from Petrol Fueled Passenger Cars at Low Ambient Temperature." VTT, Technical Research Centre of Finland, VTT Publications 348, Espoo, Finland.

Laurikko, J. and P. Aakko (1995). "The Effect of Ambient Temperature on the Emissions of Some Nitrogen Compounds: A Comparative Study on Low-, Medium- and High Mileage Three-Way Catalyst Vehicles." *Society of Automotive Engineers Paper 950933*.

Leppard, W. R., V. R. Burns and L. J. Painter, Reuter, R.M., Koehl, W.J., Hochhauser, A.M., Rapp, L.A., Rutherford, J.A., Benson, J.D., Knepper, J.C., Rippon, B.H. (1995). "Effects of Gasoline Properties (T50, T90, and Sulfur) on Exhaust Hydrocarbon Emissions of Current and Future Vehicles: Speciation Analysis - The Auto/Oil Air Quality Improvement Research Program." *Society of Automotive Engineers Paper 952505*.

Leppard, W. R., R. A. Gorse, L. A. Rapp, J. C. Knepper, V. R. Burns and W. J. Koehl (1992). "Effects of Gasoline Composition on Vehicle Engine-Out and Tailpipe Hydrocarbon Emissions - The Auto/Oil Air Quality Improvement Research Program." *Society of Automotive Engineers Paper 920329*.

Liberty, T. L., A. Constantino and J. German (1997). "Availability of the Supplemental FTP Program CD-ROM." Seventh CRC On-Road Vehicle Emissions Workshop, San Diego, CA.

Long, J. R. (1998). California Air Resources Board. Personal Communication.

Long, T. W., E. L. Hanzevack, C. M. Atkinson and N. N. Clark (1997). "Virtual Sensing: A Neural Network-Based Vehicle Emissions Prediction and Modeling System for Inventory Applications." Seventh CRC On-Road Vehicle Emissions Workshop, San Diego, California.

Lorang, P. (1998). Office of Mobile Sources, U.S. EPA. Personal Communication.

Maldonado, H. (1997). "California Air Resources Board's Heavy-Duty Vehicle Research Projects." Seventh CRC On-Road Vehicle Emissions Workshop, San Diego, California.

Masters, G. M. (1991). Introduction to Environmental Engineering and Science. Prentice-Hall, Inc., Englewood Cliffs, N.J.

MathSoft, I. (1997). S-PLUS 4 Guide to Statistics. MathSoft, Inc., Seattle, Washington.

McClintock, P. M. (1998). "The Colorado Enhanced I/M Program 0.5% Sample Annual Report." Prepared by Applied Analysis for the Colorado Department of Public Health and Environment, .

McLaren, R., A. W. Gertler and D. N. Wittorff, Belzer, W., Dann, T., Singleton, D.L. (1996). "Real-World Measurements of Exhaust and Evaporative Emissions by Chemical Mass Balance Modeling." *Environmental Science and Technology* **30**: 3001-3009.

McManus, J. B. (1996). Aerodyne Research, Inc. Personal Communication.

Mercer, A. and S. McArragher (1997). "Remote Sensing Measurements of On-Road Emissions in Five European Cities." Seventh CRC On-Road Vehicle Emissions Workshop, San Diego, California.

MHD (1997). Massachusetts Highway Dept. Personal Communication.

Michaels, H. (1998). "Emissions of Nitrous Oxide from Highway Mobile Sources: Comments on the Draft Inventory of U.S. Greenhouse Emissions and Sinks 1990-96 (March 1996)." U.S. Environmental Protection Agency, EPA420-R-98-009, Ann Arbor, Michigan.

Michaels, H., C. Fulper and B. Kolowich (1998). "Nitrous Oxide Emission Factors for Mobile Sources." AWMA Emission Inventory Conference, New Orleans, LA.

Mihalcea, R. M., D. S. Baer and R. K. Hanson (1998). "Advanced Diode Laser Absorption Sensor for In-Situ Combustion Measurements of CO_2, H_2O, and Gas Temperature." 27th Symposium (International) on Combustion, Boulder, Colorado.

Miller, J. A. and C. T. Bowman (1989). "Mechanism and Modeling of Nitrogen Chemistry in Combustion." *Progress in Energy and Combustion Science* **15**: 287-338.

Moeckli, M. A., M. Fierz and M. W. Sigrist (1996). "Emission Factors for Ethene and Ammonia from a Tunnel Study with a Photoacustic Trace Gas Detection System." *Environmental Science and Technology* **30**: 2864-2867.

Mohamed, A., B. Rosier, D. Henry and Y. Louvet (1996). "Tunable Diode Laser Measurements on Nitric Oxide in a Hypersonic Wind Tunnel." *AIAA Journal* **34**(3): 494-499.

Muzio, L. J., M. E. Teague, J. C. Kramlich and J. A. Cole, McCarthy, J.M., Lyon, R.K. (1989). "Errors in Grab Sample Measurements of N_2O from Combustion Sources." *Journal of the Air Pollution Control Association* **39**: 287.

Nagali, V. and R. K. Hanson (1997). "Design of a Diode-Laser Sensor to Monitor Water Vapor in High-Pressure Combustion Gases." *Applied Optics* **36**(36): 9519-9527.

Nam, E. K. and M. Ross (1998). "A Fuel Rate Based Catalyst Pass Fraction Model for Predicting Tailpipe NOx Emissions from a Composite Car." Eighth CRC On-Road Vehicle Emissions Workshop, San Diego, California.

Nelson, D. D. and M. S. Zahniser (1994). "Air-Broadened Linewidth Measurements in the v2 Vibrational Band of the Hydroperoxyl Radical." *Journal of molecular spectroscopy* **166**(2): 273.

Nelson, D. D., M. S. Zahniser and J. B. McManus, Shorter, J., Kolb, C.E., Jiménez, J.L., McRae, G.J., and Koplow, M.D. (1996). "Infrared Laser Remote Sensing to Monitor On-Road Emissions from Motor Vehicles." *AWMA Optical Sensing for Environmental and Process Monitoring Symposium*.

Nelson, D. D., M. S. Zahniser and J. B. McManus, Kolb, C.E. and Jiménez, J.L. (1998). "A Tunable Diode Laser System For The Remote Sensing Of On-Road Vehicle Emissions." *Accepted for publication, Applied Physics B*.

NESCAUM (1997). "Heavy-Duty Engine Emissions in the Northeast." , Boston, Massachusetts.

NRC (1991). Rethinking the Ozone Problem in Urban and Regional Air Pollution. National Academy Press, Washington, DC.

Odaka, M., N. Koike and H. Suzuki (1998). "Deterioration Effect of Three-Way Catalyst on Nitrous Oxide Emission." *Society of Automotive Engineers Paper 980676*.

Petherick, D. (1996). "Ontario's Indoor, Controlled-Mode Remote Sensing Concept - An Effective I/M Prescreening Method." Sixth CRC On-Road Vehicle Emissions Workshop, San Diego, California.

Petherick, D. (1997). "Ontario's Vehicle Emissions Pilot Project - A Detailed Look at the Final Results for Cleanscreen and IM240." Seventh CRC On-Road Vehicle Emissions Workshop, San Diego, California.

Philippe, L. C. and R. K. Hanson (1993). "Laser-Diode Wavelegth-Modulation Spectroscopy for Simultaneous Measurement of Temperature, Pressure, and Velocity in Shock Heated Oxygen Flows." *Applied Optics* **32**(30): 6090-6103.

Pierotti, D. and R. A. Rasmussen (1976). "Combustion as a Source of Nitrous Oxide in the Atmosphere." *Geophysical Research Letters* **3**: 265.

Pierson, W. R., A. W. Gertler and R. L. Bradow (1990). "Comparison of the SCAQS tunnel study with other on-road vehicle emission data." *Journal of the Air & Waste Management Association* **40**: 1495-504.

References

Pierson, W. R., A. W. Gertler and N. F. Robinson, Sagebiel, J.C., Zielinska, B., Bishop, G.A., Stedman, D.H., Zweidinger, R.B., Ray, W.D. (1996). "Real-world automotive emissions--summary of studies in the Fort McHenry and Tuscarora Mountain tunnels." *Atmospheric Environment* **30 no12**: 2233-56.

Pollack, A. K., J. P. Cohen and A. M. Noda (1991). "Auto/Oil Air Quality Improvement Research Program: Description of Phase I Working Data Set." Systems Applications International, SYSAPP-91/100, San Rafael, California.

Pollack, A. K., A. M. Dunker and J. K. Fleber, Heiken, J.G., Cohen, J.P., Shepard, S.B., Schleyer, C.H., Yarwood, G. (1998). "Revision of Light-Duty Vehicle Emission Inventories Using Real World Measurements-Auto Oil Program, Phase II." *Journal of the Air and Waste Management Association* **48**(4): 291-305.

Popp, P. J. (1998). University of Denver. Personal Communication.

Popp, P. J., G. A. Bishop and D. H. Stedman (1997). "Development of a High-Speed Ultraviolet Spectrophotometer Capable of Real-Time NO and Aromatic Hydrocarbon Detection in Vehicle Exhaust." *7th CRC On-Road Vehicle Emissions Workshop*, San Diego, CA.

Popp, P. J., G. A. Bishop and D. H. Stedman (1998a). "On-Road Remote Sensing of Automobile Emissions in the Chicago Area: Year 1." Department of Chemistry and Biochemistry, University of Denver, Report to the Coordinating Research Council CRC E-23-4, Denver, Colorado.

Popp, P. J., G. A. Bishop and D. H. Stedman (1998b). "Remote Sensing of Emissions from Commercial Aircraft." Eighth CRC On-Road Vehicle Emissions Workshop, San Diego, CA.

Press, W. H., S. A. Teukolsky, W. T. Vetterling and B. P. Flannery (1992). Numerical Recipes in C. Cambridge University Press, New York, NY.

Prigent, M., F. Castagna and R. Doziere (1994). "Status on Nitrous Oxide Emissions of Three-Way Catalyst Equipped Vehicles." 6th International Workshop on Nitrous Oxide Emissions, Turku, Finland.

Prigent, M. and G. De Soete (1989). "Nitrous Oxide N_2O in Engines Exhaust Gases-A First Appraisal of Catalyst Impact." *Society of Automotive Engineers Paper 890492*.

Prigent, M., G. De Soete and R. Doziere (1991). The Effect of Aging on Nitrous Oxide N_2O Formation by Automotive Three-Way Catalysts. Catalysis and Automotive Pollution Control. A. Crucq. Amsterdam, The Netherlands, Elsevier Science Publishers B.V.

Pun, B. K.-L. (1998). Treatement of Uncertainties in Atmospheric Chemical Systems: A Combined Modeling and Experimental Approach. Department of Chemical Engineering. Cambridge, Massachusetts, MIT.

Rabl, H.-P., A. Gifhorn and R. Meyer-Pitroff (1997). "The Formation of Nitrous Oxide (N_2O) over Three-Way Catalysts." 4th International Conference on Technologies and Combustion for a Clean Environment, Lisbon, Portugal.

Ripberger, C. T., R. C. Shores and C. O. Mann (1996). "Effects of Grade and Acceleration on On-Road Emissions of Instrumented Vehicles." Sixth CRC On-Road Vehicle Emissions Workshop, San Diego, California.

Ripberger, C. T., R. C. Shores and M. O. Rodgers (1998). "Dependence of Nitrogen Oxide Emissions on Vehicle Load: Results from the GTRP Instrumented Vehicle Program." Eighth CRC On-Road Vehicle Emissions Workshop, San Diego, California.

Riveros, H. G., A. Alba and P. Ovalle, Silva, B., Sandoval, E. (1998). "Carbon Monoxide Trend, Metereology, and Three-Way Catalysts in Mexico City." *Journal of the Air and Waste Management Association* **48**(5).

Robinson, N. F., W. R. Pierson and A. W. Gertler (1996). "Comparison of MOBILE4.1 and MOBILE5 predictions with measurements of vehicle emission factors in Fort McHenry and Tuscarora Mountain tunnels." *Atmospheric Environment* **30**(12): 2257-67.

Rogak, S. N., U. Pott and T. Dann, Wang, D. (1997). "Gaseous Emissions from Vehicles in a Traffic Tunnel in Vancouver, British Columbia." *Journal of the Air and Waste Management Association* **48**: 604-615.

Ross, M., R. Goodwin and R. Watkins, Wenzel, T., Wang, M.Q. (1998). "Real-World Emissions from Conventional Passenger Cars." *Journal of the Air and Waste Management Association* **48**: 502-515.

Rothman, L. S., R. R. Gamache and A. Goldman (1987). "The HITRAN database: 1986 edition." *Applied Optics* **26**: 4058-97.

Rothman, L. S., R. R. Gamache and R. H. Tipping, Rinsland, C. P., Smith, M. A. H. (1992a). "The HITRAN molecular database: editions of 1991 and 1992." *Journal of quantitative spectroscopy & radiative transfer* **48**(5-6): 469.

Rothman, L. S., R. L. Hawkins and R. B. Wattson, Gamache, R.R. (1992b). "Energy Levels, Intensities, and Linewidths of Atmospheric Carbon Dioxide Bands." *Journal of Quantitative Spectroscopy and Radiative Transfer* **48**(5/6): 537-566.

Rothman, L. S., C. P. Rinsland and S. T. M. A. Goldman, D.P. Edwards, J.-M. Flaud, A. Perrin, C. Camy-Peyret, V. Dana, J.-Y. Mandin, J. Schroeder, A. McCann, R.R. Gamache, R.B. Wattson, K. Yoshino, K.V. Chance, K.W. Jucks, L.R. Brown, V. Nemtchinov, and P. Varanasi (1998). "The HITRAN Molecular Spectroscopic Database and HAWKS (HITRAN Atmospheric Workstation): 1996 Edition." *Unpublished; http://www.hitran.com*.

Sachse, G. (1998). "Application of a New Gas Correlation Sensor to Remote Vehicular Exhaust Measurements." Eighth CRC On-Road Vehicle Emissions Workshop, San Diego, CA.

SAE (1996). "Road Load Measurement Using Onboard Anemometry and Coastdown Techniques." *Society of Automotive Engineers Surface Vehicle Recommended Practice J2263*.

Sagebiel, J. C., B. Zielinska and W. R. Pierson, Gertler, A.W. (1996). "Real-World Emissions and Calculated Reactivities of Organic Species from Motor Vehicles." *Atmospheric Environment* **30**(12): 2287-2296.

SAI (1996). "Auto/Oil Air Quality Improvement Research Program. Phases I and II Test Data: Public Release on Compact Disc." Systems Applications International, San Rafael, California.

Sakai, I. (1998). Chief Engineer, Honda Engineering Research Department Zero. Personal Communication.

Samaras, Z. and L. Ntziachristos (1998). "Hot Emission Factors for Passenger Cars and Light-Duty Trucks." Eighth CRC On-Road Vehicle Emissions Workshop, San Diego, California.

Sawyer, R. F., R. A. Harley and S. H. Cadle, Norbeck, J.M., Slott, R. Bravo, H.A. (1998a). "Mobile Sources Critical Review: 1998 NARSTO Assessment." *Submitted to Atmospheric Environment*.

Sawyer, R. F., R. A. Harley and S. H. Cadle, Norbeck, J.M., Slott, R. Bravo, H.A. (1998b). "Mobile Sources Critical Review: 1998 NARSTO Assessment. 25 March 1998 Draft." .

SCAQMD (1994). "*Current and Future Average Annual Day Emissions in the South Coast Air Basin*." South Coast Air Quality Management District,, Diamond Bar, CA.

SCAQMD (1997). "Draft 1997 Air Quality Management Plan." South Coast Air Quality Management District,, Diamond Bar, CA.

Schiff, H. I., J. Bechara and S. D. Nadler, and Mackay, G.I. (1994a). "A Near Infrared Diode Laser System for Remote Measurement of Automobile Exhaust Gas Concentrations and Temperature." Fourth CRC-APRAC On-Road Vehicle Emissions Workshop, San Diego, CA.

Schiff, H. I., G. I. Mackay and J. Bechara (1994b). The Use of Tunable Diode Laser Absorption Spectroscopy for Atmospheric Measurements. Air Monitoring by Spectroscopic Techniques (Chemical Analysis : A Series of Monographs on Analytical Chemistry and Its Applications). M. W. Sigrist. New York, NY, John Wiley & Sons.

References

Schiff, H. I., G. I. Mackay and S. D. Nadler (1996). "Some Applications of NIR Tunable Diodes for Remote Sensing." *Infrared Physics and Technology* **37**: 39-43.

Seinfeld, J. H. and S. N. Pandis (1998). *Atmospheric Chemistry and Physics: from Air Pollution to Climate Change*. John Wiley & Sons, New York.

Shih, R., S. Fable and R. F. Sawyer (1997). "Effects of Driving Behavior on Automotive Emissions." Seventh CRC On-Road Vehicle Emissions Workshop, San Diego, California.

Shorter, J. H., M. J.B. and C. E. Kolb, Allwine, E.J., Lamb, B.K., Mosher, B.W., Harriss, R.C., Partchatka, U., Fisher, H., Harris, G.W., Crutzen, P.J., Karbach, H.J. (1996). "Methane Emission Measurements in Urban Areas in Eastern Germany." *Journal of Atmospheric Chemistry* **24**: 121-140.

Shorter, J. H., D. D. Nelson and M. S. Zahniser (1997). "Air-broadened linewidth measurements in the nu2 vibrational band of HOCl." *Journal of the Chemical Society. Faraday transactions* **93**(16): 2933.

Silfvast, W. T. (1996). Laser Fundamentals. Cambridge University Press, London, UK.

Singer, B. C. and R. A. Harley (1996). "A fuel-based motor vehicle emission inventory." *Journal of the Air & Waste Management Association (1995)* **46**: 581-93.

Singer, B. C., R. A. Harley and D. Littlejohn, Ho, J., Vo, T. (1998). "Scaling of Infrared Hydrocarbon Measurements for Quantitative Assessment of Motor Vehicle Exhaust Emissions." Eighth CRC On-Road Vehicle Emissions Workshop, San Diego, California.

Sjödin, Å., K. Andreasson and M. Wallin (1997a). "Multi-Year Repeat Remote Sensing Measurements of On-Road Emissions from Cars Subject to an Annual Centralised I/M-Program Involving an Idle Emission Test." Seventh CRC On-Road Vehicle Emissions Workshop, San Diego, California.

Sjödin, Å., D. A. Cooper and K. I. Andréasson (1995). "Estimations of Real-world N_2O Emissions from Road Vehicles by Means of Measurements in a Traffic Tunnel." *Journal of the Air and Waste Management Association* **45**: 186-190.

Sjödin, Å., J. Mellqvist and M. Wallin, Lenner, M. (1996). "Recent Developments and Applications of Remote Sensing in Sweden - A European On-Road Fleet Example." Sixth CRC On-Road Vehicle Emissions Workshop, San Diego, California.

Sjödin, Å., K. Persson and K. I. Andréasson, Arlander, B., Galle, Bo. (1997b). "On-Road Emission Factors Derived from Measurements in a Traffic Tunnel." 4th International Symposium on Transport and Air Pollution, Avignon, France.

Sjögren, M., H. Li and U. Rannug, Westerholm, R. (1996). "Multivariate Analysis of Exhaust Emissions from Heavy-Duty Diesel Fuels." *Environmental Science and Technology* **30**: 38-49.

Slott, R. (1996). "Vehicle Exhaust Emission Control Strategies Evaluated by On-Road Remote Sensing with Controlled Driving Mode." Sixth CRC Oo-Road Vehicle Emissions Workshop, San Diego, California.

Slott, R. (1997). MIT Energy Laboratory. Personal Communication.

Smith, L. R. and F. M. Black (1980). "Characterization of Exhaust Emissions from Passenger Cars Equipped with Three-Way Catalyst Control Systems." *Society of Automotive Engineers Papers*: # 800822.

Smith, L. R. and P. M. Carey (1982). "Characterization of Exhaust Emissions from High Mileage Catalyst Equipped Automobiles." *Society of Automotive Engineers Paper 820783*.

Smith, M. A. H., C. P. Rinsland and V. M. Devi, Rothman, L.S., Rao, K.N. (1992). Intensities and Collision-Broadening Parameters from Infrared Spectra: an Update. Spectroscopy of the Earth's Atmosphere and Interstellar Medium. K. N. Rao, Weber, A., Academic Press.

Sorbo, N. W. (1997). Hughes Environmental Systems. Personal Communication.

Sorbo, N. W., C. A. Gomez and M. D. Jack, Peterson, J.C., Terorde, M.J., Smith, G.A. (1997). "Selection and Repair of Vehicles Emitting High Levels of NOx Identified by an Enhanced Remote Sensing System." Seventh CRC On-Road Vehicle Emissions Workshop, San Diego, California.

Spencer, M. N., C. Chackerian and L. P. Giver (1994). "The Nitric Oxide Fundamental Band: Frequency and Shape Parameters for Rovibrational Lines." *Journal of Molecular Spectroscopy* **165**: 506-524.

Spencer, M. N., C. Chackerian and L. P. Giver (1997). "Temperature Dependence of Nitrogen Broadening of the NO Fundamental Vibrational Band." *Journal of Molecular Spectroscopy* **181**: 307-315.

Spragle, G. S., W. A. Smith and Y. Yadin (1993). "Application of an Unstructured Flow Solver to Planes, Trains, and Automobiles." AIAA 31st Aerospace Sciences Meeting & Exhibit, Reno, Nevada.

St. Denis, M. J. (1998). "Relative Effectiveness of Remote Sensing, Low Emitter Profiling, and Model Year Exemption for I&M Clean Screening." 14th Annual Mobile Sources/Clean Air Conference 98, Breckenridge, Colorado.

Stahelin, J., C. Keller and W. Stahel, Schlapfer, K., Wunderli, S. (1998). "Emission Factors from Road Traffic from a Tunnel Study (Gubrist Tunnel, Switzerland). Part III: Results of Organic Compounds, SO2, and Speciation of Organic Exhaust Emissions." *Atmospheric Environment* **32**(6): 999-1009.

Stedman, D. H., G. Bishop and P. Aldrete (1997a). "On-Road CO, HC, NO, and Opacity Measurements." Seventh CRC On-Road Vehicle Emissions Workshop, San Diego, California.

Stedman, D. H., G. A. Bishop and P. Aldrete (1997b). "On-road evaluation of an automobile emission test program." *Environmental Science & Technology* **31**: 927-31.

Stedman, D. H., G. A. Bishop and S. P. Beaton, Peterson, J.E., Guenther, P.L., McVey, I.F., Zhang, Y. (1994). "On-Road Remote Sensing of CO and HC in California." Chemistry Department, University of Denver, Denver, Colorado.

Stedman, D. H., G. A. Bishop and R. S. Slott (1998). "Repair avoidance and evaluating inspection and maintenance programs." *Environmental Science & Technology* **32 no10**: 1544-5.

Stephens, R. D. and S. H. Cadle (1991). "Remote Sensing Measurements of Carbon Monoxide Emissions from On-Road Vehicles." *Journal of the Air and Waste Management Association* **41**(1): 39-46.

Stephens, R. D., S. H. Cadle and T. Z. Qian (1996a). "Analysis of remote sensing errors of omission and commission under FTP conditions." *Journal of the Air & Waste Management Association (1995)* **46**: 510-16.

Stephens, R. D., P. A. Mulawa and M. T. Giles, Kennedy, K.G., Groblicki, P.J., Cadle, Steven H., Knapp, K.T. (1996b). "An Experimental Evaluation of Remote Sensing-Based Hydrocarbon Measurements: A Comparison to FID Measurements." *Journal of the Air and Waste Management Association* **46**(2): 148-158.

Sturm, P. J., S. Hausberger and M. Keller, de Haan, P., Schweizer, T. (1998). "Use of Instantaneous Emission Data for Estimating Emissions from Passenger Cars - Overview of European Activities -." Eighth CRC On-Road Vehicle Emissions Workshop, San Diego, California.

Tewjani, G. D. T., B. M. Golden and E. S. Yeung (1976). "Pressure-Broadened Linewidths of Nitric Oxide." *Journal of Chemical Physics* **12**: 5110-5114.

Todd, M., M. Barth and J. Norbeck (1995). "The Variation of Remote Sensing Emission Measurements with Respect to Vehicle Speed and Acceleration." Fifth CRC On-Road Vehicle Emissions Workshop, San Diego, California.

U.S. DOT (1997a). "1996 Highway Statistics." Federal Highway Administration, U.S. Department of Transportation, Washington, D.C.

U.S. DOT (1997b). "State's Successful Practices Weight-in-Motion Handbook." Federal Highway Administration, U.S. Department of Transportation, Washington, D.C.

U.S. EPA (1992). "Mobile Sources Emission Standards Summary." U.S. Environmental Protection Agency, Washington, D.C.

U.S. EPA (1993a). "Federal Test Procedure Review Project: Preliminary Technical Report." U.S. Environmental Protection Agency, EPA 420-R-93-007, .

References

U.S. EPA (1993b). "MOBILE 5.0a User's Guide." U.S. Environmental Protection Agency, Washington, D.C.

U.S. EPA (1995a). "Annual Emissions and Fuel Consumption for an "Average" Passenger Cars." U.S. Environmental Protection Agency, http://www.epa.gov/oms, Ann Arbor, Michigan.

U.S. EPA (1995b). "EPA, California Air Resources Board, and Manufacturers of Heavy-Duty Engines Sign "Statement of Principles"." , EPA420-F-95-010a, Ann Arbor, Michigan.

U.S. EPA (1996a). 40 CFR Part 86. Final Regulations for Revisions to the Federal Test Procedure for Emissions from Motor Vehicles. Federal Register, .

U.S. EPA (1996b). "National Air Pollutant Emission Trends (1990-1995)." , EPA-454/R-96-007, Research Triangle Park, NC.

U.S. EPA (1997a). "40 CFR Parts 9 and 86. Control of Emissions of Air Pollution From Highway Heavy-Duty Engines; Final Rule." Federal Register, .

U.S. EPA (1997b). "Greenhouse Gas Inventory (Chapter 3 of the 1997 U.S. Climate Action Report, submitted by the U.S.A. Under the United Nations Framework Convention on Climate Change." U.S. Environmental Protection Agency, .

U.S. EPA (1997c). "National Air Pollutant Emission Trends (1990-1996)." , EPA-454/R-97-011, Research Triangle Park, NC.

U.S. EPA (1997d). "National Air Pollutant Emission Trends, 1900-1996." US EPA, EPA-454/R-97-011, Research Triangle Park, NC.

U.S. EPA (1998a). "40 CFR Part 86. Notice of Proposed Rulemaking: Control of Air Pollution From New Motor Vehicles; Compliance Programs for New Light-Duty Vehicles and Light-Duty Trucks." U.S. Environmental Protection Agency, RIN #2060-AH06, .

U.S. EPA (1998b). "DOJ, EPA Announce One Billion Dollar Settlement with Diesel Engine Industry for Clean Air Violations." *U.S. EPA Headquarters Press Release (22 October 1998).*

U.S. EPA (1998c). "Draft Inventory of U.S. Greenhouse Gas Emissions and Sinks 1990-96." U.S. Environmental Protection Agency, .

U.S. EPA (1998d). "EPA Staff Paper on Gasoline Sulfur Issues." , EPA420-R-98-005, Ann Arbor, Michigan.

U.S. EPA (1998e). "Inspection and Maintenance (I/M) Program Effectiveness Methodologies." , EPA420-S-98-015, .

U.S. EPA (1998f). "National Air Quality and Emission Trends Report, 1996." , EPA-454/R-97-013, Research Triangle Park, NC.

U.S. EPA (1998g). "NVFEL Nitrous Oxide Testing." U.S. Environmental Protection Agency, http://transaq.ce.gatech.edu/epatac/index.htm, Ann Arbor, Michigan.

U.S. EPA (1998h). "Tier 2 Report to Congress." , EPA-420-R-98-008, .

U.S. EPA (1998i). "Update of Fleet Characterization Data for Use in MOBILE6 - Final Report." , EPA420-P-98-016, Ann Arbor, Michigan.

Urban, C. M. and R. J. Garbe (1979). "Regulated and Unregulated Exhaust Emissions from Malfunctioning Vehicles 790696." *Society of Automotive Engineers Papers*.

Urban, C. M. and R. J. Garbe (1980). "Exhaust Emissions from Malfunctioning Three-Way Catalyst Equipped Automobiles." *Society of Automotive Engineers Papers 800511*.

Verdegem, F. (1997). Flemish Technological Research Institute (VITO). Personal Communication.

Wald, M. L. (1998). "E.P.A. Says Catalytic Converter Is Growing Cause of Global Warming." *The New York Times (May 29, 1998).*

Walsh, M. P. (1998a). "Global Trends in Motor Vehicle Pollution Control: A 1998 Update." Sixth International Symposium on Highway & Urban Pollution, Ispra/Baveno, Italy.

Walsh, M. P. (1998b). "Vehicles, Fuels, and Climate Change: Recent Developments in Europe." U.S. EPA Mobile Sources Technical Review Subcommittee Meeting, Ann Arbor, Michigan.

Walsh, P. A. and A. W. Gertler (1997). "Texas 1996 Remote Sensing Feasibility Study." Desert Research Institute, Reno, Nevada.

Walsh, P. A. and C. Kite (1998). "The Influence of Speed and Acceleration on RSD Measurements." Eighth CRC On-Road Vehicle Emissions Workshop, San Diego, California.

Warner-Selph, M. A. and C. A. Harvey (1990). "Assessment of Unregulated Emissions from Gasoline Oxygenated Blends." *Society of Automotive Engineers Paper 902131*.

Watson, H. C., E. E. Milkins and M. O. Preston, Chittleborough, C., Alimoradian, B. (1983). "Predicting Fuel Consumption and Emissions - Transferring Chassis Dynamometer Results to Real Driving Conditions." *SAE paper 830435*.

Weaver, C. S. and L.-M. Chan (1996). "Draft Final Report on Mobile Source Emission Factors for Global Warming Gases." Engine, Fuel, and Emissions Engineering Incorporated, Sacramento, California.

Webster, W. J. and C. Shih (1996). "A Statistically Derived Metric to Monitor Time-Speed Variability in Practical Emissions Testing." Sixth CRC On-Road Vehicle Emissions Workshop, San Diego, California.

Wehinger, C. and R. Meyer-Pitroff (1994). "Schadstoffemissionen von Ottomotoren mit Geregeltem Dreiwegekatalysator." *Staub - Reinhaltung der Luft* **54**: 9-15.

Welstand, J. S. (1997). "Remote Sensing Readings Compared to Cyclic Mass Emissions Measurements - A Literature Review." Seventh CRC On-Road Vehicle Emissions Workshop, San Diego, California.

Wenzel, T. (1998). Lawrence Berkeley National Laboratory. Personal Communication.

Wenzel, T. and M. Ross (1996). "Relationship between Vehicle Attributes and Malfunction of Emissions Control Systems." Sixth CRC On-Road Vehicle Emissions Workshop, San Diego, California.

Wenzel, T. and M. Ross (1997). "I/M Failure Rates by Vehicle Model." Seventh CRC On-Road Vehicle Emissions Workshop, San Diego, California.

Wenzel, T. and R. Sawyer (1998a). "Analysis of a Remote Sensing Clean Screen Program in Arizona." Lawrence Berkeley National Laboratory, LBNL-41918, Berkeley, California.

Wenzel, T., R. F. Sawyer and M. Ross (1998b). "Further Analysis of I/M Failure Rates by Vehicle Model." Eighth CRC On-Road Vehicle Emissions Workshop, San Diego, California.

Werle, P. (1998). "A Review of Recent Advances in semiconductor Laser Based Gas Monitors." *Spectrochimica Acta Part A* **54**: 197-236.

West, B. H. and R. N. McGill (1997). "Emissions and Fuel Consumption Predictions from Data-Based Modal Models." Seventh CRC On-Road Vehicle Emissions Workshop, San Diego, California.

Whitfield, J. K. and D. B. Harris (1998). "Comparison of Heavy-Duty Diesel Emissions from Engine and Chassis Dynamometers and On-Road Testing." Eighth CRC On-Road Vehicle Emissions Workshop, San Diego, CA.

WHO/UNEP (1992). Urban Air Pollution in Megacities of the World. Blackwell Publishers, Oxford, UK.

Wiesen, P., J. Kleffmann and R. Kurtenbach, Becker, K. H. (1996). "Emission of nitrous oxide and methane from aero engines: monitoring by tunable diode laser spectroscopy." *Infrared physics & technology* **37**(1).

Willard, H. H., L. L. Merritt and J. A. Dean, Settle, F.A. (1988). Instrumental Methods of Analysis. Wadsworth, Inc., Belmont, California.

Wilson, R. and J. Spengler (1996). Particles in Our Air: Concentrations and Health Effects. Harvard University Press, .

References

Wormhoudt, J., M. S. Zahniser and D. D. Nelson, McManus, J.B., Miake-Lye, R.C., Kolb, C.E. (1994). Infrared Tunable Diode Laser Diagnostics for Aircraft Exhaust Emission Characterization. Laser Applications in Combustion and Combustion Diagnostics II, SPIE Proc. V.2122: 49-59.

Wormhoudt, J., M. S. Zahniser and D. D. Nelson, McManus, J.B., Miake-Lye, R.C., Kolb, C.E. (1995). Infrared Tunable Diode Laser Measurements of Nitrogen Oxide Species in An Aircraft Engine Exhaust. Optical Techniques in Fluid, Thermal, and Combustion Flows, SPIE Proc. V2546: 552-61.

Zahniser, M. S. (1998). Aerodyne Research. Personal Communication.

Zahniser, M. S. and C. E. Kolb (1994). "Tunable Infrared Laser Techniques to Quantify Real Time Vehicle Emissions." Fourth CRC-APRAC On-Road Vehicle Emissions Workshop, San Diego, CA.

Zhang, Y., G. A. Bishop and D. H. Stedman (1994). "Automobile Emissions are Statistically Gamma-Distributed." *J. Air Waste Manage. Assoc* **28**: 1370-74.

Zhang, Y., D. H. Stedman and G. A. Bishop (1993). "On-road hydrocarbon remote sensing in the Denver area." *Environmental Science & Technology* **27 no9**: 1885-91.

Zhang, Y., D. H. Stedman and G. A. Bishop (1995). "Worldwide on-road vehicle exhaust emissions study by remote sensing." *Environmental Science & Technology* **29**: 2286.

Zhang, Y., D. H. Stedman and G. A. Bishop, Beaton, S.P., Guenther, P.L., and McVey, I.F. (1996a). "Enhancement of Remote Sensing for Mobile Source Nitric Oxide." *J. Air Waste Manage. Assoc* **46**: 25-29.

Zhang, Y., D. H. Stedman and G. A. Bishop (1996b). "On-road evaluation of inspection/maintenance effectiveness." *Environmental Science & Technology* **30**: 1445-50.